VITY DEVICES: COMMERICAL USE OF SPACE

Annual Report

to

ional Aeronautics and Space Administration
Langlley Research Center
Hampton, VA 23665-5225

Period: February 1, 1995 - April 30, 1996

or:

Gene Haertling

Eugene Furman

ator:

Guang Li

1-1301

May 13, 1996

The Gilbert C. Robinson
Department of Ceramic Engineering

College of Engineering and Science

SUPERCONDUCTIVITY DEVICES: COMMERICAL USE OF SPACE

Annual Report

to

National Aeronautics and Space Administration
Langlley Research Center
Hampton, VA 23665-5225

Period: February 1, 1995 - April 30, 1996

Principal Investigator:

Gene Haertling

Co-Investigator:

Eugene Furman

Supporting Investigator:

Guang Li

Contract No. NAG-1-1301

May 13, 1996

CLEMSON
UNIVERSITY

The Gilbert C. Robinson
Department of Ceramic Engineering

College of Engineering and Science

Table of Contents

I. Introduction

This report details work that was performed in the Ceramic Engineering Department of Clemson University over the period from February 1, 1995 to April 30, 1996 under NASA Contract No. NAG-1-1301. The work described in this report covers various aspects of the Rainbow solid-state actuator and sensor technologies. It is present in five parts dealing with sensor applications, non-linear properties, stress-optic and electrooptic properties, stacks and arrays, and publications.

The Rainbow actuator technology is a relatively new materials development which had its inception in 1992. It involves a new processing technique for preparing pre-stressed, high lead containing piezoelectric and electrostrictive ceramic materials. Ceramics fabricated by this method produce bending-mode actuator devices which possess several times more displacement and load bearing capacity than present-day benders; i.e., unimorphs and bimorphs. Since they can also be used in sensor applications, Rainbows are part of the family of materials known as smart ceramics.

During this period, PLZT Rainbow ceramics were characterized with respect to their piezoelectric properties for potential use in stress sensor applications. It was found that they possess an unusually strong piezoelectric effect, and the respective piezoelectric coefficients under steady-state loading conditions can be over two orders of magnitude greater than that of normal ceramics. The voltage sensitivity to applied pressure was found to decrease continuously with increasing frequency prior to resonance. Overall results show that Rainbow ceramics are very promising for stress-sensing applications involving low stress levels such as shallow water exploration.

Studies of the non-linear and stress-optic/electrooptic birefringent properties were also initiated during this period. Large stress gradients that are internally present in the Rainbow structure are believed to cause polarization gradients which are being investigated both electrically and optically. Electrically, these polarization gradients lead to internal bias voltages that ultimately affect the switching of domains as noted in the asymmetrical hysteresis loops and mechanical displacement loops. Optically, these polarization and stress gradients cause optical birefringent gradients which are clearly visible under polarized light. This technique also reveals within the Rainbow where there is no gradient, i.e., the stress neutral plane. During operation, the stress-optic and electrooptic birefringent effects combine to produce new optical retardation color patterns, thus revealing the changing internal stress conditions as voltage is applied.

Various means for increasing the utility of stress-enhanced Rainbow actuators are presently under investigation. Among these are included the techniques for increased linear displacement using stacked actuators as well as matrix arrays for enhanced coverage in wide area sensor/actuator applications such as smart skins, autoleveling structures, antivibration devices and deformable coatings. The displacement characteristics of Rainbow stacks consisting of multiple clamshell units were determined as functions of voltage and load bearing capability. Conformal Rainbow arrays, composed of individual elements sandwiched between outer lead foil skins, were fabricated and qualitatively evaluated.

Part I.

Characterization of Rainbow Ceramics for Sensor Applications

Characterization of Rainbow Ceramics for Sensor Applications

Abstract: PLZT Rainbow ceramics of selected compositions were characterized with respect to their piezoelectric properties for potential application as stress sensors. It was found that Rainbow ceramics possess a strong piezoelectric effect when operated in the dome mode. The corresponding effective piezoelectric coefficient under steady-state loading conditions can be over two orders of magnitude greater than that of normal ceramics, depending on the dimensions, thickness ratio, and material properties of the Rainbow ceramics. The voltage sensitivity to applied pressure decreased continuously with increasing frequency before the occurrence of mechanical resonances. Results show that Rainbow ceramics are very promising for stress-sensing applications involving low stress levels and frequencies.

1. Introduction

Recent investigations of Rainbow ceramics (Reduced And INternally Biased Oxide Wafer) have shown that these devices hold high promise for actuator applications owing to their large field-induced displacement and excellent load-bearing capability [1-3]. A Rainbow is made by a special process in which a high lead-containing ferroelectric oxide ceramic wafer is chemically reduced on one major surface by placing the wafer on a graphite block and heat treating it at an elevated temperature. When the partially reduced wafer is cooled to room temperature, it develops a dome-shaped (sometimes saddle-shaped) configuration resulting from the dimensional mismatch between the reduced and unreduced layers. Large displacement is obtainable from the dome center of an electroded Rainbow sample by applying an electric field

across the unreduced layer. The high axial displacement of Rainbow ceramics results from the bending of the Rainbows under an applied field that is caused by the lateral constraint of the passive reduced layer to the electrically active piezoelectric or electrostrictive unreduced layer in a manner similar to the operation of conventional piezoelectric unimorph benders. However, due to their unique dome structure and associated high internal stress, Rainbow actuators can sustain external stresses or loads higher than normal.

The concept of "smart" materials and devices has recently been widely adopted in the field of material science and technology. Smart devices are able to adjust some of their own properties in response to changing ambient conditions. This generally requires them to be multi-functional, among other desired properties such as simplicity in structure, low energy consumption and good reliability. For instance, in active structural systems, "smart" piezoelectric elements act as both sensor and actuator in accomplishing a variety of sophisticated mechanical tasks in conjunction with a computer. Ferroelectric materials have long been considered as desirable materials for smart devices because of the multiplicity of their properties including piezoelectric, electrostrictive, pyroelectric effects, electrooptic and photorefractive effects for certain compositions. During the past several years the use of ferroelectric ceramics for construction of smart devices and structures has received numerous investigations and remarkable advances [4-7].

As has been mentioned, a piezoelectric Rainbow ceramic, when subjected to an applied electric field, produces a large physical displacement. The opposite is equally true; that is, a large electrical signal is generated when an external pressure or load is imposed on the Rainbow. This occurs because, with its dome-shaped structure, a Rainbow is considerably more sensitive to applied pressures than a normal bulk piezoelectric ceramic. This property of Rainbow ceramics

can be utilized to detect and measure stress or pressure. In addition, with special compositions, Rainbow ceramics can possess pyroelectric and/or photoelectronic (photoconductive, photovoltaic and photorefractive) properties. It is therefore probable that Rainbows, fabricated to perform functions of both actuator and sensor, may require different material properties.

This report is devoted to the characterization of Rainbow ceramics with respect to their piezoelectric properties for potential application as stress sensors.

2. Sample Preparation and Measurements

A number of different compositions from the PLZT system were selected to prepare the ceramic wafers for the production of the Rainbow samples. These compositions, which are located in the vicinity of the morphotropic phase boundary separating the tetragonal and rhombohedral phases, include PLZT 1.0/53/47, 5.5/56/44, and 5.5/59/41 (La/Zr/Ti). Conventional mixed-oxide processing techniques were employed to obtain the sample powders which were dry pressed into slugs of 1 and 2 inches in diameter. The slugs were then sintered in an oxygen atmosphere within closed crucibles at 1250 °C for 4 hours, or hot-pressed at 1200 °C for 6 hours at 10 MPa. Sintered ceramics were sliced with a diamond saw into disks which were lapped to wafers of desired thicknesses with 400-grit sandpaper.

In the fabrication of the Rainbow samples, a PLZT ceramic wafer was placed on a graphite block and a zirconia disk of the same size as the wafer was located on top of the wafer. The wafer was then chemically reduced by introducing the whole assembly into a preheated furnace and heat treated at an elevated temperature. After the chemical reduction, the wafer was removed from the furnace and cooled down in air to room temperature. The zirconia disk placed

on top of the wafer was used to prevent possible thermal shock during the heat treatment processing. The wafer thus obtained (a Rainbow) contains a reduced and an unreduced layer as a result of the local chemical reduction. The reduced side of the Rainbow sample was lightly sanded to eliminate any lead particles and/or thin reoxided layer. Silver paste cured at 200 °C was used as electrodes for measurements of electrical properties. While the entire surface of the reduced side was covered with electrodes, the unreduced (oxide) side was partially electroded in some cases with configurations depicted in Figure 1.

The Rainbow samples are designated in terms of the composition and processing conditions of the original, unreduced ceramic wafers. For example, RB1053HP represents a Rainbow made from a hot-pressed PLZT 1.0/53/47 ceramic. The data of the reduction temperature and time for the Rainbow samples studied, their dimensions, curvature (dome height), and thickness ratio are given in Table 1. The dome height of a Rainbow was measured with reference to the thickness of the corresponding unreduced wafer. The different values of the thickness ratio, which is defined as the ratio of the reduced layer thickness to the total thickness of the sample, were achieved by reducing the ceramic wafers for different periods of time at a constant temperature. Typical samples had dimensions of 1.25 in × 20 mil (diameter × thickness) or 0.88 in × 17 mil, and a thickness ratio of approximately 0.3.

Table 2 lists the measured values of capacitance, dielectric loss, piezoelectric constant d_{33}, the resonant and antiresonant frequencies of the radial vibrational mode, and the resonant frequency of the dome mode for some of the samples indicated in Table 1. The d_{33} data were determined on a Berlincourt-type Piezo Tester by positioning the center of the oxide and reduced sides of a Rainbow to the two oppositely mounted measuring probes. The d_{33} values thus

4

determined represent the effective d_{33} coefficient of the Rainbow's oxide layer. The dielectric properties were measured at 1 kHz using an LCR meter. The resonant characteristics of the samples were obtained from an impedance analyzer (HP 4194A).

3. Experimental Results

Response of Rainbow to Steady-State Pressure and Point Load

The response of Rainbow ceramics to uniform pressure and point load was studied. The samples used for this purpose include RB1053HP, RB1053S, RB5556S and RB5559S. Electroded Rainbow samples were poled at room temperature for a few minutes under suitable applied electric fields, normally twice the coercive field of the ceramics. For the point load testing, a sample was placed on a metal ring with the reduced side facing downward; and the load was gradually applied to the center of the sample through a metal tip as illustrated schematically in a setup in Figure 2. The electrical charge and voltage signals generated by the loading were measured using an electrometer (Keithley Instruments, 610CR). As for the measurements with uniform pressure, a small cylindrical metal chamber was built. The cross-sectional view of the chamber is diagrammed in Figure 3. A sample was placed on the flat bottom of the chamber, with a soft silver foil being inserted between the sample and the bottom plate to keep the air from leaking through, the edges during application of pressure. Desired pressure levels inside the chamber were achieved by gradually applying air pressure to the inlet of the chamber. The induced electrical signal on the sample's electrodes was measured by connecting them to an electrometer.

The polarization change in the oxide layer of a Rainbow generated by external mechanical loading gives rise to unbalanced electrical charges on the sample electrodes, and consequently an open-circuit voltage across them. Under steady-state loading, the unbalanced charges are slowly compensated by free charged ions from the environment as well as through the limited conductivity of the ceramic oxide layer. Accordingly, the generated voltages diminishes gradually. Since the electrometer used for the measurement of the voltages has a very high input impedance ($>10^{14}$ Ω versus $\sim 10^{10}$ Ω of typical Rainbow samples), its effect on the measured electrical signals can generally be ignored. Figure 4 shows the change of the induced voltages as a function of time for several Rainbow samples under steady-state point loading. It was found that, depending on specific samples, the voltages decreased only by 10 to 20 % over a time period of 2000 seconds due to the high electrical resistance of the samples. The slight fluctuations of the data for RB1053S-1 were caused by the background noises. When a metal shield was used to block the ambient radiation, the irregular variations disappeared, as is the case for the other three samples in the figure.

When a Rainbow is subjected to an instant loading, the induced signal does not rise to the maximum value instantly, but rather with a finite response time. The initial rise of the induced voltage under instant loading for several Rainbow samples was determined and is illustrated in Figure 5. The data were collected every one second automatically via a computer, while the mechanical point load was applied and removed alternately every one minute by changing the weights on the samples instantaneously. It was seen that the voltages increased from zero to the maximum in terms of a trace similar to the charging curve of a capacitor. The times required to reach the maximum values were found to be dependent upon the compositions and geometrical

6

factors such as the thickness ratio and diameter of the Rainbows. In other words, the time response characteristics of the induced signals to instant loading were of both mechanical and electrical origin. For a majority of the samples studied, the maximum output signals were reached within two minutes after loads were applied. Thereafter, the signals decreased gradually through the mechanisms described earlier. The induced electrical charges and voltages given in the following discussions were determined at their maximum values upon the application of mechanical loads.

Figure 6 shows the induced voltage of RB1053HP-4 sample as a function of point load for three loading cycles between zero and a maximum value. The voltage-load relationship given in Figure 6 is typical of all the piezoelectric Rainbow samples investigated. A salient feature of this relationship is the hysteresis of the induced voltage versus loading, which is attributed to the behavior of ferroelectric domains under stress for which the domain state, and therefore the induced strain of a ferroelectric ceramic, is dependent on the history of stressing. In addition, a residual voltage was observed at zero load after the first loading cycle. This residual voltage increased slightly for the next few loading cycles. Beyond that, the change of the residual voltage was small and irregular; and the voltage-load loop resulting from further loading cycles became relatively stable. It was found that, when the same sample was left unloaded for a few hours and the same testing was performed, a very similar voltage-load relationship was obtained. In other words, the residual voltage reoccurred. This phenomenon seems to suggest that some preferential domain alignment created by the loading relaxed gradually with time. The magnitude of the residual voltage and the degree of the hysteresis were found to be closely related to the geometry

and composition of Rainbow ceramics as well as the maximum value of load for the loading cycles.

Figure 7 displays the induced voltage versus the maximum value of loading cycles for a number of RB5556S samples having different total thicknesses but identical diameter. The samples were cycled with a given maximum value of load until a stable loop of voltage versus loading was obtained. The influence of the residual voltage was eliminated by short-circuiting the samples after each loading cycle. The same steps were repeated with different maximum values of load. The measured voltages were then plotted against the maximum loads. The results in Figure 7 indicate that the relation between the induced voltage and external mechanical loading is approximately linear when the effects of the residual signals are excluded. The RB1053S-a sample, which had the smallest thickness among them, fractured at the load of 1200g.

As mentioned earlier, the electrical signals generated by external loading are primarily contributed from the change of the dome curvature of the Rainbow. The piezoelectric effect in the thickness direction, i.e. d_{33}, is negligible compared to the lateral effect resulting from the change of the curvature. The change of the curvature and hence the induced signals are strongly dependent on the location of the Rainbow to which a point load is applied. Figure 8 shows the induced voltages obtained by applying a constant point load to different locations across the Rainbow diameter. The maximum induced signals were observed when loads were acted on the center area of the samples. This is simply because a larger curvature change was produced by a load on the center area.

The variation of the induced electrical charge and voltage with distributed load or pressure was given in Figures 9 through 11 for RB5556S samples. Similar to the case of point load, the

hysteresis and residual signals were observed. The relationship between voltage and pressure was less hysteretic for RB5556S-h sample in comparison with that of electrical charge versus pressure, as is evidenced by comparing Figure 10 with Figure 11. This may imply that the capacitance of the sample was also hysteretic under applied stress, which compensated for part of the hysteresis in the voltage curves through the simple relation, $Q = C \times V$, where Q = charge, C = capacitance, and V = voltage.

In addition to material properties, the shape and dimensions of a sample may have significant influence on the characteristics of pressure-induced charge and voltage. As applied pressure is increased, a Rainbow will become less curved and, eventually, its reduced side will touch the plate on which the Rainbow is placed. When this happens, the induced signals will decrease markedly since the dome mode contribution diminishes considerably. Under sufficiently high pressure, the Rainbow will become completely flat. In this situation the Rainbow will behave like a normal piezoelectric ceramic working in its longitudinal stretching mode. Figure 12 shows the change of the induced voltage with pressure for RB1053HP-4, in which the sudden change of the curve slop was caused by the fact that the reduced side began to touch the supporting plate under applied pressure. The transition point of the curves was found to be a strong function of the sample thickness and diameter as well as other parameters that govern the mechanical stiffness of the sample.

The magnitude of the induced signals was also dependent on the thickness ratio (the reduced layer thickness over the total thickness) of the Rainbow sample under testing. Figures 13 and 14 illustrate the induced signals as a function of the thickness ratio for RB1053S and RB5556S samples. The induced charges tended to increase with increasing thickness ratio, but

the voltages exhibited a maximum at a thickness ratio around 0.4. The occurrence of the maximum in the voltage curves was primarily attributed to the drastic increase of sample capacitance with increasing thickness ratio, since these samples had identical total thickness. Based on the relation $Q = C \times V$, when the increase of charge under constant pressure is less than the increase of capacitance, the voltage should decrease.

The influence of sample capacitance on the induced signals is further revealed by the results shown in Figures 15 and 16, where the voltage and charge were plotted as a function of the electroded area relative to the entire sample surface. In this measurement, the upper surface of a Rainbow was electroded from the center out toward the edge to obtain different sizes of electroded area, as, for example, is depicted in Figure 1 for a fully electroded and a 50% electroded sample. As can be seen in Figure 15, the induced voltage increased approximately linearly with decreasing electroded area for three RB5559S samples of different thickness ratios. The charges, on the other hand, exhibited a maximum with decreasing electroded area. The maximum in the charge curves implies that the induced charges from the regions near Rainbow's edge possess an opposite sign to those generated in the center area, since, if the induced charges had the same sign across the samples, the cumulative result would decrease monotonically with decreasing electroded area. This characteristic was further justified by examining the induced signals from a sample with separate electrodes for the edge and center regions as shown in Figure 1. The data given in Table 3 clearly show that the charges and voltages from the center regions are opposite in sign to those from the edge regions and, as a result, the signals obtained from fully electroded samples are lower in magnitude than those from the samples with center electrodes only. Table 3 also shows that bonding of sample's edge to a rigid plate (clamped condition) could

lead to significant reduction of induced signals. This is ascribed to a smaller induced strain in an edge-clamped Rainbow. The degree of signal reduction due to clamping depended closely on the manner in which the edge was clamped.

Owing to the dome-shaped configuration of Rainbow ceramics, their induced strain and electrical signals under either pressure or point load are difficult to study analytically. For this reason, the finite element method (FEM), which is based on a commercial software package ABAQUS, was used. Details of the procedure for the finite element modeling can be found elsewhere [8]. The material parameters used for the modeling which include elastic, dielectric, and piezoelectric coefficients were those of PZT-5 piezoelectric ceramics obtained from reference [9]. Figure 17 shows the change of the induced voltage from the center to the edge of a Rainbow under an applied pressure of 1 psi. It is seen that, when the edge is clamped, the voltage decreases continuously toward the edge without change in sign. However, in the case of a free edge (the edge is allowed to move freely in the radial direction as pressure is applied to the Rainbow), the voltage output changes sign at a location close to the edge, which is in agreement with the testing results given earlier. Similar results of finite element modeling were obtained for point loading, as is indicated in Figure 18. In this case, very small signals are generated near the edge area for an edge-clamped Rainbow. The signal from a free Rainbow changes sign across the radius, which again is consistent with the experimental observations. The abrupt changes at the zero position (i.e., the center of a Rainbow) shown in Figure 18 are caused by the singularity of the point load in the modeling.

Figure 19 shows the FEM results of the relationship between the induced voltage and electroded area for three Rainbows with different thickness ratios. These results qualitatively

11

agree with the experimental data given in Figure 15. It was found that the nonuniform stress and strain induced by external loading is mainly responsible for the nonuniform distribution of the induced electrical signals across a Rainbow. Figure 20 is the FEM results of the planar stress distribution across a Rainbow under uniform applied pressure. As is shown, the induced stress changes from compression (negative values) to tension along the radius direction for the edge-free condition, which leads to a change in the sign of the electrical signals.

Frequency Response

The dependence of the induced voltage on the frequency of applied pressure for Rainbow ceramics was determined via the comparison method described in American National Standard for calibration of underwater electroacoustic transducers [10]. A closed cylindrical coupling chamber with inner dimensions of 5.25 inches high and 2 inches in diameter was constructed for the low-frequency measurements, as is schematically illustrated in Figure 21. One Rainbow ceramic placed on the bottom plate of the coupling chamber was used as the sound pressure generator. The Rainbow samples to be tested or the standard pressure sensor used for comparison was located on the top of the chamber as indicated in the figure. The chamber was filled with pure mineral oil, and then evacuated for 15 min to eliminate any trapped air bubbles. Note that water is equally valid as the pressure medium for this kind of measurement. The mineral oil was used merely for convenience since insulating encapsulation was otherwise needed for the Rainbow samples to prevent crosstalk. Because the dome shape of a Rainbow is sensitive to any biasing pressure inside the chamber, to obtain consistent results, a tiny pressure-relieving outlet was let open as the sample holder was threaded into the chamber. The chamber was evacuated once

again for a few minutes before closing the outlet. The Rainbow samples used for this measurement had approximately 80% electroded area on their unreduced surface, and were attached to the sample holder.

A hydrophone made by Benthos, Co. (Model AQ-17 with AQ-201 preamplifier) was used as the standard sensor for pressure calibration. This hydrophone possesses a flat frequency response from 1 Hz to 12 kHz with a corresponding sensitivity of 176.5 dB based on information from the company. The Rainbow pressure generator had dimensions of 1.35 in × 30 mil (diameter × thickness) which was bonded to the bottom plate of the coupling chamber with superglue and then covered by a thin layer of resin epoxy. The generator was driven by an amplitude-adjustable, sinusoidally varying voltage source. The electrical signals from Rainbow samples or the hydrophone were connected to the input of a lock-in amplifier (EG&E 5302) which was interfaced with a computer for data acquisition. A diagram of the experimental setup is depicted in Figure 22.

Figure 23 shows the frequency dependence of the output voltages obtained from a Rainbow sample and the hydrophone. The voltage signals decreased rapidly with decreasing frequency in the frequency range below 5 Hz. The reasons for this will be discussed later. There is a relatively flat frequency dependence from 5 Hz up to approximately 1000 Hz. The marked variations in the output signals at higher frequencies were caused by the mechanical resonances of the Rainbow sample, as well as the resonances of the Rainbow pressure generator.

The normalized frequency response of RB1053HP-2 sample under two different magnitudes of driving voltage on the sound pressure generator is given in Figure 24. The normalized data were obtained by dividing the signals of the Rainbow sample by those of the

13

hydrophone. Since the hydrophone has a pressure sensitivity of 176.5 dB, the value of unity on the vertical scale represents the same sensitivity for the Rainbows. The two curves in the figure agree well with each another, as anticipated.

Figure 25 displays the frequency response of several RB5556S samples having different total thicknesses. A very similar sensitivity-frequency relationship was observed for these samples. Generally speaking, the characteristics of frequency response are affected by both the material properties and the geometrical factors such as thickness of the Rainbows. The similarity in the curves of Figure 25 implies that the influence of thickness of the samples was not significant, due probably to the low pressure levels on the samples. In other words, noticeable difference in the frequency response for these samples may be observed if the pressure level is sufficiently high. The different values of sensitivity at a given frequency can be ascribed to the different thickness ratios of these samples. The resonant frequencies revealed in Figures 24 and 25 were found to correspond to those obtained from the impedance analysis as shown in Figure 26

As indicated previously in the steady-state studies, the induced voltage signals can be enhanced by reducing the electroded area on a sample because of the nonuniform distribution of the induced stresses as well as reduction in sample capacitance. Figure 27 shows the change of the normalized signals with frequency for three different sizes of electrode on the unreduced side of RB5556S-2. Significant difference exists in the low-frequency range for these cases, as is clearly shown in the figure. The signals are generally stronger at higher frequencies for samples with a smaller electroded area.

4. Discussion

Rainbow ceramics exhibit a very strong piezoelectric effect when operated in their dome mode, i.e., when external load is applied vertically to the convex side of the Rainbows. The corresponding effective piezoelectric coefficient, defined as induced charge divided by magnitude of the applied load, is generally several tenths up to one hundred times greater than the longitudinal piezoelectric coefficient d_{33} of the normal bulk ceramics. The voltage sensitivity (volt per micropascal) of selected Rainbow samples under steady-state loading conditions was calculated and is given in decibels in Table 4. It was found that the value of the sensitivity is strongly dependent on the dimensions and thickness ratio of the Rainbows in addition to the material properties such as piezoelectric and elastic constants. The high sensitivity of Rainbow ceramics to applied stress can potentially be utilized for detection and measurement of pressures and loads. The major drawbacks of Rainbows as a stress sensor may be the hysteresis of signal-stress relationship and the preferred domain alignment under the influence of stress which leads to a residual signal upon each stressing cycle. It was however found that the effect of the residual signal can be minimized by increasing the number of stressing cycles in conjunction with a short-circuiting operation.

The frequency response of Rainbow ceramics given in Figures 24, 25 and 27 was determined without taking into consideration of the voltage coupling loss resulting from the direct connection of the high-impedance Rainbows to the relatively low-impedance input channel of the lock-in amplifier. Also, the sensitivity data in the high-frequency range are of less reliability because at these high frequencies the pressure inside the coupling chamber can no longer be presumed to be uniform. The high-frequency limit for this type of measurement is set by the

longest dimension of the coupling chamber and the sound velocity of the pressure medium (pure mineral oil in this case). Specifically, to obtain uniform pressure in magnitude and phase throughout the chamber, the longest dimension of the chamber should be smaller than 0.1 wavelength in the pressure medium [10]. Although the value of the sound velocity of the mineral oil used was not available, it should not be much different than that of the oils listed in reference [11]. According to the sound velocity data provided by the reference, the high-frequency limit for the present measurement was estimated to be approximately 1100 Hz.

Because of its very large resistance, the electrical impedance of a typical Rainbow is dictated by its capacitance for the frequency range above 1 Hz. The drastic reduction of the voltage sensitivity at low frequencies for samples of small electroded area as shown in Figure 27 is ascribed to the increasing coupling loss due to the decrease of sample capacitance with decreasing electroded area. The voltage coupling loss due to the relatively low impedance of the lock-in amplifier can be readily corrected via simple electrical network treatments provided that the related parameters such as the capacitance and resistance of the Rainbow and the lock-in amplifier are known. Figure 28 shows the corrected sensitivity in decibels of two Rainbow samples as a function of frequency from 1 Hz to 1000 Hz together with the original uncorrected curves. Similar correction was made to the frequency response in Figure 27 and the results are given in Figure 29. Since the impedance of the Rainbows dropped drastically with increasing frequency, the correction was significant only in the low-frequency range. It should be mentioned that the change of the Rainbow capacitance with frequency was not included in the above corrections. The capacitance values used for the corrections were those measured at 20 Hz. In addition, the frequency response of the Rainbow samples was determined on the basis of the assumption that

16

the calibrating hydrophone has a flat frequency response in the frequency range investigated. In reality, the frequency response of the hydrophone is flat in the sense of 3 dB down at the corner frequency of 1 Hz. For this reason, further corrections are needed for more accurate results in the low-frequency range.

As is evidenced in Figures 28 and 29, the voltage sensitivity of Rainbow ceramics decreases rapidly with increasing frequency in the low frequency range, followed by a relatively flat response zone prior to the occurrence of mechanical resonances. Similar characteristics were observed for the field-induced axial displacement of Rainbow ceramics versus the frequency of driving electric field in the previous work [8]. The sensitivity values in the flat response zone are comparable to those of the piezoelectric elements of some commercial hydrophones (in reference to the Benthos products). This result indicates that Rainbow ceramics are more advantageous for stress-sensing applications involving low frequencies.

5. Summary

The stress-induced electrical charge and voltage of certain Rainbow ceramics and their frequency response have been investigated. Rainbow ceramics exhibit a strong piezoelectric effect when operated in the dome mode. The corresponding effective piezoelectric coefficient under steady-state loading conditions can be over two orders of magnitude greater than that of normal ceramics, depending on the dimensions, thickness ratio, and material properties of Rainbow ceramics, as well as the mechanical boundary conditions on Rainbow's edge. The voltage sensitivity of the Rainbow samples to applied pressure decreases continuously with increasing frequency prior to the occurrence of mechanical resonances. Results show that

Rainbow ceramics are very promising for stress-sensing applications involving low stress levels and frequencies.

6. References

1. G. H. Haertling, *Am. Ceram. Soc. Bull.*, **73**, 93 (1994).

2. S. Sherrit, H. D. Wiederick, B. K. Mukherjee and G. H. Haertling, in Proceedings of the Ninth IEEE International Symposium on Applications of Ferroelectrics, pp. 390-393, (1994).

3. E. Furman, G. Li and G. H. Haertling, *Ferroelectrics*, **160**, 357 (1994).

4. H. S. Tzou and M. Gadre, *Journal. of Sound and Vibration*, **132**, 433 (1989).

5. Y. Sugawara, K. Onitsuka, S. Yoshikawa, Q. Xu, R. E. Newnham and K. Uchino, *J. Am. Ceram. Soc.*, **75**, 996 (1992).

6. C. -J. Cheng and D. C. Timm, *Journal of Intelligent Material Systems and Structures*, **6**, 436 (1995).

7. Jonathan D'Cruz, *Journal of Intelligent Material Systems and Structures*, **6**, 419 (1995).

8. "Superconductivity Devices: Commercial Use of Space", an annual report to NASA submitted by Department of Ceramic Engineering, Clemson University, March 17, 1995.

9. D. Berlincourt, D. R. Curren and H. Jaffe, "Physical Acoustics", Part A, 1, 169 (1964).

10. "American National Standard: Procedures for Calibration of Underwater Electroacoustic Transducers", ANSI S1.20-1988, ASA 75-1988 (Revision of S1.20-1972).

11. G. W. C. Kaye and T. H. Laby, "Tables of Physical and Chemical Constants", Fifteenth Edition, Longman Group Limited, London and New York (1986).

Table 1　Sample dimensions and reduction conditions.

Sample	Diameter (mm)	Thickness (μm)	Curvature (μm)	Thickness Ratio	Reduction Temp (°C)	Reduction Time (min)
RB1053HP-1	31.75	508	750	0.18	975	30
RB1053HP-2	31.75	508	890	0.25	975	60
RB1053HP-3	31.75	508	740	0.55	975	150
RB1053HP-4	31.75	457			975	60
RB1053HP-a	31.75	508	560	0.13	975	20
RB1053HP-b	31.75	508	710	0.23	975	40
RB1053HP-c	31.75	508	800	0.32	975	60
RB1053HP-d	31.75	508	850	0.45	975	90
RB1053HP-f	31.75	508	790	0.59	975	120
RB1053HP-g	31.75	508	840	0.74	975	180
RB5556S-1	22.35	432	419	0.13	975	20
RB5556S-2	22.35	432	635	0.33	975	40
RB5556S-3	22.35	432	660		975	60
RB5556S-4	22.35	432	622	0.38	975	75
RB5556S-5	22.35	432	699	0.45	975	90
RB5556S-6	22.35	432	673		975	210
RB5556S-7	22.35	432	495	0.23	975	30
RB5556S-8	22.35	432	651	0.73	975	180
RB5556S-9	22.35	432	645	0.63	975	180
RB5556S-10	22.35	432	557		975	60
RB5556S-12	22.35	432	736		975	90
RB5556S-13	22.35	432	635		975	90
RB5556S-14	22.35	432	660		975	90
RB5556S-a	22.35	432			975	50
RB5556S-b	22.35	559			975	90
RB5556S-c	22.35	686			975	140
RB5556S-d	22.35	813			975	180
RB5556S-11	22.35	432	589		975	60
RB5556S-f	22.35	559			975	90
RB5556S-g	22.35	686			975	120
RB5556S-h	22.35	813			975	150

Table 1.   Continued.

Sample	Diameter (mm)	Thickness (μm)	Curvature (μm)	Thickness Ratio	Reduction Temp (°C)	Reduction Time (min)
RB1053S-1	31.75	508	546		950	45
RB1053S-2	31.75	508	711		950	60
RB1053S-3	31.75	508	757		950	75
RB5556S-21	31.75	508			975	60
RB5559S-1	31.75	508			975	90
RB5559S-2	31.75	508			975	90
RB5559S-3	31.75	508			975	35

HP = Hot-pressed; S = Sintered.

Table 2   Properties of Rainbow Samples.

Sample	Capacitance (nF) (V/P)	Loss Factor (%) (V/P)	d_{33} $(\times 10^{12}\,C/N)$	f_b (Hz)	f_r/f_a (kHz)
RB1053HP-1	18.7/24.3	2.8/3.5		1433	72.75/81.75
RB1053HP-2	18.9/25.0	3.0/3.4		1620	72.95/80.80
RB1053HP-3	30.2/28.2	5.0/4.8		1310	66.45/69.45
RB1053HP-4	27.1/27.7	2.8/2.9	328	1200	71.18/78.88
RB1053HP-a	21.7/20.4	2.3/2.8			
RB1053HP-b	15.9/19.7	1.7/1.9			66.75/70.75
RB1053HP-c	16.5/15.9	2.0/3.0			65.35/70.75
RB1053HP-d					
RB1053HP-e	35.4/38.2	3.3/3.9			64.75/66.62
RB1053HP-f	19.2/19.3	2.6/2.4			64.65/64.65
RB5556S-1	12.7/16.7	3.6/4.7	551	2000	93.3/104.4
RB5556S-2	17.0/22.1	3.0/3.1	442	2190	94.1/103.1
RB5556S-3	13.7/17.5	4.0/4.9	385	2240	99.2/104.7
RB5556S-4	14.5/18.8	4.6/5.5	505	2290	95.0/103.3
RB5556S-5	14.5/18.2	5.3/6.5	410	2050	96.3/101.1
RB5556S-6	20.7/27.3	6.6/6.9	274	2130	93.9/96.0
RB5556S-7	15.0/17.9	10.6/23.6	523	2020	99.1/104.0
RB5556S-8	20.2/24.8	5.9/6.3	370		94.1/96.6
RB5556S-9	19.4/24.7	7.1/7.6	455	2360	96.9/98.3
RB5556S-10	17.4/18.2	4.2/4.9		2160	100.2/104.0
RB5556S-12	17.2/23.9	4.4/5.8		2240	94.8/103.3
RB5556S-13	17.2/24.1	4.1/5.7		2330	94.8/103.9
RB5556S-14	17.6/24.6	4.2/5.6		2250	96.3/105.1
RB5556S-a	11.3/14.5	3.3/3.6		2340	101.0/107.7
RB5556S-b	10.0/ --	3.4/ --		2690	96.00/108.3
RB5556S-c	9.57/ --	4.8/ --		2550	95.4/105.0
RB5556S-d	9.42/ --	5.7/ --		2375	95.6/104.00
RB5556S-11	17.9/20.6	4.0/6.3		2160	94.8/105.0
RB5556S-f	15.9/ --	2.0/ --		2229	98.7/106.0
RB5556S-g				2570	101.0/105.6
RB5556S-h	5.74/7.06	3.5/19.1		2580	98.9/104.9

Table 2. Continued.

Sample	Capacitance (nF) (V/P)	Loss Factor (%) (V/P)	d_{33} (x10^{12} C/N)	f_b (Hz)	f_r/f_a (kHz)
RB1053S-1	20.1/19.7	2.5/2.6			60.064.9
RB1053S-2	23.9/24.6	2.2/2.1			59.4/64.2
RB1053S-3	-- /23.5	-- /2.2			60.7/65.5
RB5556S-21	--/19.6	--/3.7			
RB5559S-1	--/19.5	--/6.6			
RB5559S-2	--/18.0	--/6.6			
RB5559S-3	--/23.6	--/3.6			

V/P = Virgin/Poled; f_b= Resonant frequency of bending mode; f_r/f_a = Resonant/antiresonant frequency of radial mode.

Table 3. Induced charges and voltages from different regions on the surface of Rainbow samples with an applied pressure of 1 psi.

Sample	Edge Regime		Center Regime		Whole Surface	
	Charge (μC)	Voltage (volts)	Charge (μC)	Voltage (volts)	Charge (μC)	Voltage (volts)
RB5559-1 (edge free)	-0.005	-0.890	0.192	12.92	0.173	11.84
RB5559-1 (edge clamped)	-0.003	-0.463	0.048	3.56	0.040	2.34
RB5559-2 (edge free)	-0.011	-1.06	0.203	14.4	0.177	7.95
RB5559-2 (edge clamped)	-0.011	-1.26	0.084	7.02	0.067	3.46

Table 4. Voltage sensitivity of selected Rainbow samples under steady-state loading conditions. The sensitivity data were determined according to the induced voltages at the applied pressure of 2 psi.

Sample	RB5556S-1	RB5556S-11	RB5556S-5	R5556S-6	RB1053HP-2	RB1053HP-4
Induced Signal (volts) at 2 psi	5.5	13.2	20.2	14.4	20.3	24.3
Sensitivity (dB V/μPa)	-188	-181	-177	-180	-177	-175
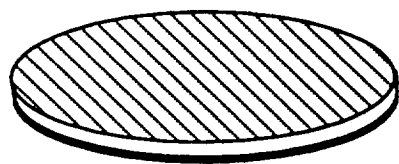
Full Electrode
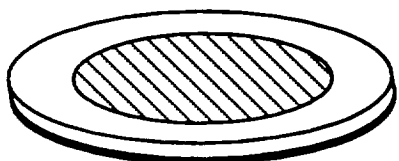
50% Electrode
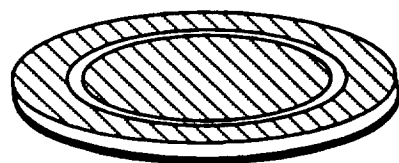
Separate Electrodes

Figure 1.   Different electrode configurations for Rainbow samples (the curvature of
Rainbows is not shown).
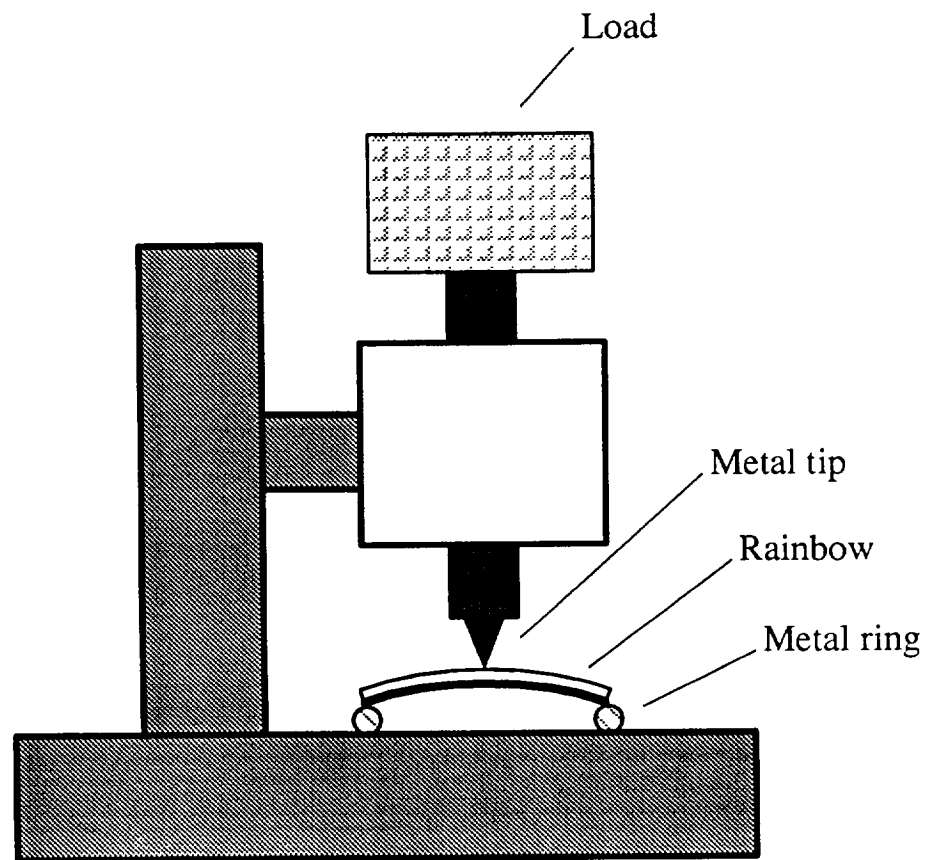
Figure 2. Schematic of setup for measurements involving point load.

Pressure inlet

Spring

Sample

Silver foil

To Electrometer
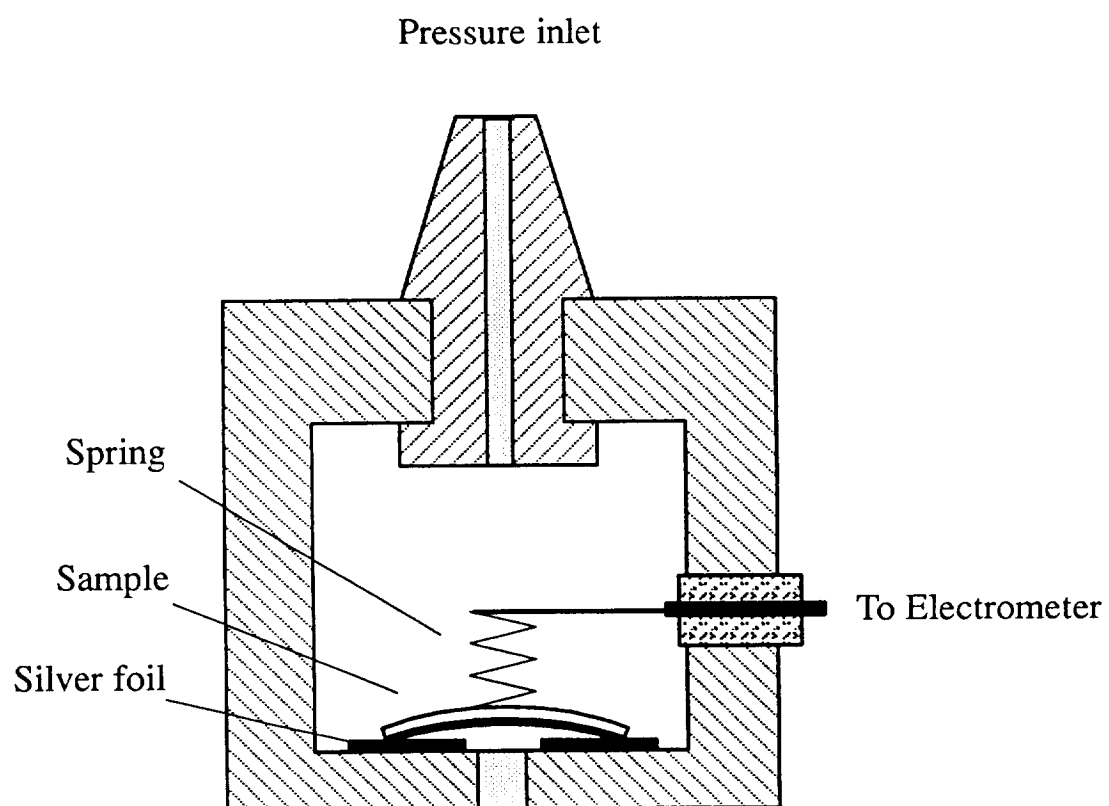
Figure 3.   Schematic of chamber for measurements involving uniform pressure.
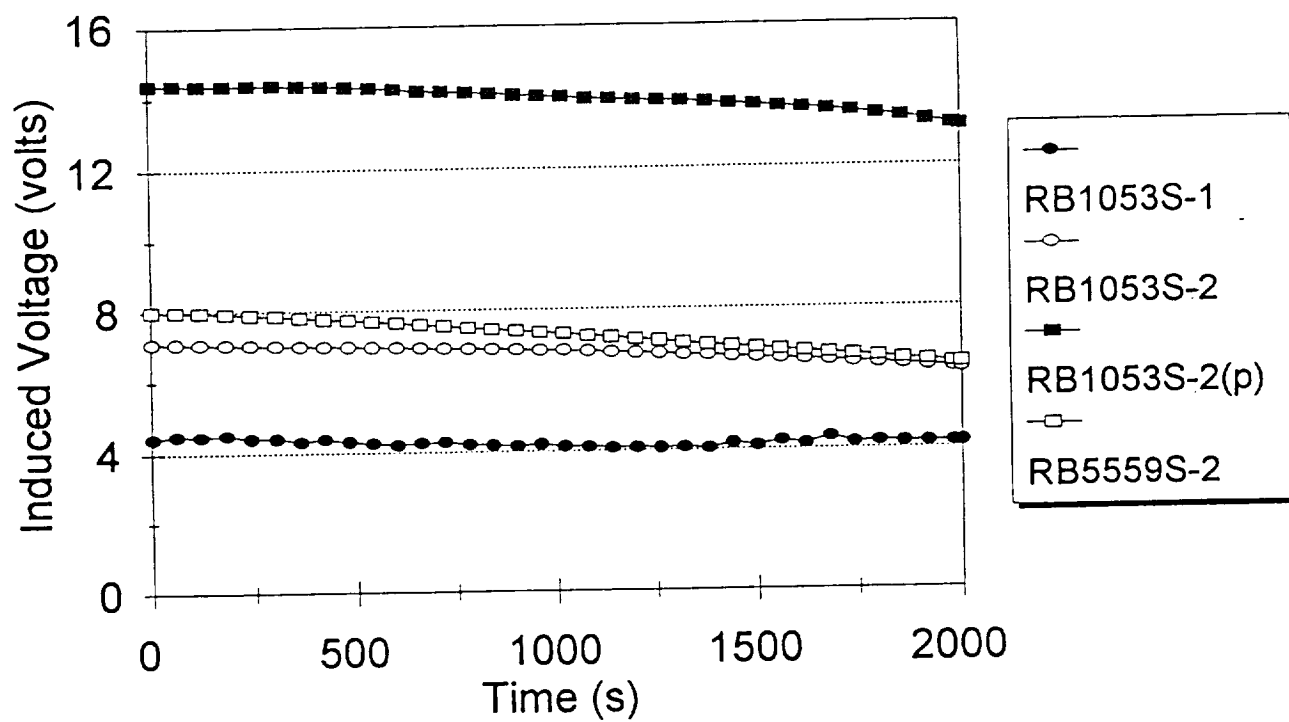
Figure 4. Time dependence of induced voltages for selected Rainbow ceramics. The curve for RB1053HP-2(p) represents RB1053HP-2 sample under applied pressure of 2 psi. The other three curves were obtained with a point load of 200g.
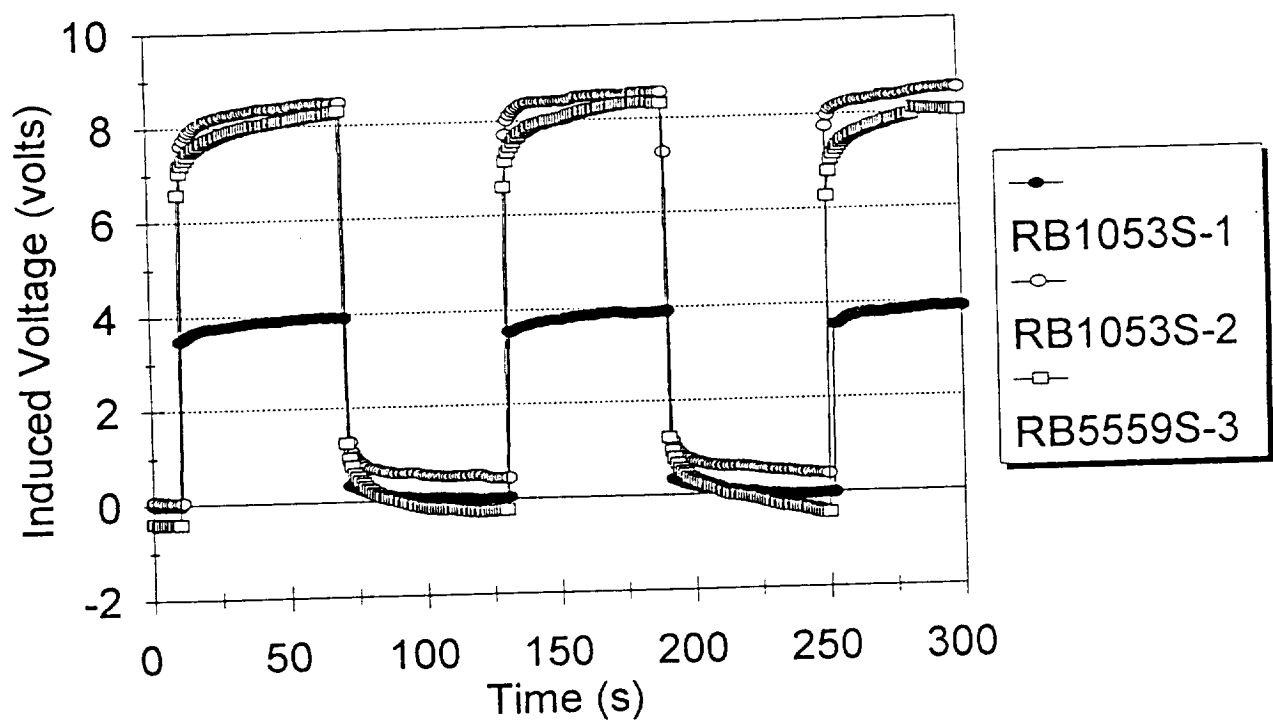
Figure 5. Variation of induced voltage with time for selected Rainbow samples under instant loading. The applied load was 200g.
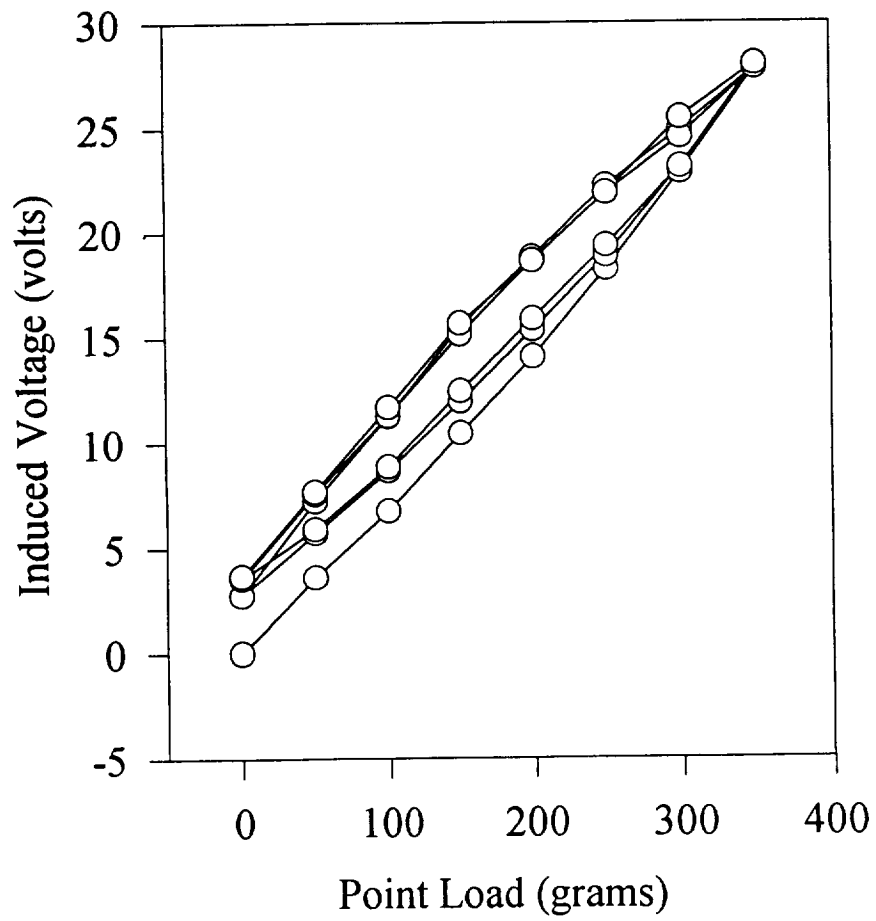
Figure 6. Changes of induced voltage under cyclic point loading for RB1053HP-4.
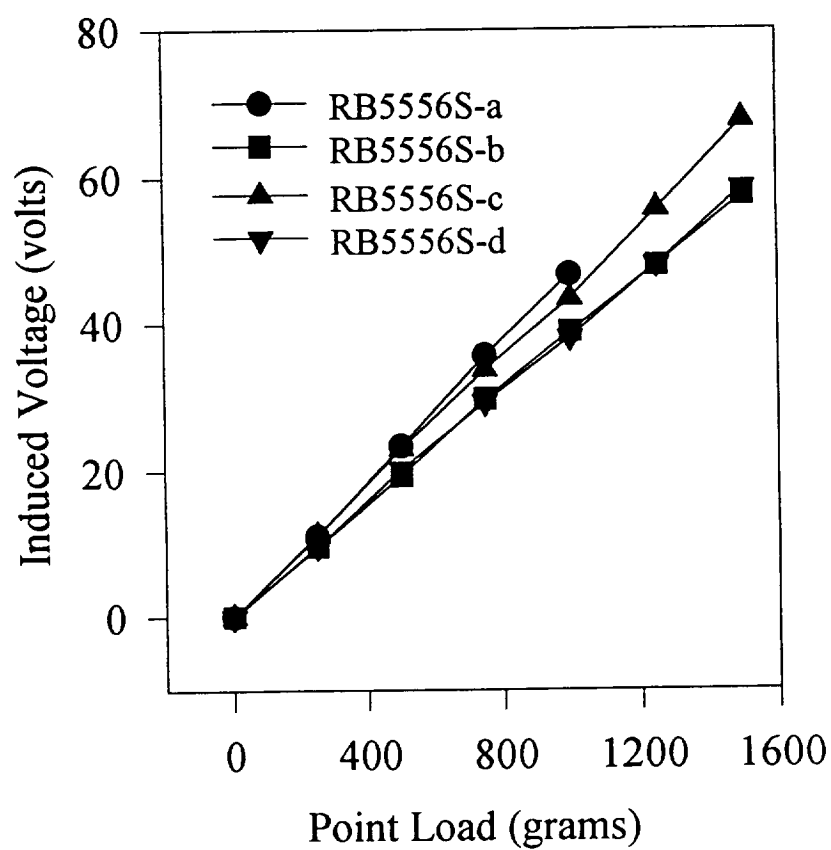
Figure 7. Change of induced voltage with the maximum value of loading cycles for RB5556 samples.
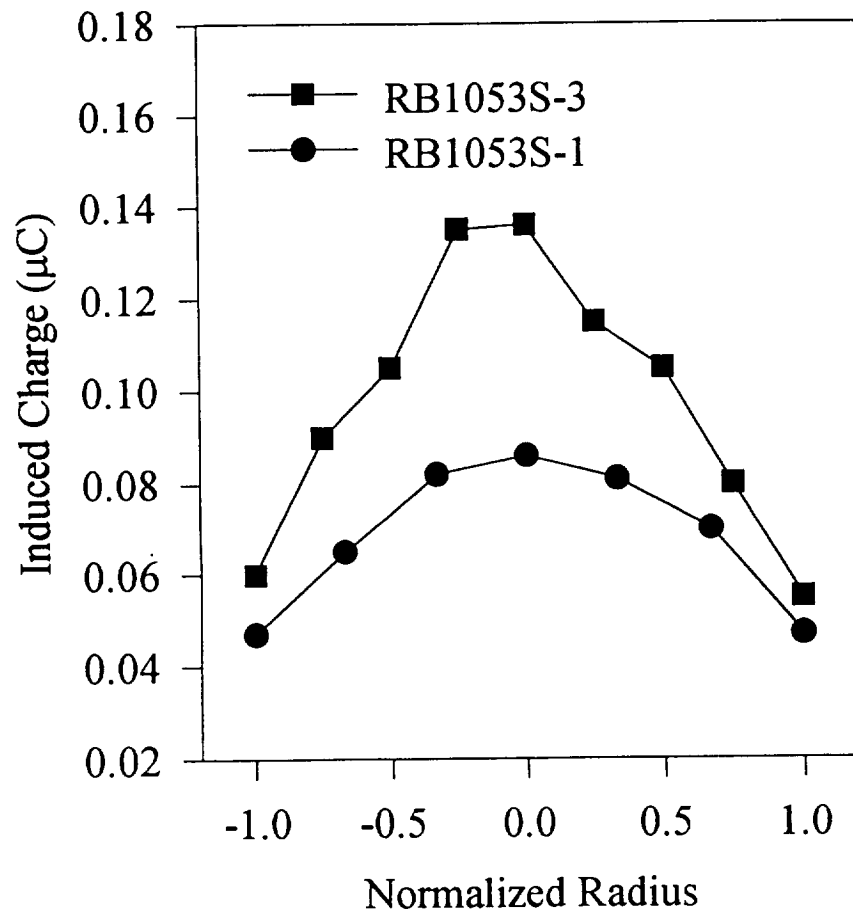
Figure 8. Variation of induced charges with location to which a point load of 200g was applied.
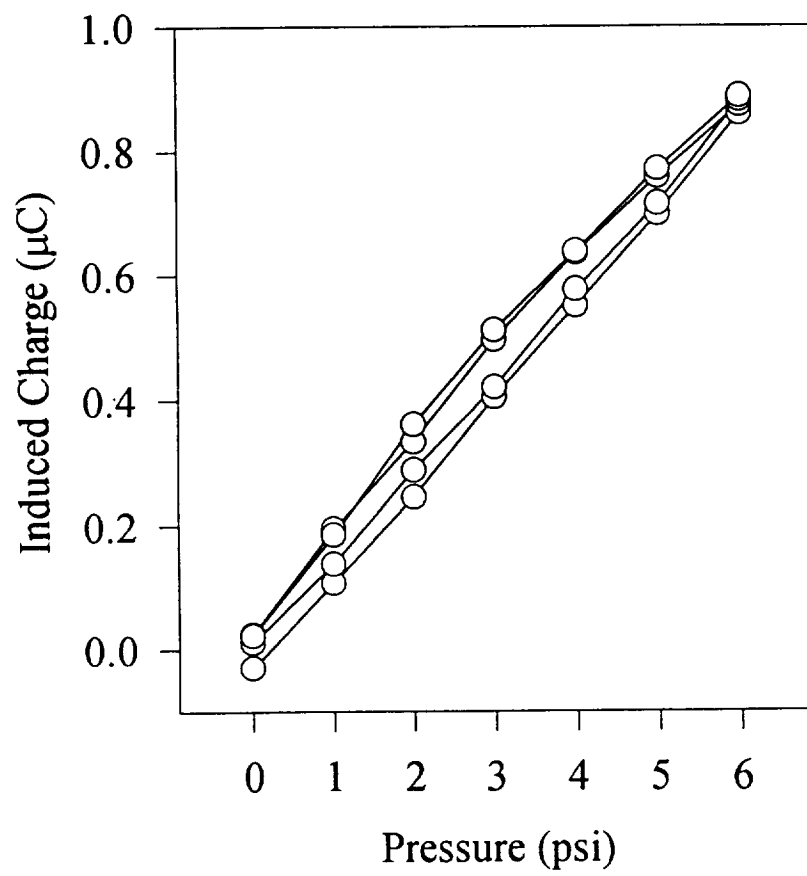
Figure 9. Variation of induced charge with applied pressure for RB5556S-2 sample.
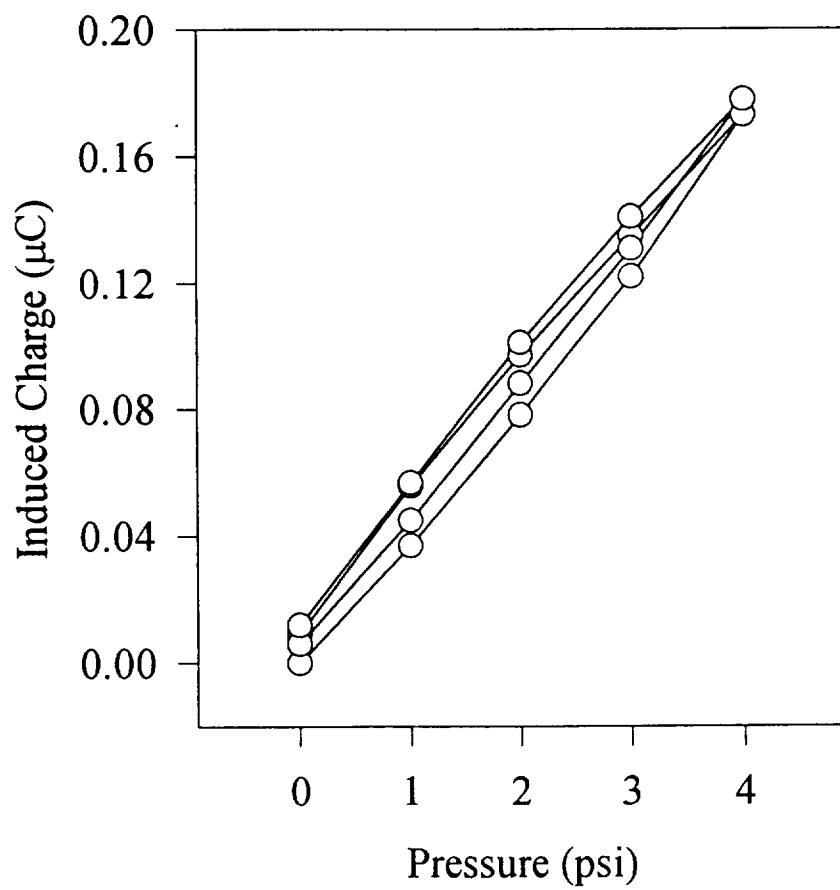
Figure 10. Changes of induced charge under cyclic pressure for RB5556S-h sample.
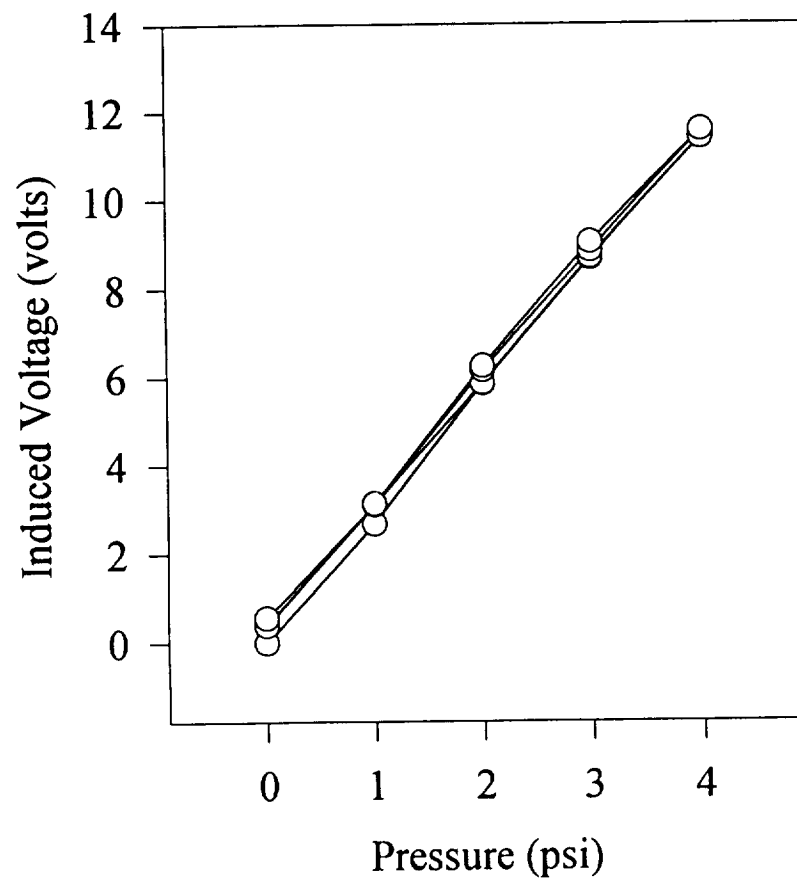
Figure 11. Changes of induced voltage under cyclic pressure for RB5556S-h sample.
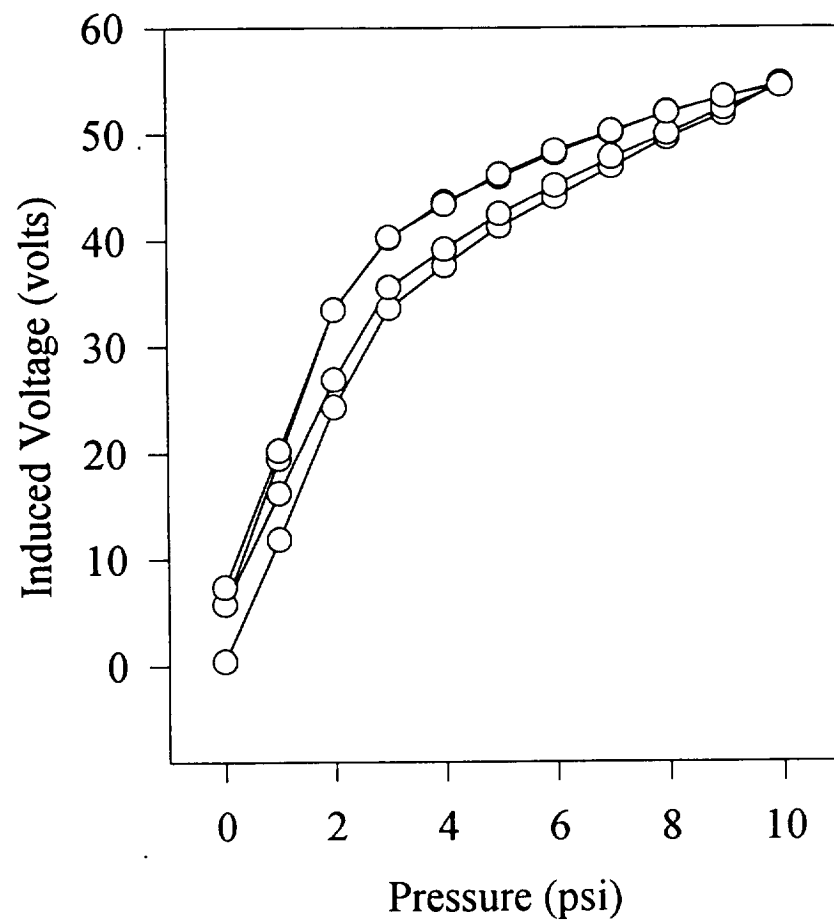
Figure 12. Variation of induced voltage with applied pressure for RB1053HP-4 sample. The sudden change of the curve slope around 3 psi indicates the contact of the sample to the supporting plate under pressure.
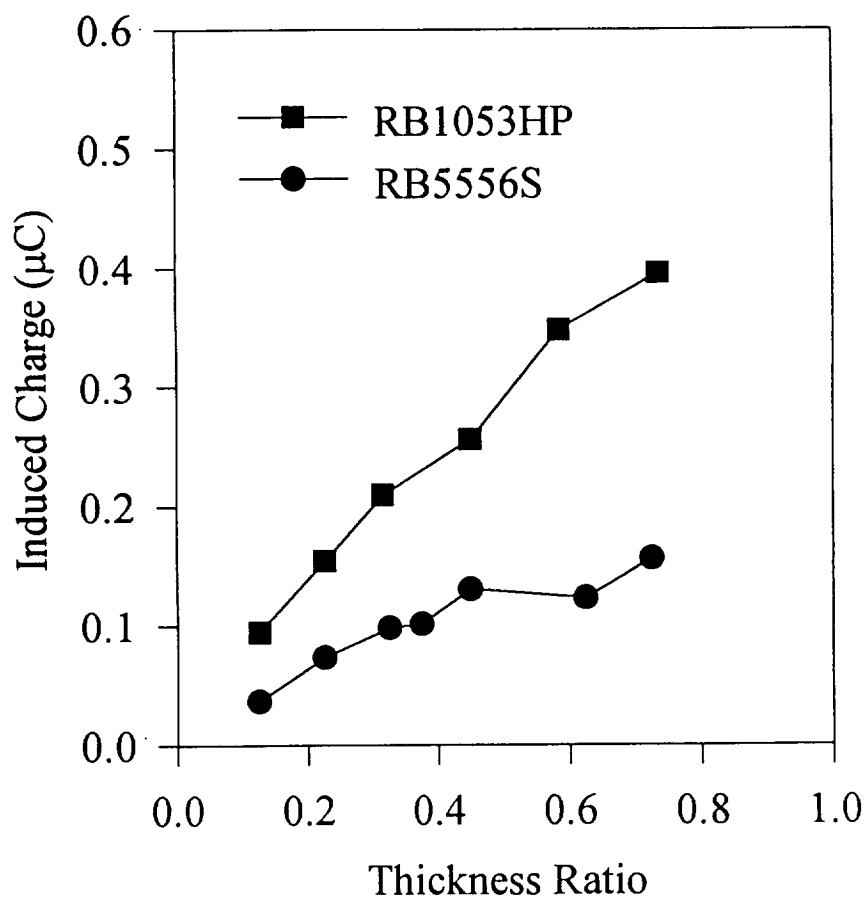
Figure 13. Induced electrical charge as a function of the thickness ratio for RB5556S and RB1053HP samples with an applied pressure of 1 psi.
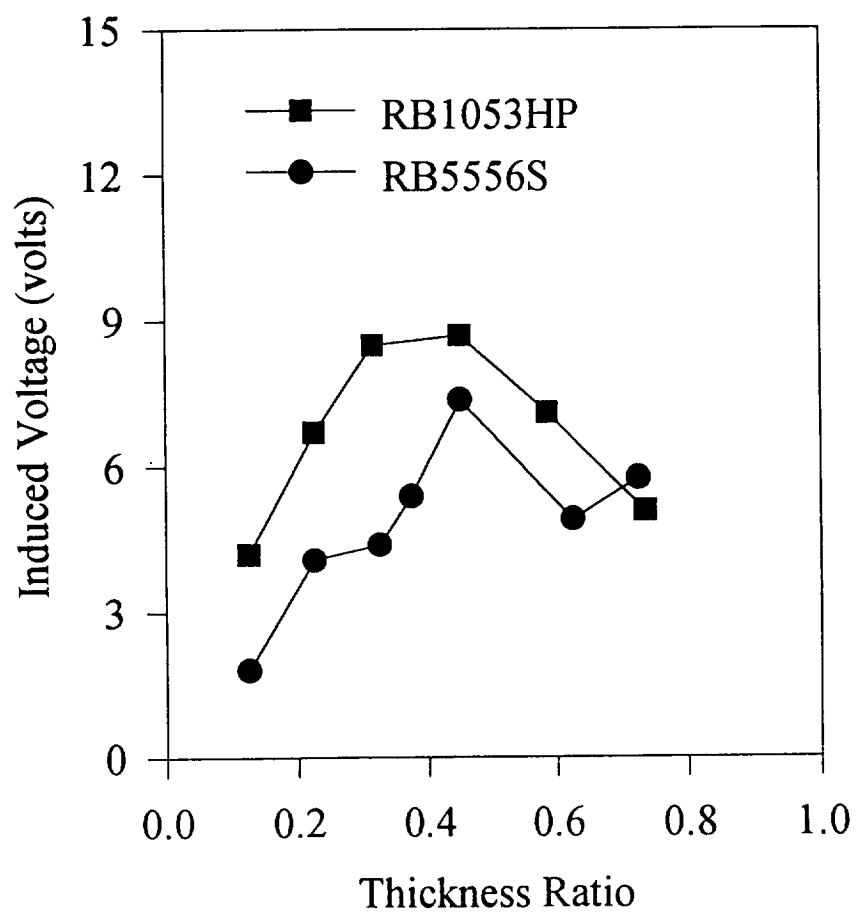
Figure 14. Induced voltage as a function of the thickness ratio for RB5556S and RB1053HP samples.
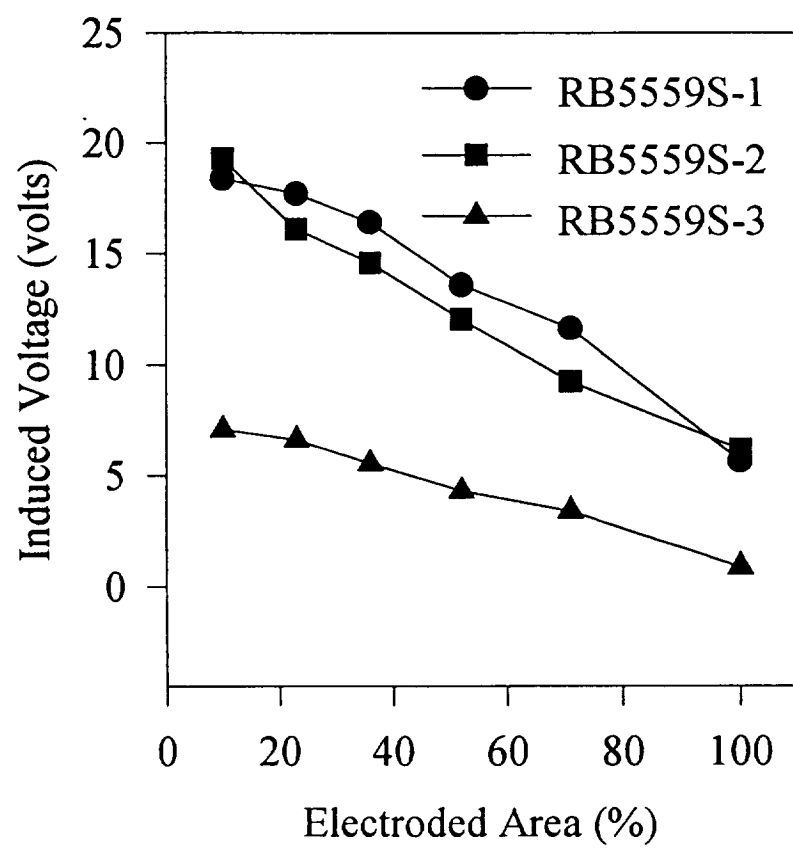
Figure 15. Variation of induced voltage with electroded area for RB5559S samples.
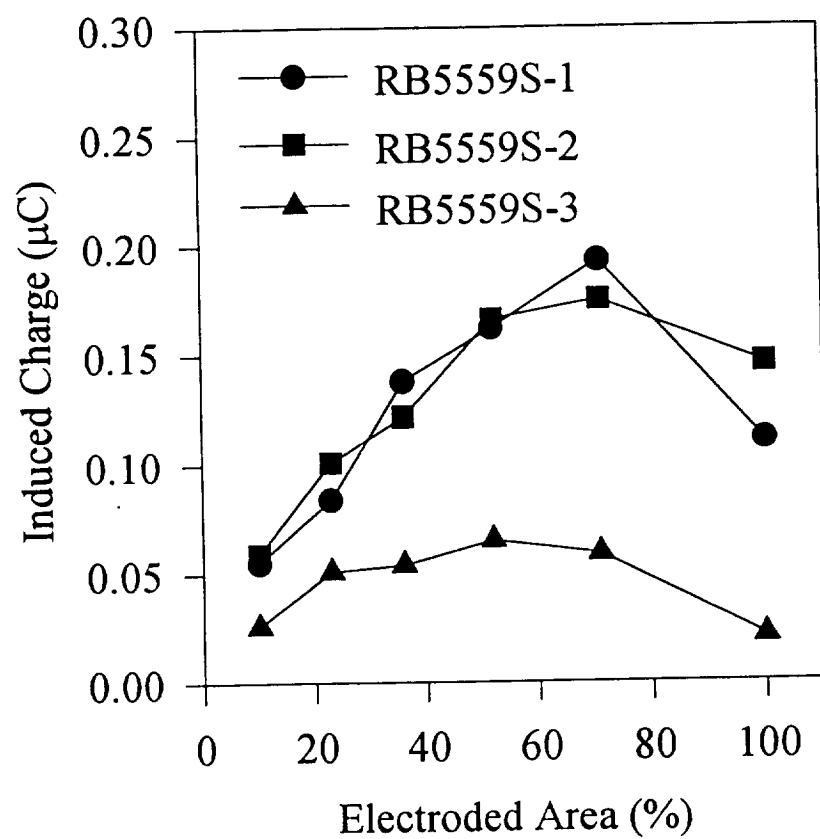
Figure 16. Variation of induced charge with electroded area for RB5559S samples.
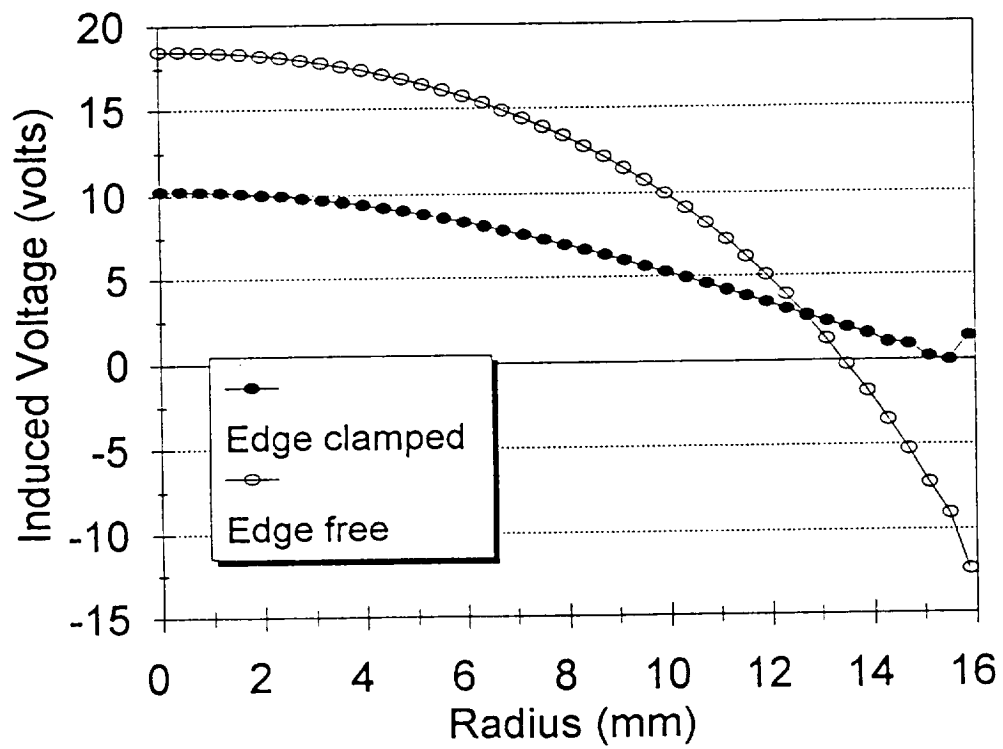
Figure 17. Results of finite element analysis on the induced voltage as a function of location along the radius of a Rainbow. The applied pressure is 1 psi.
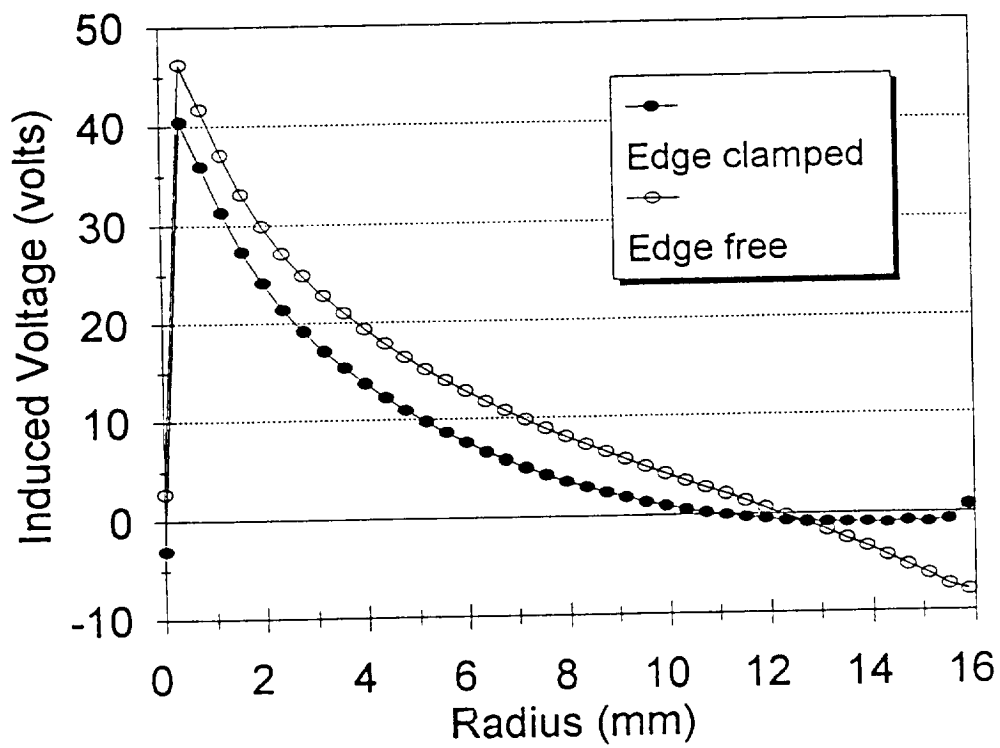
Figure 18. FEM results of induced voltage versus location across a Rainbow with an applied point load of 200g.
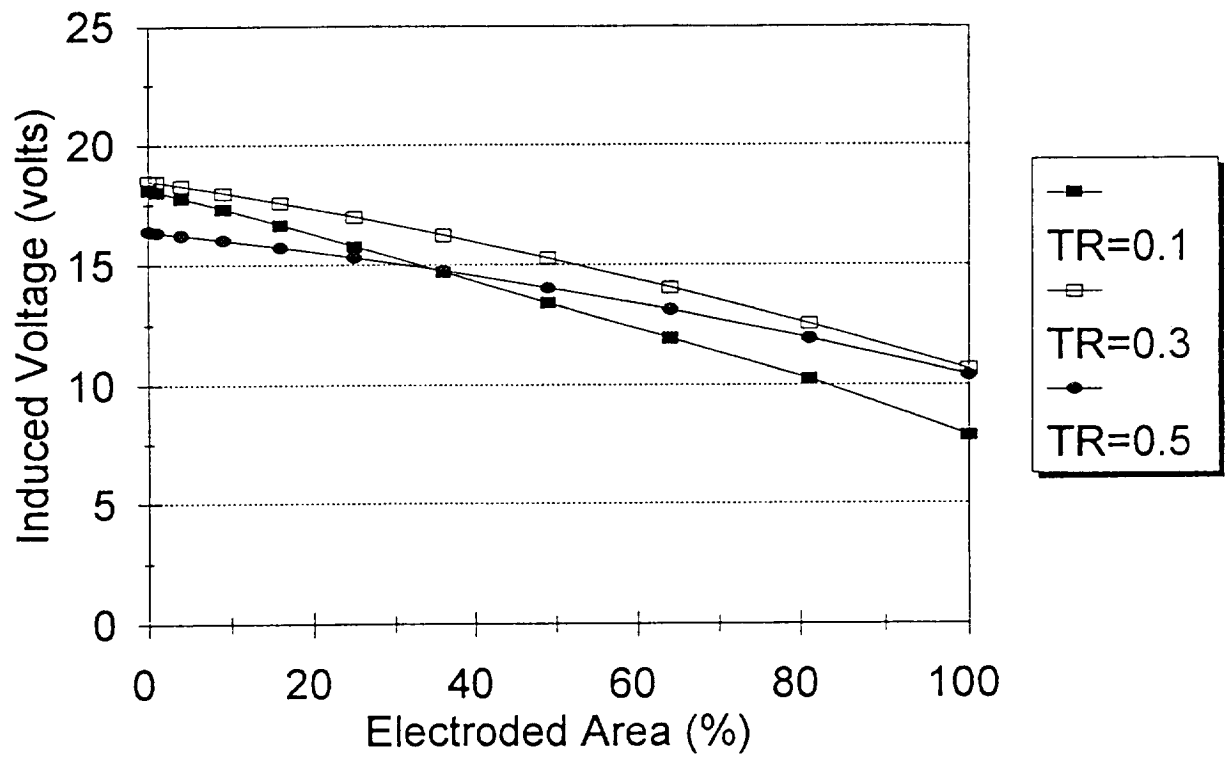
Figure 19. FEM results of induced voltage as a function of electroded area for three Rainbows of different thickness ratios (TR). The edge of the Rainbow is assumed to be free and the applied pressure is 1 psi.
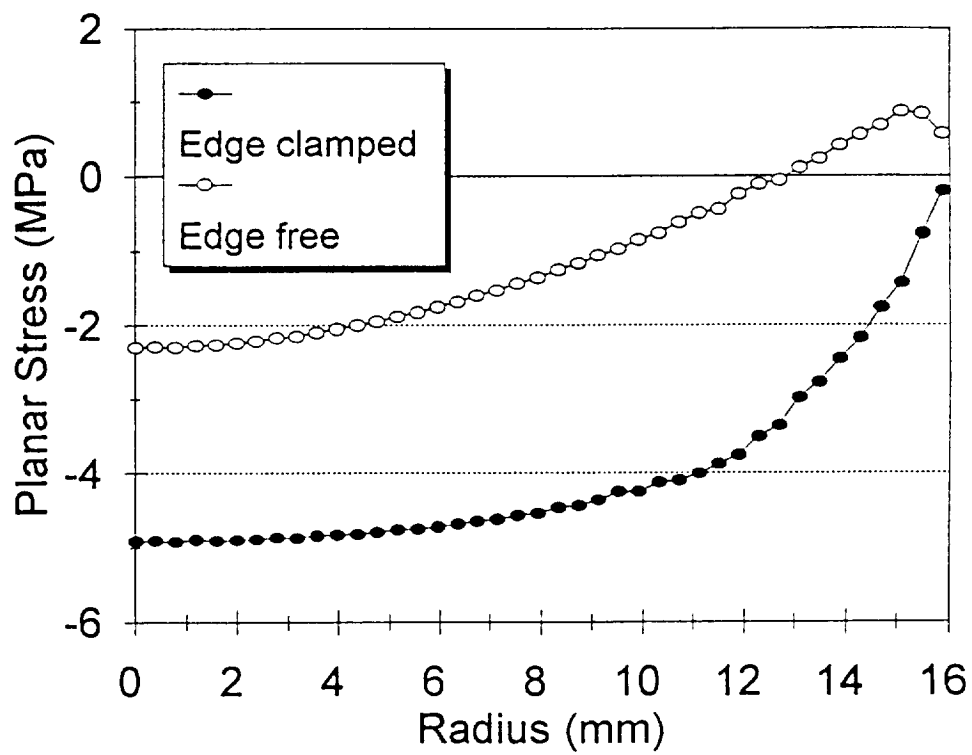
Figure 20. Variation of planar stress across the surface of a Rainbow with an applied pressure of 1 psi.

Plastic sample holder

Benthos hydrophone
with preamplifier

Inner chamber filled
with miniral oil

Tiny outlet

Rainbow sample

Rainbow pressure
generator
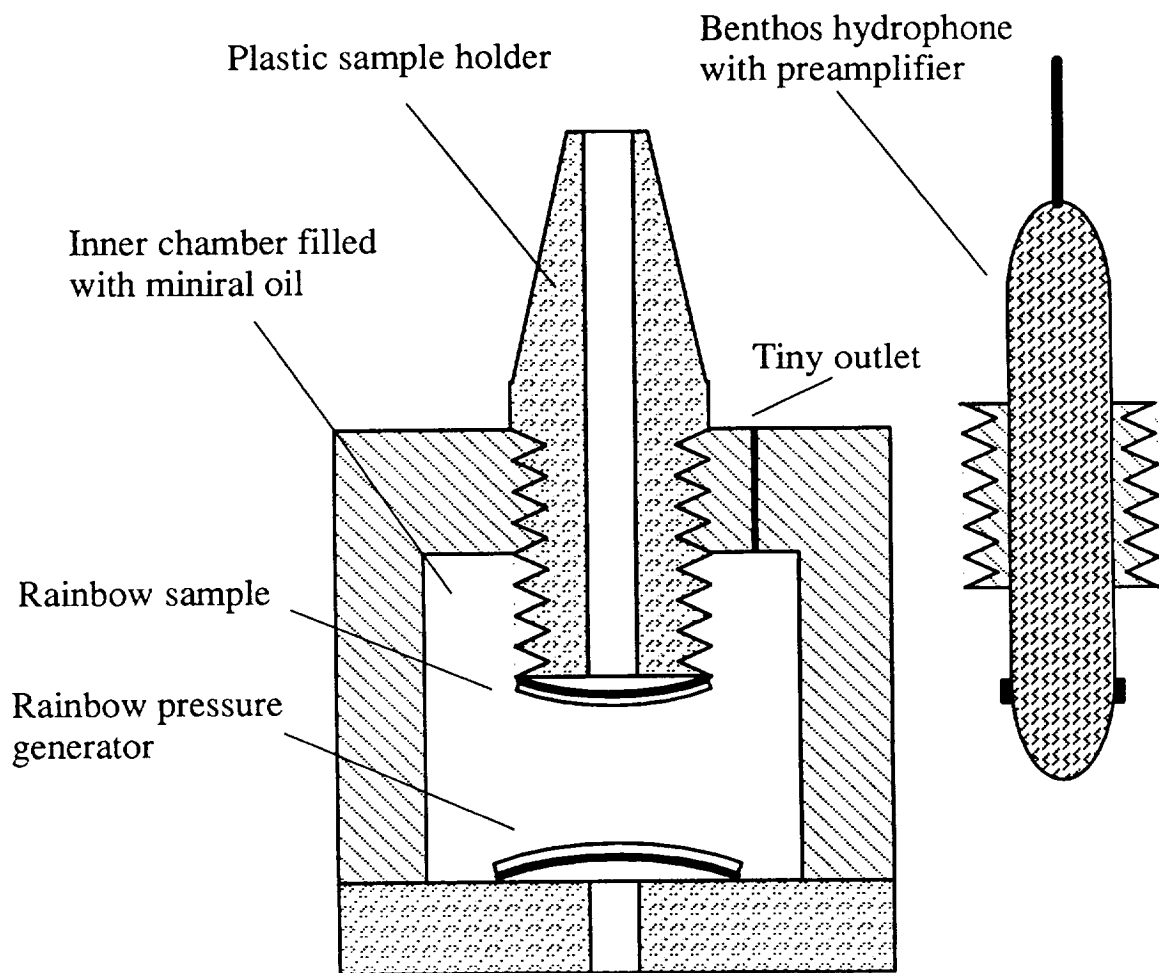
Figure 21.   Pressure chamber for measurement of frequency response of Rainbow sample
and hydrophone (not to the scale).
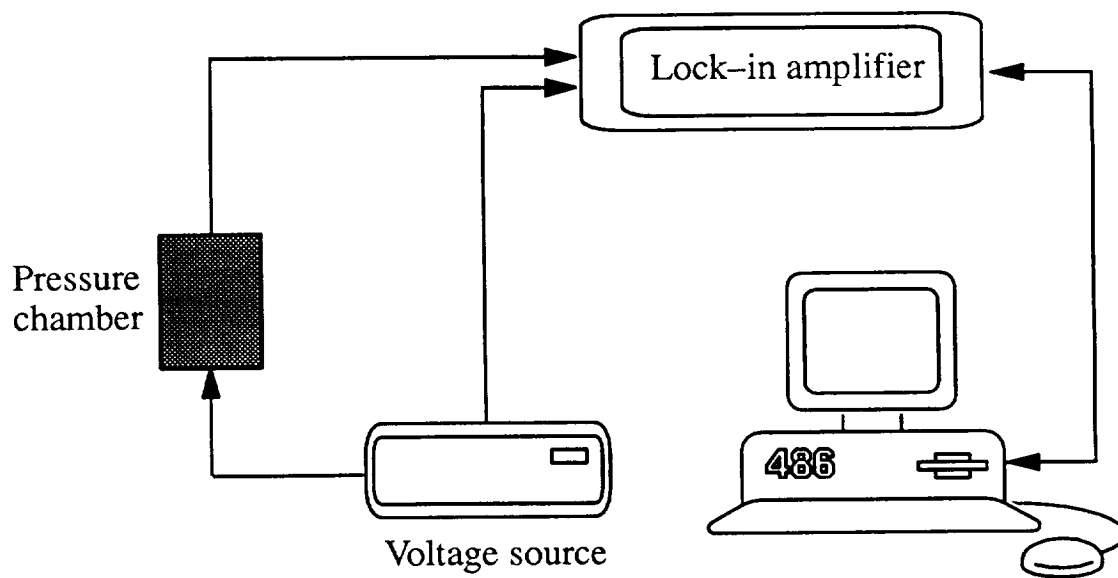
Figure 22. Diagram of experimental arrangement for frequency response measurement.
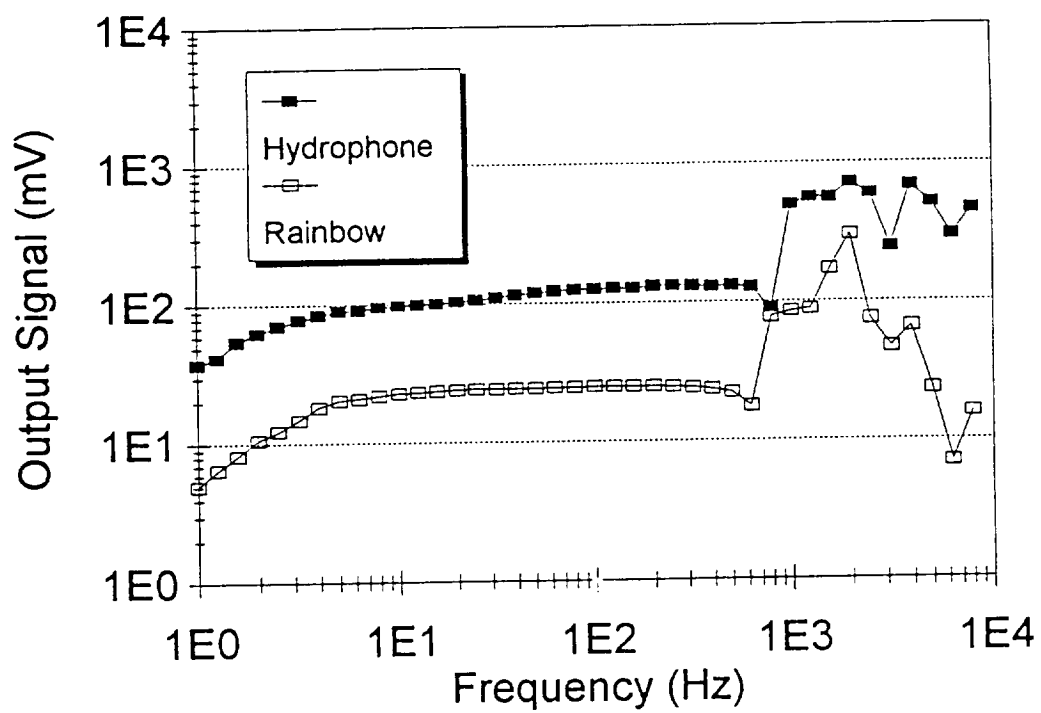
Figure 23. Dependence of output voltage signals on frequency for RB5556S-21 and the Benthos hydrophone.
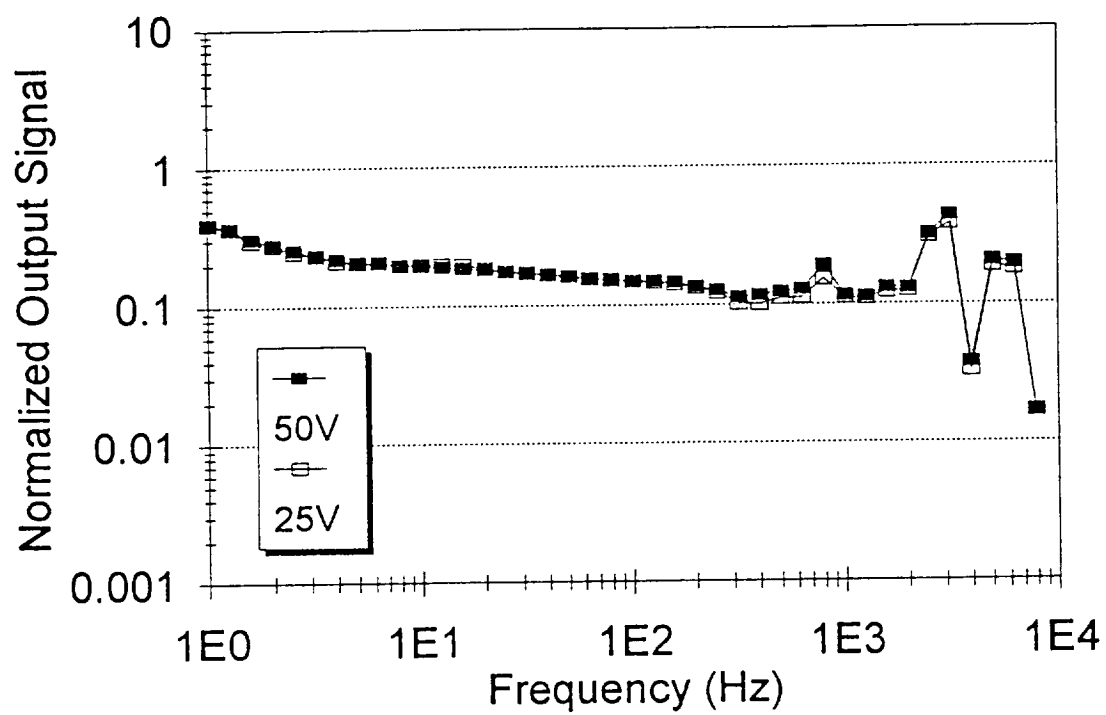
Figure 24. Frequency response of RB1053HP-2 sample under two different values of driving voltage on the pressure generator.
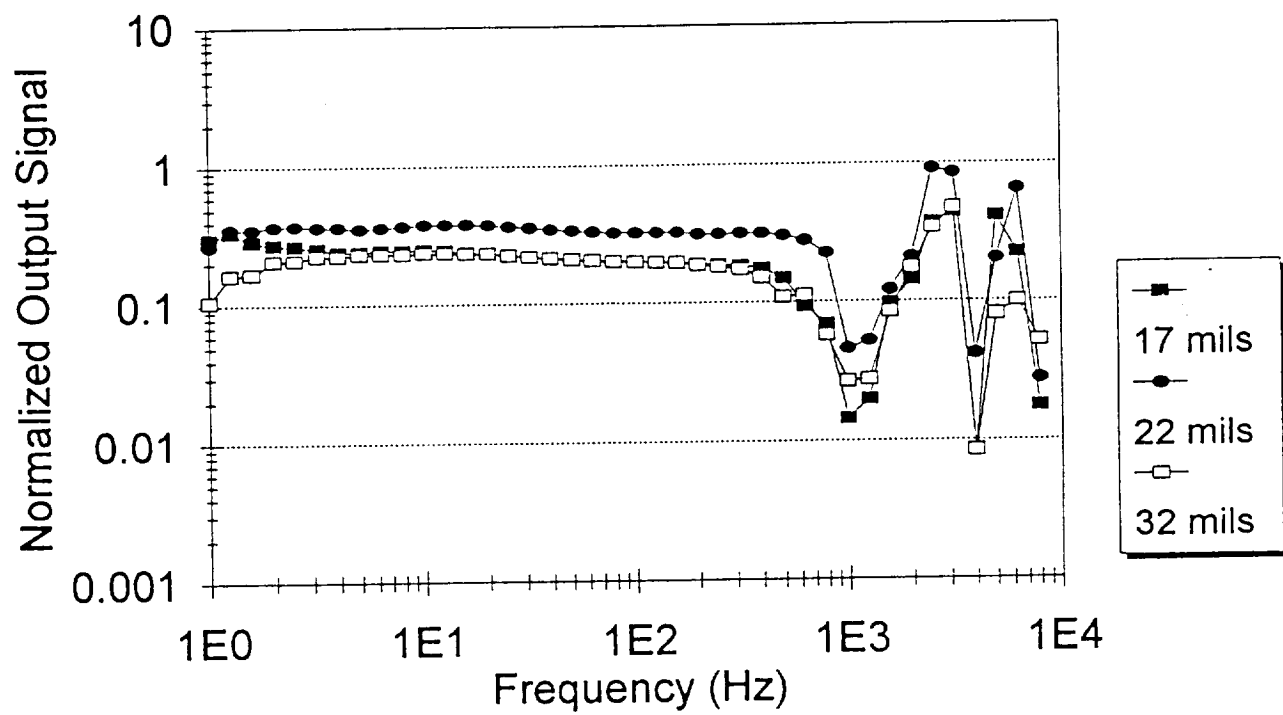
Figure 25.   Frequency response of three RB5556S samples with different total thicknesses of 17, 22, and 32 mils.
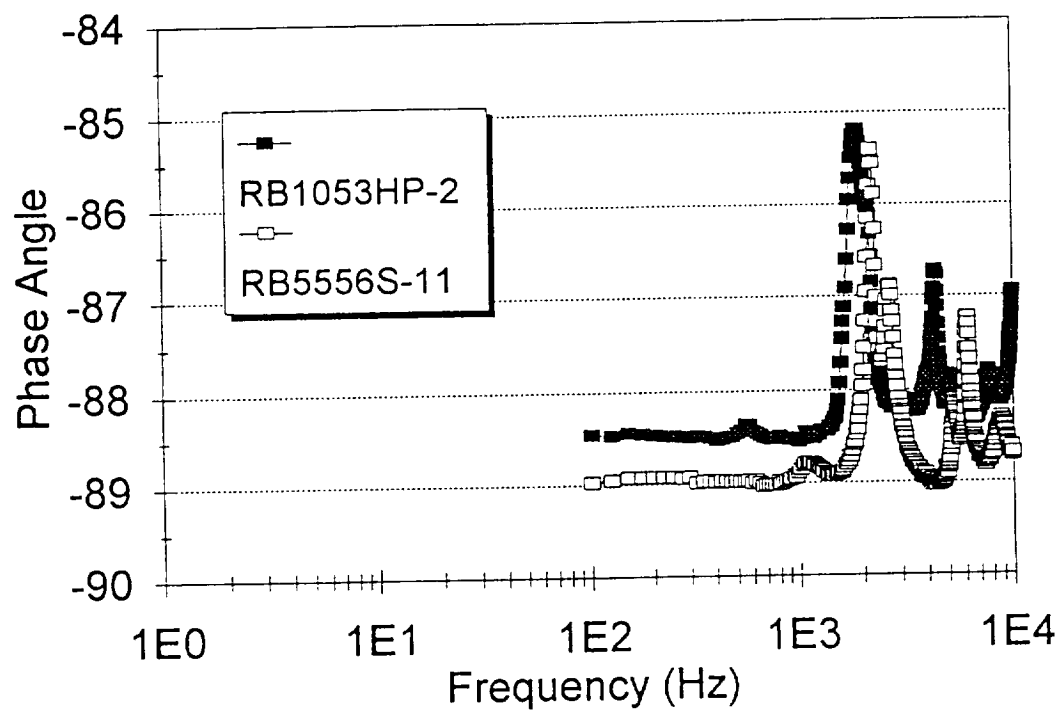
Figure 26. Change of the phase angle of impedance with frequency for selected Rainbow samples. The peaks signify the electromechanical resonances of the samples.
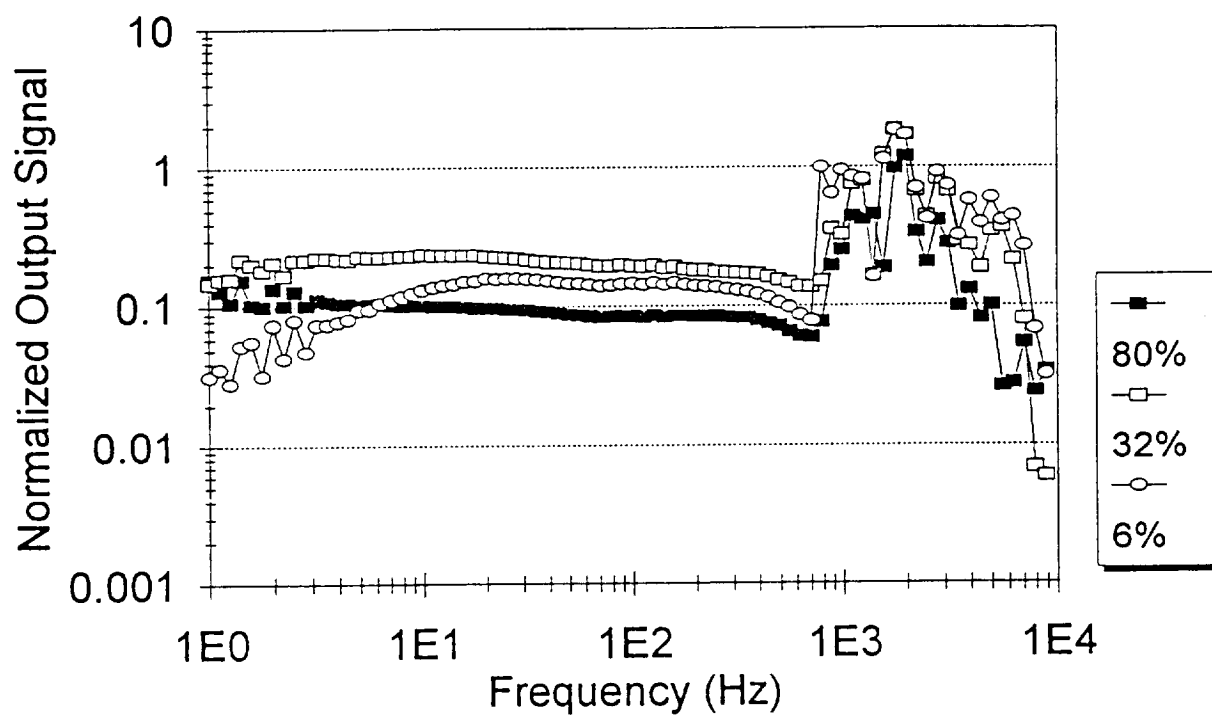
Figure 27. Frequency dependence of induced signals for RB1053S-21 sample having three different sizes of electrode on the unreduced surface.
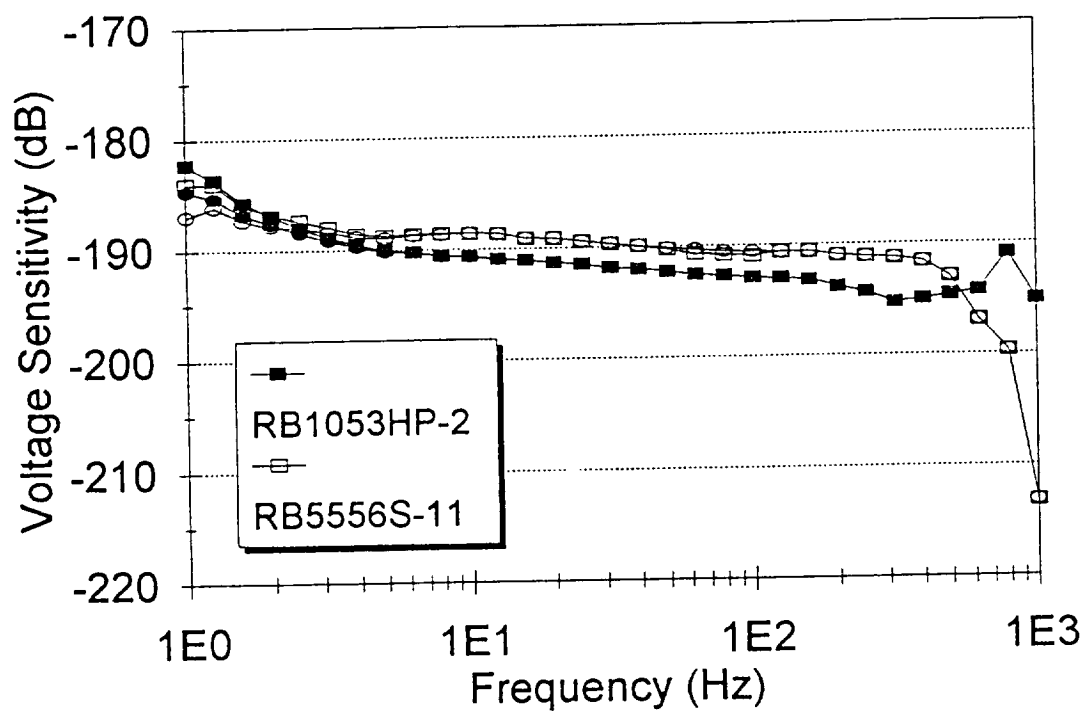
Figure 28. The corrected and uncorrected voltage sensitivity of RB1053HP-2 and RB5556S-11 samples as a function of frequency. The parameters for the correction were 18.6 nF and 10^4 MΩ for RB1053HP-2, 20 nF and 10^4 MΩ for RB5556S-11, and 25 pF and 10 MΩ for the lock-in amplifier.
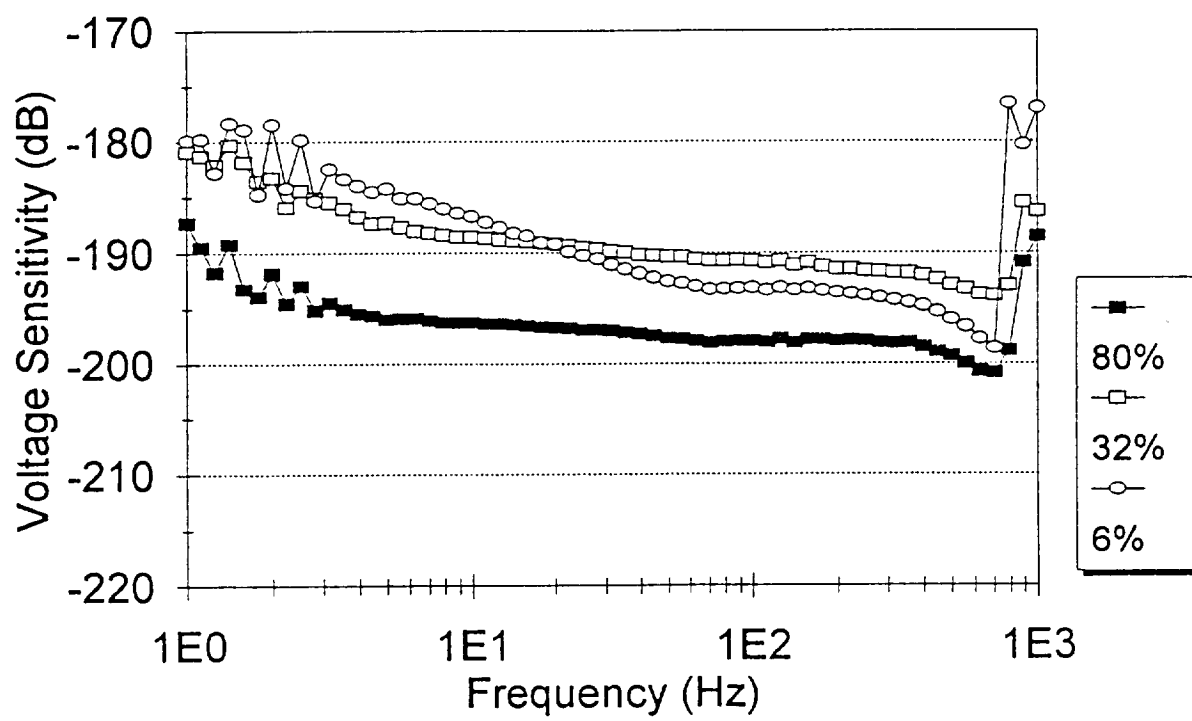
Figure 29. The corrected voltage sensitivity as a function of frequency for the samples shown in Figure 27. The parameters for the correction were 13.5 nF and 10^4 MΩ for RB5556S-21, and 25 pF and 10 MΩ for the lock-in amplifier.

Part II.

Nonlinear Properties of Rainbow Devices

Introduction

In this report nonlinear properties of Rainbow actuators and the internal voltage effects will be described. Since benders, including Rainbow (**R**educed **A**nd **IN**ternally **B**iased **O**xide **W**afer) devices, are often used in applications requiring a high drive, the nonlinearity of the response and the asymmetry of the hysteresis loops due to the presence of internal voltages are of practical importance.

In a number of ferroelectrics, including both soft and hard PZT ceramics, the hysteresis loop can be shifted along the field axis by a number of methods. The shift is characterized by an internal bias field E_i. The internal bias field usually is explained by citing reorientable dipolar defects. Defects are assumed to gradually orient in a direction corresponding to the minimization of the free energy. With benders it is more appropriate to specify internal voltages rather than internal fields since the electric field inside a bender is not uniform.

In addition to the orientable, homogeneously-distributed defects, there is another possible mechanism to account for loop asymmetry in Rainbow devices: the stress gradient. Rainbow devices consist of intimately bonded oxide and reduced layers. Large stress gradients which are present in the structure are likely to cause the polarization gradient in the oxide layer. The polarization gradient causes asymmetry in the hysteresis loop if the component of polarization is not switchable in a portion of the device.[1]

In Robels' *et. al.* model[1] a composite is considered which consists of two dielectric phases in series with different dielectric constants, ε_i, and spontaneous polarizations, P_i. Phase 1 has nonswitchable polarization, P_{1s}, and occupies volume fraction c of the

1

device. Phase 2 is ferroelectric. The following expression gives the electric field of the ferroelectric phase, E_2, in terms of the applied field, E_0:

$$E_2 = (1 - \frac{c(\varepsilon_2 - \varepsilon_1)}{B_l})E_0 + \frac{-cP_2}{\varepsilon_0 B_l} + \frac{cP_{1s}}{\varepsilon_0 B_l} \qquad (1)$$

where $B_l = \varepsilon_1 + c(\varepsilon_2 - \varepsilon_1)$

The presence of the nonswitchable polarization, P_{1s}, causes a shift of the hysteresis loop along the applied field direction.

An additional benefit of studying the internal field effects in Rainbow actuators is an opportunity to compare the internal voltages measured from the displacement and polarization measurements. Normally, only the internal electric field is determined from polarization hysteresis measurements. A comparison of the displacement and polarization internal voltages will contribute to the understanding of the polarization switching mechanism in Rainbow devices.

Experimental Procedure

For this report, primarily PLZT 9.5/65/35 samples were used because of their slim hysteresis loops. Rainbow samples were prepared using the procedures described previously.[2] Samples used in this report were provided by Dr. G. Haertling and Dr. G. Li.

An LVDT setup was used to measure the displacement for the samples driven electrically at 1 Hz. A Zygo ZMI–1000 interferometer was adapted for high-frequency, non-contact displacement measurements. An HP 4194 impedance analyzer was used for the

characterization of Rainbow samples at resonance. Details of the experimental procedures are given in previous reports.[3]

The voltages corresponding to the displacement maxima for displacement loops, V_{max1} (negative polarity) and V_{max2} (positive polarity), and the coercive voltages for polarization loops, V_{c1} (negative polarity) and V_{c2} (positive polarity), were measured. Figure 1 shows how the voltages are determined (the internal voltages are exaggerated for clarity). The following expressions were used to calculate the internal voltages for displacement and polarization:

$$V_{iD} = \frac{V_{max2} + V_{max1}}{2} \qquad (2)$$

$$V_{iP} = \frac{V_{c2} + V_{c1}}{2} \qquad (3)$$

Results and Discussion

Field-induced resonance characteristics of several PLZT 9.5/65/35 Rainbow samples with different oxide to reduced thickness ratios were explored. The strongest resonance was observed for a sample with an oxide to total thickness ratio of 0.5. This sample was used extensively in this study. It has a diameter of 2.22 cm and a total thickness of 0.043 cm.

The frequency corresponding to the maximum resistance, the parallel resonance frequency, for the fundamental bending mode was measured as a function of dc bias applied to the sample. The convention adopted in Figure 2, and throughout this report, is for a positive dc bias to represent an electric field pointing into the oxide layer from the

3

```
A/DIV   20.00   Ω   START        2 100.000 Hz
B/DIV   50.00   Ω   STOP         2 400.000 Hz
OSC=_1.00E-01 V
```
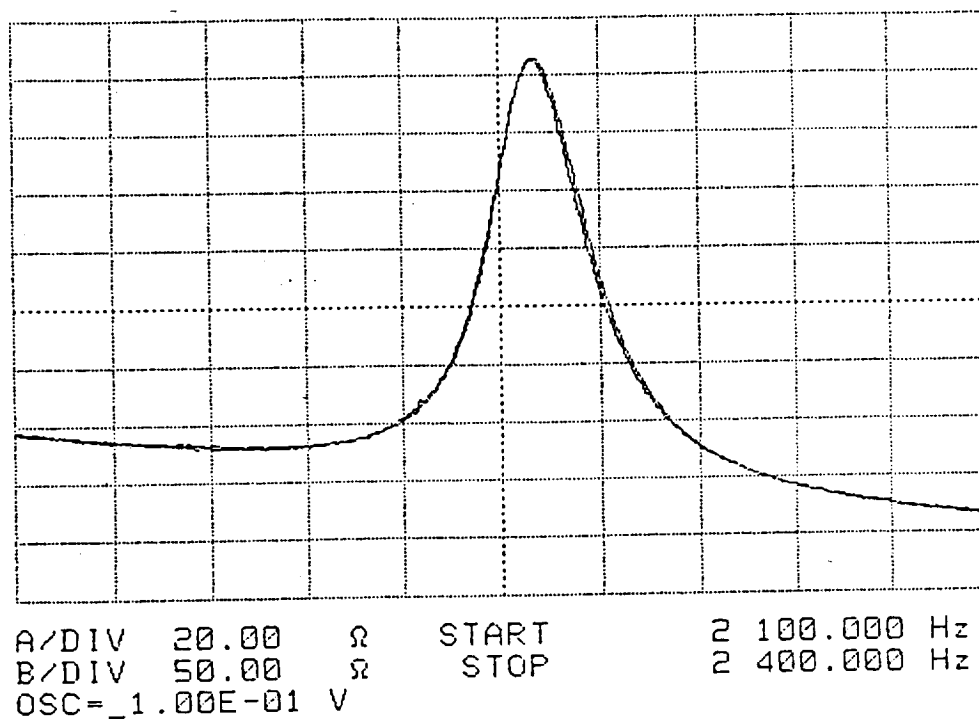
Figure 4.   Parallel resonance spectrum for increasing and decreasing frequency sweeps for PLZT 9.5/65/35 Rainbow sample under low drive conditions. ac voltage = 0.1 V, dc bias = –40 V.
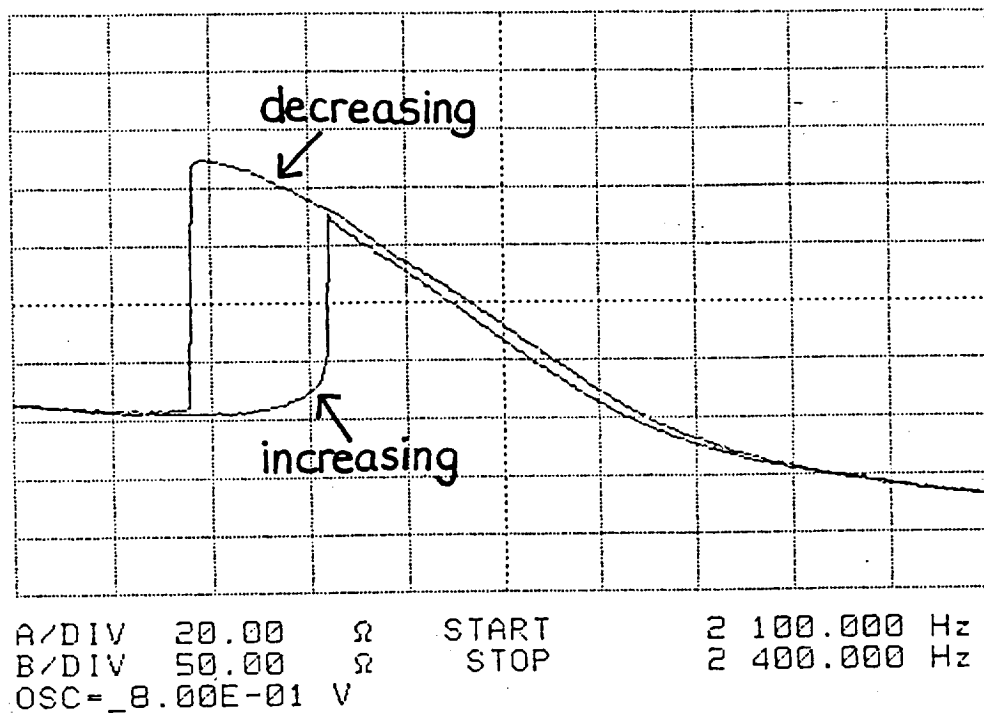
```
A/DIV   20.00    Ω    START        2 100.000 Hz
B/DIV   50.00    Ω    STOP         2 400.000 Hz
OSC=_8.00E-01 V
```

Figure 5. Parallel resonance spectrum for increasing and decreasing frequency sweeps for PLZT 9.5/65/35 Rainbow sample under high drive conditions. ac voltage = 0.8 V, dc bias = −40 V.

reduced layer – oxide layer interface. The break in the data for moderate negative bias is due to extremely weak resonances which could not be characterized. The results shown in Figure 2 indicate that there is a softening of the mode for sufficiently large applied voltages of either polarity, with the maximum parallel resonance frequency shifting away from the origin towards negative bias. The sample behaves as an internally biased electrostrictive dielectric. The internal bias is consistent with the polarization pointing away from the interface being the energetically favorable orientation. The reduction of the resonance frequency at high bias voltages is consistent with the flattening of the sample, with a corresponding reduction of sample stiffness, as predicted by Finite Element Modeling.[4]

The parallel resonance frequency for the fundamental bending mode is highly sensitive to the ac driving voltage level, as shown in Figure 3. The reduction of the resonance frequency is partly due to both the flattening of the sample for the higher drive condition and the contribution of higher order elastic constants. The splitting of the resonance curves for the up and down frequency sweeps is known to occur in bulk ceramics,[5,6] and is explained in terms of elastic nonlinearity.

The shapes of the resonance curves for the low and high drive conditions are shown in Figures 4 and 5. For the low drive of 0.1 V in Figure 4, the sample shows symmetric and overlapping resonance peaks. For the high drive of 0.8 V in Figure 5, a jump phenomenon[6] occurs, causing appreciable hysteresis between the two sweeps. The jump phenomenon arises from elastic nonlinearity, which contributes to the observed resonance mode softening. The nonlinearity is enhanced by the low frequency at which the resonance occurs, since the ferroelastic contribution from domain wall motion should be inversely proportional to the resonance frequency. It would be interesting to determine if there is a sample diameter dependency of the nonlinear response of the

fundamental resonance. A high mechanical Q, the reciprocal elastic loss tangent, should also contribute to the nonlinear response, since the induced stresses in a resonator are proportional to Q.[7] The Q for this sample was determined from the radial mode resonance to be approximately 75. Higher Qs (90 – 120) were estimated for Rainbow samples with lower La contents, as expected.[8]

The third order compliance, s_{111}, also gives rise to the excitation of resonance by subharmonic drive.[9] This effect was observed for the 6.0/56/44 PLZT Rainbow sample using the ZMI–1000 interferometer. At constant applied voltage magnitude, the voltage frequency was swept through the range which included the half subharmonic of the fundamental bending mode. The observed displacement as a function of frequency is shown in Figure 6, which indicates the generation of the fundamental mode response at a modest driving voltage.

In Figure 7, peak-to-peak displacement of PLZT 9.5/65/35 Rainbow is plotted as a function of the applied voltage. The displacement curve indicates that the sample follows an electrostrictive response up to approximately ±150 Volts, then levels off at higher voltages.

The maximum displacement voltages, V_{max2} and $|V_{max1}|$,* and the displacement internal voltage, V_{iD}, from the displacement loop measurements as a function of driving voltage are shown in Figure 8. The magnitude of the voltage for negative polarity, V_{max1}, is higher than for positive polarity, V_{max2}, and the displacement internal voltage, V_{iD}, is approximately independent of the applied voltage magnitude. The sign of V_{iD} is consistent with that deduced from Figure 2.

---

*V_{max1} is plotted as a positive value for ease of comparison to V_{max2} in Figures 8 and 14, similarly for V_{c1} in Figures 9, 10, and 13.

The coercive voltages, V_{c2} and $|V_{c1}|$, and the polarization internal voltage, V_{iP}, from the polarization loop measurements as a function of driving voltage are shown in Figure 9. The magnitude of the coercive voltage for negative polarity, V_{c1}, is higher than for positive polarity, V_{c2}, at high voltages, but there is a change in sign at low voltages. Unlike the displacement internal voltage, V_{iD}, the polarization internal voltage, V_{iP}, shows an approximately linear increase with driving voltage. The polarization coercive voltages level off and the displacement deviates from quadratic behavior in the same applied voltage range, as comparison of Figures 7 and 9 shows. Indeed, inspection of Figure 10 indicates that a plot of the coercive voltages as a function of the induced polarization has a more linear slope.

The fact that the coercive voltages differ from the maximum displacement voltages is noteworthy. For the ideal square loop hysteresis, the coercive voltages from polarization measurements and the maximum displacement voltages from displacement measurements are identical. The large discrepancy from the ideal behavior is related to Rainbows being prestressed benders. The stress gradient contributes to different regions trying to switch at different field levels. In particular, the ferroelastic domain switching, which is likely to dominate in unstressed ceramics, should be enhanced by the tensile stress existing near the oxide surface. In fact, XRD in the presence of an electric field indicated enhanced ferroelastic domain switching at the surfaces of Rainbow devices.[2]

Even if stress effects are ignored, since a Rainbow is a bender, the closer a portion of the oxide layer is to the free surface, the greater its contribution to the displacement. The above statement is supported by a simple argument: Assume a Rainbow sample with a reduced to oxide layer thickness ratio of 1 to 2. Further assume that the elastic properties of the two layers are identical. If the half of the oxide layer closest to the top surface is shorted, no bending would occur when voltage is applied. If, instead, the half of the

oxide layer closest to the interface with the reduced layer is shorted, the Rainbow will bend in response to the applied voltage. Therefore, enhanced domain switching and thus the effective d_{31} is especially beneficial if present near the top surface. Unlike the displacement, the polarization switching in all regions of a Rainbow contributes equally to its hysteresis loop. The lower coercive voltages for the displacement switching are due to the lower activation threshold for the ferroelastic domain switching near the free interface, compared to the rest of the oxide layer. It would be beneficial to repeat the displacement and polarization voltage measurements for a sample with a thin oxide layer which is in compression throughout the volume.

The opposite signs for the displacement and polarization internal voltages, V_{iD} and V_{iP}, observed at low driving voltages (Figures 8 and 9) suggest the possibility that the internal field has opposite signs in different parts of the Rainbow sample. In this case, trapped positive charge is expected to be present at the interface where the regions with opposite internal fields come into contact. The sign of the trapped charge is consistent with PLZT ceramics being p-type conductors.

The effect of a point load on the displacement is shown in Figure 11. The highest displacement is obtained when the maximum point load of 700 grams was applied to the sample.

In contrast to the internal voltage calculated values (Equations 3 and 4), the magnitude of the voltages is used to calculate the average switching voltages for displacement and polarization, as follows:

$$V_{aveD} = \frac{|V_{max2}| + |V_{max1}|}{2} \tag{4}$$

$$V_{aveP} = \frac{|V_{c2}| + |V_{c1}|}{2} \tag{5}$$

The average switching voltages for polarization and displacement, V_{aveP} and V_{aveD}, as a function of the applied point load are shown in Figure 12. While the polarization average switching voltage, V_{aveP}, is practically independent of the load level, the displacement average switching voltage, V_{aveD}, shows a gradual increase with load. V_{aveP} remains higher than V_{aveD} over the entire range of applied loads but the difference between the two diminishes as load increases.

The coercive voltages, V_{c2} and $|V_{c1}|$, and the polarization internal voltage, V_{iP}, from the polarization loop measurements as a function of applied point load are shown in Figure 13. The curves for the two polarities mirror each other, which is why the polarization average switching voltage, V_{aveP}, in Figure 12 is approximately independent of load level. However the polarization internal voltage, V_{iP}, (Figure 13) decreases with increasing load. In comparison, the displacement internal voltage, V_{iD}, shown in Figure 14 is independent of applied load.

Polarization hysteresis loops for no load and maximum load are shown in Figure 15. The two loops have very similar shapes. Large coercive voltages observed in the hysteresis loops suggest that some La was lost during processing. In contrast, there is noticeable difference between the displacement hysteresis loops shown in Figure 16. The upper portion of the displacement loop is elongated when load is applied.

8

Several of the observed effects of the applied load can be accounted for as flattening of the sample. Greater displacement with load (Figure 11) is in part due to the reduction of the stiffness of a loaded Rainbow structure. A smaller difference between the average switching polarization voltages for polarization and displacement, V_{aveP} and V_{aveD}, for the loaded Rainbow sample (Figure 12) can be accounted for by a more uniform stress in a Rainbow sample flattened by a load. A reduction in the polarization internal voltage, V_{iP}, with increasing load (Figure 13) suggests that it may also be stress-controlled.

The relative independence of the displacement internal voltage, V_{iD}, as a function of both applied voltage (Figure 8) and applied load (Figure 14) suggests that the internal voltage in the upper part of the oxide layer of a Rainbow sample is highly stable and uniform. Stability of internal voltage implies the presence of a stable nonswitchable polarization component which is only present in a portion of the sample. Therefore, according to Equation (1), the reaction field contributing to the field in the rest of the oxide layer (E_2) is produced. The combination of internal voltages throughout the oxide layer add up to the observed shifts in the hysteresis loops. The origin of the internal fields remains to be understood. It would be useful to study Rainbow samples with the oxide layer in a paraelectric state where internal stresses are present, but ferroelastic domains are not.

The results obtained in this study suggest further work. A promising area to pursue is to extend this study to PLZT 9.5/65/35 Rainbow samples with different oxide to reduced layer thickness ratios.

9

References

1. U. Robels, J. H. Calderwood, and G. Arlt, "Shift and Deformation of the Hysteresis Curve of Ferroelectrics by Defects: An Electrostatic Model," *J. Appl. Phys.*, **77** (8), 4002 (1995).

2. G. Li, "Influence of Internal Stress on the Electromechanical Properties of PLZT Stress-biased (Rainbow) Ceramic Actuators," Ph.D. thesis, Department of Ceramic Engineering, Clemson University, 1995.

3. G. H. Haertling, "Superconductivity Devices: Commercial Use of Space," Annual Report to NASA, Contract #NAG–1–1301 (1994).

4. E. Furman, G. Li and G. H. Haertling, "An Investigation of the Resonance Properties of Rainbow Devices", *Ferroelectrics*, **160**, 357 (1994).

5. R. S. Woollett and C. L. LeBlanc, "Ferroelectric Nonlinearities in Transducer Ceramics," *IEEE Trans. Sonics and Ultrasonics*, **SU-20** (1), 24 (1973).

6. K. Negishi, "Jump Phenomenon in Resonance Curve of Ferroelectric Ceramic," *J. Phys. Soc. Japan*, **15**, 534 (1960).

7. R. Holland and E. P. EerNisse, "Accurate Measurement of Coefficients in a Ferroelectric Ceramic", *IEEE Trans. Sonics and Ultrasonics*, **SU-16**, 173 (1969).

8. C. Elissalde and L. E. Cross, "Dynamic Characteristics of Rainbow Ceramics," *J. Am. Cer. Soc.*, **78** (8), 2233 (1995).

9. H. Beige and G. Schmidt, "Electromechanical Resonances for Investigating Linear and Nonlinear Properties of Dielectrics," *Ferroelectrics*, **41**, 39 (1982).
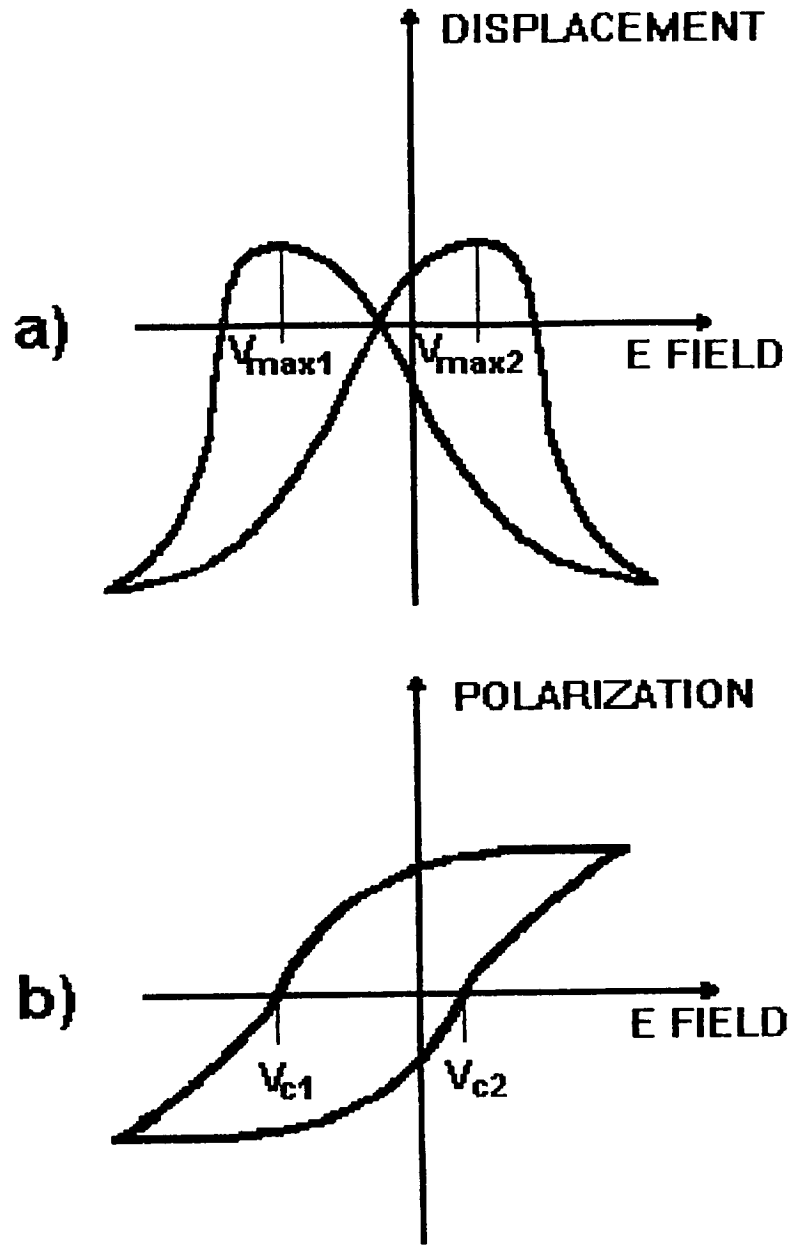
Figure 1. Measurement of voltages: a) V_{max1} (negative polarity) and V_{max2} (positive polarity) = voltages corresponding to the displacement maxima in displacement loops. b) V_{c1} (negative polarity) and V_{c2} (positive polarity) = coercive voltages in polarization loops. Diagram exaggerated for clarity.
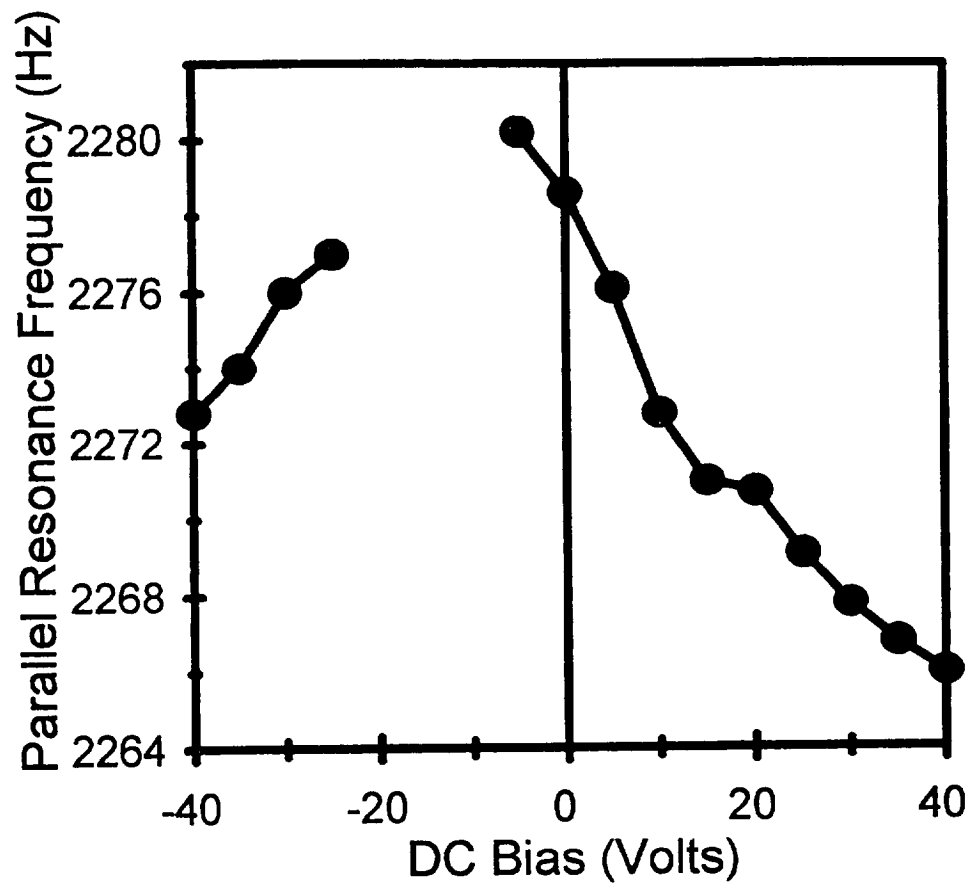
Figure 2. Parallel resonance frequency vs. dc bias for PLZT 9.5/65/35 Rainbow sample. ac voltage = 0.1 V.
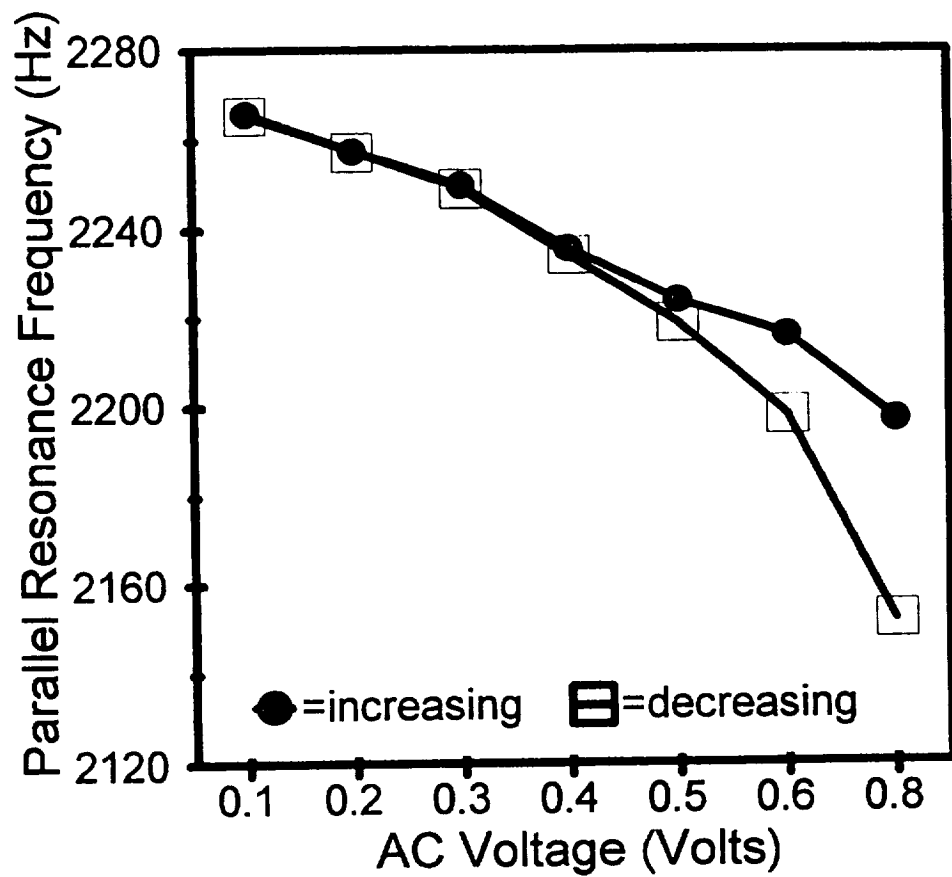
Figure 3. Parallel resonance frequency vs. ac voltage for increasing and decreasing frequency for PLZT 9.5/65/35 Rainbow sample. dc bias = –40 V.
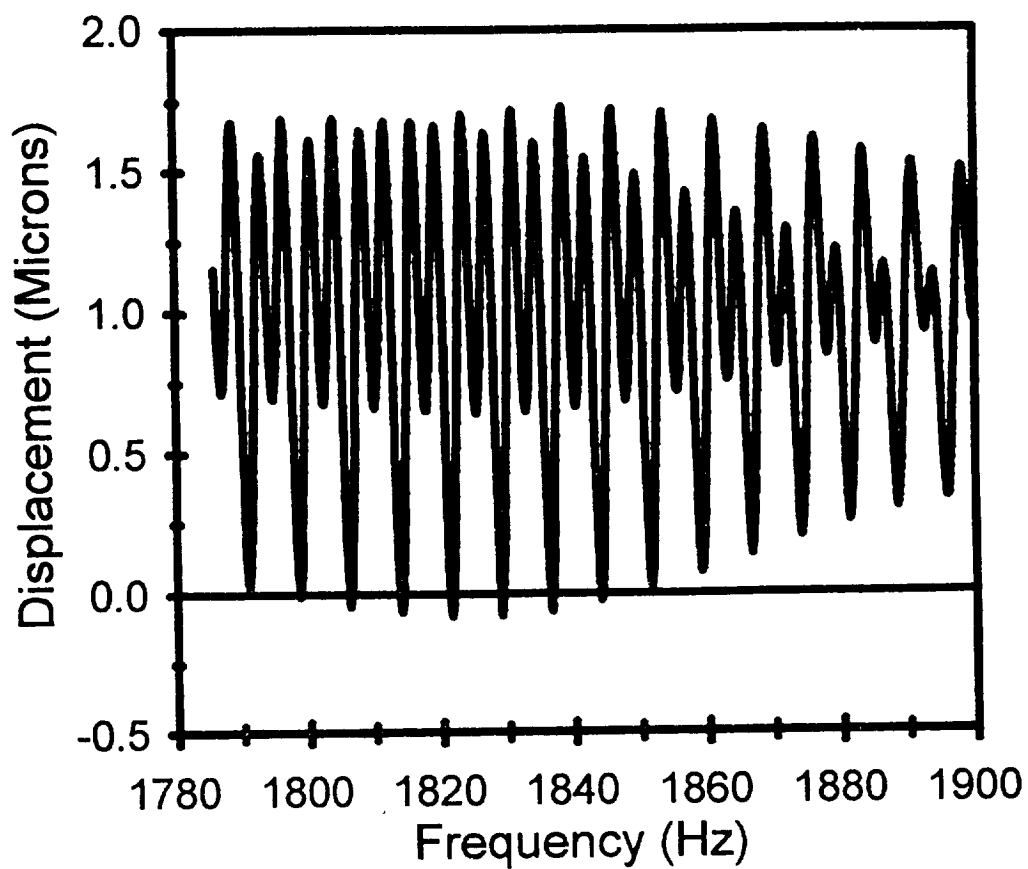
Figure 6. Displacement vs. frequency for PLZT 6.0/56/44 Rainbow sample, showing resonance response generation in the subharmonic frequency range. diameter = 3.18 cm, thickness = 0.051 cm, ac voltage = ± 10 Vpp.
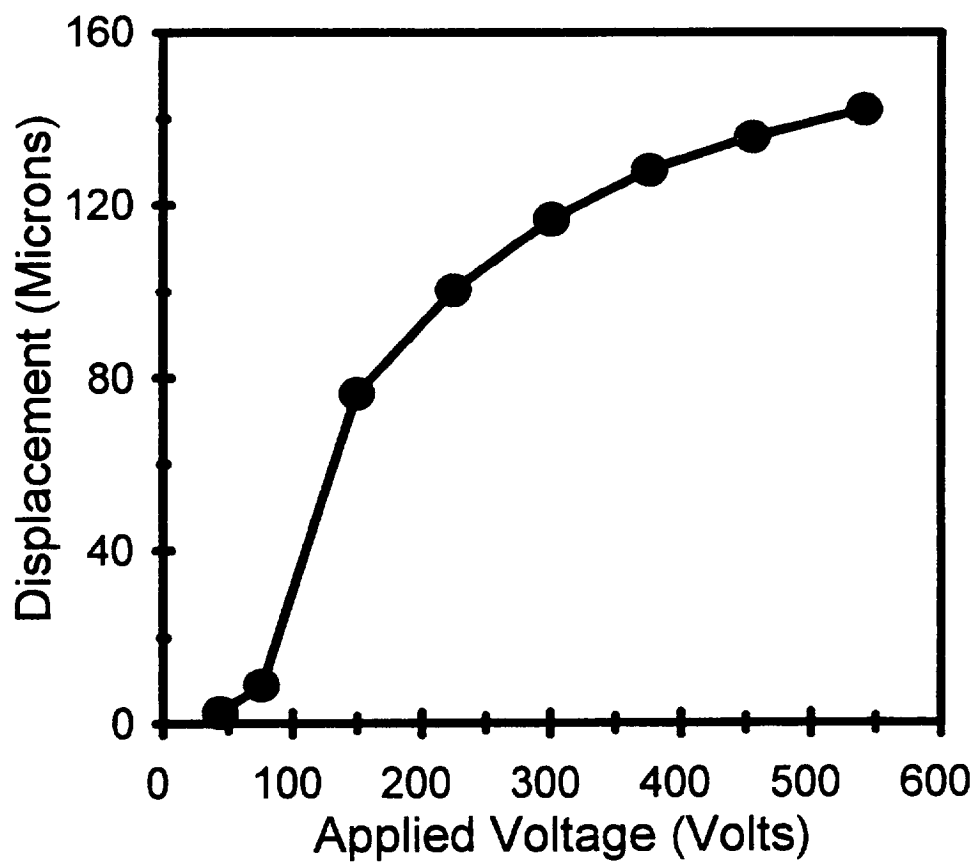
Figure 7.   Displacement vs. applied voltage for PLZT 9.5/65/35 Rainbow sample. ac voltage applied at 1 Hz.
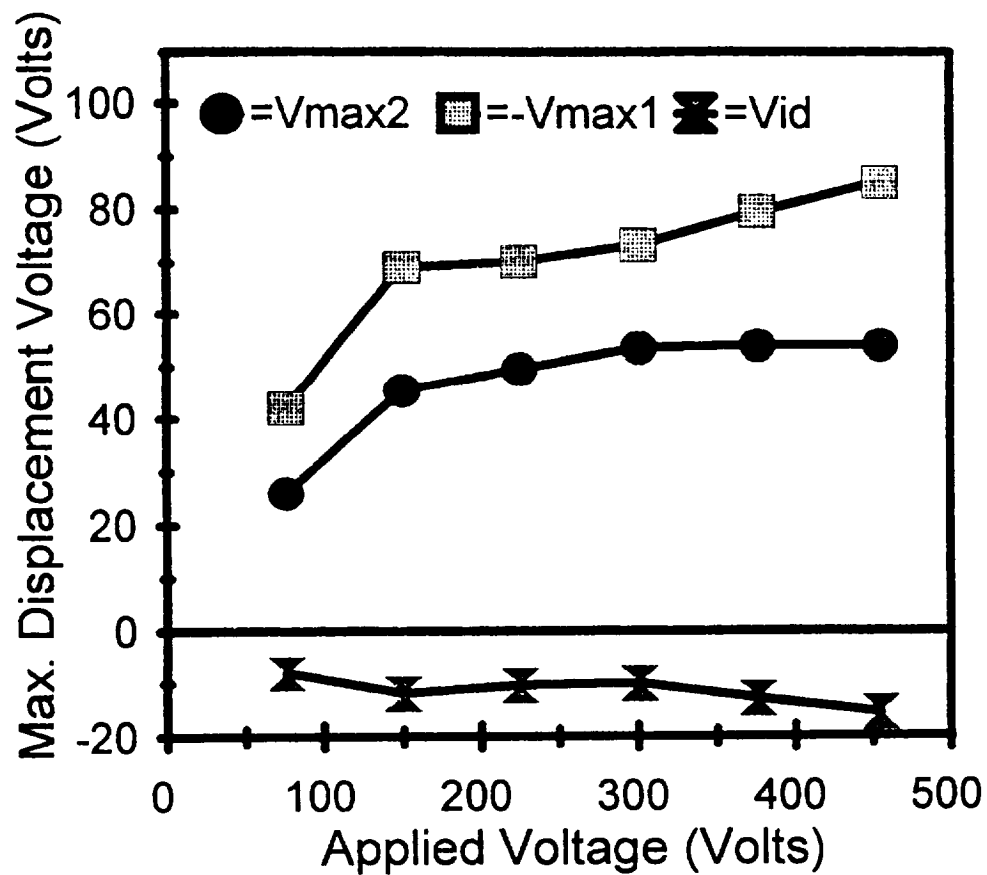
Figure 8.   Voltages corresponding to the displacement maxima, V_{max2} and $|V_{max1}|$, and displacement internal voltage, V_{iD}, vs. applied voltage for PLZT 9.5/65/35 Rainbow sample.
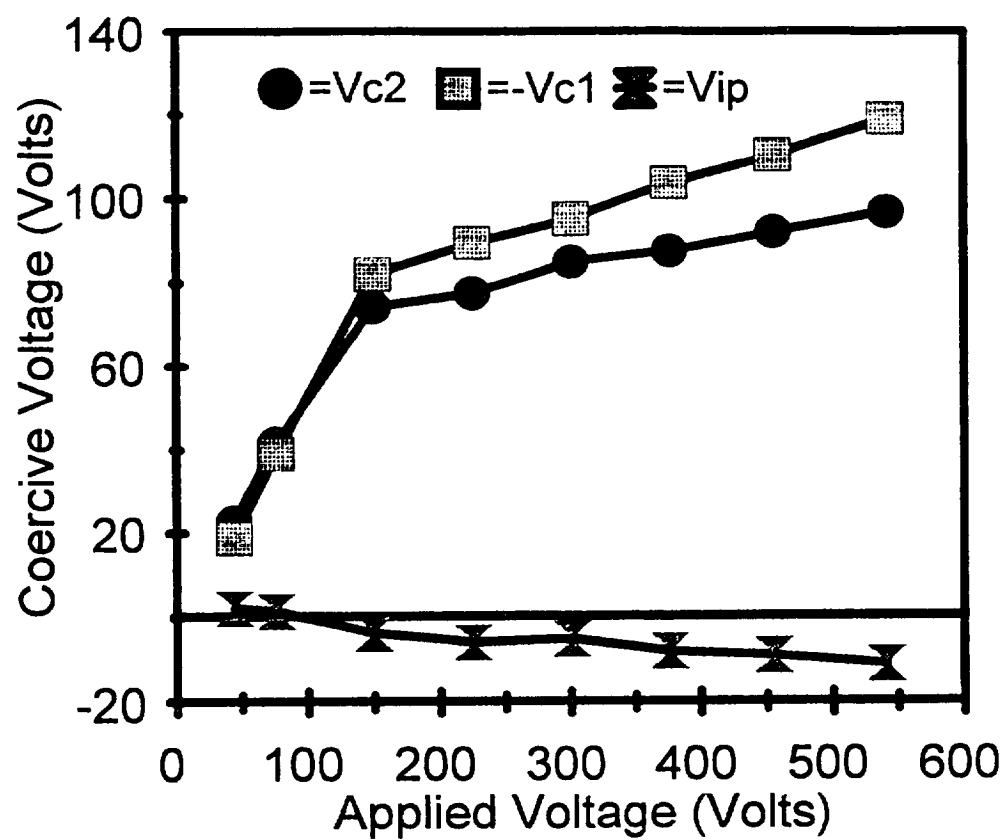
Figure 9.   Coercive voltages, V_{c2} and $|V_{c1}|$, and polarization internal voltage, V_{ip}, vs. applied voltage for PLZT 9.5/65/35 Rainbow sample.
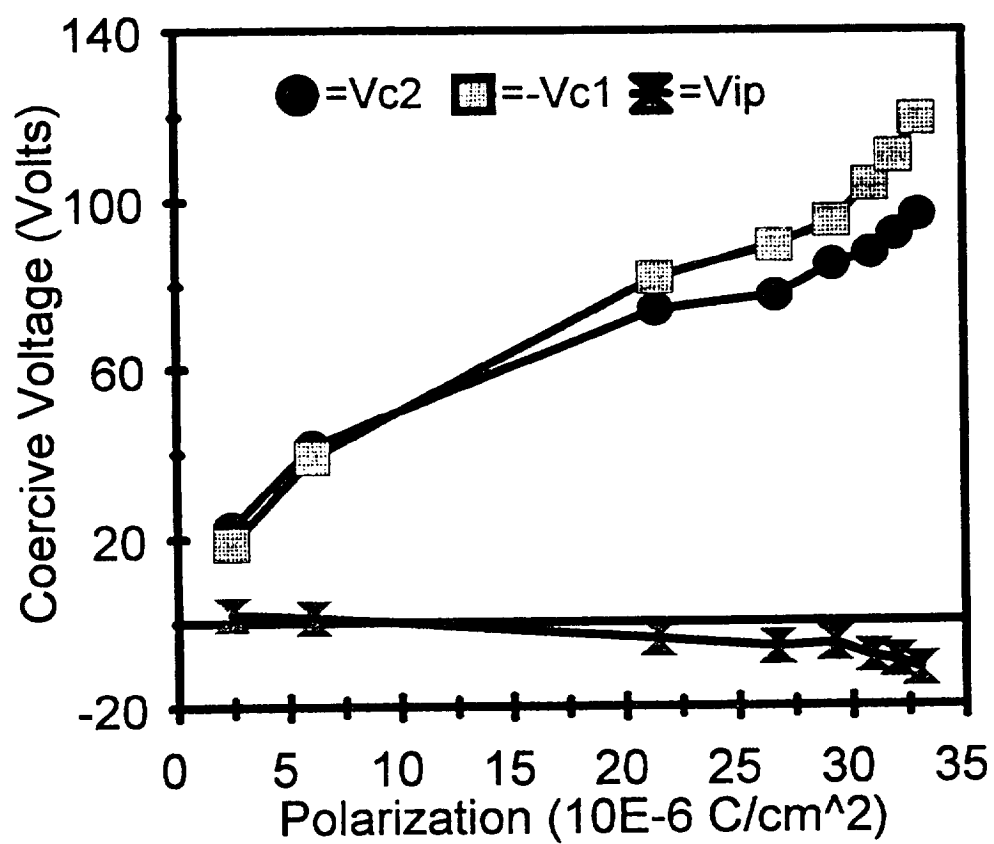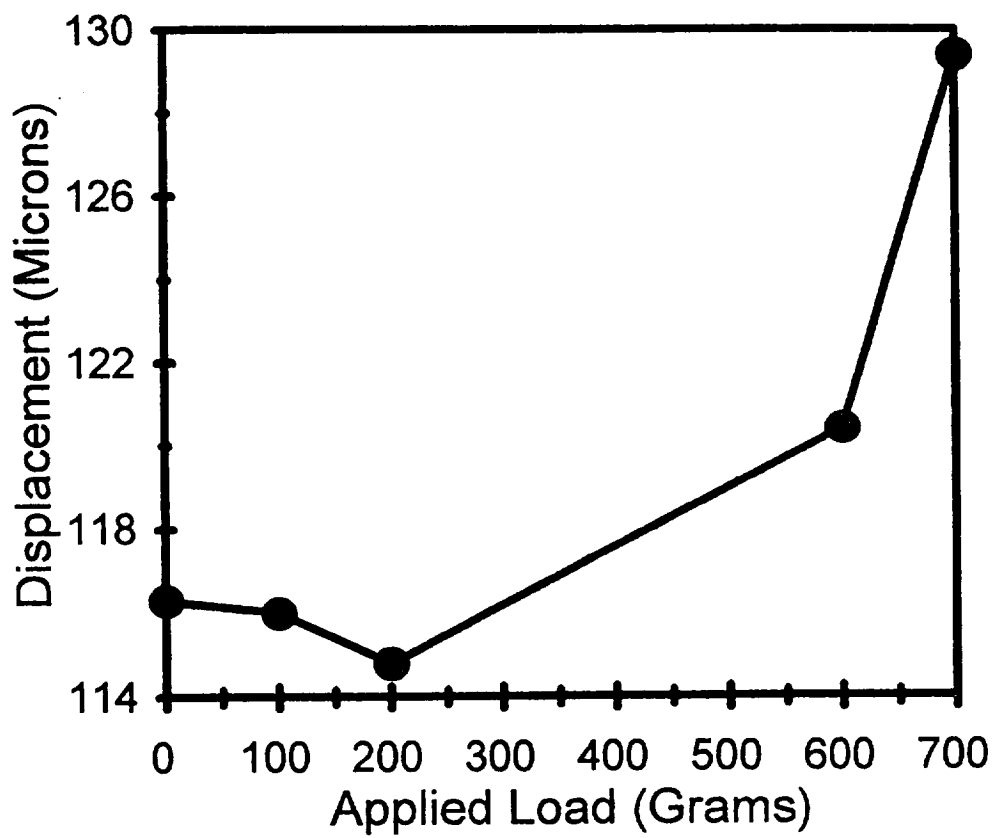
Figure 10. Coercive voltages, V_{c2} and $|V_{c1}|$, and polarization internal voltage, V_{iP}, vs. induced polarization for PLZT 9.5/65/35 Rainbow sample.

Figure 11.   Displacement vs. applied point load for PLZT 9.5/65/35 Rainbow sample.
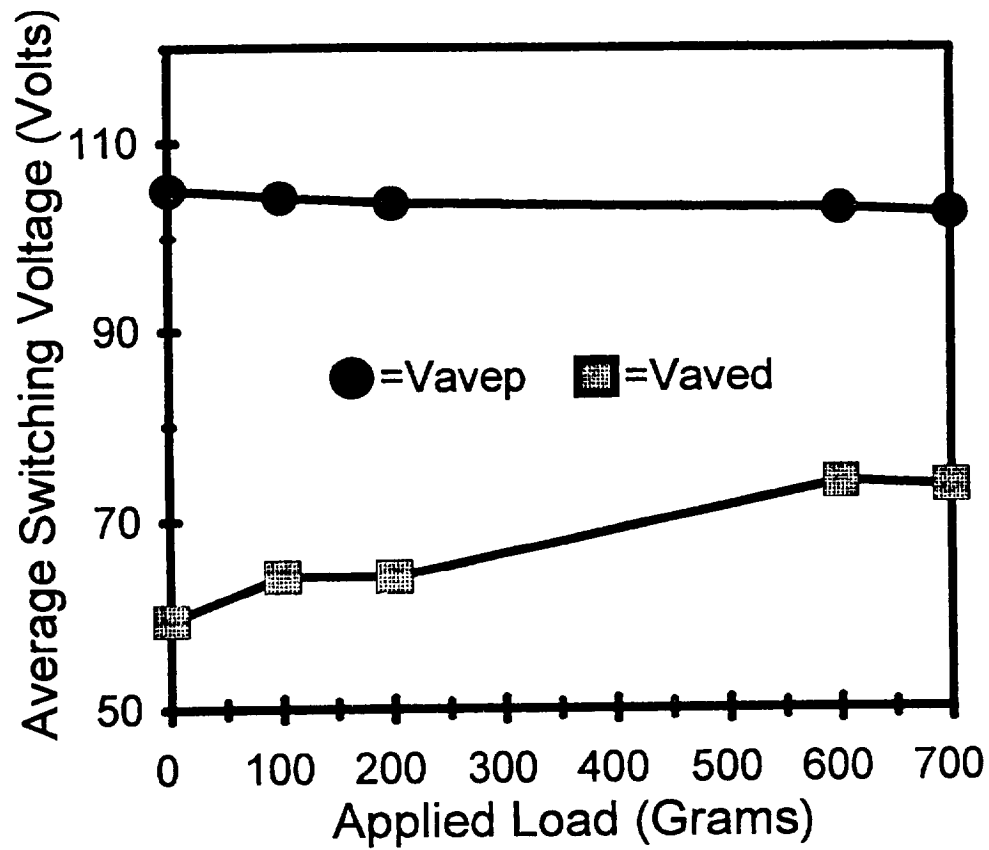
Figure 12. Polarization average switching voltage, V_{aveP}, and displacement average switching voltage, V_{aveD}, vs. applied point load for PLZT 9.5/65/35 Rainbow sample. ac voltage = ± 376 V.
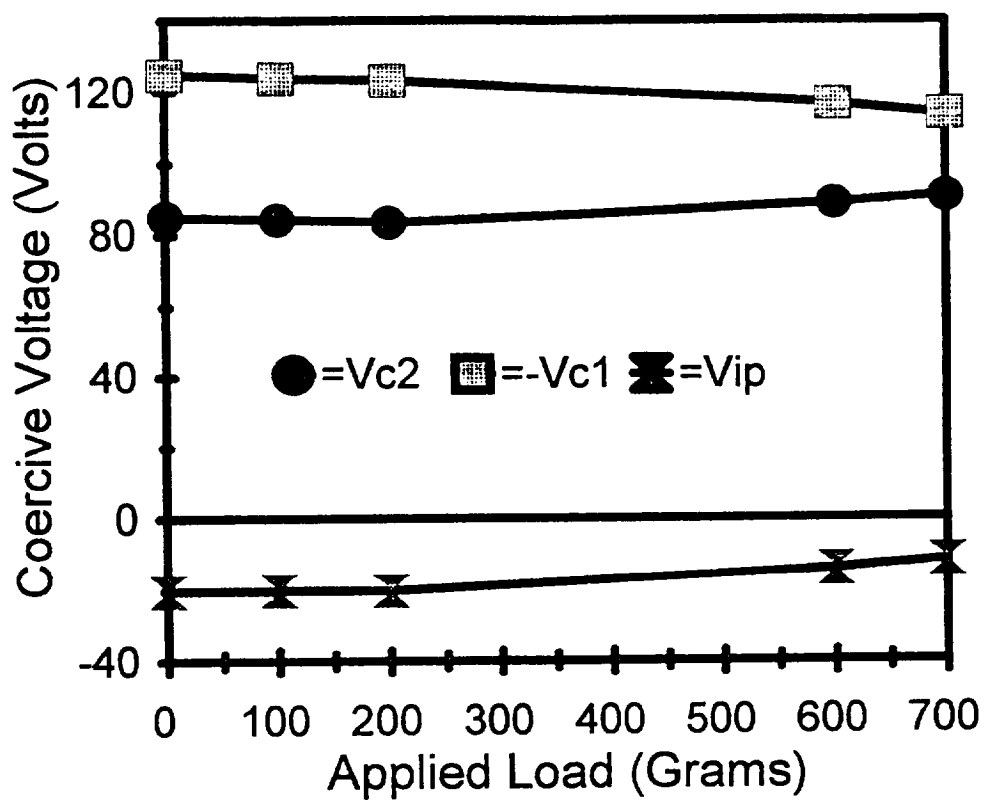
Figure 13. Coercive voltages, V_{c2} and $|V_{c1}|$, and polarization internal voltage, V_{ip}, vs. point load for PLZT 9.5/65/35 Rainbow sample.
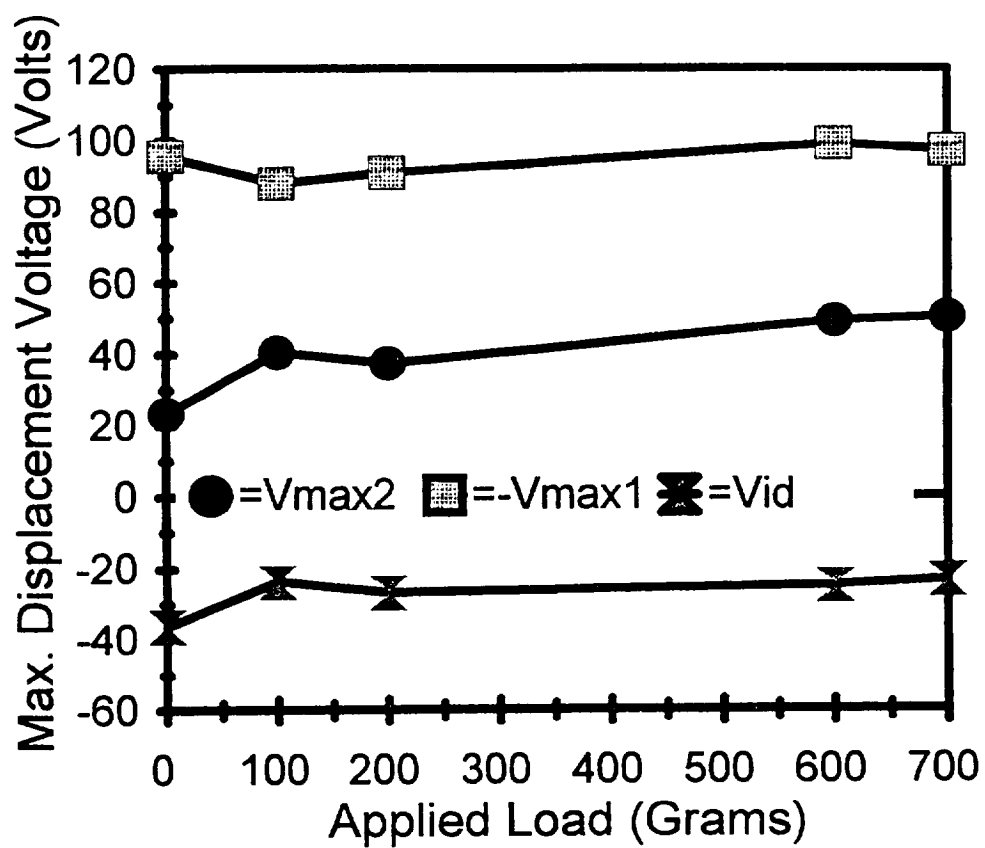
Figure 14. Voltages corresponding to the displacement maxima, V_{max2} and $|V_{max1}|$, and displacement internal voltage, V_{iD}, vs. point load for PLZT 9.5/65/35 Rainbow sample.
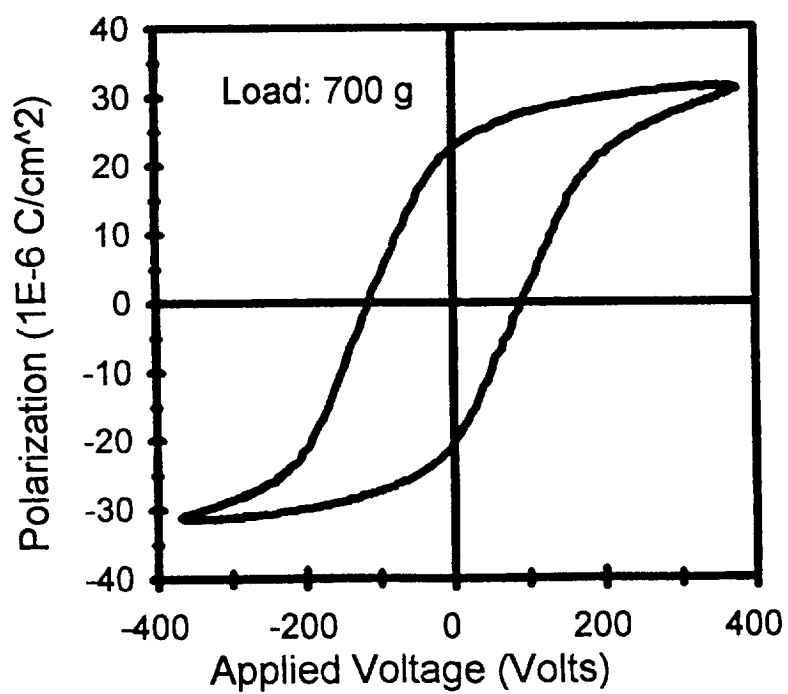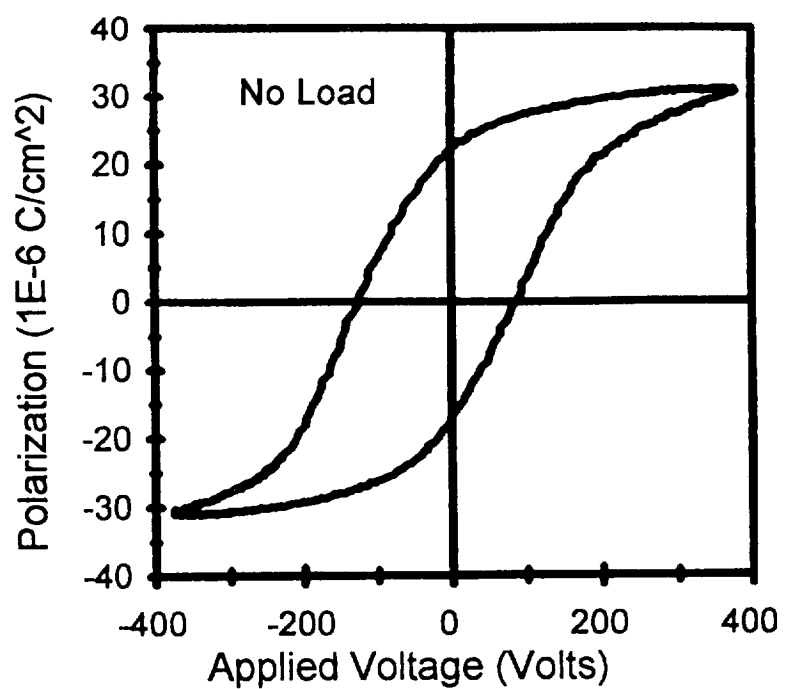
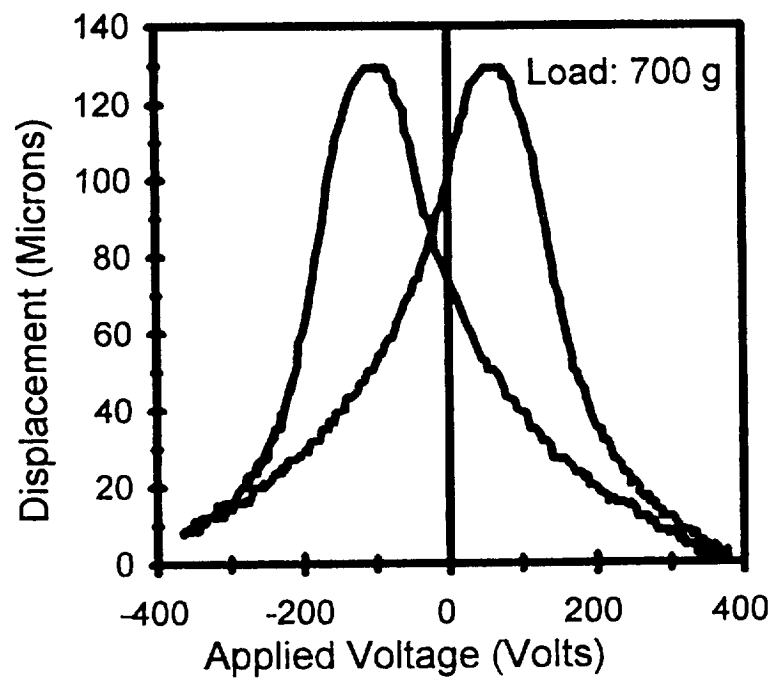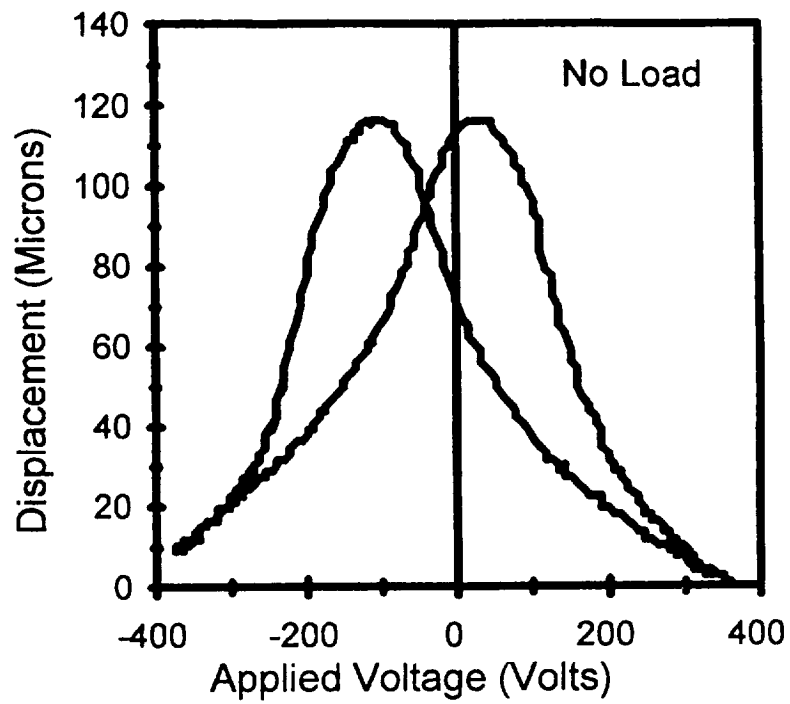Figure 15. Polarization loops for PLZT 9.5/65/35 Rainbow sample.

Figure 16.   Displacement loops for PLZT 9.5/65/35 Rainbow sample.

Part III.

A Study of Stress-Optic and Electrooptic Birefringence in Rainbow Actuators

A Study of Stress-Optic and Electrooptic Birefringence in Rainbow Actuators

I. Introduction

The concept of achieving ultra-high displacements and moderate load-bearing capability by means of stress-enhanced structures has been shown to be a valid one and has been amply demonstrated by the recent development of the Rainbow actuators. Displacements as high as 1-3 mm for individual wafers of varying thicknesses and diameters have been reported for this technology with the prospects for even higher displacements as the actuators are mechanically bonded together to form linear stacks. Recent modeling studies have also shown that the stresses which exist in the Rainbows are non-uniform and are a function of the ratio between the reduced and unreduced layers. Furthermore, the pattern of these internal stresses is expected to change significantly as (1) load is applied or generated and (2) voltage is applied during operation.

With this in mind, an investigation has been initiated to study the stress patterns which are internally generated in pre-stressed Rainbow structures and to note the change in these patterns as load and voltage are applied. The analytical method selected for this study is an optic/electrooptic one, i.e., the stress-optic birefringence achieved by mechanically producing stress and the electrooptic birefringence produced by applying voltage, the effects of both being observed and studied under crossed polarizers and white light. Although this is only a qualitative exercise, it nevertheless will provide some useful insights into how these structures operate internally and can provide very interesting information about the long term creep, fatigue and stability of the stresses.

II. Experimental

Since the Rainbow actuators are made from PLZT materials of both the ferroelectric and electrostrictive types and the electrostrictive materials such as 9/65/35 (La/Zr/Ti) are highly transparent, the 9/65/35 composition was selected as the basic material of study for this investigation. PLZT wafers, 31.75 mm in diameter and 0.5 mm thick, were processed into Rainbows by chemically reducing one surface of the wafers at 975°C for various times (20 minutes to one hour) while resting on a graphite (carbon) block. After cooling to room temperature, the wafers were sliced into bars, 3 mm wide x 25 mm long, with a low speed diamond saw. The major cross-sectional surfaces (25 mm x 0.5 mm) of the bars were then lightly sanded flat on 400 grit sandpaper and polished with 6 um diamond paste on a Buehler Texmet pad. Electrically conductive silver epoxy electrodes were applied to the major planar surfaces of the bars and cured at 200°C for 0.5 hour.

Stress-optic and electrooptic observations were performed on the Rainbow elements with a polarizing microscope using white light as the illumination source. The experimental setup is shown in Figure 1. Stress-optic birefringence patterns were noted before and after the application of mechanical stress and voltage. Mechanical stress was applied to the normal PLZT ceramic and to the Rainbows by means of a second Rainbow which was used as an actuator with a fulcrum point located at the center of the bar being observed. Documentation included both color photographs and video tape.

III. Results and Discussion

The effects of unpolarized and polarized light upon the internal stresses in a Rainbow bar are seen by comparing Figures 2 and 3. Unpolarized light in Figure 2 does not reveal any stress-optic birefringent effects whereas the polarized light of Figure 3 very clearly shows the neutral plane (dark line) where there is no stress, and hence, no birefringence. Other parts of the wafer display varying amounts of birefringence by means of shades of gray in the black-and- white photographs or different retardation colors in the color photographs. With this experimental setup, as shown, it was not possible to distinguish the type of stresses (compressive or tensile) which were present in the Rainbow since the birefringence of either type would produce the same effect optically; however, when a gypsum compensator plate (first order red retardation) was used in conjunction with this arrangement, it was determined that the stress below the neutral axis (i.e., toward the reduced layer) was compressive and above the neutral axis it was tensile since the retardation colors increased (birefringences added) in the lower region and decreased (birefringences subtracted) in the upper region. Previous X-ray and modeling studies have also served to establish that the stresses below the neutral plane are compressive while those above the neutral plane are tensile in nature.

A clearer picture of the stress distribution can be seen in the color photographs of Figures 4 and 5 where the colors indicate stress; i.e., white, yellow, red, blue, and green represent increasing amounts of stress. Figure 5 illustrates a somewhat more complicated stress pattern near the edge of the bar. Not all edge effects are of this nature; and in this case, the pattern may be a result of the reduction which has extended around the edge of the bar toward the top.

Figures 6 through 9 are video photographs of similar stress-optic effects as well as field-induced electrooptic behavior under crossed polarizers. The pattern in Figure 7 with no voltage applied can be seen to change to that of Figure 8 as voltage is applied causing the field-induced electrooptic birefringence to be superimposed (added) upon that of the stress-optic birefringence. The net effect of superimposing both of these effects can be noted in Figure 8 where the neutral plane is no longer evident since the electrooptic birefringence has been added to the compressive stress-optic birefringence and substracted from the tensile stress-optic component, in effect moving the neutral axis toward the tensile side of the bar during the application of voltage. However, it is quite evident that the non-uniform stress-optic birefringence is still present to some degree since it can be seen that optical retardation bands (yellow, green, red) are still present. If this were not the case, the electrooptic birefringence would produce a uniform retardation color depending on the magnitude of the voltage as noted in previous work on electrooptic shutters. The edge of the bar during application of voltage is shown in Figure 9. Examples of edge effects in two other Rainbow bars are given in Figures 10 and 11.

In a closer examination of the strain-optic and electrooptic birefringent effects, a PLZT bar the same size as the Rainbow bar was mated to a Rainbow actuator with a center fulcrum, such that when voltage was applied to the Rainbow, it would impart stress to the PLZT bar. The effect of this applied stress on the PLZT bar under crossed polarizers is shown in Figure

12. As with the Rainbow shown earlier in Figure 7, the PLZT bar exhibited a zero birefringence (neutral plane) area separating the top tensile stress and the bottom compressive stress. Increasing the stress by increasing the voltage on the Rainbow actuator did not substantially change the situation; i.e., the outer surfaces of the PLZT bar experienced higher stresses (higher birefringence) but the neutral plane remained near the center of the bar. Furthermore, when voltage was applied to the PLZT bar in order to produce an electrooptic effect, the neutral plane was observed to mimic that of the Rainbow by moving up toward the top surface of the bar, leaving optical retardation bands in the bar which revealed the existence of non-uniform stress gradients. This effect is illustrated in Figure 13. Removing the voltage from the PLZT bar caused the reappearance of the neutral plane, as in the case of the Rainbow.

An explanation for what is believed to be occurring in the Rainbows before and during operation is summarized in Figure 14. The top row of Rainbow cross sections describes the optical behavior, and the bottom row the polarization/domain behavior. Column one (left column) illustrates both of these behaviors as they are noted and believed to occur in an as-processed, virgin Rainbow which exhibits only the internally pre-stressed condition (stress-optic effect) as a result of the reduction process; column two illustrates the known effect of electric field on the optical properties (electrooptic effect) of a slim-loop, quadratic, relaxor such as PLZT 9/65/35; and column three illustrates the combined effect of the uniform electrooptic birefringence superimposed on the non-uniform stress gradients created from the reduction process.

Regarding the optical behavior (top row), it may be seen that both the compressive and tensile stress gradients produce mirror-image color patterns (gray, yellow, red) which are centered on the neutral plane which is black because of the crossed polarizers where there is no birefringence since there is no stress in the neutral plane. When the uniform electrooptic birefringence is superimposed on the stress-optic birefringence, new color gradients (bands) form which tend to shift the neutral axis toward the top surface of the bar; however, this is simply a result of the electrooptic birefringence canceling the tensile stress-birefringence above the neutral plane and augumenting the compressive stress-birefringence below the neutral plane. Of course, during operation the situation is somewhat more complicated than this since the internal stress patterns are actually changing in magnitude and position due to the piezoelectric d_{31} and d_{33} coefficients; i.e., a lateral shrinkage and longitudinal expansion of the bar, itself. The overall effects, though, are similar in nature. Since the color bands usually persist, at least at the lower voltages of operation, it is obvious that the original stress gradients from the Rainbow process are present to some degree.

The polarization/domain behavior shown in the bottom row of Figure 14 illustrates the alignment of the domains as a result of the Rainbow stresses. Tension toward the top surface aligns the domains (polar axes) parallel to the surface, and compression toward the bottom reduced surface aligns the domains perpendicular to the surface. When a voltage is applied during operation, the compressively-stressed, perpendicular domains are favored to grow at the expense of the tensionally-stressed, parallel domains; thus leaving the Rainbow in varying degrees of compressive stress which is less than that originally present in the virgin Rainbow. Upon removing the voltage, the original pre-stressed state of the Rainbow is restored.

IV. Conclusions

Polarized light studies involving the stress-optic and electrooptic effects present in Rainbow ceramics have revealed the existence of the neutral plane of zero stress (i.e., zero birefringence) which parallels the major surfaces of the wafer and is highly uniform in nature. The stress-optic birefringent effects were investigated separately from the electrooptic effects by studying the birefringent color patterns in as-processed bars cut from PLZT 9/65/35 Rainbow wafers. Following this, the combined effects of stress-optic and electrooptic birefringences were studied by observing the change in the retardation color patterns as voltage was applied to the Rainbow bars. The findings include:

1. A neutral plane; i.e., a planar region of zero stress, was observed in cross-sectional views of Rainbow ceramics under crossed polarizers with white light transmissive illumination.

2. Both tensile and compressive stresses exist in a Rainbow -- tensile above the neutral plane and compressive below (toward the reduced region) the neutral plane.

3. As revealed by the optical retardation color patterns, both the compressive and the tensile stress gradients are planar and highly uniform, except near the edges of the Rainbow.

4. During voltage activation of the Rainbow, the normal, transverse-mode electrooptic effect is superimposed upon the stress-optic effect, thus producing a new series of birefringent color bands which are mobile and move upward into the tensile stress region as voltage is increased.

5. At moderate voltages, the internal stresses in a Rainbow are still evident as indicated by the persistence of the birefringent color bands.

6. At maximum voltages, the birefringent color bands become indistinguishable and blend together into a homogeneous region which is white in color.

7. As indicated by the birefringent colors, applying an external load to the Rainbow also causes the neutral plane to move upward into the tensile region, thereby neutralizing some, if not all (depending on the magnitude of the stress), of the tensile stress on the top surface of the Rainbow.

In general, it can be stated that cross-sectional observations of Rainbows under polarized light has revealed a considerable amount of information about the actual internal stress condition of the devices. All of the observed results served to confirm previously determined characteristics of the internal stresses both in the virgin state of a Rainbow and during operation.
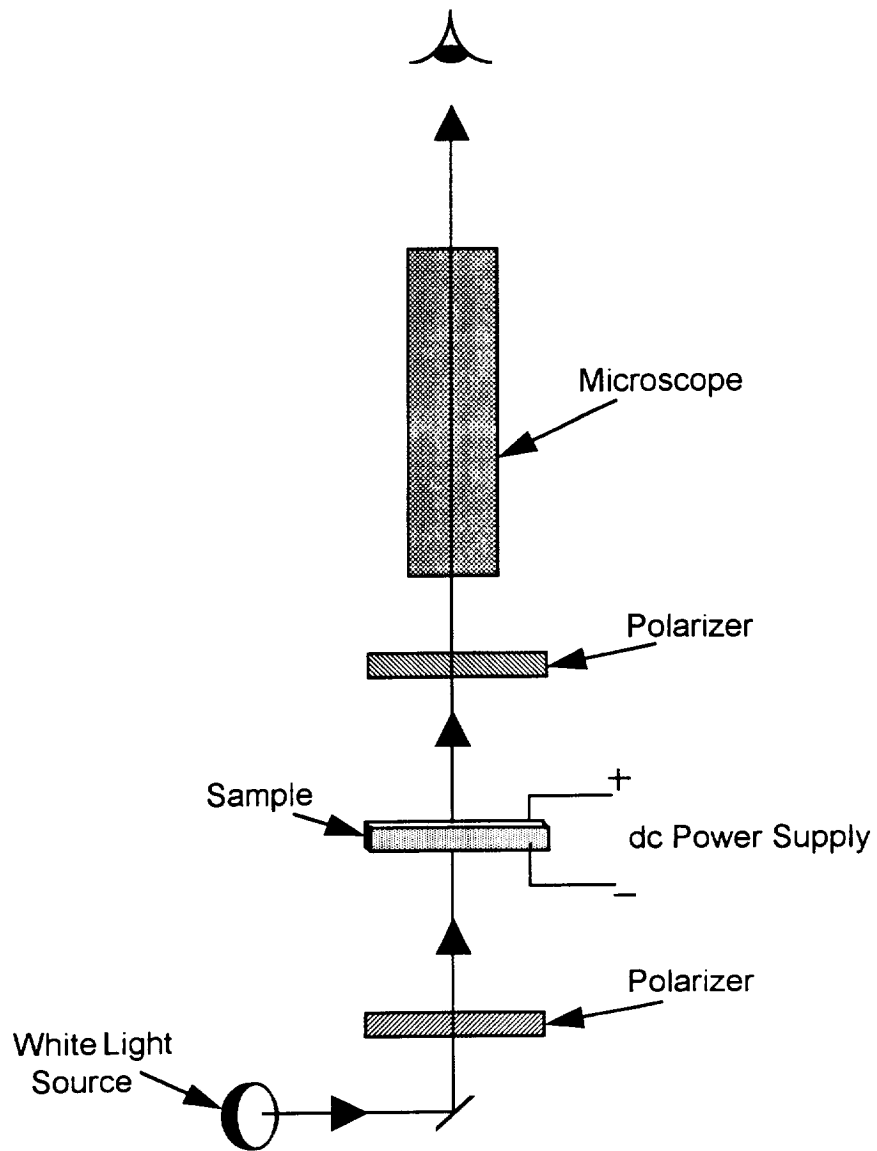
Figure 1. Measurement Setup for Observing Stress-Optic
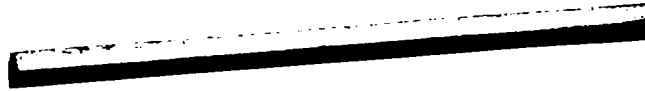and Electrooptic Birefringence in Rainbows

Figure 2. A PLZT 9/65/35 Rainbow Bar as Observed with Transmitted Unpolarized Light. Note that the Bottom Reduced Part of the Rainbow Does Not Transmit Light.
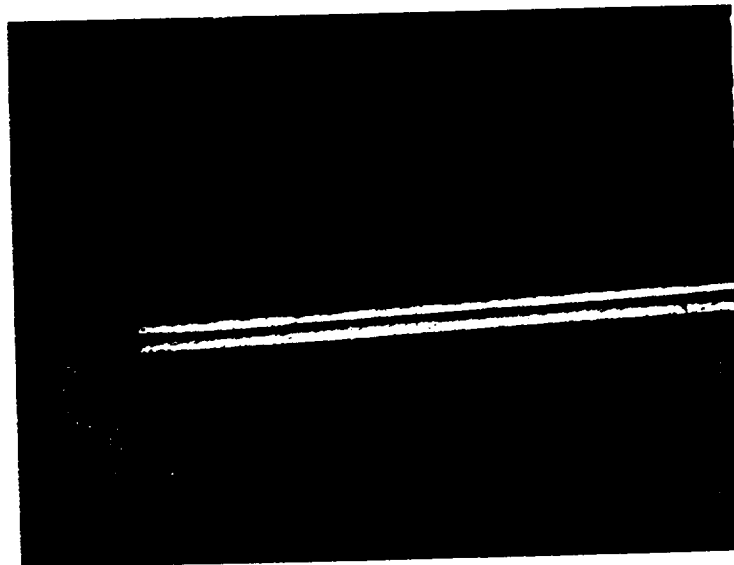

Figure 3. The Same Bar as Above Under Crossed Polarizers. Note that the Neutral Axis (Dark Line) Separating Compressive and Tensile Stresses is Uniform Throughout the Wafer.

Figure 4. A Rainbow Bar at Higher Magnification (x50) and in Color.

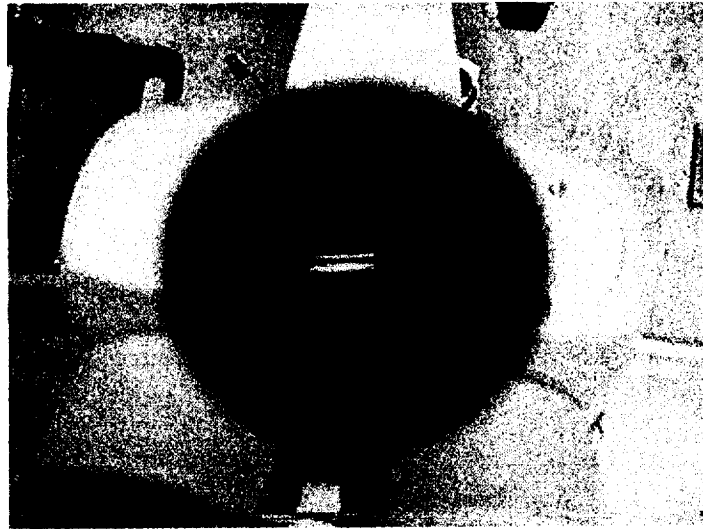Figure 5. The Same Bar as Above Showing the Stress Patterns at the End of the Bar.

Figure 6. Strain-Optic Birefringence in Unreduced Portion of Rainbow
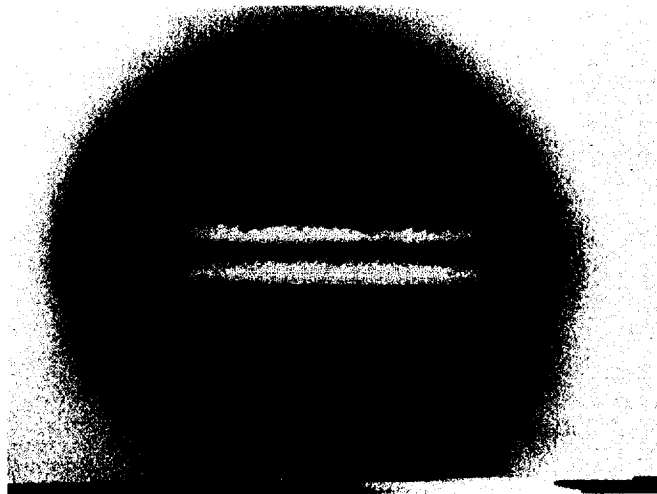When Viewed in Cross Section Under Crossed Polarizers

Figure 7. Strain-Optic Birefringence in Rainbow Bar with No Voltage
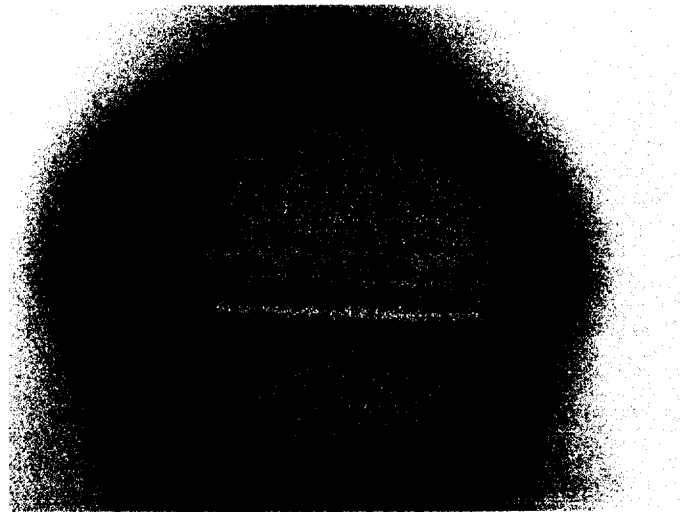Appllied, Neutral Axis (dark band) is Clearly Visible (x20)

Figure 8. Birefringence in Rainbow Bar with Voltage Applied.
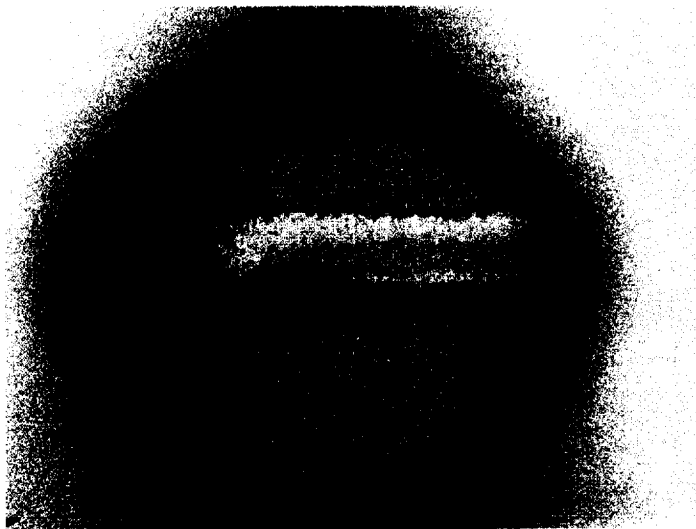

Figure 9. Birefringence in Rainbow Bar with Voltage Applied,
Same as Above at the Edge of the Bar.

Figure 10. Birefringence Pattern in Another Rainbow Bar with Voltage Applied, Cross-sectional View at Edge of Bar.
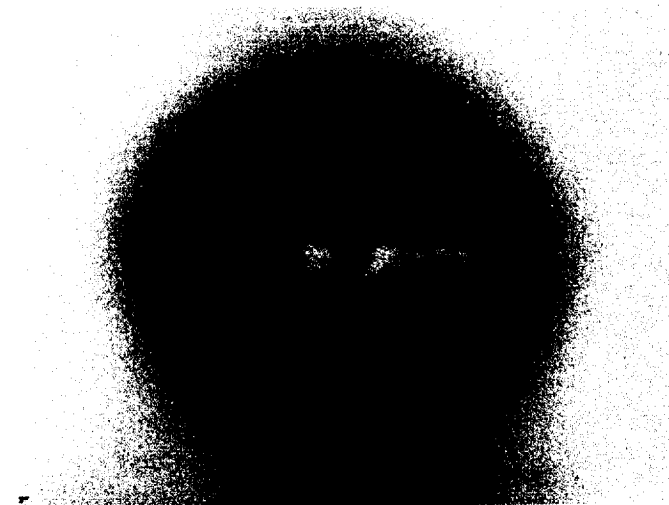

Figure 11. Birefringence Pattern in Another Rainbow Bar with Voltage Applied, Cross-sectional View at Edge of Bar.

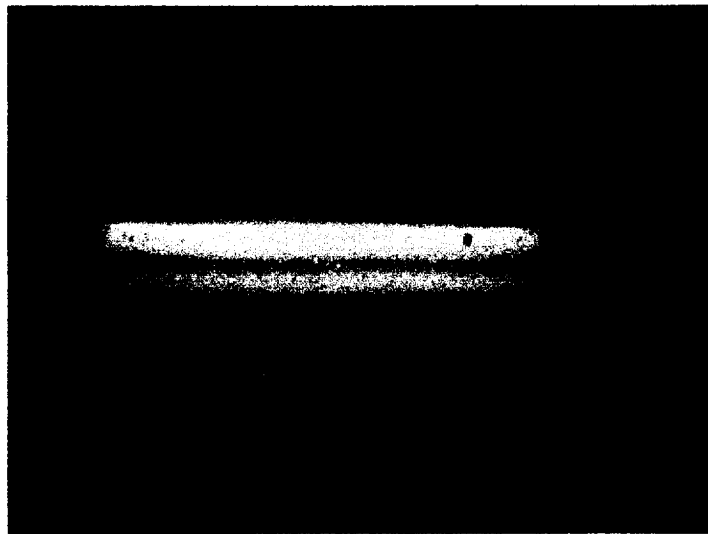Figure 12. A PLZT Bar Which is Being Stressed at the Bottom
Fulcrum Point With a Rainbow Actuator, Putting Tensile
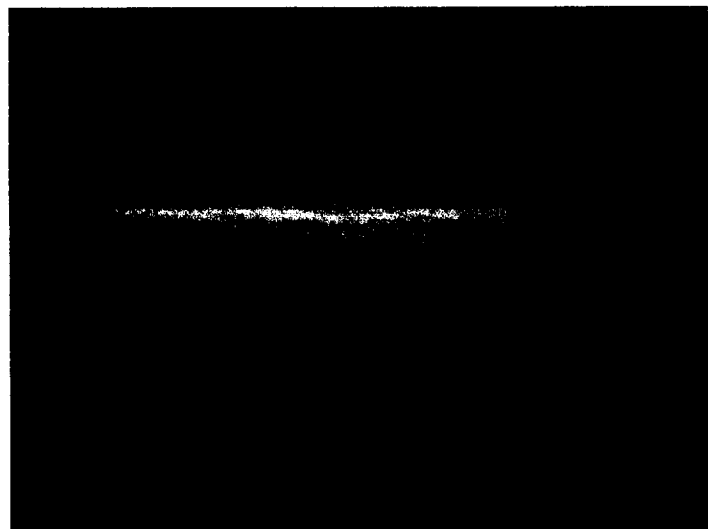Stress on the Top and Compressive Stress on the Bottom.

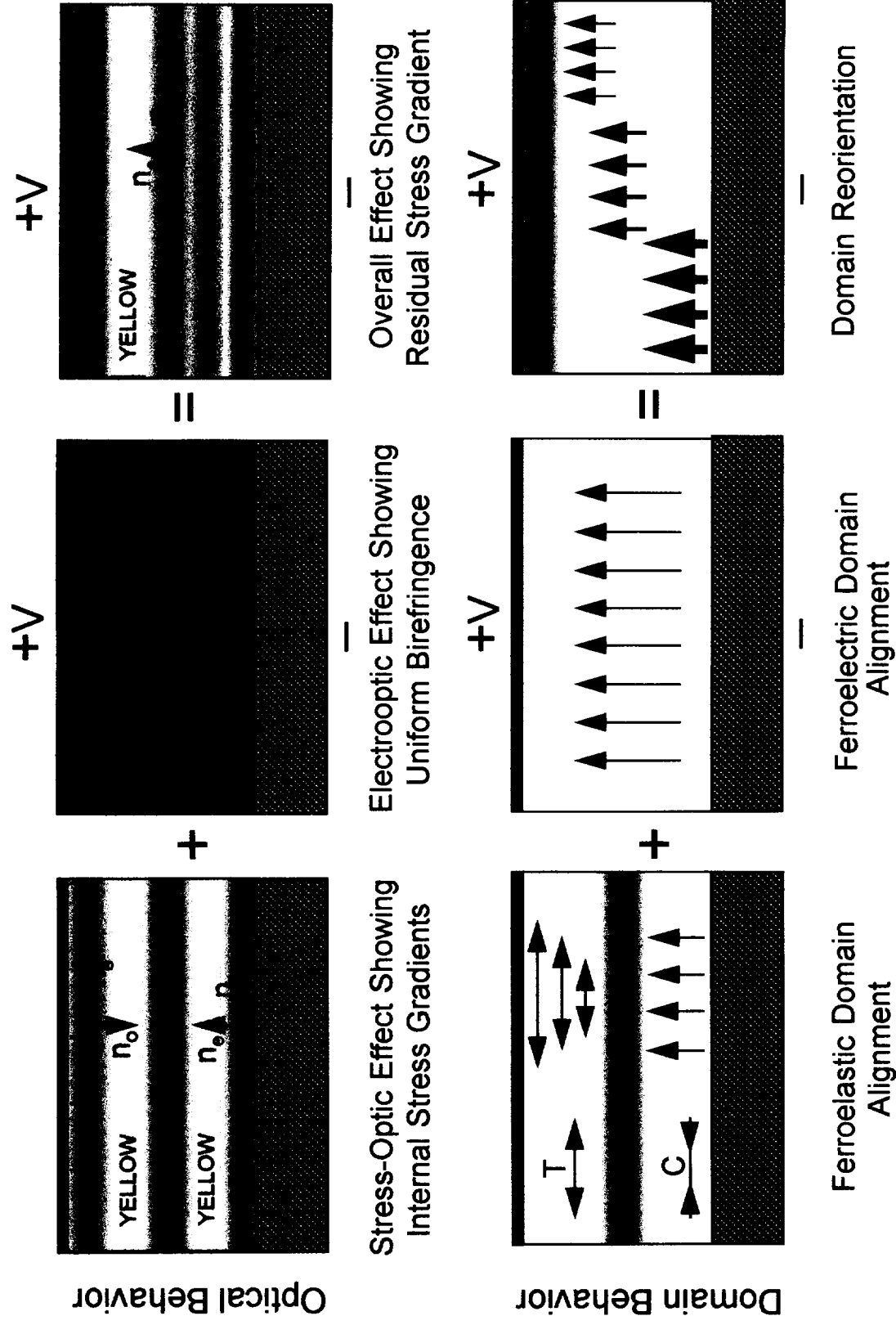Figure 13. The Same Bar as Above With Voltage Applied.

Figure 14. Explanation of Stress-Optic and Electrooptic Effects Observed in Rainbow Ceramics Before and During Application of Voltage.

Part IV.

Rainbow Actuator Stacks and Arrays

RAINBOW ACTUATOR STACKS AND ARRAYS

Gene H. Haertling

The Gilbert C. Robinson Department of Ceramic Engineering
Clemson University, Clemson, SC 29634-0907

Abstract

Various means for increasing the utility of stress-enhanced Rainbow actuators are presently under investigation. Among these are included the techniques for increased linear displacement using stacked actuators as well as matrix arrays for enhanced coverage in wide area sensor/actuator applications such as smart skins, autoleveling structures, antivibration devices and deformable coatings. The displacement characteristics of Rainbow stacks consisting of multiple clamshell units were determined as functions of voltage and load bearing capability. Total displacements were found to scale linearly with the number of Rainbow units. Conformal Rainbow arrays, composed of individual elements sandwiched between outer lead foil skins, were fabricated and qualitatively evaluated.

Introduction

Previous work on high displacement Rainbow actuators has shown that they possess the capability to be configured into linear stacks for higher displacement devices or into larger area arrays for actuator/sensor functional components. The subject of this investigation was to further demonstrate this capability by constructing working models of each type, i.e., actuator stacks and arrays. Since it is already known that individual Rainbow actuators elements have the ability to achieve high electromechanical displacements (up to 200 microns for a 31.75 mm dia. x 0.5 mm thick wafer) with unipolar voltage (450 volts) and twice that amount for bipolar operation in a dome mode, the present work focused on linearly stacking several Rainbow elements together in multiple groups of two in a clamshell arrangement and then bonding them together into a single unit. Sending/receiving arrays, on the other hand, were individually placed side-by-side in order to maximize their area while minimizing their thickness. Thus, stacks consisted of Rainbows arranged mechanically in series and electrically in parallel while arrays were Rainbows arranged both mechanically and electrically in parallel.

Experimental

The materials chosen for this study were fully dense, hot pressed PLZT 1/53/47 and 8.5/65/35 having grain sizes of about 8 microns. Wafer diameters ranged from 12.7 mm to 31.75 mm and thicknesses from 0.5 mm to 1.125 mm. For Rainbow processing, the lapped, planar wafers were placed on a graphite block and introduced into a furnace previously heated to 975°C. After 1.25 hr. at temperature, the assembly was removed and allowed to cool to room temperature. Epoxy Ag electrodes were then applied. Each Rainbow wafer was evaluated and tested prior to assembly into a stack or array.

For stacks, Rainbow wafers were bonded together in units of two, as in a clamshell arrangement. These clamshell units, in turn, were bonded together to form a complete stack which would usually consist of four to eight clamshells. All Rainbow elements in the stack were then electrically connected in parallel for final evaluation. Typical examples of stacks are shown in Figure 1.

For arrays, Rainbow wafers were laid out in a square or rectangular pattern and bonded to a supporting lead foil (0.2 mm thick) with electrically conducting Ag epoxy. A matching piece of lead foil was then placed on top of the element array and bonded to the array with conducting Ag epoxy. An insulating spacer

was also sandwiched between the two lead foils in order to prevent shorting. The two outer lead foils served as the electrodes for the array. Lead foil was selected as the supporting material because of its high ductility which allowed the final assembly to be used as a conformal actuator/sensor when mated to either a flat and/or curved surface. Process steps for assembly of the arrays are shown in Figures 2 and 3. Electrical continuity was verified after final assembly by means of an audio output from a radio or tape recorder as illustrated in Figure 4.

Results and Discussion

The characteristics of the PLZT 1/53/47 and 8.5/65/35 Rainbow stacks were evaluated as a function of voltage and load bearing capability. These data are shown in Figures 5, 6, 7, 8, 9 and 10. First, it can be seen that bipolar operation always achieves higher displacement but at the expense of higher non-linearity. Secondly, in unipolar operation the SFE, relaxor 8.5/65/35 material achieved higher displacements and could sustain higher loads than the FE 1/53/47 material; however, in bipolar operation the FE 1/53/47 was found to be superior in terms of displacement. And thirdly, small compact actuators, 12.7 mm dia. x 24 mm long, are capable of achieving moderate displacements (380 um) under modest loads of one kg. or less. This 8-unit 1/53/47 stack also achieved 635 um

displacement with no loading and 180 um with 3.5 kg point load. A similar stack with dimensions of 31.75 mm dia. and 35 mm long, using 1.125 mm thick, wafers achieved 318 um displacement with a point load of 5.5 kg. In general, total displacements were found to scale linearly with the number of individual Rainbow elements.

Three different Rainbow arrays (9.5x11, 11.5x16, and 14x17 cm) consisting of 42 ea. 12.5 mm dia. elements, 18 ea. 31.75 mm dia. elements and 20 ea. 31.75 mm dia. elements, respectively were fabricated and evaluated for sensor and actuator functions. The sensitivity and output from the arrays emulated these same characteristics from the individual elements.

Acknowledgments
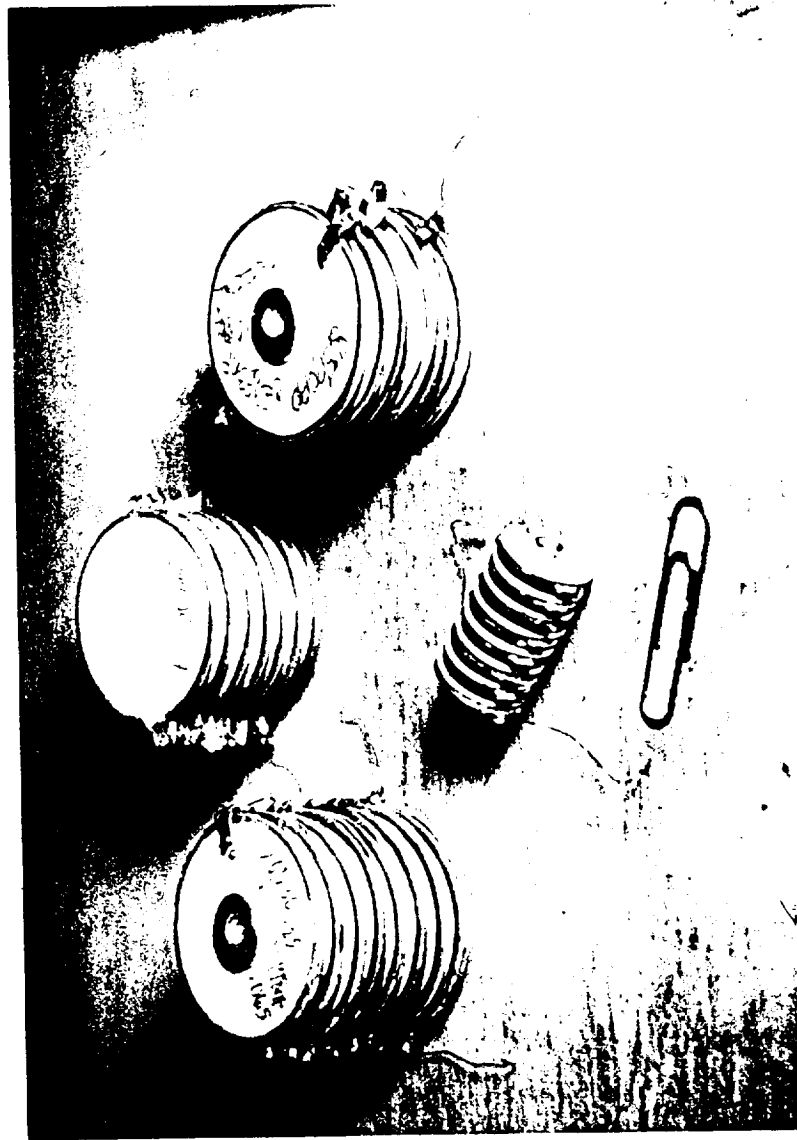
Typical Examples of Rainbow Actuator Stacks for Amplified Displacement

Figure 1
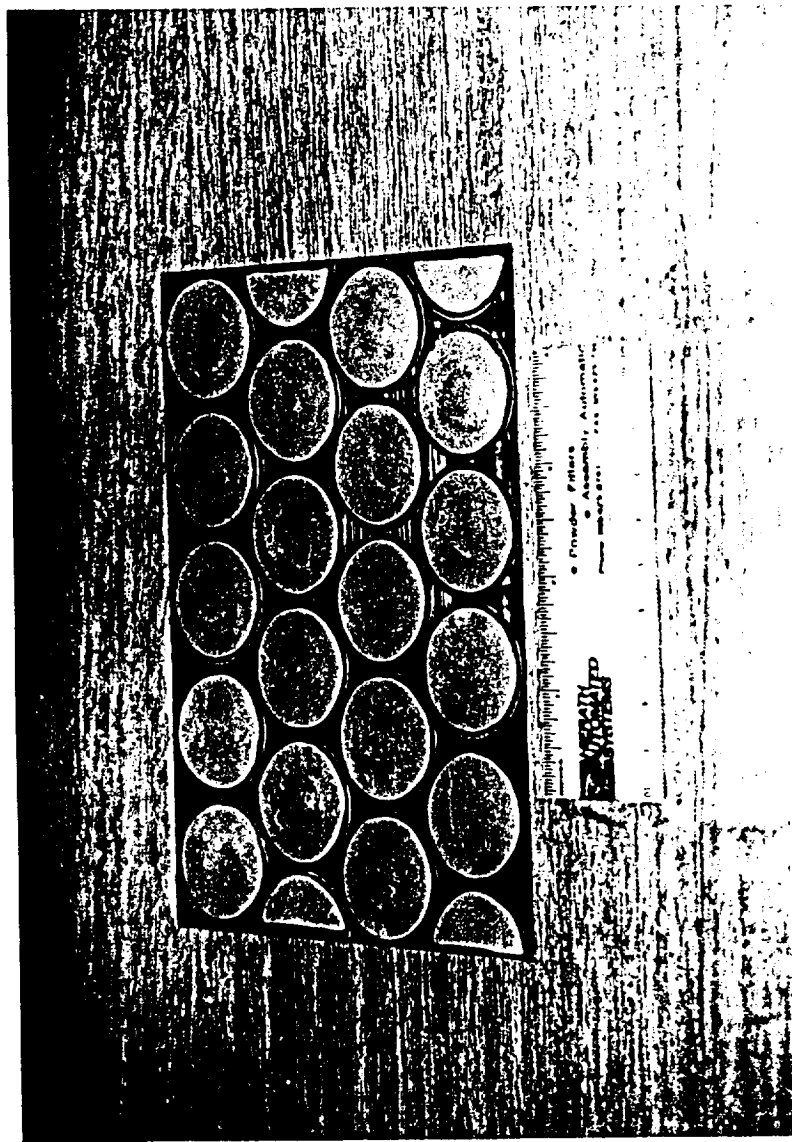
Rainbow Elements in a Rectangular Array with Top Layer Missing

Figure 2
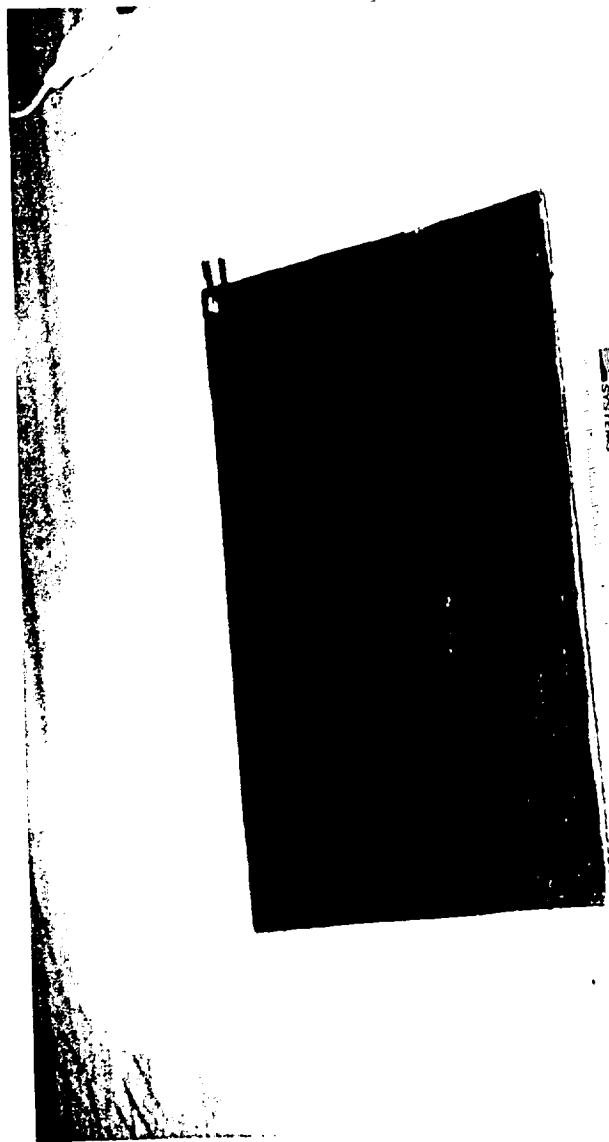
Fully Assembled Rainbow Actuator/Sensor Array

Figure 3
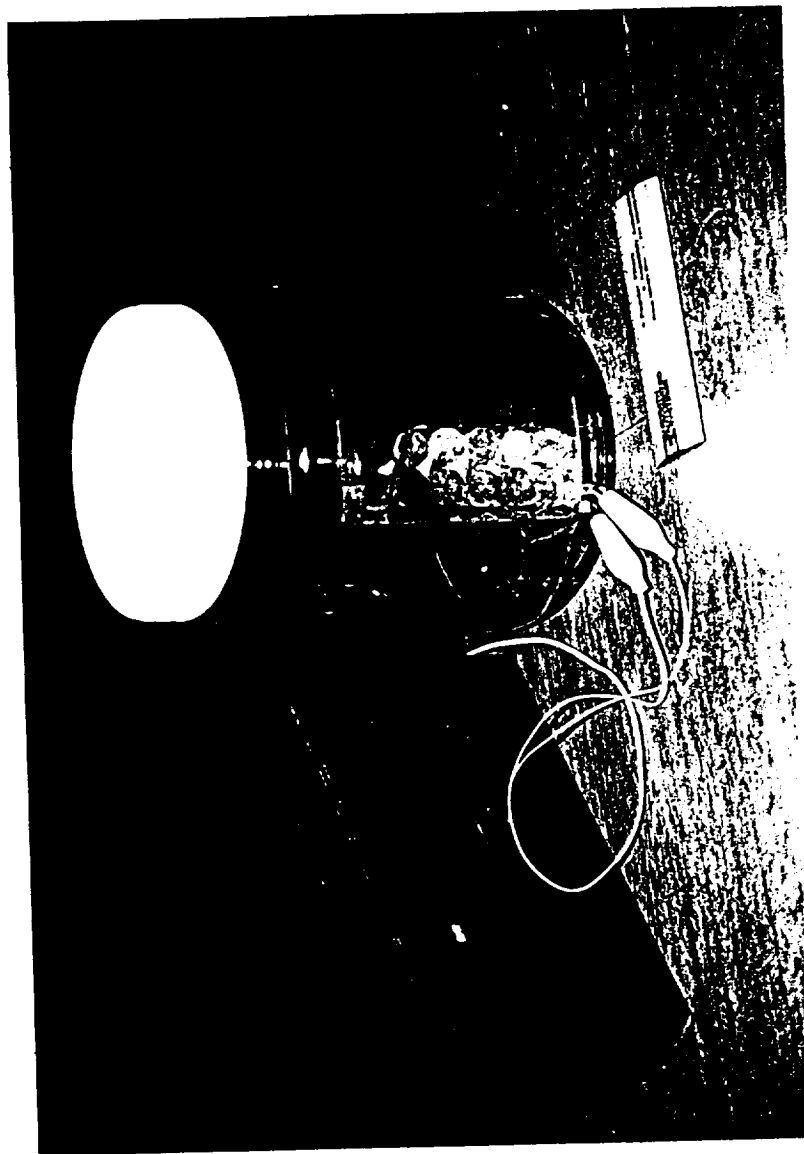
Rainbow Conformal Array Mounted on a Curved Surface

Figure 4
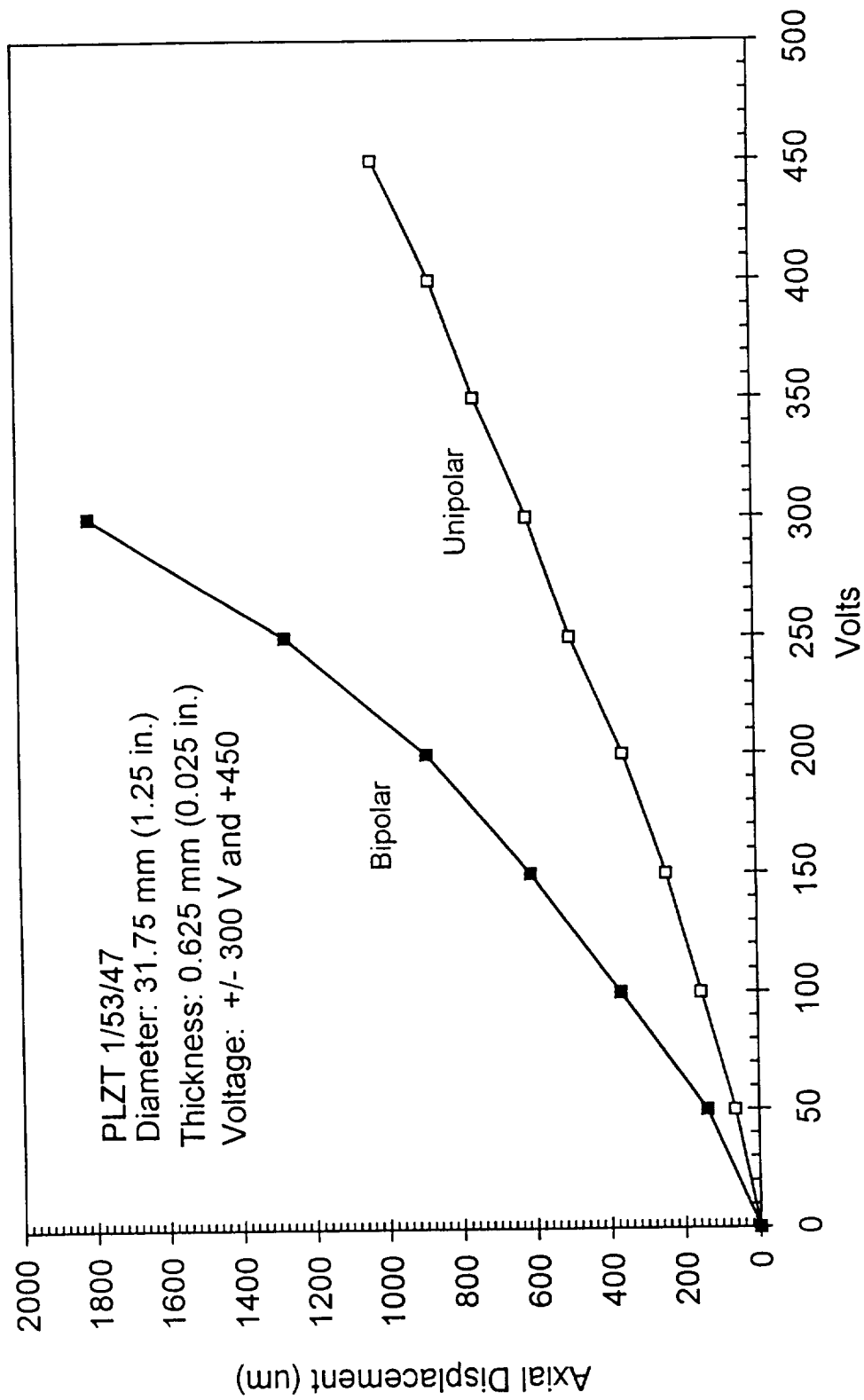
Figure 5. Axial Displacement as a Function of Bipolar and Unipolar Voltage for a PLZT 1/53/47 Eight-Unit Clamshell Rainbow Actuator with No Load
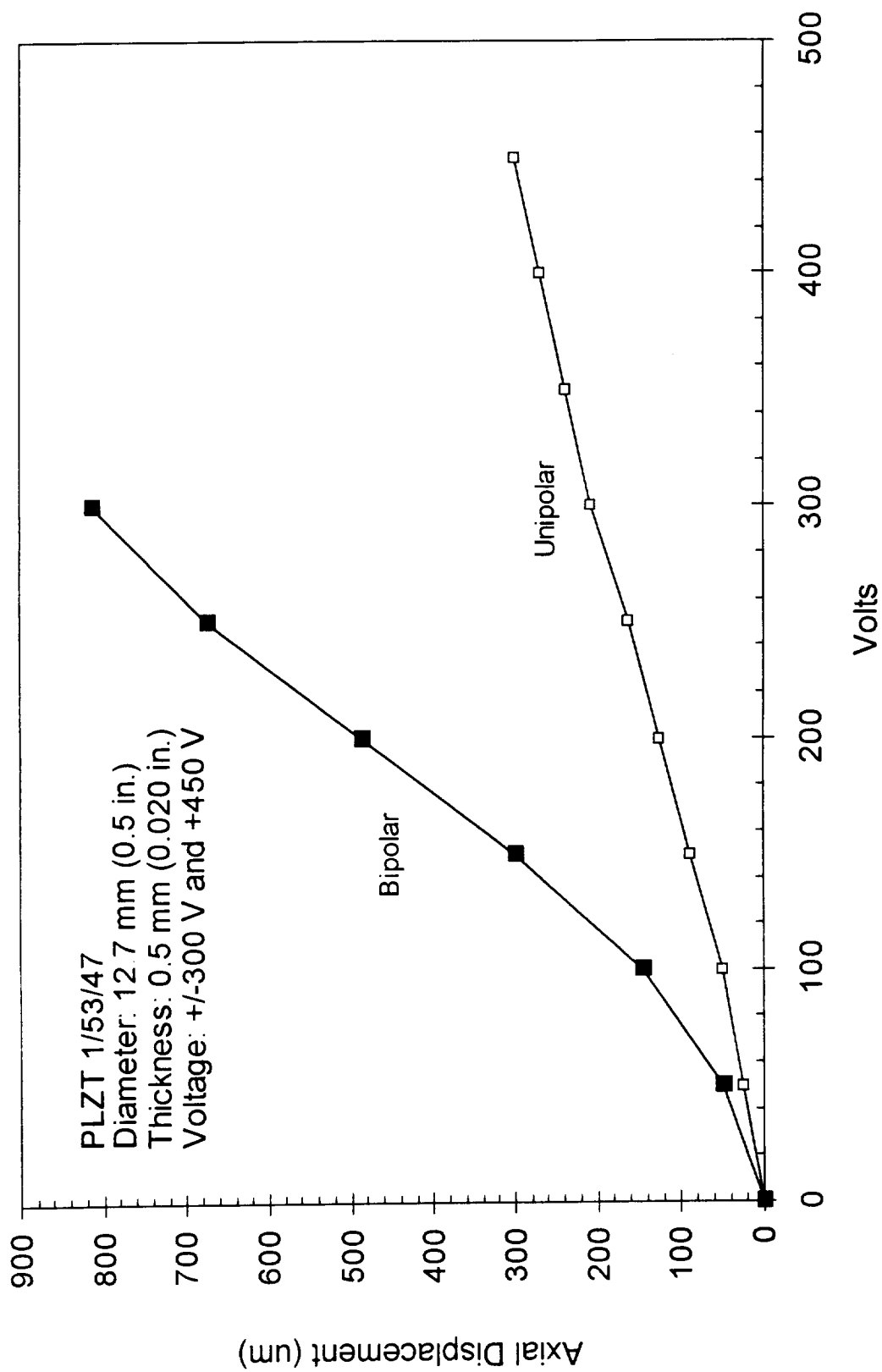
Figure 6. Axial Displacement as a Function of Bipolar and Unipolar Voltage for a PLZT 1/53/47 Eight-Unit Clamshell Rainbow Actuator with No Load, 12.7 mm diameter
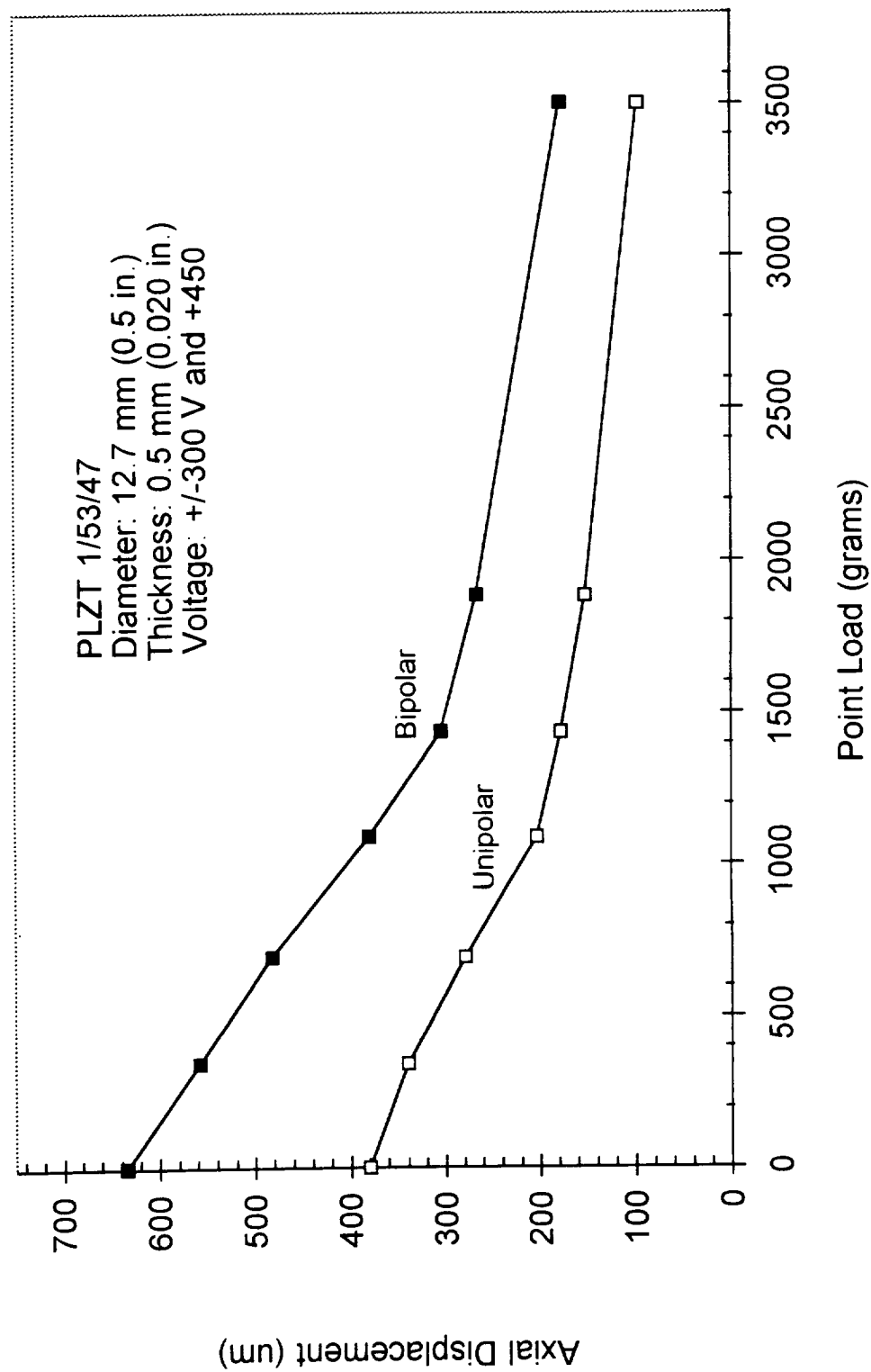
Figure 7. Effect of Point Load on Axial Displacement of a PLZT 1/53/47 Eight-Unit Clamshell Rainbow Actuator, 12.7 mm diameter.

PLZT 1/53/47
Diameter: 31.75 mm (1.25 in.)
Thickness: 1.125 mm (0.045 in.)
Voltage: +/- 350 V and +600V

Unipolar

Bipolar

Axial Displacement (um)

Volts
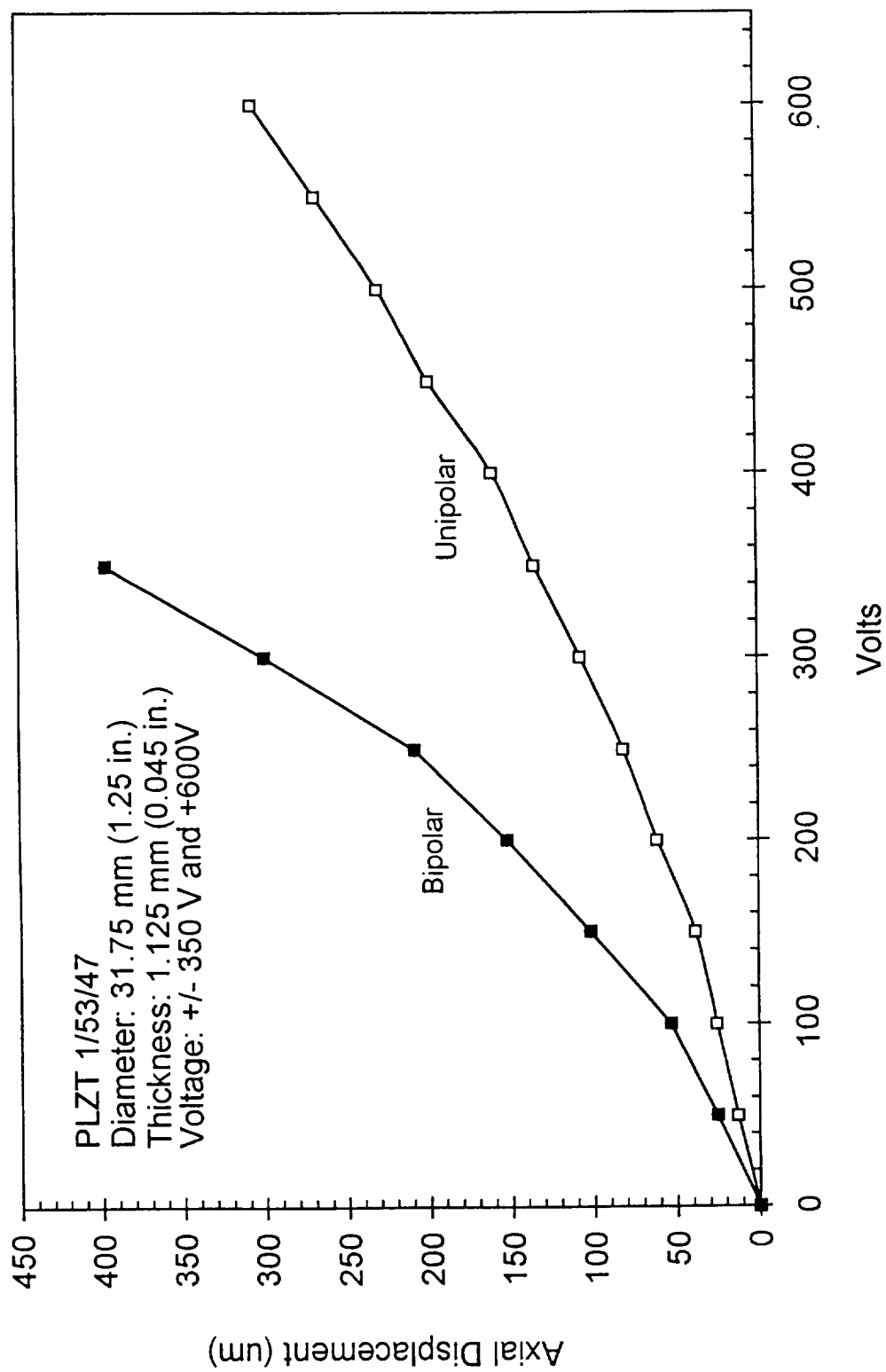
Figure 8. Axial displacement as a Function of Bipolar and Unipolar Voltage for a PLZT
1/53/47 Eight-Unit Clamshell Rainbow Actuator with No Load
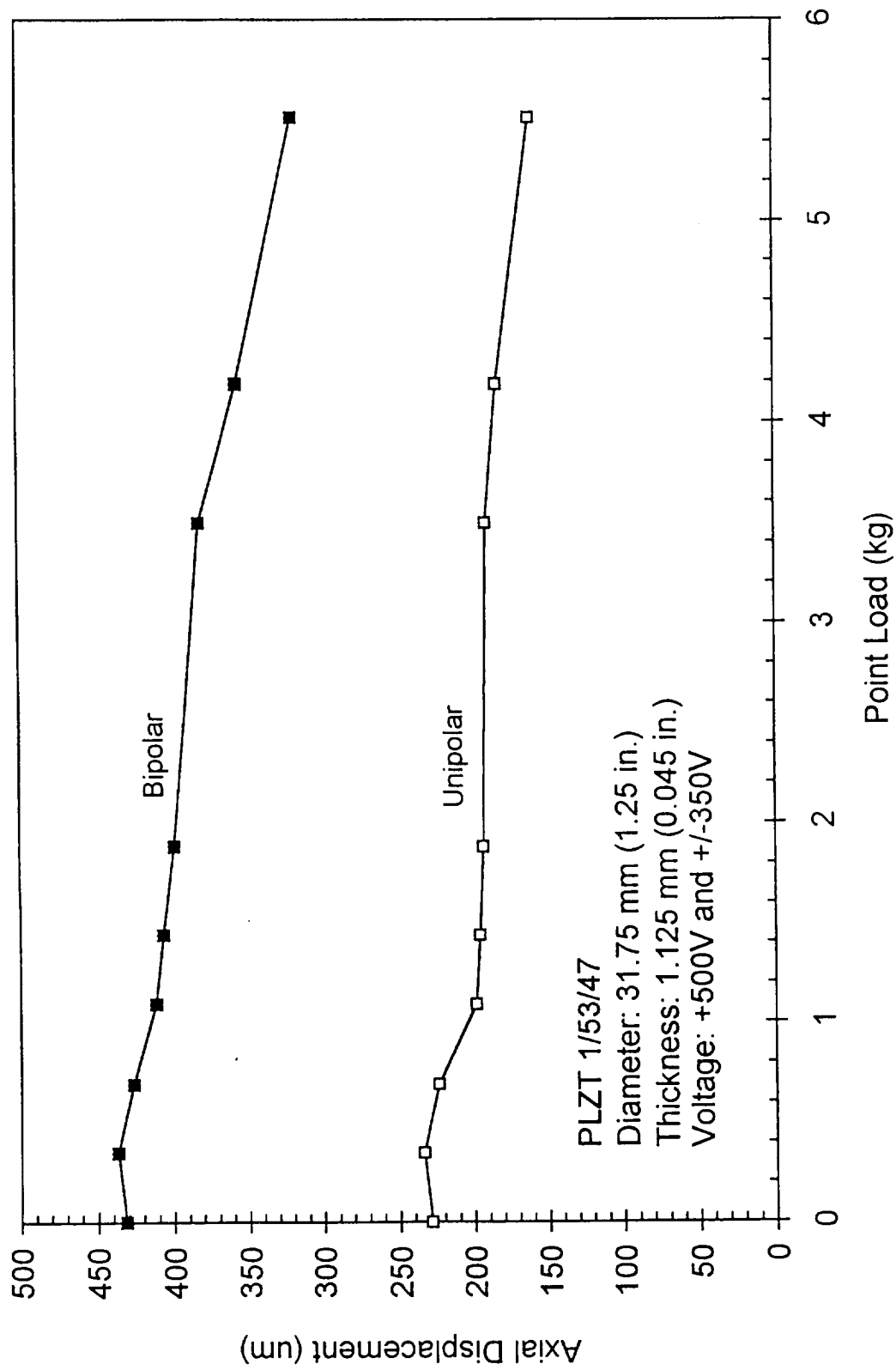
Figure 9. Axial displacement as a Function of Point Load for a PLZT 1/53/47 Eight-Unit Clamshell Rainbow Actuator Operated +500V (Unipolar) and +/- 350V (Bipolar)

PLZT 1/53/47
Diameter: 31.75 mm (1.25 in.)
Thickness: 1.125 mm (0.045 in.)
Voltage: +500V and +/-350V

Bipolar

Unipolar

Point Load (kg)

Axial Displacement (um)
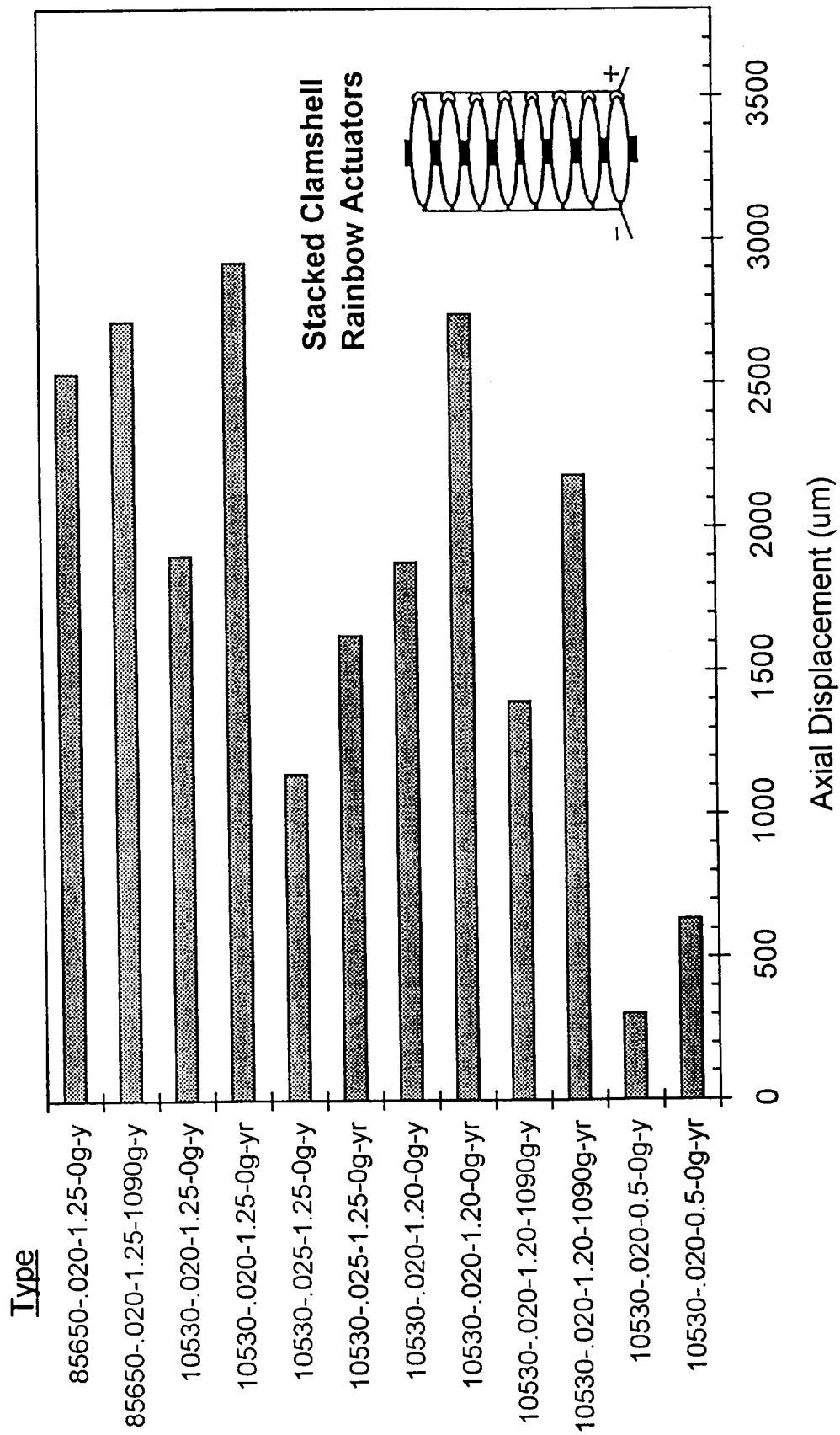
Figure 10. Displacement Characteristics of Various Types of Eight-Unit Rainbow Clamshell Actuators; Type Legend: Composition/Wafer thickness/Wafer diameter/Point load/Bipolar (yr) or Unipolar (y) voltage displacement

Conclusions

1. PLZT Rainbow clamshell stacks are a viable means for achieving both high displacement and high load bearing capability

2. When arranged mechanically in series and electrically in parallel, total displacements were found to scale linearly with the number of individual Rainbow units.

3. The SFE 8.5/65/35 Rainbows achieved higher diplacements and could sustain higher loads that the FE 1/53/47.

4. Rainbow arrays are useable and effective as conformal smart (send/receive) skins.

Part V.

Publications

Gene H. Haertling

Gilbert C. Robinson Department of Ceramic Engineering

Clemson University, Clemson, SC 29634-0907

Abstract -- On-going studies have shown that the PLZT compositional system is one which yields materials possessing some of the highest coefficients for piezoelectric and electrostrictive actuators. It has also been found that PLZT ceramics are near ideal for achieving the ultra-high displacements recently reported for the Rainbow (Reduced and INternally Biased Oxide Wafer) actuators. In order to determine the optimum composition or compositions for these Rainbow actuators, a study was conducted by preparing and processing selected formulations throughout the PLZT system. Results from this study indicate that, like the conventional direct extensional-mode materials, the maximum Rainbow bending displacements occur in materials located compositionally at the morphotropic $(FE_{rhomb} - FE_{tet})$ and Curie point (FE - PE, PE - AFE) phase boundaries. Examples of specific compositions for each of these regions are 2/53/47, 9/65/35 and 8.5/70/30 (La/Zr/Ti), respectively. Microstructural (grain size), electrical (dielectric constant, dissipation factor) and electromechanical (axial displacement) data are presented for selected compositions in the system.

INTRODUCTION

It has long been known that the PLZT compositional system is a very versatile one which yields materials possessing maximum dielectric properties and some of the highest known electromechanical coefficients for piezoelectric devices such as speakers, hydrophones, ignitors, accelerometers, motors, sensors and actuators [1-2]. In general, these optimum properties are found in materials located compositionally along the morphotropic (MPB) phase boundary $(FE_{th} - FE_{tet})$ separating the rhombohedral and tetragonal ferroelectric phases, as shown in Figure 1 by the double cross-hatched region. Other properties of interest (e.g., pyroelectric and electrooptic) are optimized in compositions located along the boundaries separating the FE polar phases from the antiferroelectric (AFE) and paraelectric (PE) non-polar phases. Compositions which typify these materials are more popularly known as electrostrictive relaxors and are indicated in Figure 1 by the single cross-hatched region identified as the SFE (slim FE hysteresis loop) region [3].
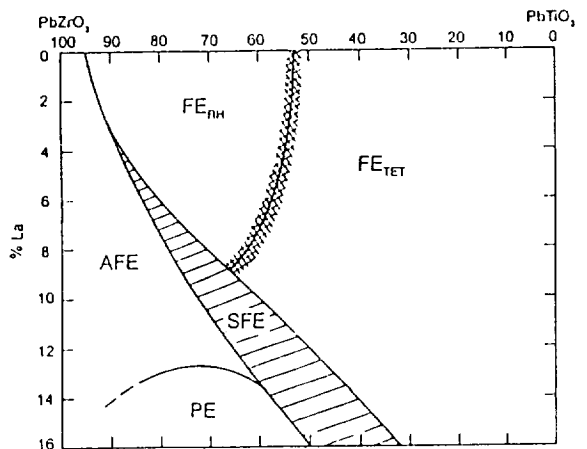

Figure 1. Room temperature phase diagram of the PLZT system showing phase stability regions and phase boundaries of interest.

Although the PLZT relaxor materials were developed over two decades ago for electrooptic applications such as shutters, displays and modulators, they have now been found to be quite suitable for electrostrictive actuator devices where non-memory, lower hysteresis properties are required.

Also, it has recently been reported that PLZT ceramics are excellent materials for achieving ultra-high displacements when they are processed into Rainbow actuator benders which are similar in operation to the unimorph benders with the exception that the Rainbows are a monolithic structure [4-5]. As single-element Rainbows, the PLZT materials are able to achieve very high displacements (up to 3mm) at moderate loading or lesser displacements at loads of up to 10 kg. A variety of applications are foreseen for these devices, however, before they can be developed it is necessary that the phenomena producing the high displacement in these materials be understood more thoroughly and that the composition of the material selected for a given application be the optimum one.

Therefore, it is the purpose of this investigation to (1) study the characteristics of a broad range of compositions in the PLZT solid solution system as Rainbow benders, (2) identify specific compositions with maximum displacement properties and (3) gain more insight into the strain amplification mechanisms involved in the Rainbow ceramics.

EXPERIMENTAL PROCEDURE

Several series of compositions in the PLZT system were prepared from the raw material oxides via a conventional mixed oxide process as outlined in the flowsheet of Figure 2. These
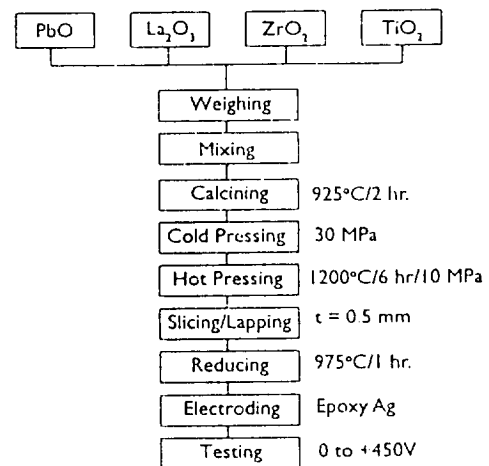
Figure 2. Flowsheet for Rainbow process.

compositions, compounded according to a B-site formula[3], ranged in Zr/Ti ratio from 90/10 to 30/70 and La content from 1 to 15 atom percent. A total of sixty individual compositions were formulated, weighed, wet mixed with distilled water, dried and calcined at 925°C for 2 hours in closed alumina crucibles. The milled and dried powders were first cold pressed as pre-form slugs and then hot pressed at 1200°C for 6 hours at 10 MPa. This procedure yielded a fully dense material with grain sizes

varying from 1.5 to 6 microns. Subsequent steps in the fabrication of the wafers included slicing and lapping them to a thickness of 0.5 mm.

A Rainbow was produced from a lapped part by placing the wafer on a flat graphite block which was supported on a zirconia carrier plate. A second zirconia plate of the same size as the wafer was placed on top of the wafer in order to shield the top side of the wafer from chemical reduction and to minimize thermal shock to the part during processing. The assembly was placed into a furnace preheated to 975"C and held there for one hour, removed from the furnace while hot and cooled naturally to room temperature in about 45 minutes. When cool, the dome shaped wafer was lifted from the graphite block, sanded lightly on the reduced (concave) side to remove any metallic lead particles and to expose the reduced layer, and then electroded with DuPont 5504N epoxy silver paint cured at 200°C for 30 minutes. Although a silver electrode was applied to the reduced side of the wafer, it was used primarily to insure good electrical contact to the conductive reduced PLZT which actually was the bottom electrode. Since the reduced PLZT layer was measured to be 0.15mm thick for the selected reducing conditions, the net thickness of the PLZT piezoelectric was 0.35mm.

Standard electrical measurements of capacitance (1 kHz), dissipation factor and dc hysteresis loops were run on all of the samples after electroding. Displacement measurements were usually made using a positive pulse voltage source and a mechanical dial indicator [8], however, selected tests were also run using a LVDT in order to compare results and to obtain the full displacement loop with + and - voltages.

Grain size measurements were determined from optical micrographs of polished and etched parts at a magnification of x1250 using the linear intercept method.

RESULTS AND DISCUSSION

Grain Size

Grain sizes of the hot pressed PLZT parts ranged from 1.5 microns (um) average diameter to 6.0 um. In general, the larger grain size materials were found to be located along each of the phase boundaries mentioned previously; i.e., between the AFE, PE and FE phases, while compositions in the interior of the phase stability regions possessed minimal grain sizes with the 4% La series having the smallest. Examples of this behavior are illustrated in Figures 3 and 4 as functions of Zr/Ti ratio and La content, respectively. The reason for this behavior is not
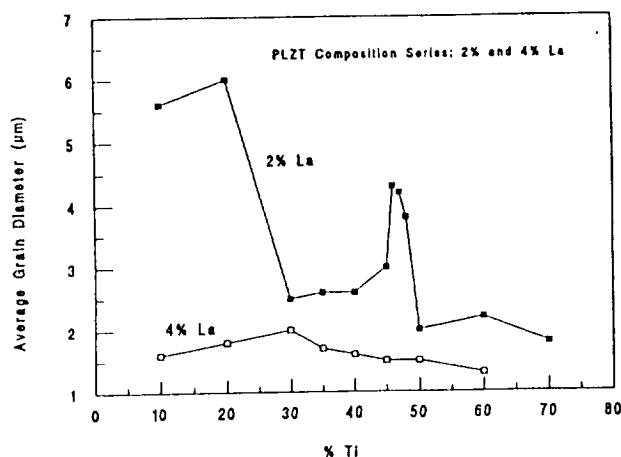

Figure 3. Grain size as a function of composition for materials in the PLZT system at 2 and 4 atom % La.
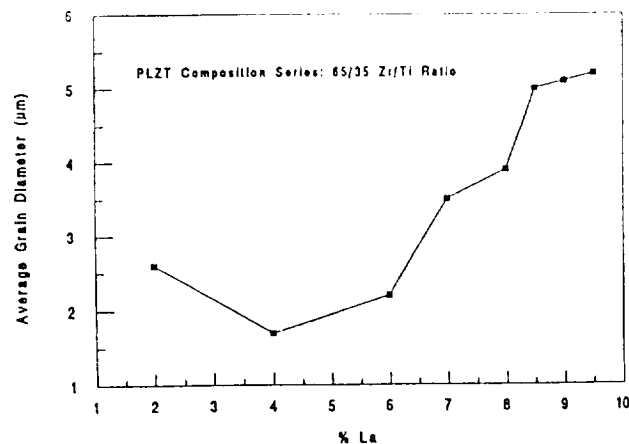

Figure 4. Grain size as a function of composition for materials in the PLZT system at a Zr/Ti ratio of 65/35.

understood at this time; however, previous experience with PLZT materials for electrooptics confirms the existence of large grain sizes (up to 15 um) for 9/65/35. Obviously, this present set of grain sizes exists for the materials hot pressed at the selected conditions, and this would change as the as the temperature or time was varied; but when comparing all compositions at the same conditions, one can only speculate at this stage that chemical and structural factors such as excess lead oxide in the B-site formula, vacancies in the lattice or mixed phases in the phase boundary compositions are instrumental in producing these results.

Grain size is an important factor in the displacement characteristics of Rainbows just as it is already known to be a significant factor in other properties of piezoelectrics such as dielectric constant, coupling and d constant. Figure 5 shows the effect of grain size on axial displacement for composition 1/53/47.
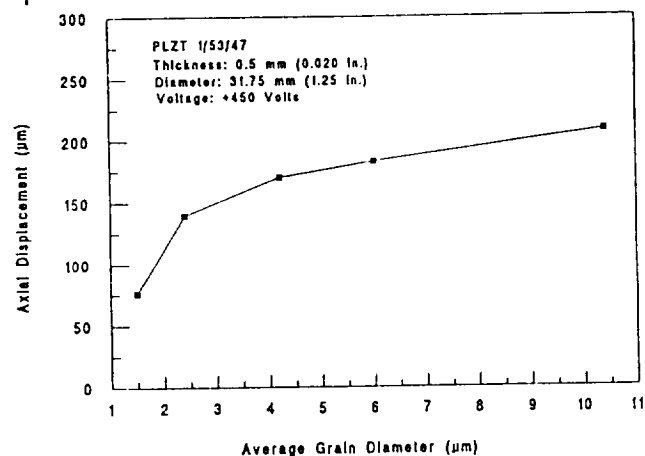
Figure 5. Grain size dependence of axial displacement for PLZT 1/53/47 Rainbow.

The grain sizes for this composition were obtained by hot pressing at temperatures from 1000 to 1200°C. As can be seen, grain sizes less that approximately 2 um lessen the displacement characteristics and those greater than about 8 microns are of little additional benefit. An optimum grain size range is estimated to be from 6 to 7 microns.

Electrical Properties

Dielectric Properties - Small-signal dielectric properties of

several compositions of varying Zr/Ti ratio at 2% and 6% La concentration are given in Figures 6 and 7, respectively. Values
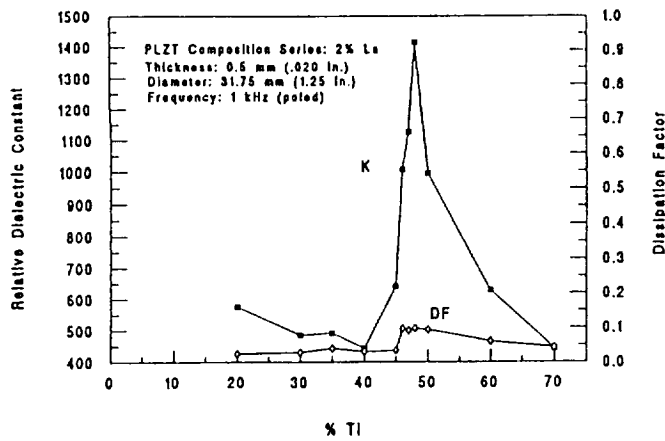
Figure 6. Small signal dielectric properties of composition series at 2% La.
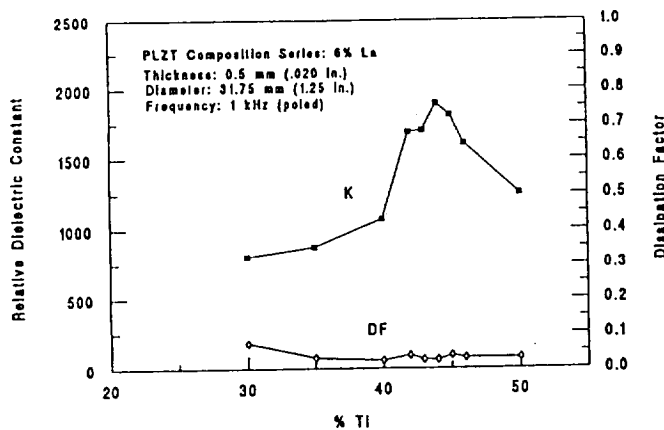
Figure 7. Small signal dielectric properties of composition series at 6% La.

Figure 8. Small signal dielectric properties of composition series at 65/35 Zr/Ti ratio.
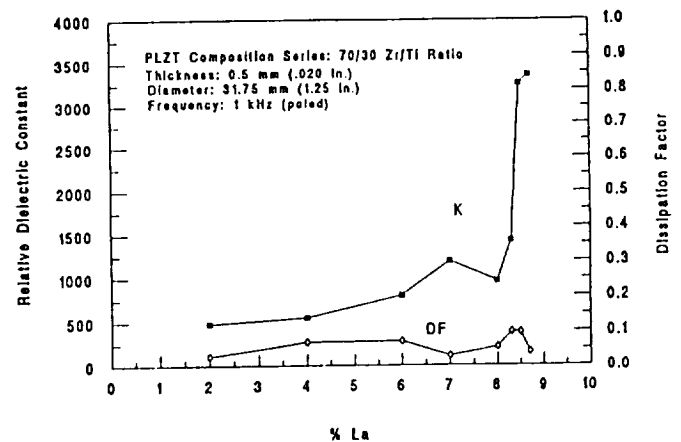
Figure 9. Small signal dielectric properties of composition series at 70/30 Zr/Ti ratio.

ranged from a low of 444 for 2/60/40 to a high of 1896 for 6/56/44. As expected, dielectric constant peaked at the MPB for both series of compositions, however, the anomaly was especially pronounced for the 2% La series. The maximum value of 1416 was possessed by composition 2/52/48. Dissipation factors ranged from 2.4% to 9.7% with the higher values occurring in the MPB compositions.

A second series of compositions with varying La contents at Zr/Ti ratios of 65/35 and 70/30 are shown in Figures 8 and 9, respectively. In this series, dielectric constants were observed to increase in a regular manner from low values at 2% La to maximum values at 8.5 - 9% La. Actual values ranged from 486 to 3264 for the 70/30 group, and the 65/35 values also fell within this range. Dissipation factors as high as 9.8% and as low as 2.8% were measured, again with the higher values occurring at the FE - AFE and FE - PE phase boundaries. These values are typical of those obtained in previous work on PLZT materials.

Hysteresis Loops - Typical examples of dc hysteresis loops for compositions 1/53/47 and 9/65/35 are given in Figure 10. The loop in Figure 10 (A) was taken on the ferroelectric Rainbow element (1/53/47) in its virgin condition before any other measurements were made. It should be noted that on the initial application of positive voltage to +450V there was approximately 60% of the total remanent polarization switched rather than the usual 50% one ordinarily observes in a virgin,

randomly oriented ceramic. This behavior is highly unusual and indicates that the Rainbow ceramic was partially poled before testing. Additional audio and piezoelectric tests of other virgin parts also indicated that the elements were partially poled to varying degrees; i.e., some very little and others as high as 75%.

One explanation for this condition occurring in the electrically virgin state is that the mechanical compressive and tensile stresses produced in the Rainbow wafer during processing are acting together to switch some of the domains in this soft ferroelectric/ferroelastic material. Since uniform stress is a
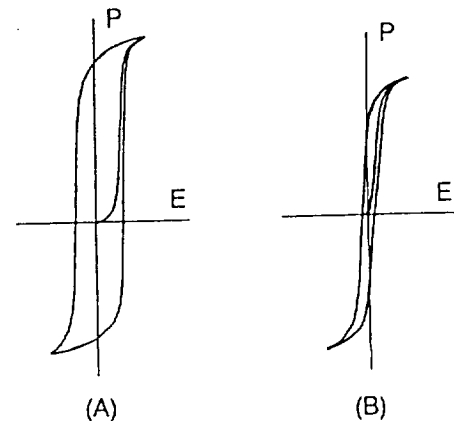
Figure 10. Typical hysteresis loops for Rainbow PLZT compositions (A) 1/53/47 and (B) 9/65/35.

symmetrical quantity, it is recognized that it alone is insufficient to produce a net polarization in a given direction even though it may be of sufficient magnitude to switch domains; however, a stress gradient such as produced by the Rainbow bending process is a vector quantity and can, indeed, produce the observed effect. This non-uniform stress is believed to be responsible for the partial poling of the Rainbow wafers.

Measured properties on the above wafer were: P_R = 44.8 uC/cm^2, E_C = 7.5 kV/cm, dielectric constant = 1210 and dissipation factor = 0.047.

The virgin loop of Figure 10(B) is a typical one for the electrostrictive (9/65/35) type of Rainbow materials and is very similar to that obtained on bulk electrooptic material. Measured properties on this wafer were: $P_{10KV/CM}$ =28.3 uC/cm^2, dielectric constant = 3142 and dissipation factor = 0.085. As a matter of course, no unsymmetrical hysteresis loops were observed in the electrostrictive materials, and none was expected, since there are no stable domains in these materials at zero electric field. Conceivably, a high enough stress could precipitate stable domains in a very near-ferroelectric material, however, a study of this effect is beyond the scope of this investigation.

Displacement Loops - Displacement vs. electric field (butterfly) loops for the Rainbow wafers described above are shown in Figure 11. As before, Figure 11(A) illustrates the Rainbow axial motion as the sample is electrically switched from zero to +450V, to -450V and back to zero, however, in this case this loop was not taken on the virgin wafer. It may be noted that this loop is remarkably similar to that observed when measuring the direct extensional (longitudinal, lateral) displacements via the piezoelectric d_{33} or d_{31} coefficients. The value of displacement in the + voltage direction was measured at 190.5 um, and the total amount of displacement (+/-) was 432 um.
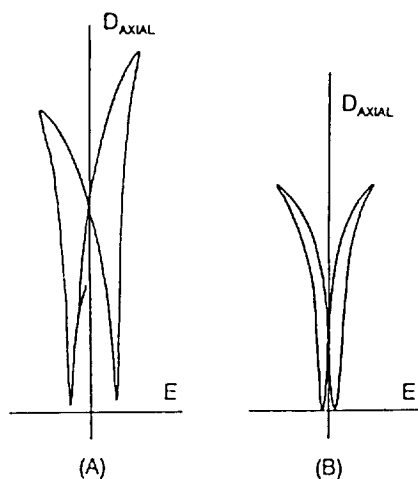

Figure 11. Axial displacement loops of samples in Figure 10.

Figure 11(B) shows the displacement loop of the electrostrictive Rainbow material (9/65/35) mentioned above. Since 9/65/35 is a relaxor material there should be little or no memory, and the same value and sign of displacement should be obtained whether a + or a - voltage is applied. One can see by switching this sample through a full voltage loop that a small amount of remanent displacement (strain) is present which is probably due to the close proximity of this composition to a FE phase. A further indication of this incipient FE phase is the higher than normal value of P_{10} (P_{10} = 28.4 vs. 18.0 uC/cm^2) as given above. Measured value of total displacement for this wafer was 178 um.

Displacement vs. Composition - Displacement data as a function of composition in the PLZT phase diagram is shown in Figure 12. In this figure, the stars indicate the location of most
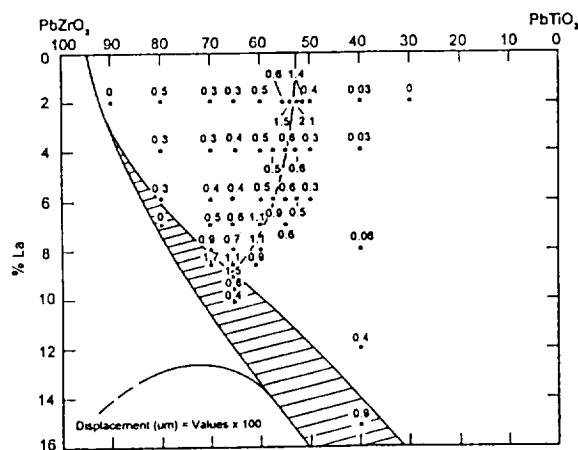
Figure 12. Rainbow displacement data for the PLZT system overlaid with the phase diagram of Figure 1 (values in microns are to be multiplied by 100).

of the compositions prepared, and the values given are those obtained from the dial micrometer measurements at zero to +450 volts. As such, they represent approximately one-half of the total switching displacement available from the FE materials but all of the displacement available from the SFE relaxor materials. It may be noted in this diagram that the maximum displacements were found to occur along the same phase boundaries mentioned previously; i.e., the FE_R - FE_T, FE - PE and FE - AFE boundaries, where other properties also are maximized. It should also be mentioned that the phase boundaries shown in Figure 12 are the same as those of Figure 1 because Figure 1 was simply overlaid on the displacement data and drawn in. The location of these boundaries were determined to be nearly identical to those which could be located by the displacement data. A comparison of these boundary locations at various levels of La are given in Table 1.

Table 1. Morphotropic phase boundary compositions determined from displacement data compared with ref. 3.

% La	PLZT (Ref. 3)	PLZT Rainbow (This Work)
2	2/53/47	2/53/47
4	4/55/45	4/55/45
6	6/58/42	6/57/43
7	7/60/40	7/61/39
8	8/62/38	8/60/40
Boundary	8.6/65/35	8.5/70/30

The values of displacement varied from essentially zero (equivalent to the direct extensional modes) to a high of 210 um for composition 2/52/48, which would indicate that maximum displacement occurs just on the tetragonal side of the MPB boundary. Other maxima occur at 9/65/35 (152 um) and 8.5/70/30 (168 um) for the electrostrictive materials at their respective boundaries. It is interesting to note that no significant anomaly or trend occurred near the AFE - FE boundary where one would expect a large electric field induced volume change in

going from a small AFE unit cell to a larger FE unit cell. For compositions 2/90/10 and 4/90/10 which are near this boundary, it was observed that the Rainbow curvature was reversed from convex up (reduced side concave) to near flat or convex down (reduced side convex). In some cases, an electroded part of this type exhibited an axial displacement which could be tested simply by turning the wafer upside down and then operating as normal. Obviously, this region of the phase diagram should be studied further, but such depth was beyond the scope of this investigation.

Some of the possible reasons for maximum Rainbow displacements to occur at phase boundaries are (1) maximum piezoelectric constants (d_{33} and d_{31}) occur at the boundary, (2) mixed or metastable phases exist, (3) maximum domain reorientation is possible, (4) higher mechanical compliance of the structure exists, (5) electric field enforced phases are possible and even probable in some cases and (6) larger grain sizes may occur in the mixed phase region at the boundary. To some degree, all of these effects are probably operative in the Rainbow devices, however, a more in-depth study is required to identify the dominant mechanisms.

Figures 13 through 17 deal with a closer look at the compositional variation of displacement as a function of Zr/Ti

Figure 15. Displacement characteristics of PLZT Rainbow ceramics as a function of La content at a 65/35 Zr/Ti ratio.

Figure 13. Displacement characteristics of PLZT Rainbow ceramics as a function of Zr/Ti ratio at selected levels of %La.

Figure 16. Displacement charcteristics of PLZT Rainbow ceramics as a function of La content at a 60/40 Zr/Ti ratio.
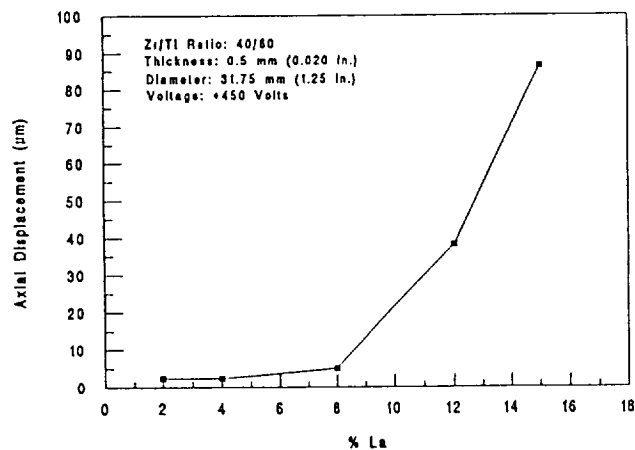
Figure 17. Displacement characteristics of PLZT Rainbow ceramics as a function of La content at a 40/60 Zr/Ti ratio.

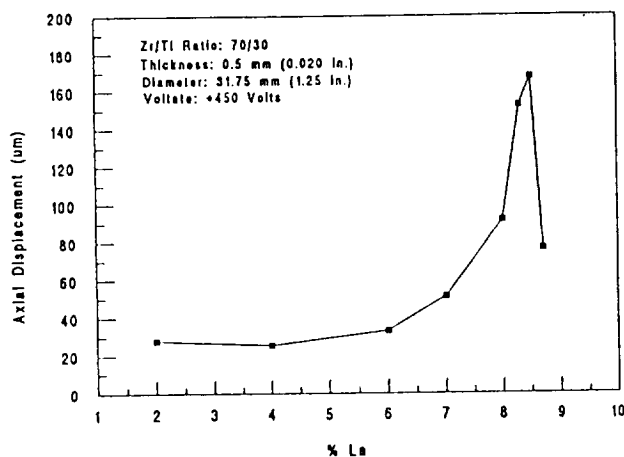Figure 14. Displacement characteristics of PLZT Rainbow ceramics as a function of La content at a 70/30 Zr/Ti ratio.

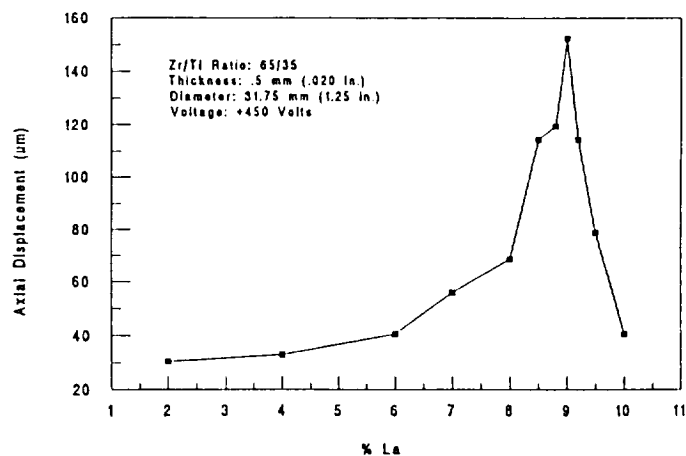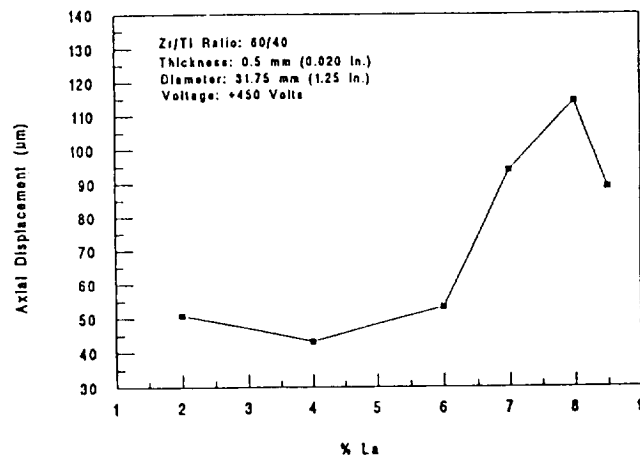ratio (% Ti) at several levels of La concentration or of % La at several different Zr/Ti ratios. Each of these figures again emphasizes the significantly larger displacements existing in the phase boundary compositions.

CONCLUSIONS

This investigation indicates that the PLZT compositional system is a very fruitful area for producing and studying the unique characteristics of the Rainbow ceramics. No difficulty was experienced in fabricating any of the compositions into Rainbow wafers with the exception of four compositions near the AFE - FE phase boundary.   The results of this investigation clearly show that (1) maximum axial displacement is obtained in compositions in or near the morphotropic phase boundary or the phase boundary separating the FE phases from the non-polar (AFE, PE) phases, (2) grain size is a factor in achieving high displacement, i.e., larger grain size is desirable, (3) the compressive and tensile stresses produced in the Rainbow process are instrumental in partially pre-poling the Rainbow ceramic and (4) other mechanisms, in addition to the piezoelectric d_{31} coefficient, are very likely responsible for the unusually large displacements observed.   A maximum displacement of 210 microns for a single, dome-mode Rainbow ceramic was found to occur in PLZT 2/52/48 when activated from zero to +450 volts. Since all of the displacements in this investigation were obtained on Rainbow ceramics with a diameter-to-thickness ratio (31.75 mm x 0.5 mm or 63.5 to 1) conducive to producing a dome-type displacement rather than a saddle type, significantly higher displacement values are to be expected for larger diameter and thinner parts with a higher ratio [4].

REFERENCES

1. D. Berlincourt, "Current Developments in Piezoelectric Applications of Ferroelectrics," Ferroelectrics, 10, 111-119, 1976.

2. G.H. Haertling, "Piezoelectric and Electrooptic Ceramics," in Ceramic Materials for Electronics, Relva Buchanan, ed., 139-225, Marcel Dekker, Inc., New York, 1986.

3. G.H. Haertling and C.E. Land, "Hot Pressed (Pb,La)(Zr,Ti)O$_3$ Ferroelectric Ceramics for Electrooptic Applications," J. Am. Ceram. Soc., 54, 1-11, 1971.

4. Gene H. Haertling, "Rainbow Ceramics - A New Type of Ultra-High-Displacement Actuator," Bull. Am. Ceram. Soc., 73, 93-96, 1994.

5. Gene H. Haertling, "Chemically Reduced PLZT Ceramics for Ultra-High Displacement Actuators," Ferroelectrics, 154, 101-106, 1994.

The Dielectric, Piezoelectric and Hydrostatic Properties of PLZT Based Rainbow Ceramics

S. Sherrit, H.D. Wiederick and B.K. Mukherjee
Royal Military College of Canada, Kingston, Ontario K7K 5L0, Canada

and

G.H. Haertling
Clemson University, Clemson, South Carolina 29634-0907, USA.

ABSTRACT

It has recently been shown that the selective reduction of one surface of a high-lead-containing piezoelectric or electrostrictive ceramic wafer results in a stress-biased wafer with a unique domed structure that leads to high electromechanical displacement and enhanced load-bearing capability. These ceramics have been called rainbow ceramics and their very high displacements make them very promising materials for transducers and actuators. The dielectric, piezoelectric and hydrostatic properties of a variety of PLZT based rainbow ceramics have been measured and analysed. The samples exhibited a strong piezoelectric effect in the poling direction (effective d_{33} of the order of 10^{-8} C/N) under low planar and hydrostatic pressures but as the pressure was increased there was a marked decrease in the strength of the piezoelectric response which passed through a minimum and then increased to the level of typical values for PZT ceramic. Some samples were plated and these had a low pressure hydrostatic voltage coefficient that was considerably greater than that of PZT along with a reasonable level of thickness mode electromechanical coupling. However, as the hydrostatic pressure was increased, the hydrostatic voltage coefficient decreased towards typical values for PZT. The rainbow ceramics show considerable promise as material for actuators and, possibly, for shallow water sonar transducers.

INTRODUCTION

A new type of ceramic bender has recently been produced by the high temperature chemical reduction of one surface of a high-lead-containing piezoelectric or electrostrictive ceramic wafer which results in a stress-biased dome like structure that is capable of achieving very high axial displacements [1]. The reduced (concave) side of the wafer can serve as one of the electrodes. This type of ceramic has been called a "rainbow" (reduced and internally biased oxide wafer) ceramic. When a voltage is applied to a rainbow ceramic, the dome height varies as a function of the magnitude and polarity of the voltage and this motion is largely a consequence of the lateral contraction produced in the material due to the lateral piezoelectric coefficient d_{31}. Rainbow ceramics have been produced using ceramics such as lead zirconate titanate (PZT), lead lanthanum zirconate titanate (PLZT) and lead magnesium niobate (PMN). Single elements of rainbow ceramics, 0.2 mm thick, have produced displacements of 1 mm which represents a very high strain of 500%. Since rainbow ceramics are also easy and cheap to produce, they show considerable promise as materials for actuators and sonar activators. This paper reports on the measurement and analysis of the dielectric, piezoelectric

and hydrostatic properties of a range of PLZT based rainbow ceramic specimens which are described in Table 1. The specimens had a lanthanum content of 1.0 % and a lead zirconate content of 53 %. The samples were 0.5 mm thick discs which were electroded with Dupont 5504N silver epoxy and they all had a dome like appearance. Samples 4 and 5 had their rims glued to 1 mm thick brass plates whose diameters are given in Table 1. A specimen without electrodes was used to determine the density which was found to be 7575 ± 100 kgm^{-3}.

Table 1: The Specimens

Sample Number	Diameter/ Plate Diameter (cm)	Plate
1	1.31	none
2	3.15	none
3	3.14	none
4	3.16 plate - 3.4	brass
5	1.31 plate - 1.32	brass

RESONANCE MEASUREMENTS

A Hewlett Packard Model 4192 Impedance Analyser was used to measure the impedance of the samples as a function of frequency. In addition to radial and thickness mode resonances, the samples showed bending mode resonances; in the case of sample 1 the bending mode resonance occurred at about 30 kHz. The impedance spectra of the samples have been analysed using Smits' method [2] and our own techniques [3] although it should be stressed that the geometry of these dome shaped samples does not correspond strictly to the geometry assumed in deriving the resonance equations. An analysis of the thickness and radial mode resonances of samples 1, 2 and 3 gave the material constants shown in Tables 2 and 3 in which the symbols used have the usual definitions as given in the IEEE Standard on Piezoelectricity [4]. These tables show that there are large differences in the material constants measured for the various samples and this is likely to be due to small differences in the curvatures and aspect ratios of the dome shaped samples. The curvature is a result of the reduction process and small variations in composition and processing conditions would produce differences in

Table 2: Thickness mode material constants measured at 4 MHz and 20°C

	Sample 1	Sample 2	Sample 3
k_t	0.359(1 - 0.12i)	0.355(1 - 0.31i)	0.327(1 + 0.12i)
c_{33}^D (10^{11}N/m^2)	1.35(1 + 0.020i)	1.06(1 + 0.069i)	1.19(1 + 0.068i)
ε_{33}^S (10^{-9}F/m)	6.39(1 - 0.33i)	6.87(1 - 1.1i)	11.3(1 - 0.35i)
h_{33} (10^9V/m)	1.62(1 + 0.049i)	1.23(1 + 0.15i)	0.99(1 + 0.33i)

Table 3: Radial mode material constants measured at 20°C

	Sample 1	Sample 2	Sample 3
s_{11}^E (10^{-11}m^2/N)	1.55(1 - 0.023i)	1.81 (1 - 0.023i)	2.15(1 - 0.038i)
s_{12}^E (10^{-11}m^2/N)	-0.517(1 - 0.023i)	-0.742(1 - 0.023i)	-1.22(1 - 0.038i)
d_{31} (10^{-12}C/N)	-140(1 - 0.088i)	-123(1 - 0.085i)	-83(1 - 0.22i)
ε_{33}^T (10^{-9}F/m)	13.3(1 - 0.0915i)	11.6(1 - 0.077i)	7.8(1 - 0.21i)
σ^p	0.334	0.410	0.566
k_p	0.52(1 - 0.043i)	0.48(1 - 0.047i)	0.43(1 - 0.11i)

the curvatures of the samples which would significantly affect the material constants.

In Figure 1, which shows the thickness resonance of sample 1, the experimental points are compared to the fit obtained by using the material constants found for this sample. It can be seen that the fit is acceptable around the fundamental mode but there is significant dispersion at higher frequencies. Besides, the first thickness resonance occurs close to 4 MHz and it follows that a non-dispersive material would have a second resonance at around 12 MHz whereas this occurs at about
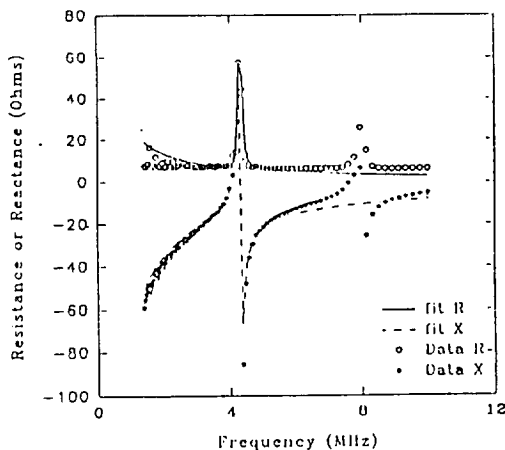

Figure 1. The resistance and reactance versus frequency for sample 1. The experimental points are compared with the lines which represent fits obtained by using the derived material constants.

7.5 MHz in the figure. Finally the figure shows that the baselines for the data and the fit differ substantially at frequencies higher than the first resonance frequency. All of this evidence points to a significant dispersion in the dielectric, elastic and piezoelectric constants of the material.

Another interesting feature is that the second thickness mode resonances of the larger samples are inductive and yield negative values of permittivity; this is due to the high conductivities of these samples at high frequencies.

Samples that were bonded to plate electrodes had thickness resonances that saturated the measuring circuit while their radial modes were smaller than those for the unbonded samples. This suggests that the electrode plate acts to clamp d_{31} more than d_{33} with a resulting enhancement in k_t.

DIELECTRIC MEASUREMENTS

The capacitances of the specimens were measured at a frequency of 1000 Hz at room termperature. The average values for the permittivity, the dielectric constant and the loss tangent for samples 1, 2 and 3 are given in Table 4.

Table 4: Dielectric Constants (averaged over samples 1, 2 and 3)

Property	Units	Value
Permittivity ε_{33}^T	10^{-9} F/m	14 ± 1
Dielectric Constant K_{33}^T		1540 ± 110
Loss Tangent tan δ		0.086 ± 0.012

THE PIEZOELECTRIC CHARGE CONSTANT

The value of the piezoelectric charge constant, d_{33}, for the material was obtained by using a point force head on a Berlincourt type d_{33} meter which was operated at a frequency of 200 Hz. The value of d_{33} was found to vary over the surface of the samples; to find if this was due to coupling to the bending mode of the sample, measurements were made at 12 points spaced 1 mm apart along a diameter of the slightly domed samples. Our results for sample 1 are shown in Figure 2 where the three curves represent the values obtained (a) when the measurements were made with the curvature of the dome shaped sample facing downwards so that the sample formed a cavity with the base plate of the meter with the positive terminal at the point head (indicated as "+ up" data in the figure, (b) when the measurements were made with the sample curvature facing upwards ("+ down" data in the figure) and (c) the average of the two measurements made in (a) and (b). Figure 4 shows that the apparent d_{33} values are quite large and can reach up to 12,000 pC/N at the centre of the specimen. It is likely that this large value is due to the addition of the normal uniaxial compression of the ceramic material and the bending modes of the dome shaped sample. In order to elucidate this better the d_{33} was measured as a function of uniaxial compres
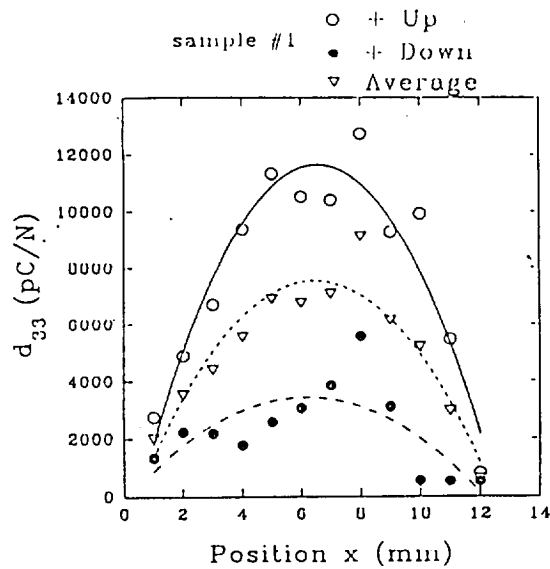
Figure 2. The effective d_{33} value as a function of distance along a diameter of sample 1. The significance of the three curves has been explained in the text.
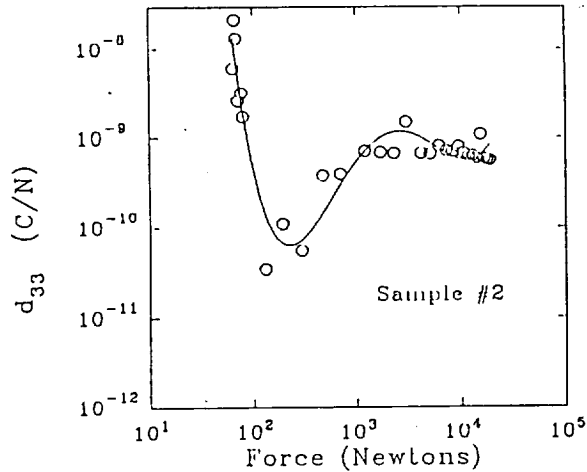

Figure 3. The effective d_{33} as a function of the compressional force applied to sample 2.

sion using a method which has been reported earlier [5]. Our results for sample 2 are shown in Figure 3 and it can be seen that d_{33} has a value of about 10,000 pC/N at low applied force but it then decreases rapidly as the dome shaped sample is flattened out as a result of increasing force and it passes through a minimum at a force of about 200N from which point it rises up to typical ceramic values as the ceramic undergoes compression. It can therefore be concluded that the large d_{33} values are indeed caused by the bending of the dome shaped sample when a stress is applied; after the rainbow material has become flat, it begins to act like a plain bulk ceramic disc.

It should be noted that the voltage - force curves of the specimens show hysteresis and this behaviour is very similar to that shown by bulk PZT discs [5]. The hysteresis is due to the time-dependence of the piezoelectric response of the rainbow ceramic.
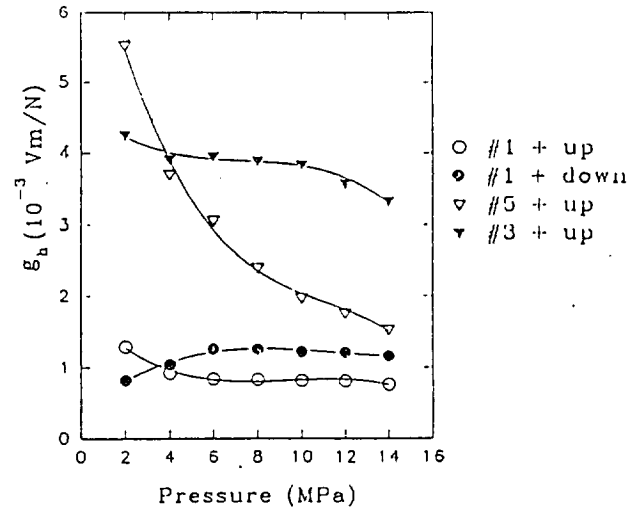

Figure 4. The hydrostatic voltage coefficient, g_h, as a function of the hydrostatic pressure for different samples and orientations.

HYDROSTATIC PROPERTIES

The hydrostatic voltage constants, g_h, of the rainbow specimens have been measured at a frequency of 400 Hz and as a function of pressure using a SENSOR g_h apparatus. Our results for samples 1, 3 and 5 are shown in Figure 4. Two series of measurements were carried out on sample 1: the results indicated by "+ up" correspond to the dome shaped sample being placed with its curvature facing down and forming a small cavity with the base plate of the apparatus while the results indicated by "+ down" correspond to the rainbow ceramic sitting on the base plate with its curvature facing up. The hydrostatic voltage response is the sum of the contributions arising from the bending of the dome shaped rainbow and the compression of the ceramic itself. In the case of sample 1, the bending effects are small since the edge of the rainbow ceramic can move laterally on the base plate and so the g_h value is close to that of standard bulk PZT ceramic. The small difference between the two series of measurements on sample 1 is probably due to the different contributions from the bending of the specimens. Samples 1 and 3 are similar in that both were not bonded to a base plate so that the hydrostatic pressures are identical on both faces and the dome does not undergo any flattening due to the hydrostatic pressures. Sample 3, which has the bigger radius, has a larger value of g_h and this is perhaps due to the larger bending deflections which are possible in this case. Sample 5 is a rainbow ceramic of the same radius as sample 1 but it is bonded to a brass plate about 1 mm thick so that the hydrostatic pressure is not now transmitted to the inner surface of the rainbow and the dome gradually flattens as the external static pressure is increased. At low pressures the flattening is negligible, but since the rim of the rainbow is bonded, the bending response to the signal is considerably greater than in the case where the rainbow is not bonded (as in sample 1) and hence the much larger value of g_h. As the pressure increases, the rainbow gradually flattens, the bending contributions decrease and the g_h value approaches that of a normal bulk PZT ceramic.
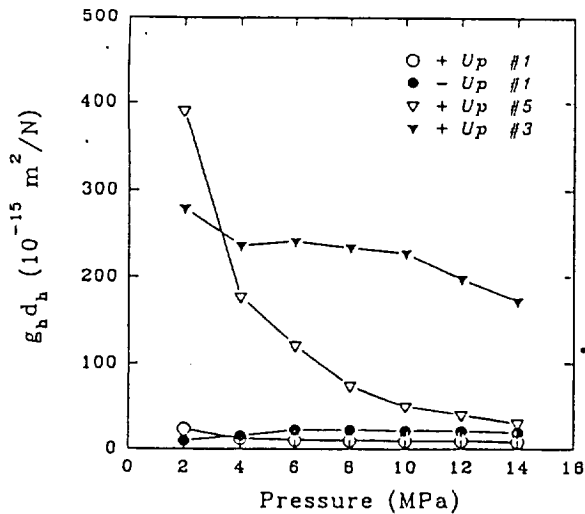
Figure 5. The hydrostatic figure of merit for samples 1, 3 and 5.

Figure 5 shows the hydrostatic figure of merit, $g_h d_h$, of samples 1, 3 and 5. The small rainbow (sample 1) has a figure of merit that is substantially lower than that of PZT while the larger rainbow ceramic (sample 3) has a figure of merit which is comparable to that of PZT.

The $g_h d_h$ values for sample 4 are shown as a function of pressure in Figure 6. This sample is a large rainbow ceramic, 3.16 cm in diameter, bonded to a 1 mm thick brass plate and its behaviour is qualitatively similar to that of sample 5 which is smaller. At high pressures the values are slightly lower than the nominal values for normal bulk PZT but they rise dramatically at low pressures. At low pressure this sample has a very high g_h value of about 0.8 Vm/N

Finally it may be noted that both Figures 3 and 6 show minima. This is explained by the fact that there are two contributions to charge generation: bending of the dome shaped samples and compression of the ceramic. These two contributions are not independent but are coupled with the strain being relieved by the bending action of the monomorph.
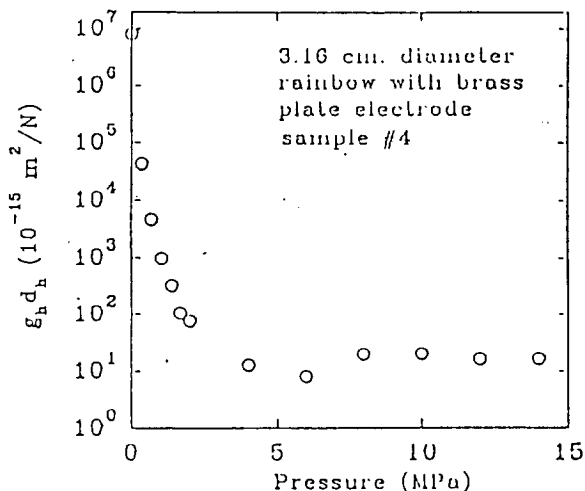
CONCLUSIONS

The set of PLZT based rainbow specimens analysed by us have shown a strong piezoelectric response under low planar and hydrostatic pressures but there is a marked decrease in the strength of the response as the pressure is increased. The larger response at low pressures is thought to be due to the bending of the samples and the consequent release of charge.

The resonance curves of the specimens were somewhat distorted by the presence of the bending modes. The material constants were determined for the radial and thickness modes of operation and these were found to exhibit geometric effects and dispersion.

The rainbow samples that were not bonded to a base plate had hydrostatic properties in the same range as ordinary bulk PLZT with some variation depending on the orientation of the sample in the measurement apparatus. However the rainbow samples that were bonded to electrode plates showed substantially better hydrostatic properties but, as the static pressure increased, these decreased to values similar to those of bulk PLZT.

The dielectric properties of the rainbow samples were similar to those of PLZT.

In conclusion, the rainbow ceramic material shows considerable promise as an actuator material where large displacements are required (solid state speakers, pumps, switches, positioners etc..) and, possibly, for shallow water sonar projectors. The large pressure dependences exhibited by the material reduce its applicability in deep water applications, although, with proper design, it may be possible to maintain a pressure-independent sensitivity that will be somewhat greater than that of PZT, the current standard in sonar transducer materials.

REFERENCES

[1]   G.H. Haertling, "Rainbow Ceramics - A new Type of Ultra-High-Displacement Actuator", *American Ceramic Society Bulletin*, vol.73, pp.93-96, January 1994.

[2]   J.G. Smits, "Iterative Method for Accurate Determination of the Real and Imaginary Parts of the Material Coefficients of Piezoelectric Ceramics", *IEEE Trans. Sonics and Ultrasonics*, vol.SU-23, pp.393-402, June 1976.

[3]   S. Sherrit, N. Gauthier, H.D. Wiederick and B.K. Mukherjee, "Accurate Evaluation of the Real and Imaginary Material Constants for a Piezoelectric Resonator in the Radial Mode", *Ferroelectrics*, vol.119, pp.17-32, 1991.

[4]   *IEEE Standards on Piezoelectricity*, ANSI/IEEE Std.176-1987.

[5]   S. Sherrit, D.B. Van Nice, J.T. Graham, B.K. Mukherjee and H.D. Wiederick, "Domain Wall Motion in Piezoelectric Materials under High Stress", *Proceedings of the Eighth IEEE International Symposium on Applications of Ferroelectrics - ISAF '92*, 1992, pp.167-170.

Figure 6. The hydrostatic figure of merit as a function of pressure for sample 4.

Electromechanical Properties of Rainbow Devices

E. Furman, G. Li and G. H. Haertling
The Gilbert C. Robinson Department of Ceramic Engineering
Clemson University, Clemson, South Carolina 29634-0907

Abstract — A stress-biased, domed, electromechanical bender called a Rainbow was recently developed. Displacement characteristics for Rainbow devices based on piezoelectric PLZT compositions were studied in the frequency range far below the fundamental resonant mode frequency. Experimentally obtained field-induced displacements were compared with those predicted by a finite element model. The model underestimated the observed displacements. Low frequency relaxation of the displacements was observed experimentally.

INTRODUCTION

There are a number of applications including pumps, speakers, laser deflectors, optical scanners, and relays for which displacements well above those obtained using linear actuators are desirable. For these applications, piezoelectric benders have traditionally been used [1-4]. Benders are based on a bimorph or unimorph structure. Bimorphs contain two electromechanically active layers, and unimorphs have an active and a constraining layer. In both cases, layers must have good bonding since bending occurs as a result of field-induced lateral strain being nonuniform in different parts of a structure. To accommodate this strain, the sample bends, producing vertical displacement. The key parameter for these devices is the piezoelectric d_{31} or electrostrictive Q_{12} coefficient, which should be maximized.

Recently, a new type of bender called a RAINBOW (Reduced And Internally Biased Oxide Wafer) was developed with promising characteristics [5]. Rainbow devices with maximum displacements of 3 mm and sustaining point loads up to 10 kg were demonstrated [6]. The trade-off between the displacement and load-bearing capabilities was established.

In this paper the electromechanical properties of Rainbow devices well below the fundamental resonance mode frequency will be described and compared to those predicted by a finite element model (FEM).

RAINBOW ACTUATORS

Rainbow actuators consist of an electromechanically active layer and a constraining layer, similar to conventional unimorphs. Unlike the unimorph, however, the Rainbow is a monolithic structure. The constraining layer is formed by exposing one side of a lead-containing ceramic to a reducing atmosphere at high temperature produced by placing a ceramic in contact with a carbon block. The reduction of lead lanthanum zirconate titanate (PLZT) ceramics occurs as a result of oxidation of the solid carbon block, first to carbon monoxide and then to carbon dioxide gases [7]. The reduced layer is no longer piezoelectric, and is, in fact, a good electrical conductor due to a presence of a large amount of lead. The reduced layer functions as the electrode and the constraining part of the bender.

Rainbows also differ from unimorph benders by the presence of large internal stresses developed during the process of reduction and cooling to room temperature. Because of the volume decrease during the reduction step and the higher thermal expansion of the reduced layer compared to the oxide layer, the stress-free equilibrium dimensions of the reduced layer are smaller than for the oxide layer. To retain continuity at the interface between the oxide and the reduced layers and to minimize stored elastic energy, the sample develops curvature. For the Rainbows with a large reduced/oxide layer thickness ratio, the oxide layer is in compression throughout its volume. For a sufficiently small reduced/oxide layer thickness ratio, the neutral axis is in the oxide layer with the oxide material close to the interface being in compression and further away in tension.

EXPERIMENTAL PROCEDURE

Batches with various PLZT compositions were prepared using the mixed oxide method. The powders were calcined at 925 °C for two hours in closed alumina crucibles. The samples were either sintered at 1250 °C for 6 hours in oxygen or hot pressed at 1200 °C for 6 hours at 14 MPa. For the reduction process, a lapped sample was placed on a graphite block and introduced into a preheated furnace held at 975 °C for approximately one hour, and then removed from the hot furnace. Silver electrodes were used throughout the testing [6].

Field-induced displacement was determined using LVDT-based apparatus. Displacements were determined for the forward-biased case and for the complete loop cycling. For the forward-biased case a Rainbow was poled at room temperature with approximately 900 volts applied until the displacement stabilized, and then the displacement was measured in the poling direction quasi-statically from zero volts to the poling voltage. The procedures for determinations of the thermal expansion coefficients and elastic constants will be published elsewhere [8].

MODELING

Finite-element modeling of complicated piezoelectric structures has been used successfully [9]. For this study the ABAQUS commercial FEM package (Hibitt, Karlsson & Sorenson, Inc., version 5.2) was used to simulate thermomechanical and electromechanical properties for the Rainbow devices. The model uses linear piezoelectric, dielectric, and elastic properties of the oxide and reduced layers..

The constituent equations for the piezoelectric media used in the modeling are:

$$S_i = s_{ij}^E T_j + d_{ij}^t E_j \qquad (1)$$
$$D_i = d_{ij} T_j + \varepsilon_{ij}^T E_j \qquad (2)$$

where S_i is the strain, D_i is the polarization, T_j is the stress,

E_j is the electric field, s_{ij}^E is the elastic compliance, ε_{ij}^T is the dielectric permittivity, and d_{ij} is the piezoelectric compliance.

Modeling of Rainbow devices includes three major parts: 1) the definition of material properties and sample geometry, 2) the modeling of the cool down from the reducing temperature to room temperature, and 3) the determination of the response to the specified set of boundary conditions.

For the modeling of the cool down step nonlinear analyses were used to account for the considerable stiffening of the Rainbow structure during this step. The model permits linear analyses of the piezoelectric properties. Currently, nonlinear piezoelectric effects and electrostrictive properties cannot be modeled. For the calculation of the field-induced displacements a structure based on 60 elements gave satisfactory results for the modeling of the quasi-static field-induced displacements.

RESULTS AND DISCUSSION

In the case of piezoelectric ceramics there are three piezoelectric, two dielectric, and five elastic coefficients which are permitted by symmetry to be nonzero. The complete set of these values are known for only a few ceramics. Fortunately, for PZT 5 all of the above properties have been characterized [10]. PZT 5 is a soft PZT, and it should have values similar to those of PLZT ceramics with low lanthanum content. Piezoelectric, dielectric, and elastic constants of PZT 5 were used in the model. In addition, Young's modulus, Poisson's ratio, densities, and thermal expansion coefficients for the reduced layer formed from PLZT 5.5/57/43 (La/Zr/Ti) ceramics have been experimentally determined [8]. The data used in the modeling work are shown in Table 1. A rate of formation of the reduced layer of 127 μm/hour was used in the model.

To verify the model, a comparison was made between the predicted displacement from the FEM model and the analytical model of the cantilevered bimorph [3]. For one bimorph, the FEM predicted a field-induced displacement of 61 microns compared to the 50 microns predicted by the analytical model. The FEM correctly predicted the field-induced displacement to be proportional to the length of the cantilever squared, again in good agreement with the analytical model.

There was reasonable agreement between the experimentally determined spontaneous displacements measured at the center of a Rainbow after cool down and the modeling predictions as is shown in Table 2. Rainbow devices were found to be partially poled during the cool down which lowers their spontaneous displacement (Rainbow devices become flatter when poled).

Table 1. (a) PZT 5 data used for the oxide layer modeling, and (b) experimental data for the reduced layer prepared from PLZT 5.5/57/43.

Material	Property	Magnitude
(a) PZT 5	c_{11}^E	$12.1*10^{10}$ N/m^2
	c_{12}^E	$7.54*10^{10}$ N/m^2
	c_{13}^E	$7.52*10^{10}$ N/m^2
	c_{33}^E	$11.1*10^{10}$ N/m^2
	c_{44}^E	$2.11*10^{10}$ N/m^2
	d_{33}	$374*10^{-12}$ C/N
	d_{31}	$-171*10^{-12}$ C/N
	d_{15}	$584*10^{-12}$ C/N
	$\varepsilon_{11}^T/\varepsilon^o$	1730
	$\varepsilon_{33}^T/\varepsilon^o$	1700
(b) Reduced Layer	Density	8.00 gm/cm^3
	Young's modulus	$6.86*10^{10}$ N/m^2
	Poisson's ratio	0.381
	Thermal Expansion	~$10*10^{-6}$ °C^{-1}

The experimentally obtained displacements are significantly higher than those predicted by the model (Table 2). There are appreciable variations from sample to sample in the ratio of total displacement to the forward biased displacement. The larger experimental displacement compared to the model may be accounted for by considering additional nonlinear contributions from the non-180° domain walls and phase boundaries [11] and higher linear piezoelectric coefficients.

The model was used to compare the effects of the reduced/oxide layer thickness ratio on a Rainbow's field-induced and cool down displacements. The magnitude of the displacement on cool down is determined by the difference in the effective thermal expansion coefficients between the oxide and reduced layers, the geometry of a sample, and the elastic constants. Figure 1 shows that the maximum predicted spontaneous displacement should occur for the reduced/oxide layer thickness ratio of approximately one. This result is in qualitative agreement with Timoshenko's model of the bi-metal thermostat [12], which also predicts maximum displacement near the layer thickness ratio of one for the two layers having properties of the oxide and reduced layers. As is also shown in Figure 1, the maximum field-induced and cool down displacements occur at the same Rainbow geometry. This result is applicable if the magnitude of the electric field is kept constant in the oxide layer as the geometry changes, which was done in the case described in Figure 1. For the case of constant voltage across the oxide

Table 2. Experimental results and FEM predictions of electromechanical properties.

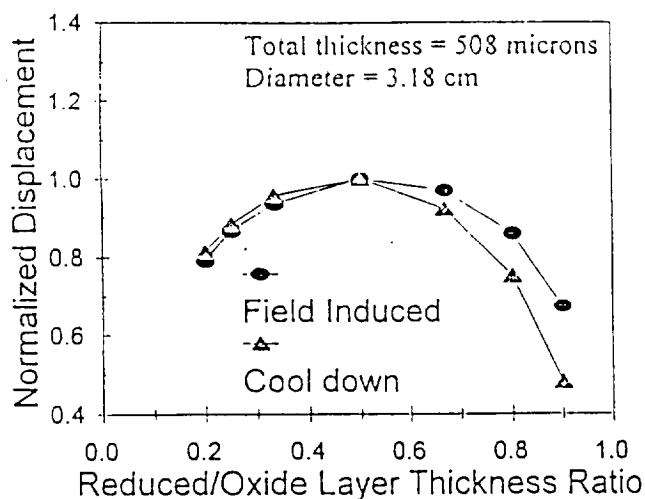| Oxide Layer Composition	Reduction Temperature/ Time (°C / minutes)	Total Rainbow Thickness (μm)	Full Cycle Voltage (Volts)	Experimental Full Cycle Displacement (μm)	Experimental Forward Bias Displacement (μm)	Calculated Forward Bias Displacement (μm)	Experimental Cool Down Displacement (μm)	Calculated Cool Down Displacement (μm)
1.0 / 53 / 47	975 / 105	762	± 1026	301	116	40	547	789
6.0 / 59.5 / 40.5	975 / 90	635	± 912	177	78	42	759	844
6.0 / 59.5 / 40.5	975 / 105	864	± 912	150	35	27	742	705
6.0 / 57 / 43	975 / 60	508	± 1026	357	129	51	1067	828
6.0 / 56 / 44	975 / 75	508	± 912	307	140	53	668	884

Figure 1. Normalized displacements induced by cool down and application of voltage.

layer the displacement continues to increase with the reduction of the oxide layer thickness. This is consistent with the electrical energy stored in the oxide layer being inversely proportional to its thickness, permitting greater field-induced lateral strain which increases the degree of bending of a Rainbow.

The shapes of the Rainbow samples having different diameters before and after the electric field application are shown in Figure 2. The flatter samples have no applied voltage; the more curved Rainbows bend up as a result of voltage applied in the opposite direction to the poling direction (the magnitude of movement is exaggerated). For the thicker Rainbows, there is less flattening in the middle portions. The model predicts this shape as a result of the nonlinear cool down step. Because FEM predicts that the

curvature of a Rainbow is nonuniform, it is not compatible with the predictions of linear models, mentioned above, which ignore nonlinear effects. In particular, the model predicted smaller displacement than the diameter squared dependence of the field-induced displacement.

Rainbow samples are capable of significant load-bearing capability. As is shown in Figure 3, there is excellent reproducibility in field-induced strain for a sample with up to 500 grams point load applied to the center of the sample.

Figure 3. Field-induced displacements as a function of voltage for different loading conditions.
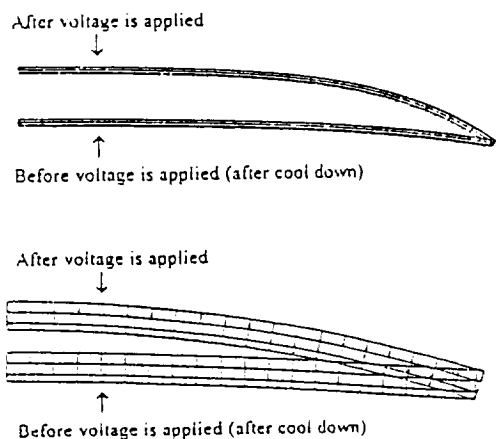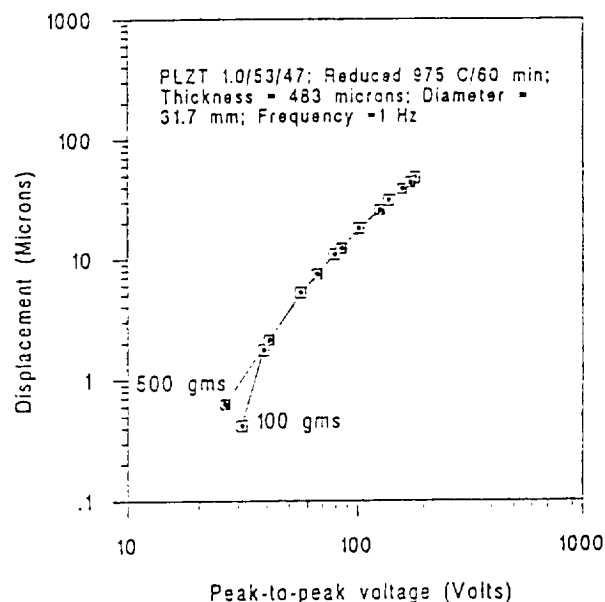

Figure 2. Shapes of Rainbows with diameter 6.35 cm (top) and 1.59 cm (bottom) before and after voltage is applied. Reduced/oxide layer thickness ratio: 1:3, thickness: 508 μm, applied voltage: 500 V for both samples.

Rainbow samples have pronounced low frequency relaxation of the field-induced strain. It usually is manifested strongly for only one polarity. The response is relatively fast for the other polarity. An example of the low frequency contribution to the Rainbow displacement is shown in Figure 4. This sample was poled at 800 volts, and the field-induced displacements were measured at ±53 volts. It can be observed that the field-induced displacement fits a straight line on semilog paper, indicating that the displacement becomes especially large at low frequencies.

The intriguing possibility to consider is whether the strong frequency-dependence of displacements and displacements exceeding the FEM's predictions are enhanced in Rainbow devices compared to conventional benders. Because Rainbows have large internal stresses it is reasonable to expect greater density of ferroelastic domain walls compared to ferroelectric devices without the macro-scale internal stresses, which could lead to enhanced displacements. Another possible contributing factor to the large displacements observed in Rainbow devices is unique to its structure.
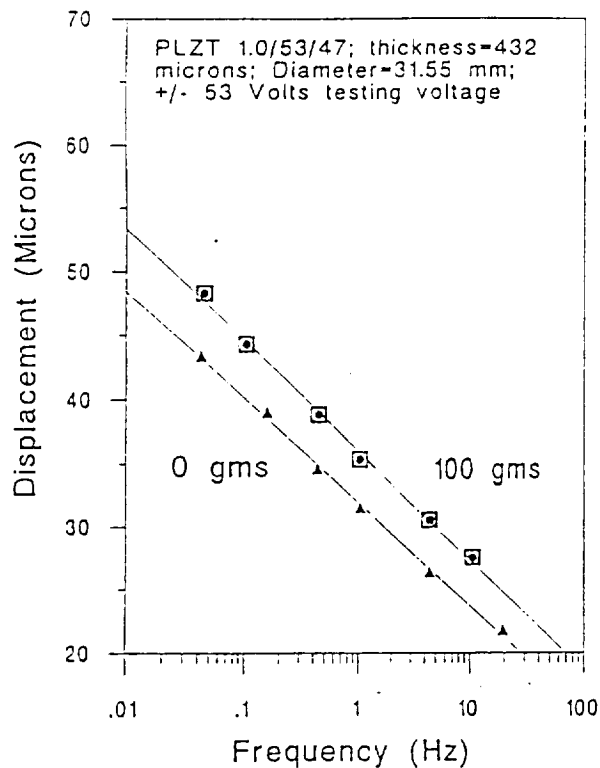
Figure 4. Field-induced displacements as a function of frequency for different loading conditions.

Because of the gradual change in the stress level in the oxide layer, different domain orientations are favored in different parts of the sample. Free charges may be trapped to compensate for polarization discontinuity at high temperature where conductivity is relatively high. As the sample is cooled down rapidly to room temperature it remains partially poled, and there may be net trapped charge in the bulk of the sample. Slow migration of charges during the domain switching may account for low frequency enhanced displacements. Finally, since a greater volume fraction of the oxide layer is in compression, higher switchable polarization should be available compared to the unstressed bender, as was shown for thin films in compression [13].

CONCLUSIONS

Electromechanical properties of Rainbow devices were studied at low frequencies and the results were compared to the FEM. The distinguishing characteristic of Rainbow devices is large and nonuniform stress on a macroscopic scale. Possible reasons for larger than expected displacements and frequency-dependent properties were discussed, and are believed to be related to a unique Rainbow structure.

ACKNOWLEDGMENT

REFERENCES

[1] J. van Randeraat and R. E. Setterington (Ed.), *Piezo-electric Ceramics*. N. V. Philips' Gloeilampenfabrieken, Eindhoven, The Netherlands, 1974.

[2] A. G. Kuzin, N. Mirgorodskii, V. Pikarnikov and V. Soroka, "Piezoelectric Light Beam Deflectors. I. Theory of Bimorph Deflectors and Experimental Tests," *Sov. Phys. Tech. Phys.*, vol. 21, pp. 1128-1130, 1976.

[3] M. R. Steel, F. Harrison and P. G. Harper, "The Piezoelectric Bimorph: An Experimental and Theoretical Study of its Quasistatic Response," *J. Phys. D.: Appl. Phys.*, vol. 11, pp. 979-989, 1978.

[4] J. K. Lee and M. M. Marcus, "The Deflection-Bandwidth Product of Poly(vinylidine Floride) Benders and Related Structures," *Ferroelectrics*, vol. 32, pp. 93-101, 1981.

[5] G. H. Haertling, "Rainbow Ceramics - A New Type of Ultra-High-Displacement Actuator," *Am. Cer. Soc. Bull.*, vol. 73, pp. 93-96, 1994.

[6] G. H. Haertling, "Chemically Reduced PLZT Ceramics for Ultra-High Displacement Actuators," *Ferroelectrics*, vol. 154, pp. 101-106, 1994.

[7] G. H. Haertling, "Reduction/Oxidation Effects in PLZT Ceramics," pp. 699-711 in *Proceedings of the 4th International SAMPE Electronics Conference, pp. 699-711*, 1990.

[8] E. Furman, G. Li and G. H. Haertling, "An Investigation of the Resonance Properties of Rainbow Devices," accepted for publication in *Ferroelectrics*.

[9] R. Learch, "Simulation of Piezoelectric Devices by Two- and Three-Dimensional Finite Elements," *IEEE Trans. Ultrasonics, Ferroel., and Frequency Control*, vol. 37, pp. 233-247, 1990.

[10] D. A. Berlincourt, D. R. Curran and H. Jaffe, "Piezoelectric and Piezomagnetic Materials and Their Function in Transducers," in *Physical Acoustics*, vol. 1 Part A, New York: Academic Press, 1964, Ch. 3.

[11] S. Li, W. Cao, R. E. Newnham and L. E. Cross, "Electromechanical Nonlinearity of Ferroelectric Ceramics and Related non-180° Domain Wall Motions," *Ferroelectrics*, vol. 139, pp. 25-49, 1993.

[12] S. Timoshenko, "Analyses of Bi-Metal Thermostats," *J.O.S.A. & R.S.I.*, vol.11, pp. 233-251, Sept. 1925.

[13] B. Tuttle, et. al., "Chemically Prepared Pb(Zr,Ti)O$_3$ Thin Films: the Effects of Orientation and Stress," in *Proc. of IEEE 8th Int. Symp. on Appl. of Ferroelectrics*, 1992, pp. 344-348.

Hybrid

Microelectronic

Materials

▼▲▼

Edited by
K.M. Nair
DuPont Electronic Materials

V.N. Shukla
Texas Instruments

▲▼▲

RAINBOWS AND FERROFILMS - SMART MATERIALS FOR HYBRID MICROELECTRONICS

Gene H. Haertling
Gilbert C. Robinson Department of Ceramic Engineering
Clemson University, Clemson, SC 29634-0907

ABSTRACT

This review paper describes the materials, processing, properties and applications of the newly developed ultra-high displacement Rainbows and thick/thin ferroelectric Ferrofilms. Their applicability to hybrid and fully integrated microelectronics is discussed in regard to each of these areas of concern.

INTRODUCTION

Current trends have shown that industrial and commercial hybrid microelectronic components designed for the automobile, home, office and factory are becoming an increasingly more important segment of present-day automation. The materials for such applications are required to be more sophisticated in that they must be able to perform more than one function (e.g., actuation and sensing) during operation or provide a unique combination of highly specialized properties. These materials are now commonly known as smart or intelligent materials and are exemplified by such general groups as ferroelectrics, piezoelectrics, pyroelectrics, electrooptics, electrostrictive materials and composites.

Key factors in the application of these materials to hybrid circuits and microelectronics are (1) their ability to be scaled down in size (i.e.,miniaturized or fully integrated) without loss of bulk properties, (2) their capability of achieving the proper form factor for the substrate and (3) their processing compatibility with other components on the substrate. Recent research and development work has shown that significant progress has been made in the last several years in each of these areas.[1-5] A new processing technique has recently led to the development of ultra-high displacement

Hybrid Microelectronic Materials

ceramic actuators which have been coined as RAINBOWS (Reduced And INternally Biased Oxide Wafers), an acronym for the chemical reduction process used to transform ordinary planar piezoelectric and electrostrictive wafers into domed, high displacement, two-dimensional bending actuators of moderate load-bearing capability.[6,7] Rainbow devices such as speakers, pumps, switches, deflectors and linear actuators have been made in sizes as large as 10 cm. in diameter and as small as 2 mm. in diameter or length.
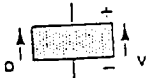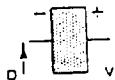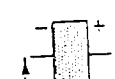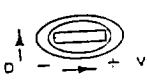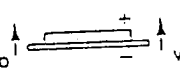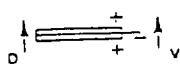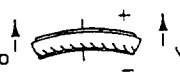
An assessment of the present-day ceramic actuator technologies for bulk materials is given in Table 1. As seen from the table, a variety of direct extensional configurations, composite flextensional structures and bending mode devices are used to achieve an electromechanical output. Trade-offs between stress generating/loading capability and displacement are commonly made when designing for particular applications. Maximum displacement can be seen to be achieved with composite or bender structures; however, this is usually accomplished at the expense of less load bearing capability, greater complexity and higher cost. The recent introduction of the Rainbow bender to this family of actuators has served to either extend the stress capability of the bender technologies without sacrificing displacement or extending the displacements achievable with equal load-bearing capacity. Additionally, because of their unique dome or saddle-type structure, small discrete Rainbow elements for hybrid circuits can be fabricated from larger, bulk processed wafers.

For the fabrication and integration of actuator/sensors and other devices at the microelectronic (micron) level, one must consider different technologies than those previously mentioned. Among these techniques are vacuum deposition, spinning, dipping, chemical vapor deposition and laser ablation; however, those which have been reported to successfully produce both thin (0.02 - 5 um in this paper) and thick (5 - 30 um in this paper) films of the above mentioned materials are considerably fewer in number, and the most promising of these, in the near term, is dipping. Using an automated dipping apparatus, Li, et.al.,[8] were successful in fabricating thin and thick films of PLZT ferroelectric and electrooptic compositions on Ag, Si, sapphire and glass substrates. Films as thick as 15 microns have yielded properties quite similar to those of the bulk material and show excellent promise for future devices.

It is the object of this review paper to describe the materials, processing and properties of two types of recently developed smart materials; i.e., Rainbows for discrete and hybrid structures and thick/thin ferroelectric films (Ferrofilms)

for hybrid and integrated structures.   Examples of typical applications are discussed.

Table 1. Present-Day Ceramic Actuator Technologies

Type	Configuration	Max. Stress* (MPa)	Actuator Movement (w/Voltage)	Actuator Type (P or E)	Actuator Displacement (%)+
Monolithic (d_{33} mode)		40	Expansion	P	0.40
Monolithic (d_{31} mode)		40	Contraction	P	-0.15
Monolithic (s_{11} mode)		40	Expansion	E	0.24
Monolithic (s_{12} mode)		40	Contraction	E	-0.08
Composite Structure (d_{33} mode) (flexten.)		10	Contraction	P	-1.0
Composite Structure (d_{33}/d_{31}) (Moonie)		0.028	Expansion	P/E	1.3
Unimorph (bender)		0.002	Expansion/ Contraction	P/E	10
Bimorph (bender)		0.002	Expansion/ Contraction	P/E	20
Rainbow Monomorph (bender)		0.020	Expansion/ Contraction	P/E	35-500

Notes: V = Voltage; D = Actuator Displacement; P = Piezoelectric; E = Electrostrictor
  * = Max. generated stress; + = Displacement at ± 10 kV/cm based on thickness

Hybrid Microelectronic Materials

73

MATERIALS

Although a number of different compositions have been successfully prepared as Rainbows and Ferrofilms, those most compatible to the specific processes used and most amenable to achieving the desired properties are in the PLZT solid solution family. Typical high displacement ferroelectric compositions are 1/53/47 (La/Zr/Ti) and 5.5/56/44 for low and high dielectric constant applications, respectively; whereas, the usual compositions for the electrooptic, electrostrictive-type applications are 9/65/35 or 8.6/65/35.[9] These specific compositions are pointed out in the PLZT phase diagram given in Figure 1. As may be noted, the ferroelectric materials are morphotropic phase boundary compositions and the non-memory, electrostrictive materials are compositionally located along the ferroelectric-to-paraelectric phase boundary.
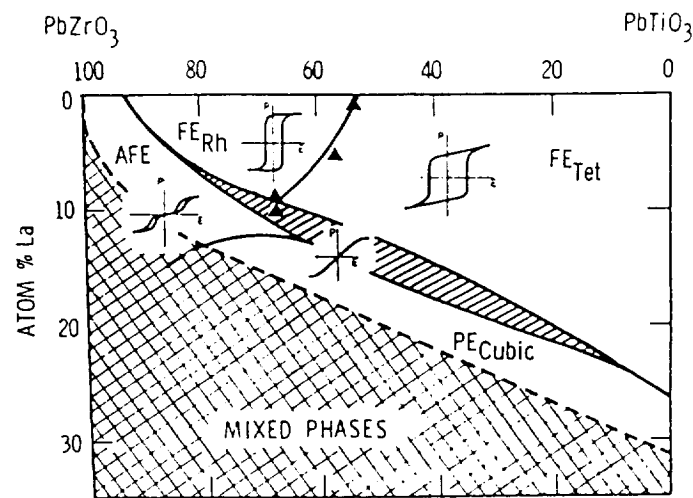
Figure 1. Room Temperature Phase Diagram of the PLZT System
Compositions are indicated by triangular markers

PROCESSES

In this section, the specific processes which have been reported for both the Rainbows and the Ferrofilms are described. Since Rainbows are produced via a bulk-type process and the Ferrofilms are fabricated with a thick/thin film technique, they are distinctly different, by nature, and thus, are discussed in

Hybrid Microelectronic Materials

separate sections.

Rainbow Process

The Rainbow technology fundamentally consists of a new processing method that is applied to standard, high lead-containing ferroelectric, piezoelectric and electrostrictive ceramic wafers which are transformed by the process into a monolithic, composite structure consisting of a stressed dielectric and a chemically reduced, electrically conductive layer which acts as the stressing element as one of the electrodes for the final device. Since all of the materials are ferroelectric or electrically-enforced ferroelectric materials, they are multifunctional and smart, by nature, and are thus capable of performing both actuator and sensor functions, simultaneously.

The high temperature chemical reduction process involves the local reduction of one surface of a planar ceramic plate, thereby achieving an anisotropic, stress-biased, dome or saddle-shaped wafer with significant internal tensile and compressive stresses which act to increase the overall strength of the material and provide its unusually high displacement characteristics. According to previously reported work, the chemical reduction process proceeds via simple reactions consisting of the oxidation of the solid carbon (graphite) block to carbon monoxide and further oxidation of the carbon monoxide gas to carbon dioxide with the associated loss of oxygen from the PLZT oxide in contact or in near contact with the graphite block.

Rainbow ceramics are produced from conventionally sintered or hot pressed ceramic wafers by means of a few simple steps requiring approximately two hours of additional time as shown in the process flowsheet of Figure 2. A Rainbow is produced from an as-received wafer by placing it on a flat graphite block, placing a protective zirconia plate of the same size on top of the wafer and introducing the assembly into a furnace held at temperature in a normal air atmosphere. The part is treated at a temperature of 975°C for one hour, removed from the furnace while hot and cooled naturally to room temperature in about 45 minutes. A reduced layer approximately 150 um thick is produced in the wafer under these treatment conditions, When cool, the dome shaped wafer is lifted from the graphite block, brushed lightly on the reduced (concave) side to remove any metallic lead particles and to expose the reduced layer, and then electroded for test and evaluation. A variety of electrodes can be used such as epoxy silver, fired-on silver and vacuum deposited metals. After depositing appropriate electrodes, the Rainbow is completed and ready for operation.

```
┌─────────────────────┐
│   PIEZOELECTRIC     │
│   CERAMIC WAFER     │
└─────────────────────┘
           │
┌─────────────────────┐
│    REDUCTION        │
│    975/1 HR.        │
└─────────────────────┘
           │
┌─────────────────────┐
│    ELECTRODE        │
│ EPOXY Ag/FIRED-ON Ag│
└─────────────────────┘
           │
┌─────────────────────┐
│      TEST           │
│   EVALUATION        │
└─────────────────────┘
```
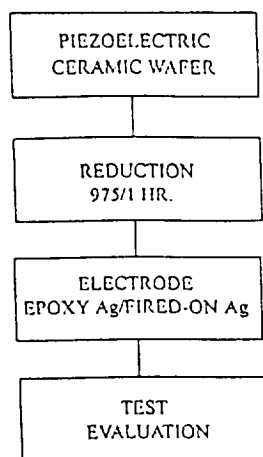
Figure 2. Process Flowsheet for PLZT Rainbow Ceramics

In regard to operation, a Rainbow is similar to a device known in the industry as a unimorph bender. A unimorph is composed of a single piezoelectric element externally bonded to a flexible metal foil which is stimulated into action by the piezoelectric element when activated with a ac or dc voltage and results in an axial buckling or displacement as it opposes the movement of the piezoelectric element. However, unlike the unimorph, the Rainbow is a monolithic structure with internal compressive stress bias on the piezoelectric element; thus producing the dome structure, rendering it more rugged and able to sustain heavier loads that normal. The integral electrode (usually the bottom electrode) consists of metallic lead intimately dispersed throughout the semiconductive oxide layer. The change in shape of the wafer after reduction is believed to be due to the reduction in volume of the bottom reduced layer (largely metallic lead) compared to the unreduced material, as well as the differential thermal contraction between the reduced and unreduced layers on cooling to room temperature.

Like other piezoelectric devices, Rainbows may be operated with a dc, pulse dc, or ac voltage; however, when driven with ac, the largest displacements are usually achieved at 100 Hz or less. In operation, the dome height of the Rainbow varies as a function of the magnitude and polarity of the voltage. When a given polarity of voltage is applied, the dome decreases in height depending on the magnitude of the voltage; and alternatively, when the polarity is reversed, the dome increases. The large axial motion of the dome

is largely due to contributions from a lateral contraction produced in the material via the d_{31} coefficient and a stress-directed domain switching process.

It should be noted that although Rainbows are processed in bulk wafer form, after heat treatment they may be diced or scribed into smaller elements for a pick-and-place operation onto a hybrid substrate. This technique is possible since each individually diced element possesses a smaller but similar dome structure with a radius of curvature identical to the larger wafer. Even though the displacements of the smaller individual elements are proportionately less than the parent wafer, they nevertheless, are large enough (5 - 50 microns) to be useful in some devices. Some typical examples of sizes and shapes of Rainbows are shown in Figure 3.
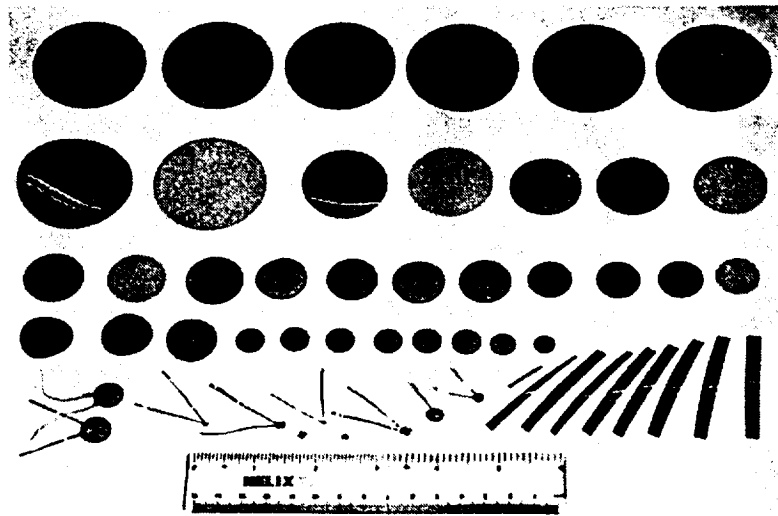
Figure 3. Typical Examples of Sizes and Shapes of Rainbows

Ferrofilm Process

Thick and thin films of ferroelectrics, piezoelectrics and electrostrictive materials are presently being fabricated from a water-soluble, acetate-precursor, liquid chemical system (Metal Organic Decomposition type) using an automated dipping process. An operational flowsheet for this process is given in Figure 4; however, the details of the process and the apparatus have

previously been reported as part of a overall effort involving the intelligent processing of ferroelectric films.[10]
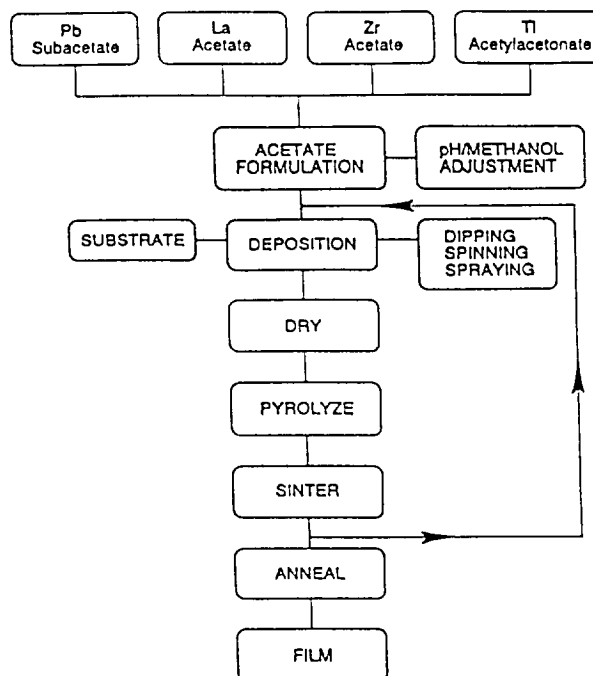
Figure 4. Process Flowsheet for PLZT Acetate MOD Process

Briefly, the process consists of formulating the stock solution from as-received precursors of Pb (lead subacetate), La (lanthanum acetate), Zr (zirconium acetate) and Ti (titanium acetylacetonate) by mixing them together in the requisite amounts along with the appropriate amount of methyl alcohol for viscosity control. This simple, five minute operation yields a clear, light yellow solution which is water soluble and stable for long periods of time. The solution is then deposited on the selected substrate via automatically controlled dipping and withdrawal operations. Drying occurs in a matter of a few seconds, and the coated substrate is subsequently sintered very quickly by introducing it directly into a furnace pre-heated to the sintering temperature. Multiple dipping, drying, sintering and cooling cycles are required in order to build up the necessary film thickness for the specific device. Depending on the dilution ratio of the solution, individually dipped layer thicknesses may vary from approximately 0.05 to 0.3 um, yielding films

78   Hybrid Microelectronic Materials

as thick as 12 um for a 40 layer device. For a cycle time of three minutes, the total time required to dip a 40-layer device is about two hours.

The final sintered film deposited on a suitable substrate such as a 0.125 mm thick Ag foil is usually transparent and crack-free with a smooth, shiny surface. After applying suitable electrodes such as air dried Ag, epoxy Ag or vacuum deposited metals, the film is ready for operation; however, it should be remembered that poling may be required if it is a ferroelectric thick film. Some examples of electroded and unelectroded thick films on Ag substrates are shown in Figure 5.
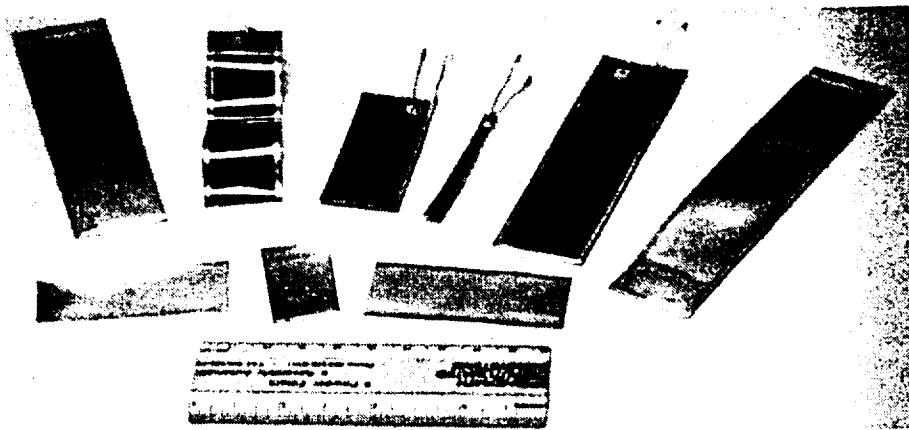
Figure 5. Typical Examples of Unelectroded and Electroded Ferrofilms

Although Ferrofilms lend themselves well to a number of different fabrication processes at the totally integrated level, for discrete components at the hybrid microelectronics level the dipping technique has been found to be reliable and predictable and can easily be implemented in a totally hands-off environment. In addition, industrial equipment is readily available to dip very large as well as small, discrete parts at minimal cost. The acetate process, being water insensitive, is especially suitable for the dipping process since the open solution is usually exposed to the atmosphere for long periods of time and during this period must withstand chemical interactions as well as minimal evaporation of solution.

PROPERTIES

In the last two years since the Rainbow ceramics were first developed at

Clemson University, there has been a considerable on-going effort to (1) understand the details of the reduction process in the PLZT materials, (2) measure their properties and characterize their unusually high displacement and load bearing capabilities as benders, (3) model their electromechanical behavior and frequency dependent properties and (4) construct working models illustrating various proof-of-principle applications. Some of this data for the Rainbow ceramics will be presented in this section, along with the limited amount of data available, to date, for the Ferrofilms. In most instances, a standard Rainbow size of 31.75 mm diameter and 0.5 mm thick was used to obtained the data. Additional technical data on the Rainbow ceramics has been reported in a document prepared by Sherrit, et.al., of the Royal Military College of Canada.[11]

Rainbows Characteristics

Dielectric Properties - The temperature dependent dielectric behavior for two PLZT compositions; i.e., 1/53/47 and 8.6/65/35, are shown in Figures 6 and 7, respectively. It can be seen from Figure 6 that a gradual rise occurs in the relative dielectric constant (1 kHz) of 1/53/47 from a room temperature value of approximately 1100 to about 2700 at 200°C. No peak is observed in this range for this composition because its Curie point is 330°C. On the other hand, composition 8.6/65/35 in Figure 7 shows a change in K from 3200 to 5700 over this same temperature range with a peak occurring at 105°C, which is its usual Curie point as determined from small signal measurements. Since this composition is an electrostrictive, relaxor-type material, this Curie point does not coincide with its loss in polarization which occurs at about 20°C; thus, making it one of the most sensitive, high displacement, electrostrictive Rainbow materials. It may be noted that the dielectric constants and dissipation factors for both compositions are comparable to previously reported values, and this indicates that the Rainbow reduction process does not change the dielectric properties of the unreduced part of the structure.

Hysteresis Loops - Typical examples of dc hysteresis loops for compositions 1/53/47 and 9/65/35 are given in Figure 8. The loop in Figure 8(A) was taken on the ferroelectric Rainbow element (1/53/47) in its virgin condition before any other measurements were made. It should be noted that on the initial application of positive voltage to +450V there was approximately 60% of the total remanent polarization switched rather than the usual 50% one ordinarily observes in a virgin, randomly oriented ceramic.. This behavior is highly unusual and indicates that the Rainbow ceramic was partially poled before testing. Additional audio and piezoelectric tests of other virgin parts also

Hybrid Microelectronic Materials

indicated that the elements were partially poled to varying degrees; i.e., some very little and others as high as 75%.
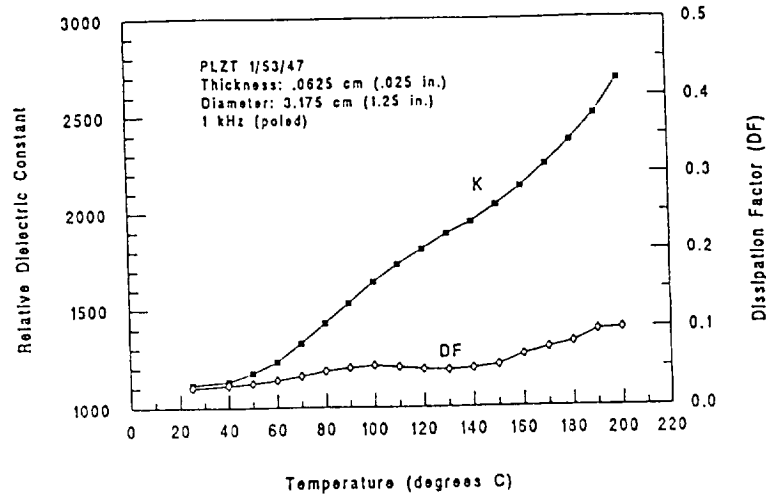

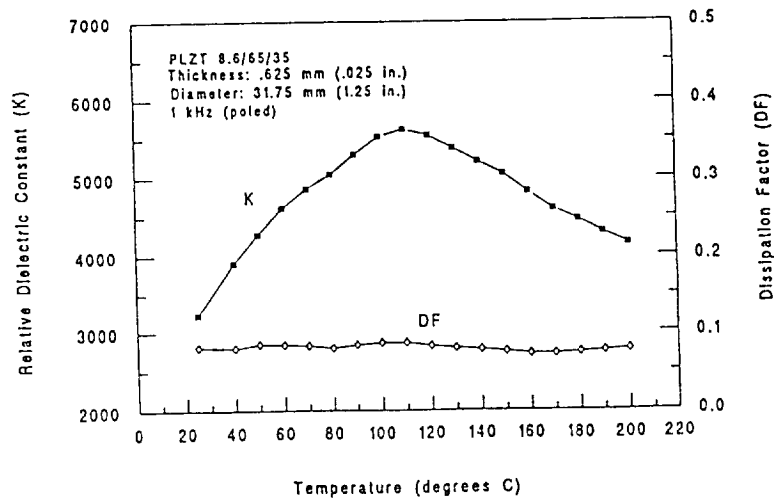Figure 6. Temperature Dependent Dielectric Properties of PLZT Rainbow 1/53/47

Figure7. Temperature Dependent Dielectric Properties of PLZT Rainbow 8.6/65/35
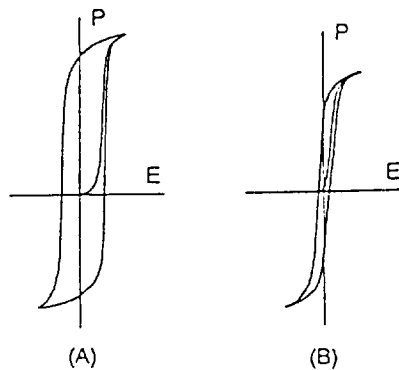
Figure 8. Virgin Hysteresis Loops for Rainbow PLZT Compositions (A)
1/53/47 and (B) 9/65/35

One explanation for this condition occurring in the electrically virgin state is
that the mechanical compressive and tensile stresses produced in the Rainbow
wafer during processing are acting together to switch some of the domains in
this soft ferroelectric/ferroelastic material. Since uniform stress is a
symmetrical quantity, it is recognized that it alone is insufficient to produce
a net polarization in a given direction even though it may be of sufficient
magnitude to switch domains; however, a stress gradient such as produced by
the Rainbow bending process is a vector quantity and can, indeed, produce
the observed effect. This non-uniform stress is believed to be responsible for
the partial poling of the Rainbow wafers. Measured properties on the above
wafer were: P_R = 44.8 uC/cm^2, E_C = 7.5 kV/cm, dielectric constant = 1210
and dissipation factor = 0.047.

The virgin loop of Figure 8(B) is a typical one for the electrostrictive (9/65/35)
type of Rainbow materials and is very similar to that obtained on bulk
electrooptic material. Measured properties on this wafer were: $P_{10kV/cm}$=28.3
uC/cm^2, dielectric constant = 3142 and dissipation factor = 0.085. As a
matter of course, no unsymmetrical hysteresis loops were observed in the
electrostrictive materials, and none was expected, since there are no stable
domains in these materials at zero electric field. Conceivably, a high enough
stress could precipitate stable domains in a very near-ferroelectric material,
however, this was not experimentally confirmed

Displacement Loops - Displacement vs. electric field (butterfly) loops for the
Rainbow wafers described above are shown in Figure 9. As before, Figure

9(A) illustrates the Rainbow axial motion as the sample is electrically switched from zero to +450V, to -450V and back to zero, however, in this case this loop was not taken on the virgin wafer. It may be noted that this loop is remarkably similar to that observed when measuring the direct extensional (longitudinal, lateral) displacements via the piezoelectric d_{33} or d_{31} coefficients. The value of displacement in the + voltage direction was measured at 190.5 um, and the total amount of displacement (+/-) was 432 um.
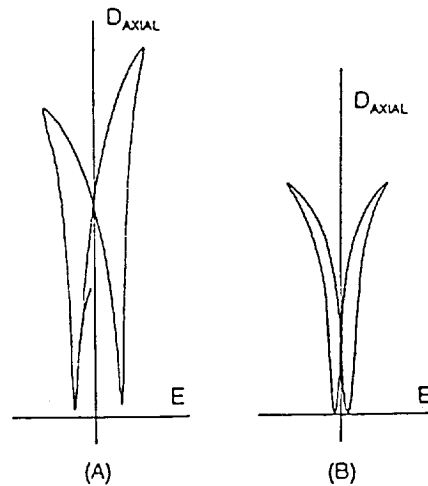
Figure 9. Axial Displacement Loops for Rainbow PLZT Compositions (A) 1/53/47 and (B) 9/65/35

Figure 9(B) shows the displacement loop of the electrostrictive Rainbow material (9/65/35) mentioned above. Since 9/65/35 is a relaxor material there should be little or no memory, and the same value and sign of displacement should be obtained whether a + or a - voltage is applied. One can see by switching this sample through a full voltage loop that a small amount of remanent displacement (strain) is present which is probably due to the close proximity of this composition to a FE phase. A further indication of this incipient FE phase is the higher than normal value of P_{10} (P_{10} = 28.4 vs. 18.0 uC/cm^2) as given above. Measured value of total displacement for this wafer was 178 um.

Displacement Characteristics - The displacement characteristics as a function of applied voltage are given in Figure 10 for some selected compositions. One of the most striking features of this figure is the very high displacements

achieved by these Rainbow ceramics at moderate electric fields; e.g., 400 volts is equivalent to an electric field of 10 kV/cm. Composition 8.6/65/35 is noted to possess the highest displacement of 210 um at a maximum voltage of 600 volts, however, its displacement is characteristically non-linear because of its electrostrictive nature. Compositions 1/53/47 and 5.5/56/44 are ferroelectric materials, and thus, are more linear in behavior. As a general rule, the displacements of the ferroelectric materials are lower than those of the electrostrictive compositions, particularly when operated at higher voltages and one polarity; however under bipolar operation, the displacement values of the ferroelectric materials will commonly be double the values shown in Figure 10.
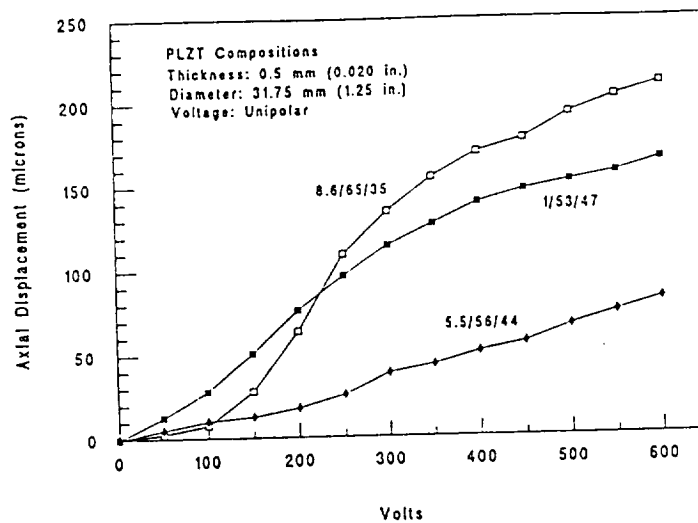
Figure 10. Axial Displacement Characteristics of Rainbow PLZT
Compositions as a Function of Voltage

A measure of the difference in displacement between the planar (lateral extensional mode) direction and the orthogonal axial (Rainbow bender mode) direction is given in Figure 11 for PLZT 8.6/65/35, which also shows the temperature dependence of these two modes. This figure clearly demonstrates the very large displacement amplification of the bending phenomenon when one considers the data showing a change in displacement from approximately 0.07% to 22% at 25°C; i.e., an amplification of 315%. Although not shown on the figure, both displacements are negative (i.e., a contraction) when voltage is applied.

Hybrid Microelectronic Materials
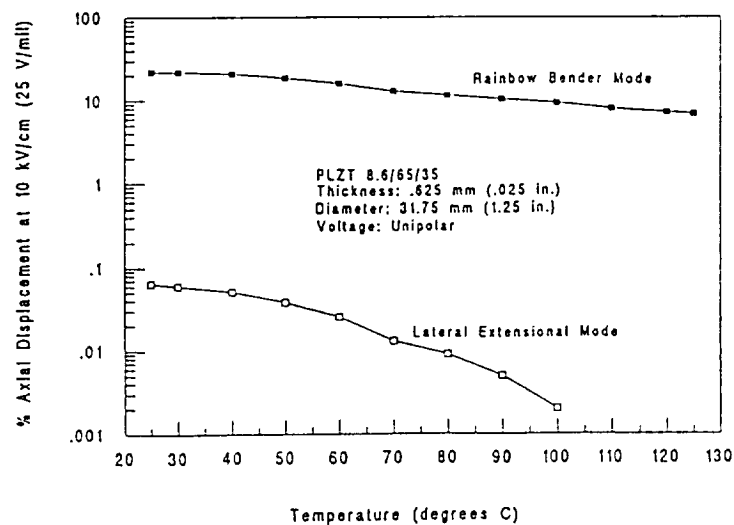
Figure 11. Temperature Dependence of Electrostrictive Lateral and Rainbow Bending Displacements in PLZT 8.6/65/35 Ceramics

Figure 12 illustrates the profile of the vertical bending displacement across the diameter of a Rainbow wafer during activation at 10 kV/cm. As might be anticipated, the highest displacement is in the center of the wafer, dropping off to zero at the circumference. This zero displacement at the edge of the wafer is beneficial because a Rainbow can be conveniently placed on a planar surface and operated as a linear actuator device or its circumference can be sealed off, and it can be operated as a cavity-mode pump.

The variation of a Rainbow's axial displacement as a function of wafer diameter is given in Figure 13. For a 0.5 mm thick wafer of composition 1/53/47, the values of displacement can be seen to vary from 170 um for a diameter of 31.75 mm (1.25 inch) to approximately 3 um at 6.5 mm diameter. Thus, a discrete 15 mm diameter Rainbow component on a hybrid substrate could be expected to have a displacement of about 40 um when operated with a single polarity and about 80 um when operated bipolar.

Wafer thickness has been found to have a significant effect upon axial displacement primarily because of the change in motional mode; i.e., from dome to saddle-type, as the wafer thickness is reduced to approximately one one-hundredth of the diameter. For example, a 31.75 mm (1.25 inch) diameter wafer usually develops a saddle-mode configuration when its
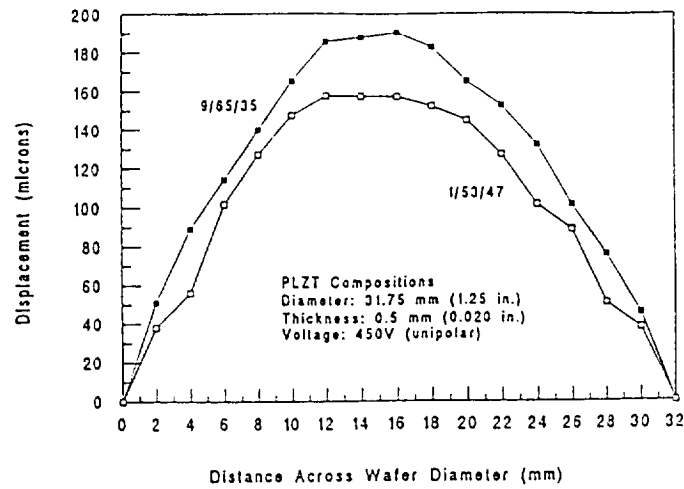
Figure 12. Profile of Displacements Measured Across Rainbow Wafer
Diameter for PLZT 1/53/47 and 9/65/35
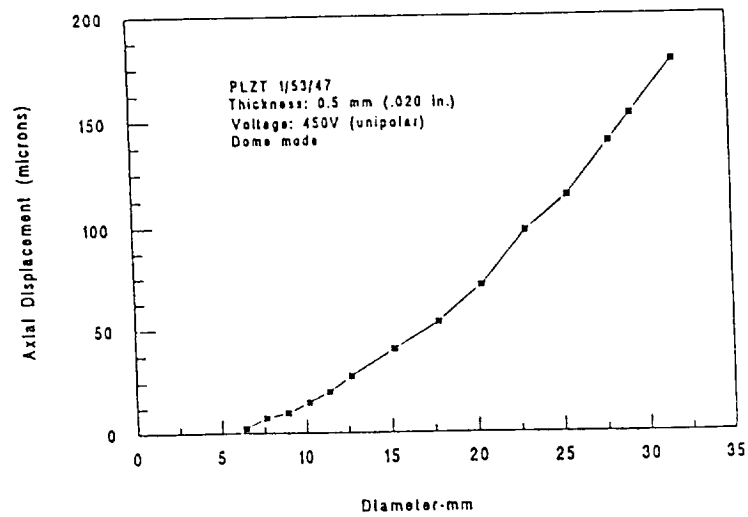
Figure 13. Variation of Axial Displacement as a Function of Rainbow Wafer
Diameter for PLZT 1/53/47

thickness is less than 0.32 mm (0.013 inch). Saddle-mode operation provides
maximum displacement with minimum load bearing capability; and therefore,

86   Hybrid Microelectronic Materials

should only be considered for special applications. Figure 14 illustrates the unusually large range of displacements obtained for Rainbows as a function of thickness. Please note that the displacement axis is a log scale.
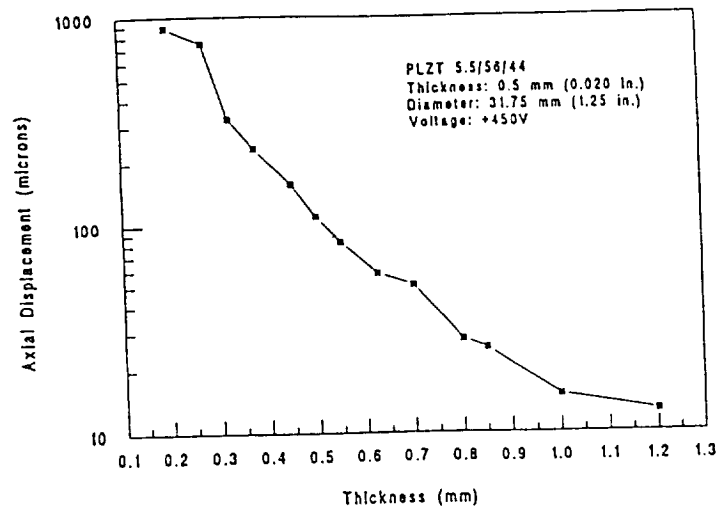
Figure 14. Effect of Thickness on Axial Displacement for PLZT 5.5/56/44
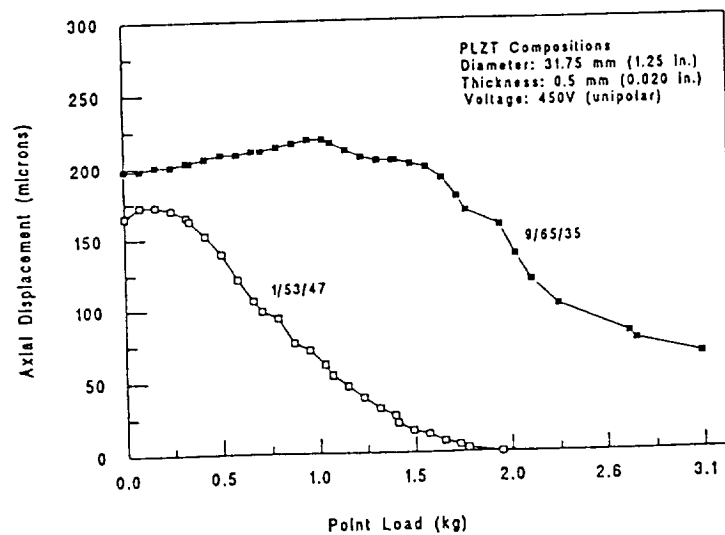
Figure 15. Point Load-Bearing Properties of Rainbow PLZT Compositions

The effect of an unconstrained point load on the displacement of an activated Rainbow is given in Figure 15 for compositions 1/53/47 and 9/65/35. PLZT 1/53/47 can be seen to be relatively ineffective when loaded with a dead weight of 1.5 kg (3.3 lbs), whereas, composition 9/65/35 is still effective at a load of over 3 kg. This result is not too surprising since the elastic modulus of 9/65/35 (10.9 x10^4 MPa) is noticeably higher than that of 1/53/47 (5.7 x 10^4 MPa). Another point to note from the figure is the increase in displacement with the introduction of a finite amount of load on the device. This effect was previously reported by Furman, et. al.[12] The tradeoff between thickness and maximum sustainable point loading is given in Figure 16 for 1/53/47.
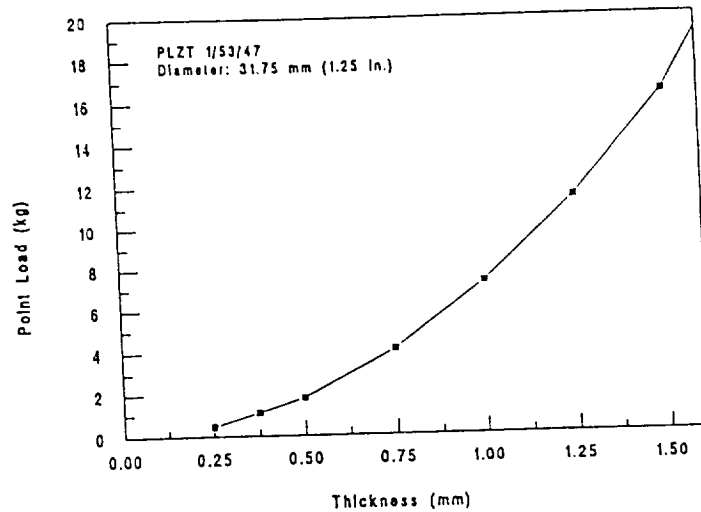
Figure 16. Maximum Sustainable Point Load for Rainbow PLZT 1/53/47 as a Function of Thickness

Another concern of actuator designers is the amount of force that can be generated by an actuator when voltage is applied. This is shown in Figure 17 for a 1/53/47 Rainbow of standard size. As can be seen, the force generated is a linear function of voltage until the onset of saturation for this particular configuration. A maximum force of 1.3 kgf was achieved at 450 volts.

Finally, displacement and sustainable overpressure data for PLZT 5.5/56/44 as a function of wafer thickness are presented in Figure 18. The left ordinate scale represents the maximum allowable pressure differential across the wafer thickness before the wafer contacts the planar surface and stops flexing
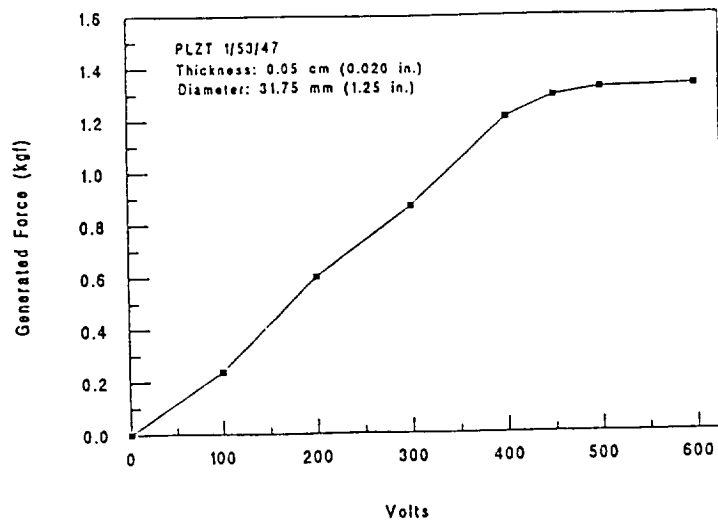
Figure 17. Effect of Applied Voltage on the Force Generated by a PLZT
1/53/47 Rainbow Wafer
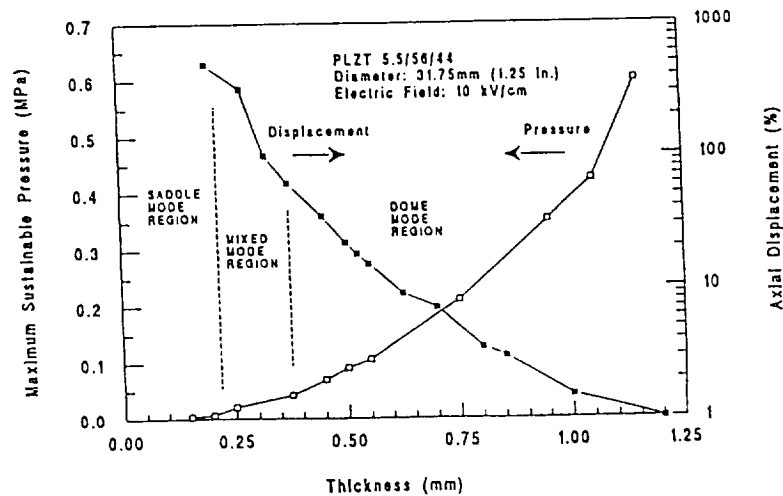
Figure 18. Sustainable Pressure and Displacement Characteristics for Rainbow
PLZT 5.5/56/44 as a Function of Thickness

usually <0.5 mm thickness) or the wafer mechanically fractures (>0.5 mm
thickness). The right ordinate log scale is the percent displacement (based on
wafer thickness) of the device when operated at 450 volts dc while only under

the loading of the dial gage (80 grams). Also indicated on the figure are the wafer thickness regions where the saddle and dome modes of operation are dominant for a wafer 31.75 mm (1.25 in.) in diameter. The data shown in the figure indicate that Rainbow displacements span an unusually large range from near zero to at least 500% with actual displacements of up to 1 mm (0.040 in.) for a 0.2 mm (0.008 in.) thick wafer. Of course, such large displacements are not possible when operating under significant pressure differentials or under moderate point loading situations near its capacity.

Resonance Characteristics - The resonant, frequency dependent properties of a standard Rainbow wafer is given in Figure 19 which displays both impedance and phase angle as a function of frequency. Some outstanding features of this figure are the large radial resonance anomaly at 70 kHz and the several bending resonances between 1 to 20 kHz. Other resonances not shown in this figure are (1) overtone resonances of the fundamental radial resonance in the range from 100 kHz to 1 MHz, (2) thickness resonances in the low megahertz range around 4 and 8 MHz for the fundamental and first overtone and (3) very low frequency structurally-dependent resonances in the range of 25 to 500 Hz which can be noted when a Rainbow is operated as part of a working device.
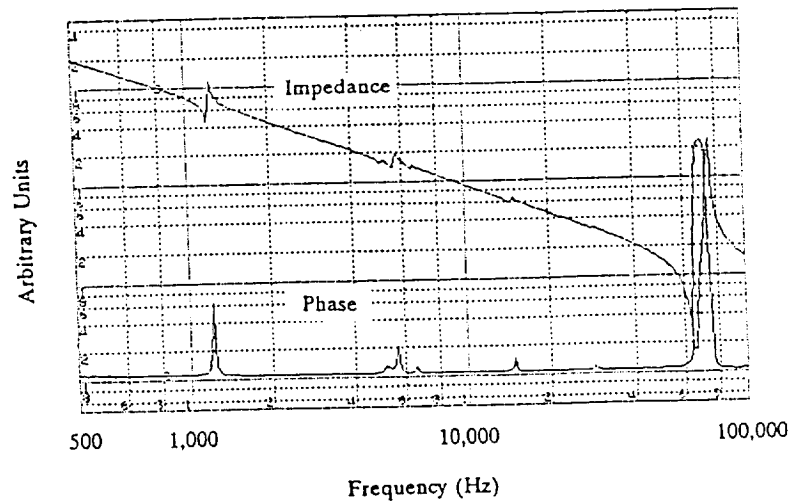
Figure 19. Resonance Characteristics of a Rainbow PLZT 1/53/47 Wafer

Table of Properties - A summary of selected properties which have been determined, to date, for the Rainbow ceramics are given in Table 2. In

Hybrid Microelectronic Materials

addition to these, a number of advantages and features of the Rainbows are: (1) simplicity, (2) solid-state type, (3) monolithic, (4) pre-stressed for greater strength and durability, (5) can sustain/generate moderate loads, (6) mechanical overload protection, (7) medium fast response, (8) very high axial displacement, (9) surface mountable, (10) above-the-plane displacement, (11) no bonding layers, (12) temperature compensation possible, (13) can be stacked to multiply strain, (14) easy to fabricate and (15) cost effective.

Table 2. Some Selected Properties of Rainbow Ceramics

Thermal Expansion -	$10.0 \times 10^{-6}/°C$ (reduced layer)
	$5.4 \times 10^{-6}/°C$ (oxide layer)
Modulus of Rupture -	1.58×10^{2} MPa (22,500 psi)
Modulus of Elasticity -	5.7×10^{4} MPa $(8.1 \times 10^{6}$psi)(bending)(1/53/47)
	10.9×10^{4} MPa $(15.5 \times 10^{6}$ psi)(bending)(8.6/65/35)
	6.9×10^{4} MPa (reduced layer)(acoustic)(5.5/56/44)
	7.8×10^{4} MPa (oxide layer) (")(")
Acoustic Velocity -	4015 m/sec (reduced layer)
	4248 m/sec (oxide layer)
Poisson's Ratio -	0.38 (reduced layer)
	0.38 (oxide layer)
Resistivity -	3.8×10^{-4} ohm-cm
Effective $d_{33\,(saddle)}$ -	2.5×10^{-6} m/V (bending mode)
$d_{33\,(dome)}$ -	2.8×10^{-7} m/V (bending mode)
Hysteresis -	5 - 35%
Displacement (31.8 mm) -	178 microns (0.007 inch)(0 - 450V)(dome mode)
	381 microns (0.015 inch)(+/- 450V)(dome mode)
	1143 microns (0.045 inch)(0 - 450V)(saddle mode)
(102 mm dia.) -	3175 microns (0.125 inch)(0 - 450V)(saddle mode)
	1016 microns (0.040 inch)(0 - 450V)(dome mode)
Capacitance (1.25" dia.) -	15 nF (PLZT composition 1/53/47) K = 1200
	30 nF (PLZT composition 5.5/56/44) K = 2400
	60 nF (PLZT composition 9/65/35) K = 3800

Ferrofilms

The properties of Ferrofilms were determined from PLZT composition 2/53/47 prepared via the acetate process and automatically dip coated for 40 layers onto Ag substrates ranging in thickness from 0.025 to 0.25 mm, yielding an overall film thickness of approximately 12 um. Standard, 1-mm diameter, vacuum evaporated Cu electrodes were deposited on the surface of the films for testing.

Dielectric Properties - The small-signal dielectric measurements of the PLZT thick films revealed that they possess properties very similar to bulk material of the same composition. For the particular composition evaluated, relative dielectric constants (1 kHz) ranged from 1400 to 1800 and dissipation factors from 3.5% to 4.6%.

Hysteresis Loops - Hysteresis loops (1 KHz) were obtained with an ac looper constructed in-house because thick films require higher voltages (>100 V) than normally available from standard thin film testers. An example of a typical loop is shown in Figure 20. As can be seen, the loop (polarization vs. electric field) is very square with sharp, saturated loop tips at maximum field, indicating a high degree of domain switching and good, insulating characteristics well into saturation at 100 kV/cm. The loop of Figure 20 displays typical properties for these films; i.e., that of: $P_R = 42$ uC/cm^2 and $E_c = 15.7$ kV/cm (40 V/mil). It should be recognized that this low value for E_c is more typical for bulk material than for thin films which characteristically possess E_cs of 75 kV/cm or higher.
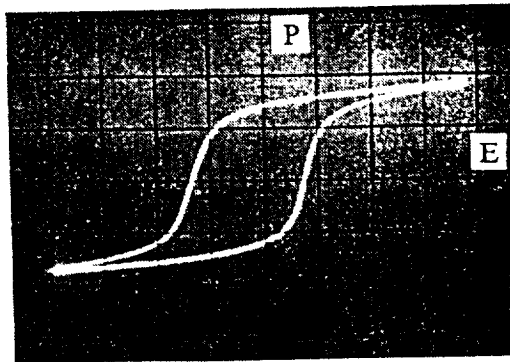
Figure 20. Typical Hysteresis Loop of Ferrofilm PLZT 1/53/47 on Ag

APPLICATIONS

A number of examples of applications are given in this section in order to demonstrate the versatility of the Rainbow and Ferrofilm technologies. These working models are essentially discrete, proof-of-principle devices which require further engineering design, miniaturization and modification in order for them to be suitable for hybrid microelectronics or integrated structures. In any case, it is believed that the Rainbow technology best serves the application range from macroelectronics to millielectronics, whereas the thick/thin Ferrofilms are best suited for the range from millielectronics to microelectronics.

The Rainbow devices shown in Figures 21 and 22 are typical examples of a number of applications envisioned for this technology. As can be seen, they range from actuators to sensors, and speakers to pumps. A more extensive list of applications include (1) linear actuators, (2) cavity/piston pumps, (3) loud speakers, (4) reciprocating motors, (5) relays/switches/thermostats, (6)

Speakers

Hydrophones

D
E
V
I
C
E
S

Motors

Pumps
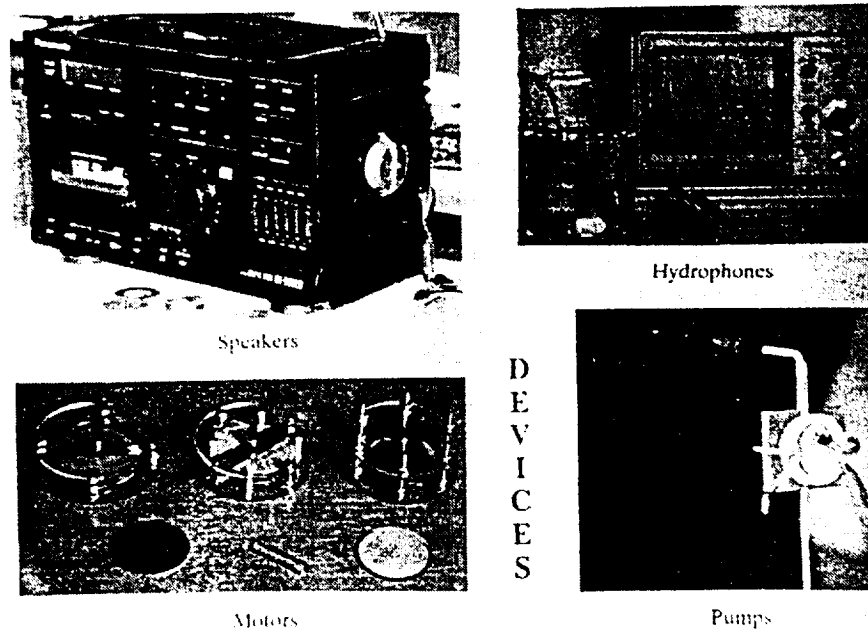
Figure 21. Examples of Working Model Devices Using Rainbow Ceramics as Actuators

sensors, (7) hydrophones/hydroprojectors, (8) variable-focus mirrors/lenses, (9) optical deflectors/scanners, (10) vibrating delivery systems, (11) liquid delivery systems, (12) antivibration/noise cancelling devices, (13) displays, (14) sonic and ultrasonic devices and (15) auto-leveling platforms.

SEND RECEIVE SENSOR

HYDRO PROJECTOR/HYDROPHONE

PISTON PUMPS
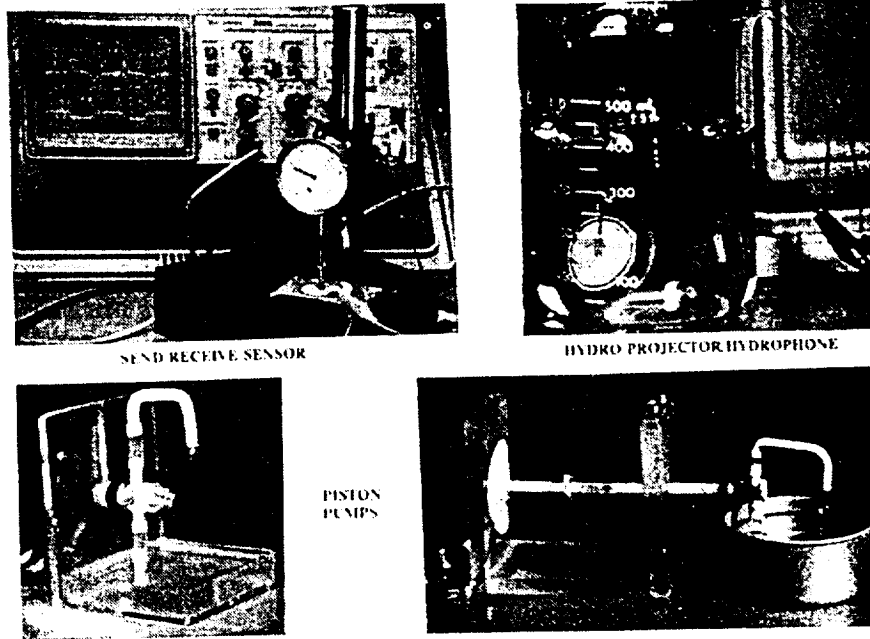
Figure 23. Additional Examples of Working Models Using Rainbow Ceramics as Actuators and Sensors

A single Ferrofilm device is shown in Figure 23. It simply consists of a 25 x 50 mm x 12 um thick film which was dip coated onto a 0.125 mm thick Ag substrate and electroded on the top major surface with vacuum-deposited Cu. After poling the film at 70 volts, the film/substrate is mounted to a resonating enclosure (in this case the enclosure is a cardboard box) and connected to the output of a radio. As with most ferroelectric/piezoelectric audio devices, the quality of the audio is only moderate, at best, when operated over the full audio range of the radio.

CONCLUSIONS

The prospects for utilizing Rainbows and Ferrofilms in discrete hybrid and

totally integrated microelectronics are promising for future applications involving smart ceramics such as ferroelectrics, piezoelectrics, pyroelectrics, electrooptics and electrostrictive materials. Rainbows have opened up a new dimension in ultra-high displacement actuators while Ferrofilms have now bridged the gap from bulk materials to thin films. The key to adapting these materials to specific devices and applications is the manner in which answers are found to questions concerning their reproducibility, reliability, longevity and cost effectiveness. Further development and design work are obviously needed in order to answer these questions.
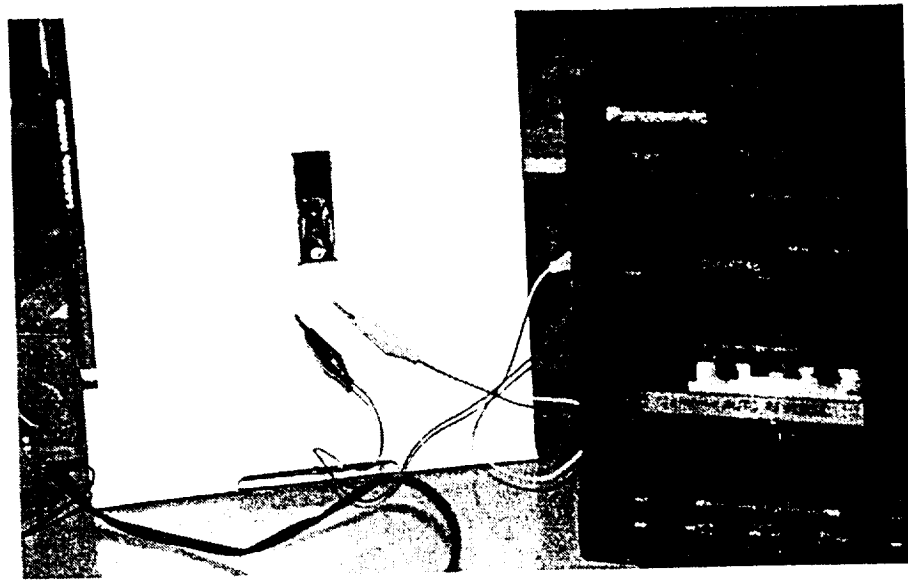
Figure 23. A Ferrofilm Speaker for a Stereo System

REFERENCES

1. L.H. Sheppard, "Advances in Processing of Ferroelectric Thin Films, Bull. Am. Ceram. Soc., 71, No. 1, 85-95 (1992)

2. P.C. Fazan, "Trends in the Development of ULSI DRAM Capacitors," Integrated Ferroelectrics, 4, 247-256 (1994)

3. R. Watton, "Ferroelectric Materials and IR Bolometer Arrays: From Hybrid Arrays Towards Integration," Integrated Ferroelectrics, 4, 175-186 (1994)

4. E.M. Lenoe, W.N. Radicic and M.S. Knapp, "Implications of Smart Materials in Advanced Prosthetics," Proceedings SPIE on Smart Structures and Materials, 2189, 84-104 (1994)

5. C.C. Hsueh, T. Tamagawa, C. Ye, A. Helgeson and D.L. Polla,"Sol-Gel Derived Ferroelectric Thin Films in Silicon Micromachining," Integrated Ferroelectrics, 3, 21-32 (1993)

6. G.H. Haertling, "Rainbow Ceramics - A New Type of Ultra-High Displacement Actuator," Bull. Am. Ceram. Soc., 73, No. 1, 93-96 (1994)

7. G.H. Haertling, "Chemically Reduced PLZT Ceramics for Ultra-High Displacement Actuators," Ferroelectrics, 154, 101-106 (1994)

8. K.K. Li, G.H. Haertling and W-Y Howng, "An Automatic Dip Coating Process for Dielectric Thin and Thick Films," Integrated Ferroelectrics, 3, 81-91(1993)

9. G.H. Haertling, "Dielectric and Electrooptic Properties of Acetate Derived PLZT X/65/35 Thin Films," Integrated Ferroelectrics, 3, 207-215 (1993)

10. G.H. Haertling, "Intelligent Processing of Ferroelectric Films," Bull. Am. Ceram. Soc., 73, No. 8, 68-73 (1994)

11. S. Sherrit, H.D. Wiederick and B.K. Mukherjee, "Evaluation of PLZT Based RAINBOW Ceramic Samples Developed by Dr. Gene Haertling at Clemson University," Report No. DREA CR/94/436, Royal Military College of Canada, Kingston, Ontario, Canada, June (1994)

12. E. Furman, G. Li and G.H. Haertling, "Electromechanical Properties of Rainbow Devices," Proceedings of the 9th ISAF Meeting, State College, June (1994)

Hybrid Microelectronic Materials

AN INVESTIGATION OF THE RESONANCE PROPERTIES OF RAINBOW DEVICES

E. FURMAN, G. LI and G. H. HAERTLING

Gilbert C. Robinson Department of Ceramic Engineering, Clemson University, Clemson, South Carolina 29634-0907 USA

In the last fifteen years considerable progress has been made in developing novel materials and devices for electromechanical actuator applications based on a variety of ferroelectric materials. Recently a novel type of high displacement actuator was developed. It is a monolithic, domed, stress-biased wafer consisting of oxide and reduced layers. These actuators are envisioned to be used in a variety of applications for which the knowledge of the resonance modes is essential. In this paper measurements of the resonant modes are compared to the predictions of the finite-element model. A number of low frequency modes were observed and identified as the bending modes. A higher frequency radial mode was determined to be less dependent on the sample dimensions than the bending modes. Effects of the boundary conditions on the resonant modes were modeled and investigated experimentally. For the modeling aspect of the study it was necessary to measure elastic constants, thermal expansion coefficients, and bulk densities of the oxide and reduced portions of the actuator. Experiments to measure these properties were performed and are described.

I. INTRODUCTION

In the last fifteen years there has been considerable progress in developing novel materials and devices for electromechanical actuator applications based on a variety of ferroelectric materials.[1] Much of the work was directed toward developing materials with enhanced electric field-induced strain. Currently linear strain actuators are based on piezoelectric, electrostrictive and antiferroelectric materials. For actuation, these devices rely on either piezoelectric d_{33}, d_{31}, electrostrictive Q_{11}, Q_{12}, or an antiferroelectric-ferroelectric phase transition volume change. Unfortunately, the maximum realizable strain in these devices is less than one percent.[2] For a multilayer actuator with a one centimeter thickness, the maximum obtainable total displacement is less than 10 microns.

There are a number of applications including pumps, speakers, laser deflectors, optical scanners and relays for which displacements well above 10 microns are desirable. For these applications piezoelectric benders have traditionally been used.[3-6] Benders are based on a bimorph or unimorph structures. Bimorphs contain two active layers bonded together, and unimorphs have an active and a passive layer. In both cases, bending occurs as a result of field-induced lateral strain. To accommodate this strain, the sample bends, producing vertical displacement. Key parameters for these devices are piezoelectric d_{31} or electrostrictive Q_{12} coefficients. A further advantage of benders is their lower mechanical impedance, which allows more effective energy coupling into gases and liquids. One consequence of the

higher compliance of benders is a reduction of the resonant frequencies compared to stiffer linear actuators.[6]

Benders are used in three types of applications: quasi-static, non-resonant dynamic, and resonant.[3] For the non-resonant dynamic and resonant applications, knowledge of resonant modes of a bender device is of crucial importance.

Recently a new type of bender called a RAINBOW (Reduced And Internally Biased Oxide Wafer) was developed which has promising characteristics.[7] Rainbow devices with 1 mm displacement and a 10 kg load-bearing capability were built.

The purpose of this paper is to describe the resonant properties of Rainbow devices. The basic structure and the principle of operation of Rainbow devices is described in section II. In section III the experimental procedures for preparation and characterization of Rainbow devices are given. Section IV describes the finite-element modeling procedure. In section V experimental results are compared with the finite-element model. Likely mechanisms for the various vibration modes are identified.

II. RAINBOW ACTUATORS

A unimorph consists of a piezoelectric or electrostrictive active layer bonded to a metal foil. Electric field induced lateral dimensional change in an active layer is opposed by a flexible metal plate. Rainbow actuators, similar to conventional unimorphs, consist of an electromechanically active layer and inactive layer. Unlike the unimorph, the Rainbow is a monolithic structure. The inert layer is formed by exposing one side of a lead-containing ceramic to a reducing atmosphere at high temperature produced by placing a ceramic in contact with a carbon block. The reduction of lead lanthanum zirconate titanate (PLZT) ceramics occurs as a result of oxidation of the solid carbon block, first to carbon monoxide and then the carbon dioxide gases.[8] The reduced layer is a good electrical conductor, and it acts both as the electrode and inert part of the bender.

Rainbows also differ from unimorph benders by the presence of large internal stresses developed in the process of reduction and cooling down to room temperature. Various steps involved in internal stress and shape development of a Rainbow are shown in Figure 1. Because of the volume reduction occurring during the reduction step and larger thermal expansion of the reduced layer compared to the oxide layer, stress-free equilibrium dimensions of the reduced layer are smaller than for the oxide layer. External stresses shown in Figure 1(b) must be present in order to prevent the composite from bending. The removal of external forces results in a net bending moment, which accounts for the Rainbow shape.

III. EXPERIMENTAL PROCEDURE

PLZT ceramics were prepared using a conventional mixed-oxide process. Following calcination at 925°C for 2 hours in a closed alumina crucible, the milled and dried powders were cold pressed as preform slugs and then hot pressed at 1200°C for 6 hours at 14 MPa. Hot pressed PLZT samples were placed on a graphite block, and
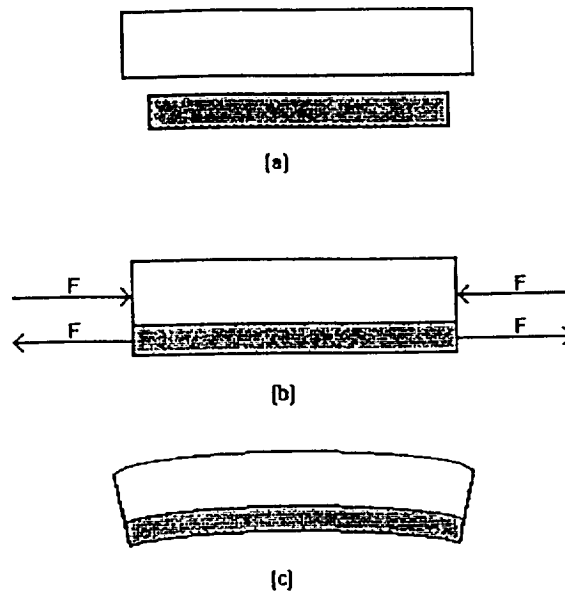
(a)

(b)

(c)

FIGURE 1   Formation of a Rainbow device, showing the oxide layer (light) and the reduced layer (dark): (a) at zero stress level; (b) with compressive force applied to the oxide layer and tensile force to the reduced layer to match the layers at the boundary; (c) after the removal of external forces.

the assembly entered into the furnace preheated to 975°C. Exposure of the samples to the reducing atmosphere ranged from 45 minutes for a typical Rainbow sample to many hours for the completely reduced samples used in the measurements of the coefficient of thermal expansion, and elastic constants of the reduced layer. For electrical studies, samples were electroded with silver epoxy paint (5504N, E. I. du Pont de Nemours & Co.) at 200°C for thirty minutes. Further details of Rainbow preparation can be found in reference 7.

The majority of the characterization work described in this paper was performed on PLZT ceramics with the nominal composition 5.5/57/43 (La/Zr/Ti). This composition was chosen because of the large lateral strain observed in PLZT samples with this composition, and its proximity to the morphotropic phase boundary insured high electromechanical coefficients.[9]

Densities of the oxide and reduced samples were measured using a water immersion method. Ultrasonic pulse-echo measurements were performed on the oxide and completely reduced samples. Panametrics model 5052PR Ultrasonic Pulser/Receiver was used with 10 MHz longitudinal and 5 MHz shear transducers acoustically coupled to samples polished with five micron powder. The samples had less than two percent variation in thickness and a diameter-to-thickness ratio sufficiently large to avoid diffraction effects.

A HP 54504A digital storage oscilloscope was interfaced with the pulser, and both excitation and echo responses were recorded. Measurements of shear velocity (v_s) and longitudinal velocity (v_l), combined with the measurements of densities, permitted calculation of Young's modulus (Y) and Poisson's ratio.

An Orton dilatometer model 1600D with an environmental chamber was used to perform thermal expansion measurements from room temperature up to 1000°C.

Completely reduced samples were measured in flowing nitrogen, and unreduced PLZT samples in air.

Resonant modes of the Rainbow devices were characterized with an HP 4194 impedance analyzer. Samples were supported at the center of the top and bottom surfaces with point contacts for the majority of the experiments.

In the model, both resonant and antiresonant modes were characterized. The resonant modes were obtained by specifying the short circuit electrical boundary conditions. The open circuit electrical boundary conditions were used for the determination of antiresonant modes.

IV. MODELING

The finite-element modeling, FEM, of complicated piezoelectric structures had successfully been used in the past.[10] For this study the ABAQUS commercial FEM package (Hibitt, Karlsson & Sorenson, Inc., version 5.2) was used to simulate thermomechanical and electromechanical properties of the Rainbow devices. The model uses linear piezoelectric, dielectric, and elastic properties of the oxide and reduced layers.

The constituent equations for the piezoelectric media used in the modeling are:

$$S_i = s_{ij}^E T_j + d_{ij}^t E_j \tag{1}$$

$$D_i = d_{ij} T_j + \varepsilon_{ij}^T E_j \tag{2}$$

where S_i is the strain, D_i is the polarization, T_j is the stress, E_j is the electric field, s_{ij}^E is the elastic compliance, ε_{ij}^T is the dielectric permittivity, and d_{ij} is the piezo-electric compliance.

Rainbow modeling includes three major parts; (1) definition of material properties and sample geometry, (2) modeling of the cool down from the reducing temperature to room temperature and (3) determination of response to the specified set of the boundary conditions.

In the case of piezoelectric ceramics there are 3 piezoelectric, 2 dielectric and 5 elastic nonzero coefficients, and their values are known only for a few ceramics. Fortunately, for PZT 5 all of the above properties have been characterized.[11] PZT 5 is a soft PZT, and it should have values similar to those of PLZT ceramics used in this study. Piezoelectric, dielectric, and elastic constants of PZT 5 were used in the model. Actual values used are listed in the Appendix. In addition, Young's modulus, Poisson's ratio, densities, and thermal expansion coefficients for the oxide and reduced layers were determined in this study and were used in the modeling.

The parameters and sample geometry were entered into two separate models. The simpler model is a two dimensional axisymmetrical model. A full three dimensional model was also developed for a more complete characterization of the resonant modes.

For the modeling of the cool down step nonlinear analyses were used because of the considerable stiffening of the Rainbow structure during this step.

For the calculation of the resonant and antiresonant modes using the axisymmetric model, a structure based on 60 elements gave satisfactory results (about 2% stiffer than the model with 120 elements). A relatively small number of elements

was sufficient because of the primary interest in the frequency range below 100 KHz.

V. RESULTS AND DISCUSSION

Measurements of densities and elastic constants for the oxide and reduced layers based on PLZT 5.5/57/43 nominal composition are summarized in Table I. A slightly larger density and Poisson's ratio for the reduced layer compared to the oxide layer is due to a large quantity of lead metal present in the reduced layer as determined by X-ray diffraction.[8] The specific gravity of lead is 11.35 and it has a large Poisson's ratio of 0.43.[12] The pulse-echo measurements used gave elastic constants at a constant displacement. A large measured value of Poisson's ratio for the oxide layer is consistent with the literature values for the PZT materials for the constant displacement condition.[13]

Lead metal with its high coefficient of thermal expansion of $16 * 10^{-6}\,°C^{-1}$ contributes to a higher value of thermal expansion of the reduced layer compared to the oxide layer.[12] It was not possible to determine the precise values of coefficient of thermal expansion up to 975°C for the oxide and reduced layers due to creep observed in both materials at high temperature. Creep in the oxide layer occurred for temperatures above 750°C, and for the reduced layer above 850°C. Creep of the oxide layer is more pronounced compared to the reduced layer, and amounted to 1.2 percent change of the measured sample length for a room temperature to 1000°C thermal cycling. CTE values in Table I represent actual values used in the modeling, and resulted in a fairly good agreement between the predicted and measured curvatures of a Rainbow on cool down. The amount of the volume change during the reduction of PLZT at 975°C was not estimated directly, but was considered as a contributor to the effective thermal expansion constant of the reduced layers. In the temperature range where creep is not significant, the following measured CTE values were obtained: for the oxide sample $6.7 * 10^{-6}\,°C^{-1}$ in the range of 27 to 700°C, and for the reduced sample $8.2 * 10^{-6}\,°C^{-1}$ in the range of 80 to 850°C. A significant creep in the oxide layer at higher temperatures is the reason for the lower oxide CTE used for the whole temperature range. Similarly, volume reduction during the reduction at 975°C is the justification for the higher value of its CTE used.

A comparison between the experimental determination of the resonant frequencies for the different boundary conditions and axisymmetric FEM is made in Table II. Experiments were performed on the Rainbow with the oxide composition of 5.5/57/43. Two boundary conditions were used: (1) a sample supported at top

TABLE I

Experimental data obtained for the PLZT 5.5/57/43 oxide and reduced layers

Property	Oxide layer	Reduced layer
Density (gm/cm^3)	7.93	8.00
Young's modulus (N/m^2)	$7.79 \cdot 10^{10}$	$6.86 \cdot 10^{10}$
Poisson's ratio	0.377	0.381
Thermal Expansion (°C^{-1})	$\sim 5 \cdot 10^{-6}$	$\sim 10 \cdot 10^{-6}$

TABLE II

Effect of the boundary conditions on antiresonant frequencies of PLZT 5.5/57/43 Rainbow determined experimentally and from the axisymmetric modeling

Boundary Condition	Experimental Frequency (Hz)	Modeling Frequency (Hz)
No Sideways Constraint	1534	1611
	1642	
	6547	
	7100	7218
	7368	
	7608	
	16816	
	18116	18544
	32290	35347
	not observed	57086
	76740	74854
Sideways Constraint	3844	2353
	4189	
	5900	
	10900	9767
	12533	
	14370	
	27000	23224
	not observed	42117
	not observed	66277
	76969	74008
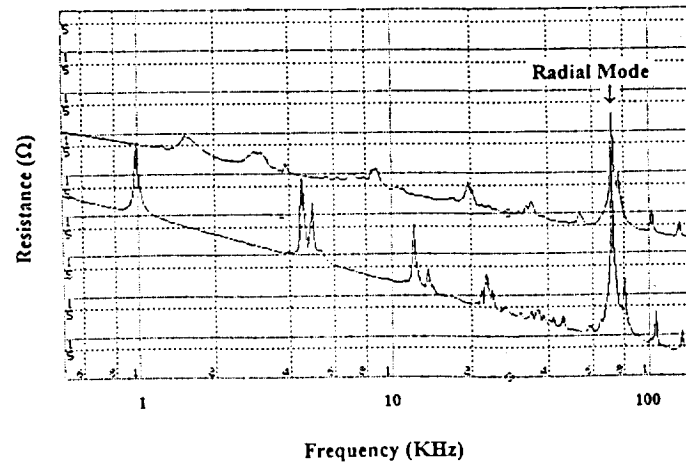
FIGURE 2 Resonance spectra for PLZT 1/53/47 Rainbow for two boundary conditions: (a) plane/ point support; (b) point/point support. The two spectra are separated vertically for clarity.

and bottom surfaces with point contacts and (2) a sample resting on a rigid plate with point contact at the top center. Good agreement between the model and experiment was observed for the point contact arrangement. The model predicted frequencies that are typically slightly higher than the experiment. Increasing the number of elements used in the modeling reduced the stiffness of a Rainbow and

TABLE III

Resonant modes of PLZT 5.5/56/44 Rainbow determined experimentally and predicted by the axisymmetric and three dimensional models.

Experimental Frequency (Hz)	Axisymmetric Model (Hz)	Three Dimensional Model (Hz)
1501	1566	1525
		1537
		3612
6200		6394
		6915
7100	7102	7179
		9929
		11344
		14366
15000		14883
		16687
		19027
	18265	19379
		19746
		23056

(Dimensions: 3.20 cm diameter; thickness 0.053 cm; reduced layer thickness 0.015 cm)

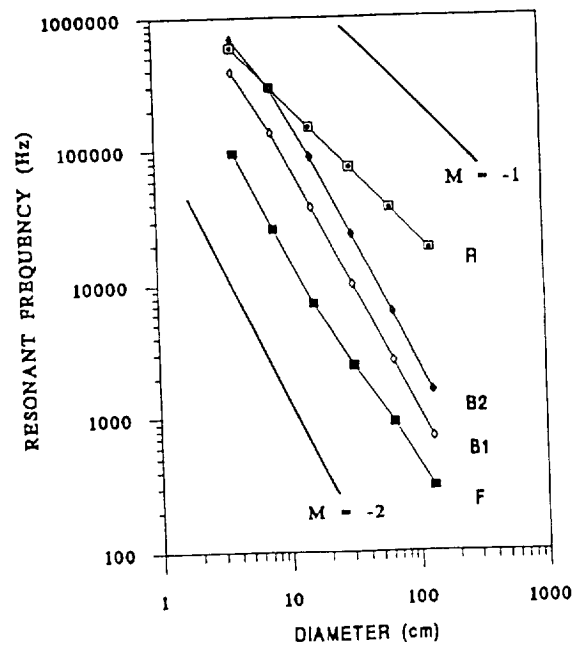FIGURE 3 Axisymmetric modeling of the effect of the Rainbow sample diameter on the resonant frequency. Modeling parameters: number of elements: 60, reduced layer thickness: 0.015 cm, total thickness: 0.053 cm. M: ideal slopes for comparison. F: fundamental mode, B1, B2: pure bending modes, R: radial mode.
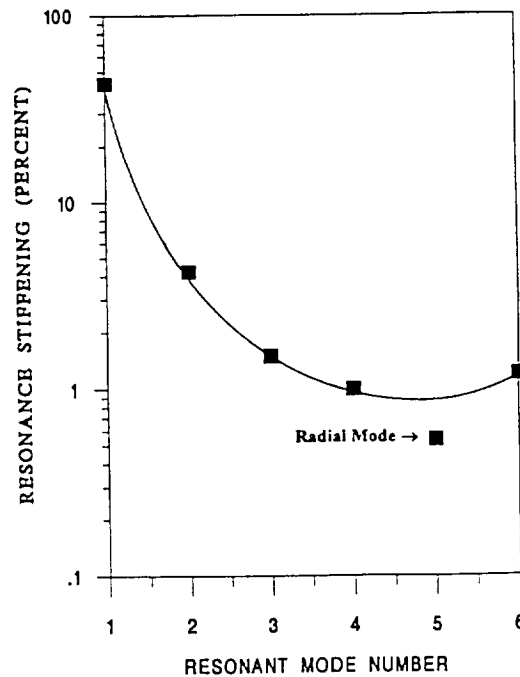
FIGURE 4   Axisymmetric modeling of the resonance stiffening during the cool down step. Stiffening is the change in frequency on cool down divided by the frequency prior to cool down, expressed in percent.

resulted in further improvement in its ability to predict actual resonant spectrum. A number of observed modes are not predicted by the axisymmetric model because they do not contain infinite fold rotational axes of symmetry. For the plane-to-point boundary condition, observed modes occur at significantly higher frequencies than those predicted by the model. The model does not account for the frictional forces present as a result of a lateral displacement of a Rainbow.

The experimentally obtained resonance spectra for PLZT 1/53/47 Rainbow for two different boundary conditions are shown in Figure 2. In addition to stiffening of the modes for plane/point support, broadening and damping of the modes occurred. As compared to the radial mode occurring at 72 KHz, the low frequency modes are weaker; in fact, some of the modes predicted by the model were not observed experimentally. The radial mode is also less sensitive to the boundary conditions as compared to low frequency modes.

The principle advantage of the three dimensional FEM model is that the full spectrum of possible resonant modes becomes available for the analyses. This is achieved at the price of significantly higher computational time. For a few samples on which three dimensional modeling was performed, good agreement with the axisymmetric model was obtained. An example of this is shown in Table III, in which the experimental data is also included.

The shape of the mode has to be consistent with the boundary conditions provided. For the case where sideways motion of the Rainbow is restricted to a planar motion, the resonant mode shapes and the order in which they occur follow the predicted modes for a circular membrane.[14]
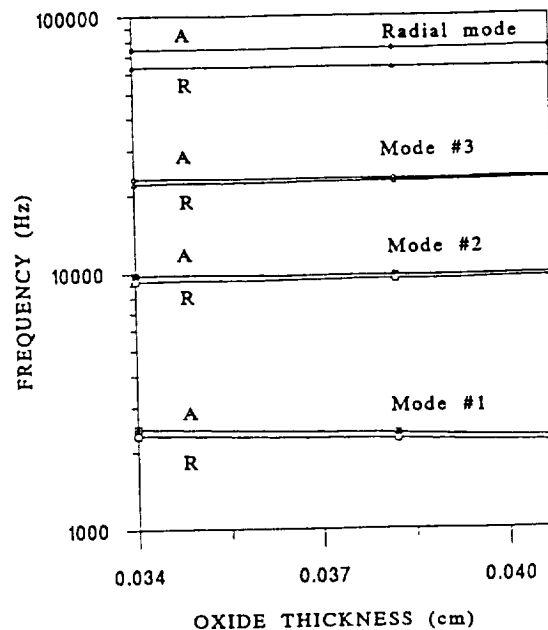
FIGURE 5 Axisymmetric modeling of the resonance and antiresonance mode frequencies as a function of the oxide layer thickness. Modeling parameters: number of elements: 60, total thickness: 0.051 cm, diameter: 3.175 cm. R: resonance mode, A: antiresonance mode.

For the oxide PLZT circular disc, the lowest frequency mode is the resonant or planar mode. In the case of a Rainbow device, the radial mode is no longer the lowest mode of resonance. There are two types of modes which may occur in a Rainbow at lower frequencies: the thin sphere breathing mode which has no harmonics, and a flexure or bending mode existing in a composite structure.[11,15] Resonance modes for the Rainbow samples with different diameters were modeled to determine the mode of vibration. The radial and the sphere breathing mode frequencies are proportional to the inverse of the diameter, for the bending mode the resonant frequency is proportional to the inverse of the diameter squared. The results of the axisymmetric modeling are shown in Figure 3. Over a wide range of frequencies, the radial mode follows a slope of − 1. Except for the smallest diameter case, the second and third lowest modes follow closely a slope of − 2 indicating a pure bending mode. For the lowest mode, Rainbows with small diameters have a bender mode resonance as deduced from the slope, but for larger diameters the slope does not fit either the thin sphere breathing mode or bending mode.

It already has been shown (Figure 2) that the low frequency modes are more sensitive to the boundary conditions as compared to the radial mode. It can be observed from Figure 4 that the low frequency modes are also more sensitive to the cool down step. The resonance modes for the Rainbow cooled down from 975°C were compared to a similar sample which was not cooled down. All of the modes for the cooled down sample were at a higher frequency implying that the stiffening of the structure occurs during the cool down step. However, the relative change of the resonant frequency, plotted on the vertical axes, is again the highest
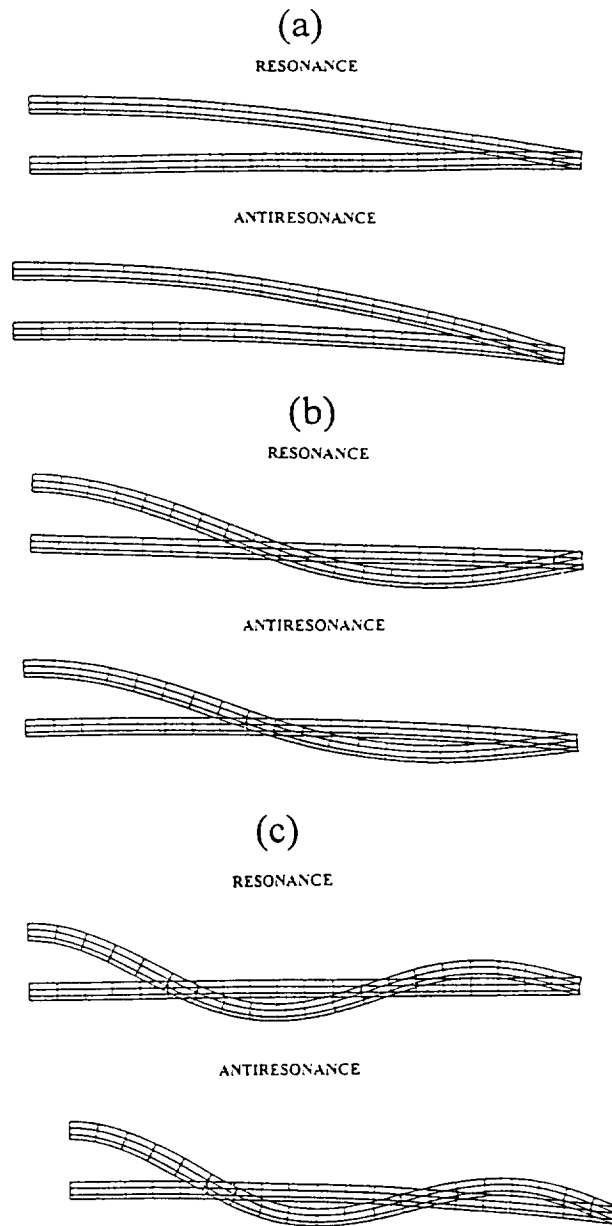
FIGURE 6   Axisymmetric modeling of the shapes of the resonant and antiresonant modes for the five lowest frequencies. (a) first mode; (b) second mode; (c) third mode; (d) fourth mode; (e) fifth mode. Modeling parameters: number of elements: 60, reduced layer thickness: 0.013 cm, total thickness: 0.051 cm, diameter: 3.175 cm.

for the low lying modes. The fifth mode is a radial mode and the least sensitive to the effect of the cool down.

In addition, the effect of the oxide to reduced thickness ratio for Rainbows with constant total thickness was modeled. The strength of the resonance is proportional

(d)

RESONANCE

ANTIRESONANCE

(e)

RESONANCE

ANTIRESONANCE

FIGURE 6   (*Continued*)

to the frequency separation between resonant and antiresonant modes divided by the resonant frequency. Figure 5 illustrates that the strengths of modes 1 through 3 are inversely proportional to the oxide layer thickness. The radial mode is the strongest mode observed since it has the largest separation between resonant and antiresonant modes.

Shapes of the modes provide useful information for possible applications, and also provide information about possible coupling between the modes. The five lowest frequency modes for the typical Rainbow device are shown in the Figure 6. For each mode, the structure which i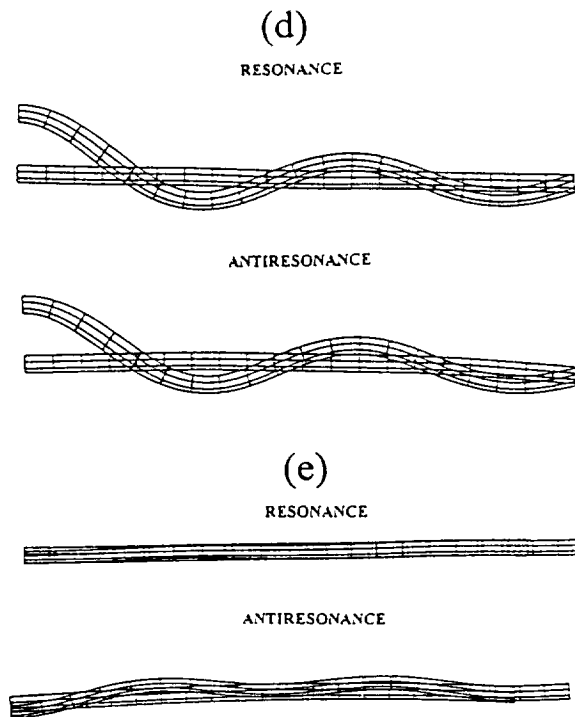s more flat represents the Rainbow after cool down. From the previous discussion, the first mode may not be a simple bending mode. Its shape is characterized by the entire surface moving in phase. The second, third, and fourth modes each have one additional nodal circle represented by a nodal point in the cross sections shown. Inner and outer surfaces of a Rainbow are now moving out of phase. Stavsky and Loewy[15] have indicated that for a composite circular plate there is a coupling between the radial and bending modes. They have considered a purely elastic system. Apparently their conclusion is also applicable for the case of a piezoelectric composite system. As can be seen from the fifth mode in addition to lateral motion associated with the radial mode, there is also bending present. Bending is more pronounced for the antiresonant mode. The radial mode is usually stronger than the bending modes, as determined by a separation in frequency between the resonant and antiresonant conditions.

(d)

RESONANCE

ANTIRESONANCE

(e)

RESONANCE

ANTIRESONANCE

FIGURE 6   (*Continued*)

to the frequency separation between resonant and antiresonant modes divided by the resonant frequency. Figure 5 illustrates that the strengths of modes 1 through 3 are inversely proportional to the oxide layer thickness. The radial mode is the strongest mode observed since it has the largest separation between resonant and antiresonant modes.

Shapes of the modes provide useful information for possible applications, and also provide information about possible coupling between the modes. The five lowest frequency modes for the typical Rainbow device are shown in the Figure 6. For each mode, the structure which is more flat represents the Rainbow after cool down. From the previous discussion, the first mode may not be a simple bending mode. Its shape is characterized by the entire surface moving in phase. The second, third, and fourth modes each have one additional nodal circle represented by a nodal point in the cross sections shown. Inner and outer surfaces of a Rainbow are now moving out of phase. Stavsky and Loewy[15] have indicated that for a composite circular plate there is a coupling between the radial and bending modes. They have considered a purely elastic system. Apparently their conclusion is also applicable for the case of a piezoelectric composite system. As can be seen from the fifth mode in addition to lateral motion associated with the radial mode, there is also bending present. Bending is more pronounced for the antiresonant mode. The radial mode is usually stronger than the bending modes, as determined by a separation in frequency between the resonant and antiresonant conditions.
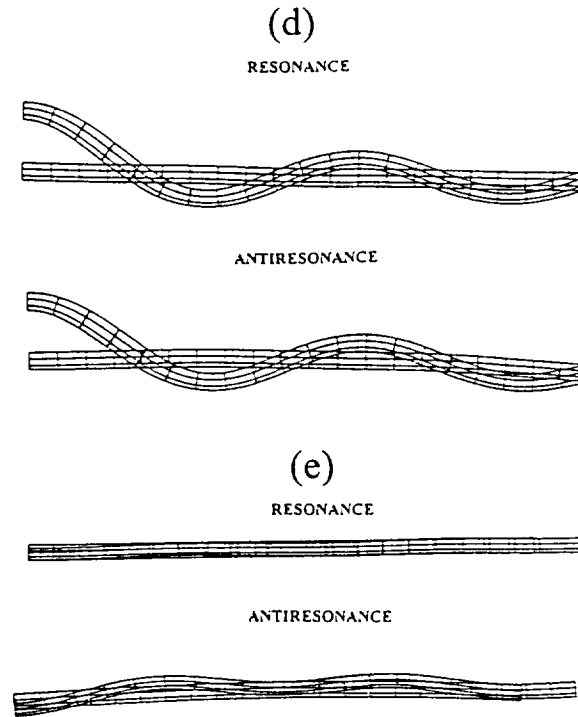
For this sample geometry, the resonant and antiresonant frequencies for the sixth mode (a bending mode) occur between the resonant and antiresonant modes of the much stronger radial mode.

The knowledge of the location and shape of the resonant modes can be beneficial in the design of Rainbow-based devices. For speaker applications it is advantageous to work well below second mode. Because of its shape, different parts of the Rainbow are being displaced out of phase near this resonance, which would diminish speaker efficiency. For pumps, it may be useful to operate at the first resonant mode, where the volume displacement should be large. Figure 3 can be used as a guideline for the determination of the appropriate geometry to operate at resonance.

VI. CONCLUSIONS

Experimental characterization and finite-element modeling of the resonant modes of Rainbow devices were presented. A good agreement between the experimentally determined resonances and finite element modeling was obtained. The identity of various modes was deduced from the frequency dependence of the resonant mode on its diameter. A large number of low frequency bending modes exist in the Rainbow devices. The coupling between the bending and radial modes was established.

The effects of the boundary conditions on the resonance behavior of Rainbow devices were investigated. The more constraining boundary conditions resulted in higher resonant frequencies. The bending modes were more affected by the boundary conditions as compared to the radial mode.

The thermal expansion coefficients, elastic constants, and densities were measured for the oxide and completely reduced samples. Higher values of the thermal expansion coefficient, Poisson's ratio, and density observed in the reduced layer are all consistent with a large amount of metallic lead present in the reduced samples.

APPENDIX

Material Parameters for PZT 5[11]

c_{11}^E	$12.1 * 10^{10}$ N/m^2
c_{12}^E	$7.54 * 10^{10}$ N/m^2
c_{13}^E	$7.52 * 10^{10}$ N/m^2
c_{33}^E	$11.1 * 10^{10}$ N/m^2
c_{44}^E	$2.11 * 10^{10}$ N/m^2
d_{33}	$374 * 10^{-12}$ C/N
d_{33}	$-171 * 10^{-12}$ C/N
d_{15}	$584 * 10^{-12}$ C/N
$\varepsilon_{11}^T/\varepsilon^0$	1730
$\varepsilon_{33}^T/\varepsilon^0$	1700

ACKNOWLEDGEMENTS

REFERENCES

1. K. Uchino, *Ceramic Bulletin*, **65**, 647 (1986).
2. L. E. Cross, *J. of Intell. Mater. Syst. and Struct.*, **2**, 241 (1991).
3. J. van Randeraat and R. E. Setterington (Ed.), "Piezoelectric Ceramics" (N. V. Philips' Gloei-lampenfabrieken, Eindhoven, The Netherlands, 1974).
4. A. G. Kuzin, *et al.*, *Sov. Phys. Tech. Phys.*, **21**, 1128 (1976).
5. M. R. Steel, F. Harrison and P. G. Harper, *J. Phys. D.: Appl. Phys.*, **11**, 979 (1978).
6. J. K. Lee and M. M. Marcus, *Ferroelectrics*, **32**, 93 (1981).
7. G. H. Haertling, *Am. Cer. Soc. Bull.*, **73**, 93 (1994).
8. G. H. Haertling, pp. 699–711 in Proceedings of the 4th International SAMPE Electronics Conference, Ed. R. E. Alfred, R. J. Martinez and K. B. Wischmann, (Society for the Advancement of Materials and Process Engineering, Covina, GA, 1990).
9. B. Jaffe, W. R. Cook, Jr. and H. Jaffe, "Piezoelectric Ceramics" (Academic Press, London, 1971).
10. R. Learch, *IEEE Trans. Ultrasonics, Ferroel., and Frequency Control*, **37**, 233 (1990).
11. D. A. Berlincourt, D. R. Curran and H. Jaffe, Ch. 3 in "Physical Acoustics," vol. 1 Part A, Ed. W. P. Mason (Academic Press, New York, 1964).
12. "CRC Handbook of Tables for Applied Engineering Sciences, Second Edition, Ed. R. Boltz and G. Tuve (CRC Press, 1973).
13. "Landolt-Bornstein Numerical Data and Functional Relationships in Science and Technology," Ed. K.-H. Hellwege and A. M. Hellwege (Springer-Verlag, Berlin, 1981) vol. 16, p. 123.
14. P. M. Morse and K. U. Ingard, "Theoretical Acoustics" (McGraw-Hill, New York, 1968).
15. Y. Stavsky and R. Loewy, *J. Acoust. Soc. Am.*, **49**, 1542 (1971).

COMPOSITION AND MICROSTRUCTURE OF CHEMICALLY REDUCED PLZT CERAMICS

G. LI, E. FURMAN and G. H. HAERTLING

*Department of Ceramic Engineering, Clemson University,
Clemson, South Carolina 29634-0907, USA*

Hot-pressed PLZT ceramic wafers were chemically reduced by a special processing technique on one of the major surfaces to form oxide-reduced layer composite structures. Devices based on such structures have promising characteristics for actuator use. The composition and microstructure of the reduced layer from several PLZT ceramics of different compositions as well as the oxide-reduced layer interface were examined and analyzed by means of X-ray diffraction (XRD) and scanning electron microscopy (SEM). A variety of the oxide phases, such as PbO, ZrO_2, $ZrTiO_4$ and $LaTiO_3$, were revealed in the reduced PLZT samples by XRD in addition to the anticipated metallic lead phase. SEM micrographs showed that the reduced PLZT ceramics were composed of various fine-grained particles, and the metallic lead formed a continuous phase. It was found that the oxide-reduced layer interface region was composed of a mixture of unreduced and reduced phases. The thickness of the mixed phase region was primarily associated with the grain size of the original unreduced PLZT ceramics.

1. INTRODUCTION

A new type of ultra-high-displacement, multi-function actuator, named RAINBOW (Reduced And INternally Biased Oxide Wafer), has recently been developed by using a special processing method. This technique involves chemical reduction of one of the major surfaces of a high lead-containing ferroelectric ceramic wafer by heat treating the wafer on a flat carbon block at an elevated temperature, thus producing a dome-shaped, oxide-reduced layer composite structure. When an electric field is applied across such a composite wafer, large axial displacement is generated. Detailed descriptions of Rainbow ceramics and their potential applications can be found in References 1 and 2. Since the electromechanical properties of a Rainbow actuator are dependent upon the physical properties such as thermal expansion, elasticity, and electrical conductivity of its reduced layer, a thorough investigation of the microstructure of reduced PLZT ceramics is significant for the characterization and application of Rainbow actuators. The PLZT ceramics were chosen for this work because they are easily reduced and have excellent electromechanical characteristics.

The phase components and microstructure of the reduced layer as well as the configuration of the oxide-reduced layer interface for several PLZT Rainbow samples have been investigated by means of X-ray diffraction technique and scanning electron microscopy.

2. SAMPLE PREPARATION AND EXPERIMENTAL PROCEDURES

The Rainbow samples used were prepared from PLZT ceramics 1.0/53/47, 5.5/57/43 and 9.5/65/35, where the numbers denote the atom ratios La/Zr/Ti of the PLZT

compositions. Conventional processing techniques combined with hot-pressing were employed to produce highly dense PLZT slugs. The ceramic wafers obtained from the PLZT slugs were chemically reduced by placing them on a graphite block and heat treating them under the conditions of 975°C/60 min (reduction temperature/time).

Fractured, polished, and etched surfaces of the samples were used in both XRD and SEM analyses. For X-ray diffraction, the reduced side of the Rainbow samples were lapped off approximately 50 μm and slightly polished to expose the internal structures. This procedure was employed because a thin reoxidized layer is often formed on reduced surfaces during processing. X-ray diffraction was first performed on the polished surfaces. Then, the same surfaces were etched with an HCl/HF solution for further study. X-ray diffraction patterns of fractured surfaces were obtained from the powders prepared by crushing the completely reduced PLZT wafers.

Cross-sectional surfaces of the Rainbow samples were usually used for the SEM analysis in this study. The fractured surfaces were obtained by breaking the Rainbow along their diameters. The surfaces were also polished by using progressively finer diamond pastes with a finish of 0.25 μm. The polished surfaces were then etched, cleaned, and coated with a carbon or gold film before examination. In some cases, the polished surfaces were directly examined under SEM.

All of the X-ray diffraction experiments were performed on an X-ray diffractometer (Scintag XDS 2000™) with Cu Kα radiation at a scan rate of 2 degrees per minute. A JOEL scanning electron microscope operating at an accelerating voltage of 15 keV was used for the SEM analyses.

3. EXPERIMENTAL RESULTS

3.1 X-Ray Diffraction Analysis

Figures 1(a)–1(c) show the X-ray diffraction patterns from the polished surface of the reduced layer of Rainbow samples 1.0/53/47, 5.5/57/43 and 9.5/65/35, respectively. The Rainbow samples in this work are indicated by their original PLZT composition; for example, Rainbow 10/53/47 represents a sample produced from PLZT 1.0/53/47 wafer. It was found that in all cases the strongest peaks in the diffraction patterns were produced by the metallic lead phase. The remaining weaker peaks were caused by a number of oxide phases formed during the reduction process. The number and composition of the phases observed in the reduced PLZT ceramics were dependent on the unreduced PLZT compositions. As is indicated in the figures, the oxide phases identified include PbO (litharge), ZrO_2, $ZrTiO_4$, TiO_2, $LaTiO_3$ and $La_{0.66}TiO_{2.99}$ (JCPDS 26-827).

The X-ray diffraction pattern of the etched reduced surface of Rainbow 5.5/57/43 is given in Figure 2. It can readily be seen by comparing Figure 2 with Figure 1(b) that, upon etching, almost all of the Pb peaks were greatly depressed while those of the oxide phases underwent little change. This result suggests that it is primarily the Pb phase that was etched away from the surface.

It should be noted that the intense diffraction peaks of the Pb phase shown in Figures 1(a)–1(c) may partly result from the grinding and polishing treatments on
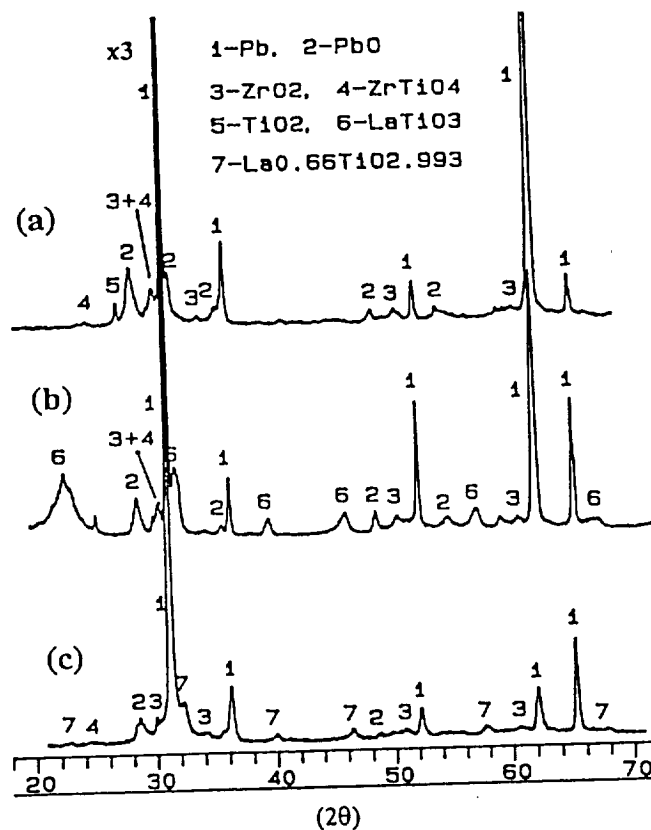
FIGURE 1 X-ray diffraction patterns from the polished surface of the reduced layer of Rainbows (a) 1.0/53/47, (b) 5.5/57/43 and (c) 9.5/65/35.
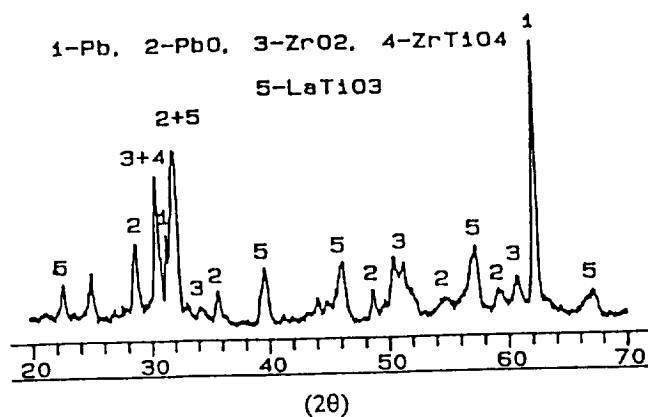

FIGURE 2 X-ray diffraction pattern from etched reduced surface of Rainbow 5.5/57/43.

1-Pb, 2-PbO (litharge)
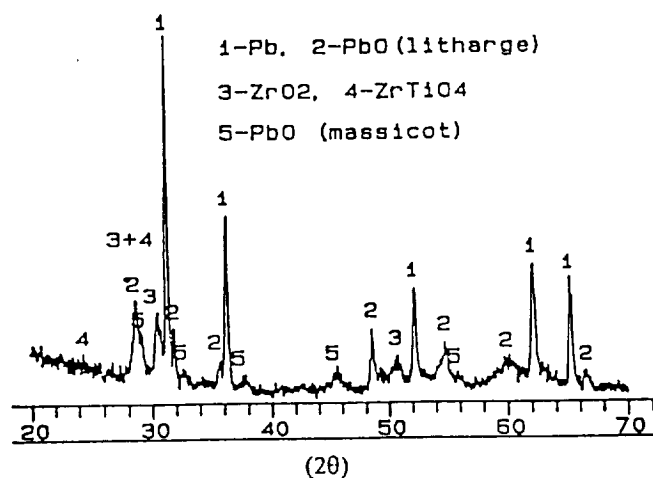
3-ZrO2, 4-ZrTiO4

5-PbO (massicot)

(2θ)

FIGURE 3   X-ray diffraction pattern of the powder obtained from reduced PLZT 1.0/53/47 sample.

FIGURE 4   SEM micrograph of fractured cross-sectional surface of Rainbow 1.0/53/47 near the PLZT-reduced layer interface.

the sample surfaces prior to analysis. Since the metal Pb is a very soft material relative to the oxide phases, when a reduced sample is ground or polished, the Pb phase is deformed and smeared over the surface. Consequently, the relative amount of Pb phase on the surface is increased, thereby enhancing the intensity of the Pb diffraction peaks.

For this reason, the X-ray diffraction of fractured surfaces better reflects the actual states of the various phases in a sample. Since it is difficult, in practice, to obtain a large fracture surface of the reduced layer, the powders from completely reduced wafers which contain various small fracture surfaces were used instead. The diffraction pattern of such powder for Rainbow 1.0/53/47 is shown in Figure 3. As can be seen, the intensity ratios of the major metallic lead peaks to the oxide phase peaks are considerably reduced compared to those of the polished surface shown in Figure 1(a), indicating the presence of smearing in the polished samples. It is, however, worth noting that the Pb diffraction peaks from the powder remain the strongest,
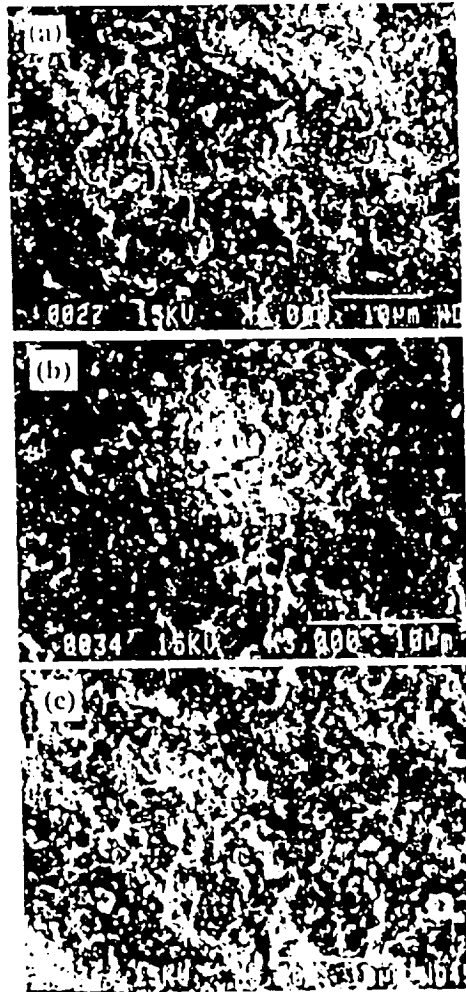
FIGURE 5   SEM micrograph of the reduced layer of Rainbows (a) 1.0/53/47, (b) 5.5/57/43 and (c) 9.5/65/35.

and this is also true for the other PLZT Rainbow samples studied. Figure 3 also shows the existence of PbO (massicot) phase which was not observed in Figures 1(a)–1(c).

3.2 SEM Analysis

Figure 4 shows the SEM micrograph of the fractured cross-sectional surface of Rainbow 1.0/53/47. The upper portion of the micrograph shows the PLZT layer, and the lower portion is the reduced layer. These layers are separated by a PLZT-reduced layer interface where both the unreduced and reduced phases were found. A micrograph of higher magnification on the reduced region, which is given in Figure 5(a),

FIGURE 6   Backscattered electron image of Rainbow 1.0/53/47 near the PLZT-reduced layer interface.

indicates that the region was composed of various fine-grained particles. A similar microstructure was also observed in Rainbows 5.5/57/43 and 9.5/65/35, as is shown in Figures 5(b) and 5(c) respectively. The small uniformly distributed pa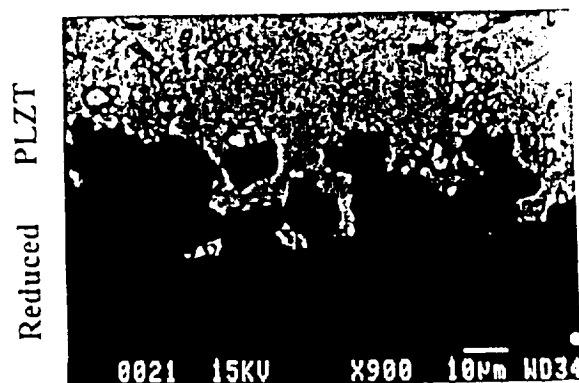rticles, about 0.2 μm in diameter, as can be seen in the figures, were identified to be the Pb grains by means of X-ray diffraction coupled with an extraction technique. The microstructure of the reduced layer seems relatively insensitive to the microstructure of the original PLZT composition.

The secondary electron image of a polished surface of the reduced layer is usually featureless. It was, however, found that some characteristics of the polished surfaces can be revealed via a backscattered electron imaging technique. Figure 6 is a backscattered electron image of Rainbow 1.0/53/47 near the PLZT-reduced layer interface. Again the lower portion is the reduced layer. The darkest areas seen in Figure 6 are most likely the thoroughly reduced regions. This is because the reduction process leads to a relatively loose structure by decomposing the original dense PLZT phase with an accompanying oxygen loss, thereby contributing less to the backscattered electron signals. From the morphology of the oxide-reduced layer interface it can be deduced that the reduction reaction was initiated along the PLZT grain boundaries and then proceeded toward the center of the grains.

The SEM image of the etched reduced surface of Rainbow 5.5/57/43, whose X-ray diffraction pattern has been given in Figure 2, is displayed in Figure 7. The grains exposed by etching, which can be seen in Figure 7, are considered to be the oxide phases identified in the corresponding X-ray diffraction pattern. The fact that the oxide grains appears isolated indicates that the Pb grains, which were mostly etched away from the surfaces, form a continuous phase. The continuity of the lead phase is further supported by high electrical conductivity of the reduced layers.

4. DISCUSSION

The results of the aforementioned X-ray diffraction analyses indicate that a number of different phases are produced as a result of the chemical reduction of a PLZT ceramic in forming the Rainbow structure. The phases found include the metallic lead phase and seven oxide phases: PbO (litharge), PbO (massicot), ZrO_2, $ZrTiO_4$,

FIGURE 7   SEM micrograph of etched reduced layer of Rainbow 5.5/57/43.

TiO_2, $LaTiO_3$ and $La_{0.66}TiO_{2.99}$. The original PLZT phase was not observed in the reduced samples. It is noted that while the exact number and composition of the phases in a particular reduced PLZT sample depend on the original PLZT composition, the phases of Pb, PbO (litharge), ZrO_2 and $ZrTiO_4$ are common among the samples studied.

Many investigations of chemical reduction of ferroelectric materials were concerned with the influence of reduction atmosphere on the electrical and optical properties of the materials.[3-7] In these studies, defects, generally vacancies, were introduced into the crystal lattice during chemical reduction, but the framework of the crystal structure underwent no substantial changes. Current work dealt with intense chemical reduction of high-lead containing ferroelectric ceramics in which the original crystal structure was completely destroyed. In his investigation of PLZT ceramics reduced by graphite blocks,[8] Haertling showed that the reduction reaction is accomplished via the interaction between carbon monoxide and loosely held oxygen atoms in the PLZT perovskite lattice. It is therefore considered that, except for the oxygen and slight Pb losses during reduction, the reduced layer should contain the same amount of chemical elements as the unreduced PLZT ceramic. In other words, the chemical reduction simply decomposes the PLZT crystal structure by attacking the lattice oxygen ions and, at the same time, produces new phases by rearranging the constituent elements.

Based on this consideration, the volume fraction of the lead phase in a reduced PLZT sample may not be as large as it seems in the X-ray diffraction as, for example, shown in Figure 3. This is reasonable since along with the volume fraction of each phase many other factors may contribute to the relative peak intensities of the X-ray diffraction pattern in a multiphase material. In fact, for the conceivable uses of Rainbow actuators, it is not critical whether the Pb phase is dominant or not. The main concern is that the Pb phase must be a continuous phase so that the reduced layer has good conductivity. The fact that the metallic lead in the reduced layer occurs with very fine particles, as was shown in the SEM micrographs, suggests that even a small volume fraction of lead phase can render the reduced layer electrically conductive. This may explain why the reduced PLZT ceramic exhibits excellent conductivity.

There is a region along the PLZT-reduced layer interface where both PLZT and

reduced phases exist. The dimension (normal to the interface) of the region is defined as the thickness of the interface in a Rainbow. It was found that the interface thickness was related to the grain size of the phase before reduction. This is easily understood considering that the reduction process is initialized along grain boundaries as illustrated in Figure 6. For Rainbow 1.0/53/47, whose PLZT layer displays a larger grain size, the thickness was found to be approximately 20 μm. Rainbows 5.5/57/43 and 9.5/65/35 have an interface thickness of about 2 μm and 5 μm, respectively. The configuration of the PLZT-reduced layer interface is probably important for some specific properties of Rainbow actuators such as fatigue and loading capability and will be investigated further.

5. SUMMARY

A number of different crystalline phases have ben found in the PLZT ceramics reduced via the RAINBOW process. The phases found include metallic lead and seven oxide phases: PbO (litharge), PbO (massicot), ZrO_2, $ZrTiO_4$, TiO_2, $LaTiO_3$ and $La_{0.66}TiO_{2.99}$. The original PLZT phase was not observed. While the exact number and composition of the phases for a particular reduced sample are dependent on the PLZT composition, the phases of Pb, PbO (litharge), ZrO_2 and $ZrTiO_4$ are commonly observed, with the Pb phase producing the strongest X-ray diffraction.

The reduced PLZT ceramics are composed of various fine-grained particles, and the smallest grains, about 0.2 μm, correspond to the lead phase. This microstructural characteristic is relatively insensitive to the PLZT composition. It is shown that the metallic Pb grains constitute a continuous phase in the reduced PLZT ceramics, which is consistent with the good electrical conductivity of these materials.

Near the interface between the PLZT and reduced phases of a Rainbow, the two phases coexist. The thickness of the interface was found to be associated with the grain size of the PLZT phase. The values of the interface thickness for Rainbows 1.0/57/43, 9.5/65/35 and 5.5/57/43 are approximately 20, 4, and 2 μm, respectively.

REFERENCES

1. G. H. Haertling, *Bull. Am. Ceram. Soc.*, 73, 94 (1994).
2. E. Furman, G. Li and G. H. Haertling, *Ferroelectrics*, 160, 357 (1994).
3. S. Ikegami and I. Ueda, *J. Phys. Soc. Jpn.*, 19, 159 (1964).
4. S. Ducharme and J. Feinberg, *J. Opt. Soc. Am., B*, 3, 283 (1986).
5. N. R. Rajopadhye, S. V. Bhoraskar, S. Badrinarayan and A. P. B. Sinha, *J. Mat. Sci.*, 23, 2631 (1988).
6. A. Dhar and A. Mansingh, *J. Phys. D: Appl. Phys.*, 24, 1644 (1991).
7. S. M. Mukhopadhyay and T. C. S. Chen, *J. Mat. Res.*, 10, 1502 (1995).
8. G. H. Haertling, in Proceedings of 4th International SAMPE Electronics Conference (Society for the Advancement of Materials and Process Engineering Covina, GA), Vol. 4, p. 699, 1990.

FABRICATION AND PROPERTIES OF PSZT ANTIFERROELECTRIC RAINBOW ACTUATORS

G. LI, E. FURMAN and G. H. HAERTLING

Department of Ceramic Engineering, Clemson University, SC 29634-0907, USA

A new type of high-displacement actuator called Rainbow (Reduced And INternally Biased Oxide Wafer) was recently developed, and it shows promising characteristics in a variety of potential applications. The fabrication and properties of Rainbow actuators from PSZT antiferroelectric ceramics with compositions near the antiferroelectric-ferroelectric (AFE-FE) phase boundary were investigated. It was found that the chemical reduction reaction proceeded much more rapidly in PSZT than in PLZT ceramics. The optimum conditions for the processing of PSZT Rainbows were determined to be 850°C for 2–3 hours. Large axial displacements ranging from 102 to 273 μm were obtained from the PSZT Rainbow samples by application of electric fields greater than the AFE-to-FE phase switching levels. The characteristics of the field-induced displacements of the Rainbow samples were dependent on the manner of applying mechanical load on the samples. At room temperature, the antiferroelectric PSZT Rainbows exhibited a concave curvature with respect to the oxide side, which was attributed to the cubic-to-antiferroelectric phase transition in the oxide layer during cooling. The dielectric and AFE-FE phase transition properties of the Rainbow samples were compared with those of the normal ceramics.

Keywords: Antiferroelectric ceramic, actuator, chemical reduction, antiferroelastic domain, internal stress.

1. INTRODUCTION

During the past several years actuators based on ferroelectric ceramic materials have received numerous investigations and undergone remarkable advances.[1] Ceramic actuators offer many advantages including quick response, high induced stress, low energy consumption and low cost which make them very attractive for a number of newer applications. When exposed to an external electric field, a ferroelectric ceramic will change its dimensions through ferroelectric domain reorientation and the intrinsic piezoelectric effect. If the ceramic is in the antiferroelectric state, strains will be developed when the antiferroelectric state is switched to the ferroelectric state under a sufficiently high applied electric field. Since the unit cell of the antiferroelectric state is generally much smaller than that of the ferroelectric state, a significant change in volume occurs during the antiferroelectric-ferroelectric transition. The field-induced dimensional changes in ferroelectric materials provide a useful mechanism for actuation application.

The electric field-induced strains from ferroelectric ceramics are relatively small although the induced stress can be substantial. They are only a few tenths of one percent for most of the compositional systems. This disadvantage considerably limits their use on advanced applications such as active structures, linear motors, cavity pumps and noise-cancelling devices that require a relatively large physical displacement. To achieve a higher displacement from the ceramics, a number of strain magnification mechanisms have been employed. Examples include the traditional uni-

morph and bimorph benders,[2] and the more recent ''moonie'' structure.[3] A bender
is able to transform a small transverse strain of the ceramic into a large displacement
in the longitudinal direction, while a ''moonie'' composite utilizes both the trans-
verse and longitudinal strains in producing a larger axial displacement. Generally, a
significant trade-off exists between induced displacement and stress for these struc-
tures. That is, an increase of induced displacement is achieved at the expense of
lowering generated stress significantly. There is, therefore, a need for mechanisms
that can provide large displacements while still sustaining reasonable load or stress.
This criterion has been met, to great extent, by a new type of stress-biased, oxide-
reduced composite ceramic wafer which was recently developed.[4] Designated as
Rainbow (Reduced And INternally Biased Oxide Wafer), the ceramic wafer is ob-
tained via chemical reduction of one major surface of a high lead-containing ferro-
electric wafer, such as PLZT, by placing the wafer on a flat carbon block and heat
treating it at an elevated temperature. As the partially reduced ceramic wafer is
cooled to room temperature, a dome-shaped (sometimes saddle-shaped), internally
stressed oxide (unreduced)-reduced layer structure is formed. Very high axial dis-
placement is obtainable from an electroded Rainbow sample by application of an
electric field across the ceramic oxide layer. Also, due to the unique dome structure,
a Rainbow can sustain a stress higher than normal. Rainbow ceramics have shown
promising characteristics for a variety of potential applications.[4-6]

It has been found that the $Pb(Sn,Zr,Ti)O_3$ (PSZT) ceramics with compositions in
the vicinity of the FE-AFE phase boundary exhibit very high field-induced strains
resulting from the transition from the AFE to the FE state.[7,8] A longitudinal strain
of 1.1% (the highest ever reported in the literature for ferroelectric ceramics) was
claimed in the PSZT system in a study by Shebanov et al.[8] Furthermore, the strain
characteristics of these ceramics can be modified through selection of appropriate
compositions.[9] For example, a PSZT ceramic may have a shape-memory effect sim-
ilar to some alloys or digital-like strain characteristics depending on the location of
its composition in the phase diagram. Ceramics with specific compositions in the
AFE phase region near the AFE-FE phase boundary are easily switched to the fer-
roelectric state by application of an electric field and remain ferroelectric upon re-
moval of the field. As a result, a shape-memory effect is achieved. The AFE com-
positions distant from the phase boundary exhibit well-defined AFE characteristics
with the digital-like strain characteristics under applied electric fields. A number of
possible applications have been proposed to utilize the strain properties of the PSZT
ceramics.[9-11]

The objective of this work was to combine the high induced strains of PSZT
ceramics with the Rainbow technology to produce high-displacement actuators. In
this paper, the fabrication and properties of PSZT antiferroelectric Rainbow actuators
with compositions in the vicinity of the FE-AFE phase boundary are described.

2. SAMPLE PREPARATION

Bulk PSZT ceramics used for the fabrication of the Rainbow samples were prepared
according to the formula $Pb_{0.97}La_{0.02}(Zr_xSn_yTi_z)O_3$. The samples studied are desig-
nated as PSZT X/Y/Z or Rainbow X/Y/Z in the following discussion, where the X,

TABLE I

Diameter and oxide/reduced thickness ratio of PSZT
Rainbow samples

Rainbow Sample	Diameter (cm)	Oxide/Reduced (μm)
66/23/11HP	2.72	302/135
64/26/10HP	2.72	294/135
64/26/10S	2.16	378/140
66/23/11S	2.16	271/190
66/24/10S	2.72	334/165
62/28/10S	2.16	195/165

HP—hot-pressed; S—sintered.

Y and Z are the molar percentage of Zr, Sn and Ti ions in the B site of the perovskite structure, respectively. The letters, HP or S, are also added to the Rainbow designation to indicate that the sample is made from hot-pressed or sintered ceramics. For example, Rainbow 64/26/10S represents a Rainbow made from a sintered PSZT 64/26/10 (Zr/Sn/Ti) wafer. A number of compositions near the AFE-FE phase boundary which were reported to have the highest field-induced strains were selected. Reagent grade PbO, ZrO_2, TiO_2, SnO_2 and La_2O_3 were used as the starting materials. Weighed components were mixed in distilled water for 30 minutes and dried at 105°C overnight. The dried powders were calcined at 925°C for 2 hours, and then milled for 8 hours in trichloroethylene using a polyethylene jar and ZrO_2 balls. Bulk ceramics were obtained either by sintering sample pellets at 1280–1320°C for 4 hours or by hot pressing the pellets at 1200°C for 6 hours at 14 MPa in an oxygen atmosphere. The sintered ceramic slugs were cut and lapped into wafers of various diameters and thicknesses.

In the fabrication of Rainbow samples, a PSZT wafer was chemically reduced on one of the major surfaces by placing the wafer on a graphite block and introducing the assembly into a preheated furnace. A zirconia disk was placed on top of the PSZT wafer to prevent possible thermal shock during processing. After the reduction, the wafer together with the graphite block was removed from the furnace and cooled down in air to room temperature. Epoxy silver electrodes cured at 200°C were used for determination of the Rainbow's electrical properties. The dimensions of the Rainbow samples are shown in Table I. Samples with two different diameters of 2.16 and 2.72 cm were studied.

3. MEASUREMENTS

The crystalline phases of reduced PSZT ceramics were examined with an X-ray diffractometer (Scintag XDS 2000™) using Cu $K\alpha$ radiation at a scan rate of 2 degrees per minute. The thicknesses of the reduced layer of the Rainbows were measured from the sample cross-sections by means of an optical microscope. Room temperature dielectric properties of the samples were determined at 1 kHz on an LCR meter (LEADER, 7450-01). Conventional dc hysteresis loop equipment was
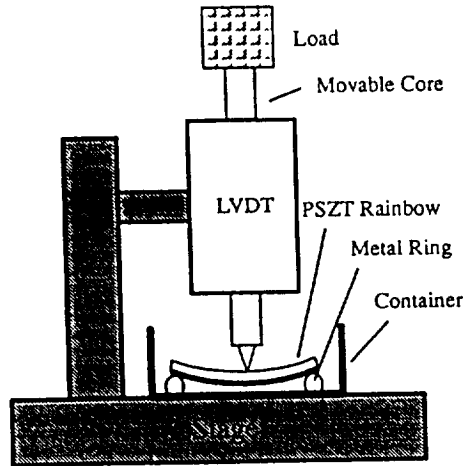
FIGURE 1   Schematic of apparatus for displacement measurement (not to scale).

employed to measure the relationship between polarization and electric field. Electric fields greater than the AFE-to-FE phase transition levels were applied gradually to the samples.

A measuring setup with an LVDT (Linear Variable Differential Transformer, 050 DC-E Lucas Schaeritz Co.), as seen in Figure 1, was used to determine the change of the field-induced displacement with electric field and the change of the dome height of a Rainbow with temperature. A Rainbow sample with electrodes on its major surfaces was placed on a metal ring in a small container. The ring supported only the edge of the sample so that the center part of the Rainbow could move up and down without touching the bottom of the container. The container was filled with silicon oil for insulating and temperature control purposes. The movable core of the LVDT was adjusted to contact the center of the Rainbow sample.

Mechanical loading on the Rainbow samples was accomplished by placing weights on top of the LVDT movable core. The variations of polarization and axial displacement with electric field were measured simultaneously as the samples were loaded.

4. RESULTS AND DISCUSSION

4.1. Chemical Reduction of PSZT Ceramics

Temperature is an important factor in controlling the reduction process during fabrication of Rainbow samples. For PLZT ferroelectric ceramics (the most frequently used Rainbow materials), the optimal reduction temperature was around 975°C. It was found that the reduction reaction was considerably more rapid in PSZT than in PLZT ceramics. A significantly thicker reduced layer in a PSZT than in a PLZT ceramic was produced when they were reduced at the same temperature for a given time. Figure 2(a) shows the reduced layer thickness of a PSZT Rainbow as a function of reduction temperature for a time of one hour. The thickness of the reduced layer began to increase rapidly at about 875°C, and tended to saturate at higher tempera-
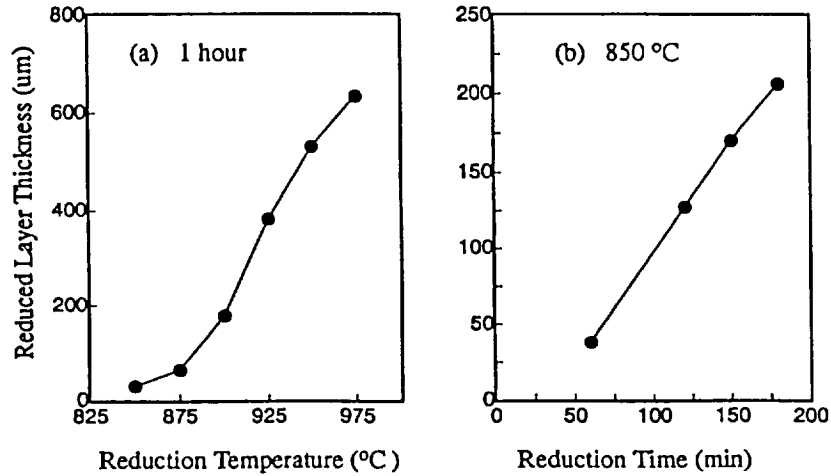
FIGURE 2 Variations of reduced layer thickness with (a) reduction temperature and (b) reduction time for PSZT Rainbow 64/26/10HP.

tures. An approximately 650 μm thick reduced layer was created in the PSZT sample at 975°C, as compared to the 150 μm thick reduced layer in a typical PLZT Rainbow obtained under identical conditions. Further manifestation of the rapid reaction in PSZT ceramics is the enhanced reoxidation of the reduced layers observed at elevated temperatures. For example, a reduced layer 200 μm thick was completely reoxidized almost instantaneously when exposed to air at a temperature used for the reduction. The reasons for the severe reactions occurring in PSZT ceramics have not been fully determined, but they seem to be related to the multivalent nature of the Sn.

Reduction time is another important factor that influences the reduction process. Figure 2(b) shows the change of the reduced layer thickness with time at a constant temperature of 850°C for hot-pressed PSZT 64/26/10. A nearly linear relationship was observed.

Although the reduction reaction is very rapid in PSZT ceramics, the reduction of the PSZT phase, unlike that of PLZT, was found to be incomplete. Figure 3(a) shows the X-ray diffraction pattern from a PSZT sample reduced at 975°C. Even at this high temperature a significant amount of the original PSZT phase remained in addition to the oxide phases such as PbO (massicot), ZrO_2, $ZrTiO_4$, and SnO_2 which resulted from the reduction process. At 975°C, the rapid reaction led to precipitation of a large amount of lead phase on the sample surface. With the additional loss of lead phase due to reoxidation during cooling, metallic lead was nearly absent from the reduced region. The diffraction pattern in Figure 3(a) was obtained after removal of the lead particles from the surface, and hence the diffraction peaks of the lead phase were not observed. Figure 3(b) shows the X-ray diffraction pattern from a sample reduced at a relatively low temperature of 850°C. At this temperature, only metallic lead and the original PSZT phases are evident, and the lead phase was uniformly distributed within the reduced layer.

As mentioned above, at a high temperature such as 975°C, the rapid reaction in PSZT ceramics leads to the loss of a large portion of lead phase from the reduced region. As a result, the reduced region has poor electrical conductivity or even be-
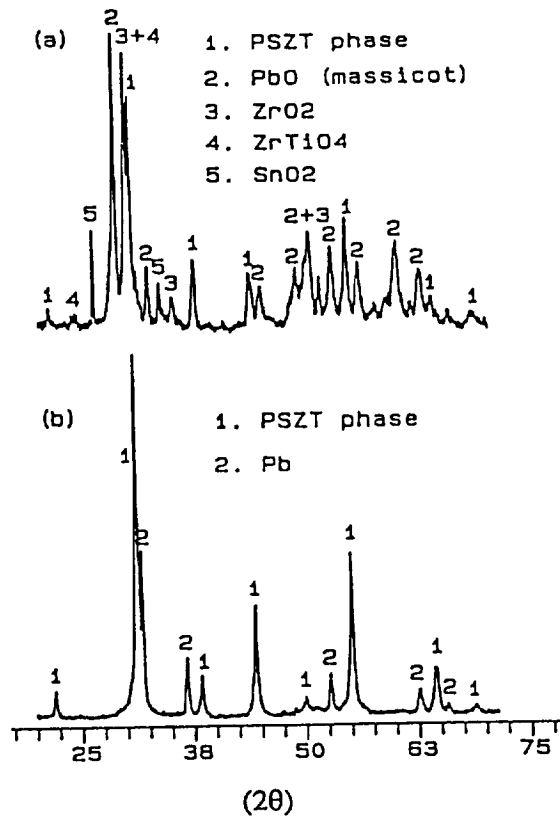
FIGURE 3   X-ray diffraction patterns of PSZT 64/26/10 ceramics reduced at (a) 975°C and (b) 850°C.

comes an insulator. This is detrimental to the performance of Rainbow actuators since the reduced layer must be electrically conductive in order for a Rainbow to operate properly. To prevent the heavy loss of the lead phase from occurring, lower reduction temperatures must be used. However, a very low temperature implies impractical and long reduction times. It was found that the useful temperature range for the production of PSZT Rainbows is actually very narrow, approximately 850 ± 30°C. The optimal conditions for producing Rainbow samples from PSZT ceramics were determined to be 850°C for 2–3 hours.

4.2. Properties of PSZT Antiferroelectric Rainbows

Figure 4 shows the polarization (P)-electric field (E) hysteresis loop of Rainbow 64/26/10HP. The hysteresis loop of a normal (non-Rainbow) sample is also given in the figure for comparison. Significant differences between the two loops are seen. First, a finite net polarization Δp, indicating a partially poled ferroelectric state of the sample, was found to exist in the virgin state of the Rainbow sample. This phenomenon, which was also observed in ferroelectric PLZT Rainbows,[12] is believed to be associated with the nonuniform internal stress in Rainbows. Second, the AFE-to-FE phase switching in the Rainbow occurred at a much lower field level and was
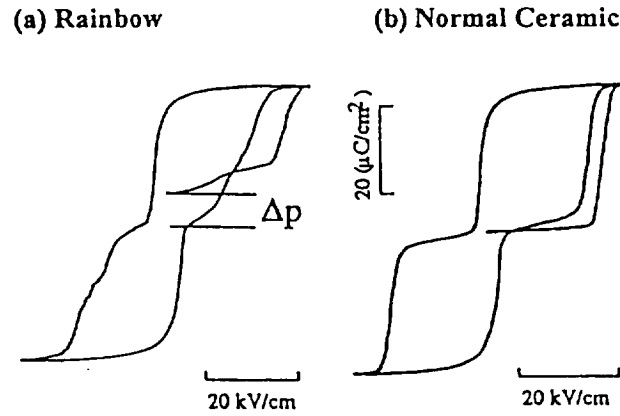
(a) Rainbow   **(b) Normal Ceramic**

FIGURE 4   Polarization-electric field hysteresis loops of Rainbow 64/26/10HP and normal (non-Rainbow) PSZT 64/26/10 ceramic.

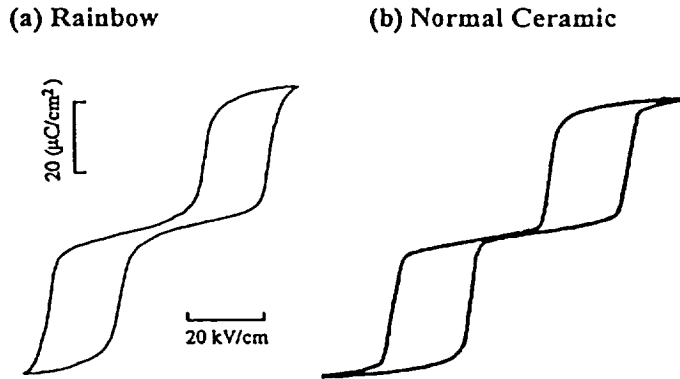**(a) Rainbow**   **(b) Normal Ceramic**

FIGURE 5   Polarization-electric field hysteresis loops of Rainbow 66/24/10S and normal PSZT 66/24/10.

less abrupt compared to the normal sample. Since the composition of PSZT 64/26/10 is located near the AFE-FE phase boundary, an intermediate P-E hysteresis loop characteristic of the two phases, namely a double hysteresis loop with an appreciable remanent polarization, was observed.

The hysteresis loops of Rainbow 66/24/10S and the corresponding normal sample are shown in Figure 5. Because the composition is well inside the AFE phase region, a typical double hysteresis loop with no remanent polarization is seen for the normal sample. The marginal remanent polarization observed in the Rainbow was probably caused by the internal stress, which will be discussed later.

Figure 6 shows the variation of axial displacement with electric field for Rainbows 64/26/10HP and 66/24/10S. A displacement as large as 273 μm was obtained from Rainbow 64/26/10HP accompanying the AFE-FE phase switching. The remanent displacement at zero field was attributable to the remanent polarization as shown in Figure 4(a). Rainbow 66/24/10S also exhibited a large axial displacement resulting from the phase switching, but little remanent displacement was found to exist. The step-like displacement-field relationship of Rainbow 66/24/10S was similar to the field-induced strain curve of the normal sample as indicated in Figure 7.

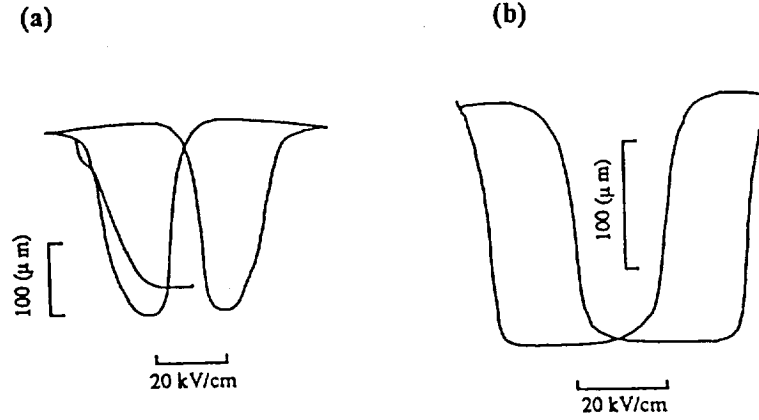**(a)**   **(b)**

FIGURE 6   Change of axial displacement with electric field for (a) Rainbow 64/26/10HP and (b) Rainbow 66/24/10S.
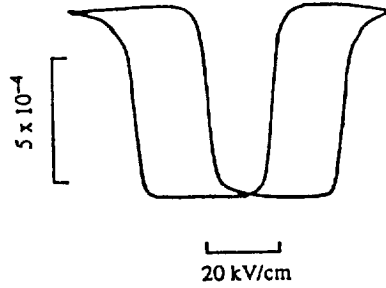

FIGURE 7   Change of transverse strain of PSZT 66/24/10 ceramic with electric field.

The axial displacement- and polarization-electric field relationships of Rainbow 66/23/11HP are given in Figure 8. Of the antiferroelectric samples studied, this sample is closest to the FE phase region. As can be seen in the figure, Rainbow 66/23/11HP is antiferroelectric in the virgin state, but stabilized into the ferroelectric state after being switched by the applied electric field. A large displacement, approximately 145 μm, was produced during the initial AFE-to-FE phase switching. The reorientation of ferroelectric domains after the initial phase transition led to a butterfly-like loop of typical ferroelectrics and moderate changes in the displacement.

Tables II and III summarize the properties obtained from the PSZT Rainbows and normal ceramics, respectively. The Rainbow samples, in general, possessed a lower dielectric constant and a higher loss factor than the normal samples. The phase switching fields, E_{AF} and E_{FA}, of the Rainbow samples were lower than those of the normal ceramics, varying with composition. The saturated polarization, however, was similar in the Rainbows and the normal samples. The total field-induced axial displacement of the Rainbows due to the phase transitions varied from sample to sample and was in the range of 102 to 273 μm depending on the geometry as well as the material properties of both the oxide and reduced layers. The largest displacement was found in Rainbow 64/26/10HP, which is equivalent to a strain of 0.63 relative to the total thickness of the sample. This is over 200 times larger than the longitudinal strain of the corresponding normal ceramic.
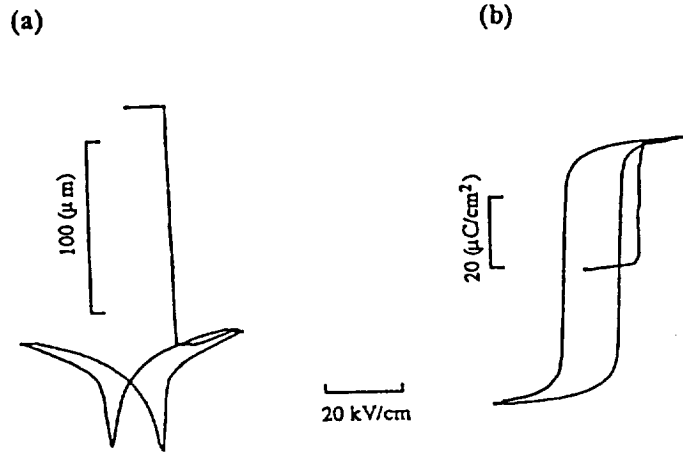
(a)   (b)

FIGURE 8 Variations of axial displacement and polarization with electric field for Rainbow 66/23/11HP.

TABLE II

Properties of PSZT Rainbow samples

Rainbow Sample	Dielectric Constant	tanδ (%)	E_{AF}/E_{FA} (kV/cm)	P_S or P_R ($\mu C/cm^2$)	y_M (μm)	S_M (%)
66/23/11HP	796	2.2	7.5 (Ec)	35	195*	45
64/26/10HP	730	3.4	19.5/–4.0	33	273	63
64/26/10S	821	3.9	16.5/–3.0	30	187	37
66/23/11S	734	3.1	7.0 (Ec)	31	102*	22
66/24/10S	626	5.4	28.5/10.0	31	208	42
62/28/10S	826	2.3	27.5/6.5	31	110	31

The effects of axial mechanical loading on the field-induced displacement and P-E hysteresis loops of Rainbow 66/24/10S are shown in Figures 9 and 10 for loads applied to the surfaces of the oxide and reduced layers, respectively. The maximum displacement from each displacement-electric field loop was determined, and plotted against loading in Figure 11. Clearly, the displacement characteristics of the Rainbow are dependent on the manner in which load is applied. There is only a slight change in the displacement up to 570 grams when load was placed on the oxide layer. The displacement with load on the reduced layer, however, decreased continuously with increasing loading. In both cases, it was found that loading has no significant influence on the polarization-electric field hysteresis loop. It is obvious that a PSZT Rainbow is more advantageous when operated with loading on the oxide side.

The different characteristics under the two loading conditions just discussed may be accounted for by the behavior of ferroelastic domains under stress. Ferroelastic domains tend to be in line with the directions in which stress is effectively relieved. When load is applied vertically to the oxide layer surface of a Rainbow, ferroelastic domains are preferably aligned parallel to the surface due to the compressive stress in the planar directions produced by the loading. This occurs because the lattice

TABLE III

Properties of PSZT normal (non-Rainbow) ceramics

Normal PSZT	Dielectric Constant	tanδ (%)	Density (g/cm³)	E_{AF}/E_{FA} (kV/cm)	P_S or P_R ($\mu C/cm^2$)	$S_{2,S}$ (x10⁴)	$S_{1,S}$ (x10⁴)
66/23/11HP	810	2.3	8.11	7.0 (E_C)	35	5.5	45.2*
64/26/10HP	876	1.6	8.22	23/-2.0	36	6.8	29.5
64/26/10S	913	1.9	8.05	28/1.0	31	7.9	28.0
66/24/10S	990	1.2	7.93	30/11.5	31	8.2	45.3
62/28/10S	882	1.9	7.97	30/9.5	32	8.5	45.7

E_{AF} – Antiferroelectric to ferroelectric switching field.
E_{FA} – Ferroelectric to antiferroelectric switching field.
P_S – Saturated polarization.
P_R – Remanent polarization.
E_C – Coercive field.
y_M – Maximum axial displacement with an applied electric field of $1.2 \times E_{AF}$.
S_M – Maximum axial displacement (y_M) divided by Rainbow thickness.
$S_{2,S}$ – Transverse field–induced strain.
$S_{1,S}$ – Longitudinal field–induced strain.
* obtained from initial phase switching.

(a)   (b)
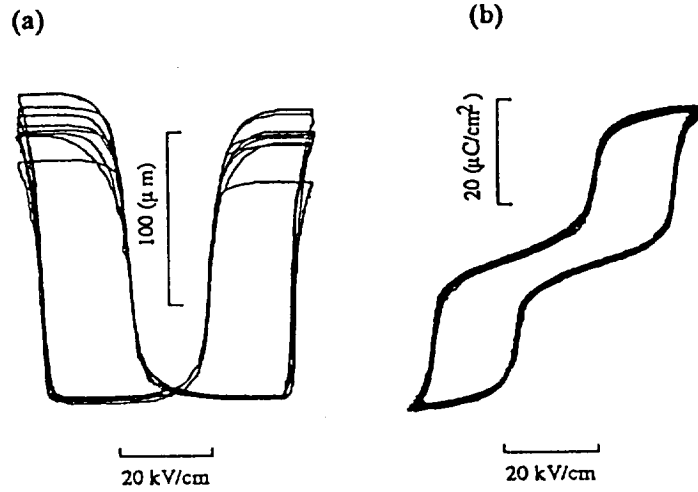

20 kV/cm   20 kV/cm

FIGURE 9   Influence of axial mechanical loading on (a) field-induced axial displacement and (b) hysteresis loop of Rainbow 66/24/10S for loads on the oxide layer.

constant of the c-axis (antipolar direction) is smaller than that of the a-axis for the PSZT antiferroelectric phase.[8] Similarly, when load is placed on the reduced layer, ferroelastic domains tend to be oriented vertical to the surface as a result of planar tensile stress. These situations are schematically depicted in Figure 12. Since the axial displacement of a Rainbow is dictated by the field-induced transverse strain in the oxide layer, a larger transverse strain should represent a larger axial displacement. Due to the different states of preferential domain alignment under the two loading conditions, different transverse strains occur under an identical applied electric field. As is shown in Figure 12, a sample with load applied to the oxide layer will exhibit
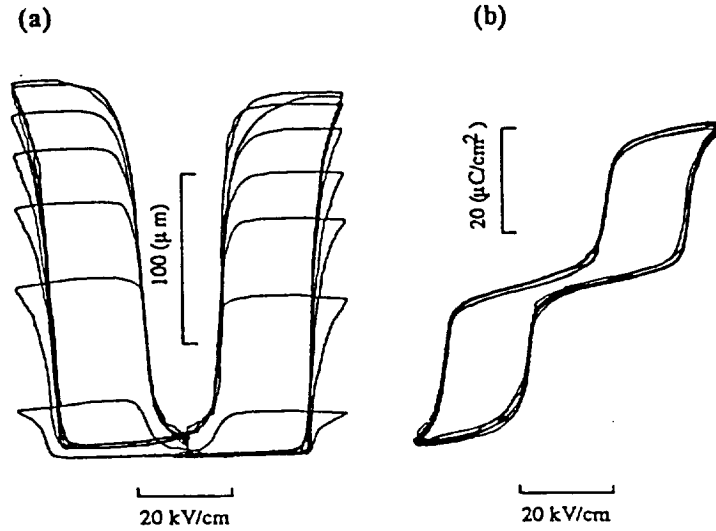
(a) (b)

20 kV/cm   20 kV/cm

FIGURE 10 Influence of axial mechanical loading on (a) field-induced axial displacement and (b) hysteresis loop of Rainbow 66/24/10S for loads on the reduced layer.
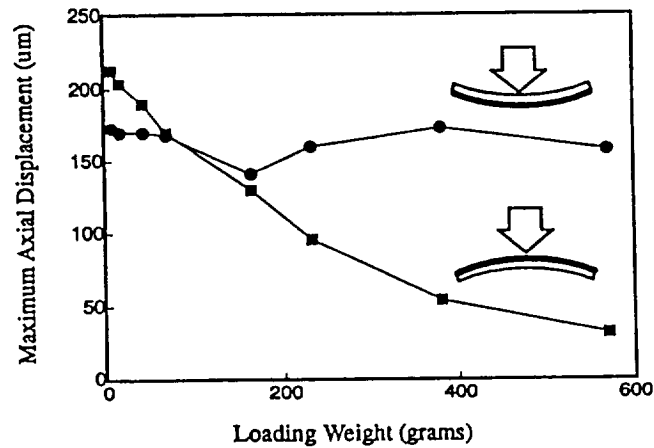

Loading Weight (grams)

FIGURE 11 Variation of maximum axial displacement with loading for Rainbow 66/24/10S, ● for load on oxide layer and ■ for load on reduced layer.

a larger field-induced displacement than one with load applied to the reduced layer. It should be pointed out that the geometrical stiffness (e.g., the reduced/unreduced layer thickness ratio and the ratio of the total thickness to diameter), dome curvature and initial internal stress of a Rainbow also have influences on the characteristics of displacement versus loading. The combined effects of the geometrical stiffness, curvature and domain alignment lead to the variations of the displacements indicated in Figure 11. Because ferroelastic domains are not polar, the domain alignment under stress will not affect the P-E hysteresis loop, which is in good agreement with the experimental observations.
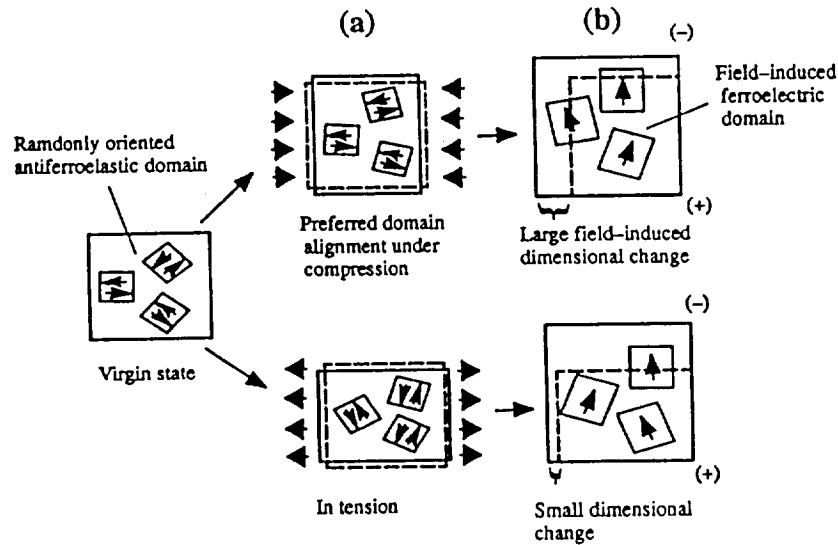
FIGURE 12　Schematic diagram of the transverse dimensional change in the oxide layer due to load-induced stresses and electric field. Dashed lines in (a) and (b) represent the shape of a portion of the oxide layer prior to the application of mechanical loading and electric field, respectively.

4.3.　Curvature and Internal Stress of PSZT Rainbows

At room temperature, a typical Rainbow possesses a dome-shaped configuration and an internal stress field as a result of the dimensional mismatch between the oxide and reduced layers produced during processing. Note that the internal stress refers to the stress inside a free Rainbow and is distinguished from the stresses created by loading as described earlier. Many of the characteristics of Rainbows have been found to be closely related to this dome structure and internal stress. The major contributions to the dimensional mismatch are considered to include: (1) the difference in thermal expansion coefficient between the oxide and reduced layers, (2) the dimensional change of the reduced layer due to oxygen (and possibly lead) loss, and (3) the dimensional change of the oxide layer resulting from phase transitions. Generally, Rainbow samples made of ferroelectric ceramics have a concave curvature with respect to the reduced side, which is defined as positive curvature. It was found that all the PSZT Rainbows prepared in this study exhibited a negative curvature, i.e. the reduced side is convex. Negative curvature implies that the oxide layer of a virgin Rainbow is predominantly, or completely, in tension depending on the reduced/unreduced layer ratio. If the composition of a PSZT Rainbow is close to the AFE-FE phase boundary, the internal tensile stress is sufficient to induce a
change from the antiferroelectric to ferroelectric phase. The net polarization observed in virgin Rainbow 64/26/10HP and the reduction of the AFE-FE switching fields in the PSZT Rainbows with respect to normal ceramics are probably the consequences of this tensile stress.

The results in Figure 13 are presented to show that the negative curvature in the PSZT Rainbows is attributable to the cubic-to-AFE phase transition. Specifically, the curvature with the concave oxide layer is caused by the fact that the reduction in
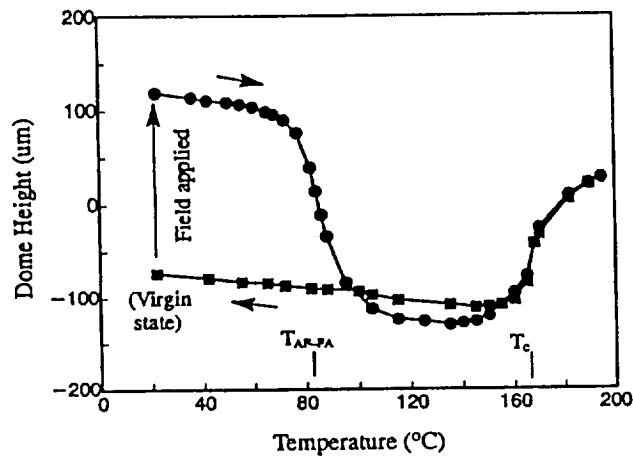
FIGURE 13   Changes of the dome height with temperature for Rainbow 66/23/11HP.

the dimensions of the oxide layer at the cubic-to-AFE phase transition exceeds the dimensional reduction of the reduced layer during cooling of a sample to room temperature. The dome height shown in Figure 13 is defined as the axial height of a Rainbow with respect to the unreduced wafer. Positive dome height corresponds to positive curvature. The curvature of Rainbow 66/23/11HP, which is antiferroelectric, was seen to change from negative to positive when the Rainbow was switched from the virgin antiferroelectric to ferroelectric state by an applied electric field. As the temperature was increased, the positive curvature changed back to a negative value at the FE-to-AFE phase transition T_{FE-AFE}. The curvature remained negative within the AFE phase range and became positive again near the Curie point. The reduction of temperature brought the sample back to the original antiferroelectric state and thus a negative curvature, as is indicated in Figure 13. All these clearly show that the antiferroelectric state is responsible for the negative curvature of PSZT Rainbows.

5.   CONCLUSION

The fabrication and properties of PSZT antiferroelectric Rainbow actuators have been investigated. The reduction reaction in PSZT ceramics proceeds much more rapidly than in PLZT ceramics. The optimal reduction conditions for the fabrication of PSZT Rainbows are 850°C for 2–3 hours. The antiferroelectric-ferroelectric phase transitions occur at a lower field strength in Rainbows as compared to normal ceramics. Large axial displacements in a range of 102 to 273 μm were obtained from the Rainbow samples by application of electric fields exceeding the phase switching levels. The field-induced displacements of the PSZT Rainbows are dependent on the manner of applying load to the samples. When load is placed on the oxide layer, there is only a slight change in the displacements for loads up to 570 grams. The displacement with load on the reduced layer, however, decreases markedly with increasing load. This behavior can be explained by the preferential alignment of

ferroelastic domains under stress. Antiferroelectric PSZT Rainbows generally have negative curvature at room temperature due mainly to the paraelectric to antiferroelectric phase transition in the oxide layer during cooling. The changes of material properties of PSZT Rainbows with respect to normal ceramics are associated with the internal stress resulting from processing.

ACKNOWLEDGEMENT

REFERENCES

1. K. Uchino, in Proceedings of the Ninth IEEE International Symposium on Applications of Ferro-electrics, pp. 319–324, 1994.
2. J. M. Herbert, "Ferroelectric Transducers and Sensors," Gordon and Breach Science Publishers, New York, 1982, Chap. 6, pp. 227–243.
3. Y. Sugawara, K. Onitsuka, S. Yoshikawa, Q. Xu, R. E. Newnham and K. Uchino, J. Am. Ceram. Soc., 75, 996 (1992).
4. G. H. Haertling, Am. Ceram. Soc. Bull., 73, 93 (1994).
5. S. Sherrit, H. D. Wiederick, B. K. Mukherjee and G. H. Haertling, in Proceedings of the Ninth IEEE International Symposium on Applications of Ferroelectrics, pp. 390–393, 1994.
6. E. Furman, G. Li and G. H. Haertling, Ferroelectrics, 160, 357 (1994).
7. W. Pan, C. Q. Dam, Q. M. Zhang and L. E. Cross, J. Appl. Phys., 66, 6014 (1989).
8. L. Shebanov, M. Kusnetsov and A. Sternberg, J. Appl. Phys., 76, 4301 (1994).
9. A. Furuta, K. Oh and K. Uchino, Sensors and Materials, 3–4, 205 (1992).
10. L. E. Cross, J. Intel. Mat. Sys. & Struc., 6, 55 (1995).
11. K. Uchino, Am. Ceram. Soc. Bull., 65, 647 (1986).
12. G. H. Haertling, in Proceedings of the Ninth IEEE International Symposium on Applications of Ferroelectrics, pp. 313–318, 1994.